STEADY STATE ANALYSIS OF INTEGRATED A.C. and D.C. SYSTEMS

A thesis

presented for the degree of

Doctor of Philosophy in Electrical Engineering

in the

University of Canterbury,

Christchurch, New Zealand.

by

B.J. HARKER B.E.(HONS), M.E.

1980

TABLE OF CONTENTS

APPENDICES

LIST OF ILLUSTRATIONS

LIST OF TABLES

LIST OF PRINCIPAL SYMBOLS

The majority of symbols are defined as they appear in the text and a comprehensive system of scripting is used for clarity. For convenience the principal symbols are redefined below.

I	:	current
V	:	voltage
Y	:	admittance
G	:	conductance
B	:	susceptance
Z	:	impedance
R	:	resistance
X	:	reactance
R_e	:	real part
I_m	:	imaginary
E	:	voltage
θ, ϕ	:	angles associated with a voltage vector
Z_0, Z_1, Z_2	:	zero, positive and negative sequence impedances
$[T_s]$	:	sequence to phase transformation matrix
$[C]$	:	connection matrix
$[J], [B'], [B'']$	:	jacobian matrices
P, Q	:	real and reactive power
$\bar{F}$	:	set of equations
$\bar{x}$	:	vector of variables
$\bar{F}(\bar{x})$	:	set of equations in terms of $\bar{x}$.
$\bar{R}$	:	set of d.c. residual (mismatch) equations
a	:	transformer tap ratio
p.u.	:	per unit
V_d	:	d.c. voltage

I_d	:	d.c. current
μ	:	commutation angle
α	:	firing delay angle
γ	:	extinction delay angle
U	:	phase-phase source voltage referred to transformer secondary
C	:	zero crossing of phase-phase source voltage
T	:	period between iniation of valve conduction and start of valve extinction
Z_0	:	characteristic impedance of transmission line
γ	:	propagation constant of transmission line
λ	:	wavelength
FFT	:	fast Fourier transform
SZC	:	shift in zero crossing
S.C.R.	:	short circuit ratio

Subscripts and superscripts

abc	:	three phase quantity
012	:	sequence component
int	:	internal or excitation busbar of a generator
reg	:	voltage regulator
gen	:	generator
term	:	terminal busbar of a generator or convertor
prim	:	primitive
p	:	primary
s	:	secondary
X_k	:	value of X at busbar k
X_k^i	:	value of X at phase i, busbar k
X^{sp}	:	specified value of X
X_{ik}^{ab}	:	value of X associated between phase a busbar i and phase b busbar k.

ABSTRACT

This thesis describes the development of a general method for the analysis of integrated a.c. and d.c. systems under normal, but not necessarily balanced, steady state operation.

Phase component three phase system modelling is reviewed and the relationship of the well known symmetrical components to the three phase modelling is discussed.

Using as a reference the single phase fast decoupled algorithm the modifications required to produce an efficient three phase fast decoupled load flow are described. It is demonstrated that the three phase fast decoupled load flow displays all the characteristics of the original single phase version.

Single phase balanced convertor modelling is reviewed and several techniques for the integration of such models with the single phase fast decoupled load flow are developed and their performance is compared.

The methods for single phase convertor modelling are extended to allow unbalanced convertor operation to be analysed. The integration of the unbalanced convertor model into the three phase fast decoupled load flow is described. Convergence properties are examined and detailed results given.

The extension of steady state analysis techniques to the consideration of harmonic frequencies is discussed. The unbalanced convertor model is used as a basis to enable the harmonic interaction of d.c. convertors and the a.c. system to be studied.

ACKNOWLEDGEMENTS

I express my thanks to my supervisor Professor J. Arrillaga for his advice, assistance and friendship during the elaboration of this work.

Also, the value of the many discussions with my post-graduate colleagues is gratefully acknowledged.

Special recognition is made of the financial and technical assistance provided by my employer, New Zealand Electricity. I thank the staff of the Christchurch Drawing Office of New Zealand Electricity for the preparation of the many diagrams in this thesis.

Finally, I thank my wife Jenny for her patience and encouragement during the course of my work.

CHAPTER 1

INTRODUCTION

The undesirable influence of steady state power system unbalance[1] on the conventional system loads and generators has required power system planners to be very conscious of any features which may create unbalance among the three phases. With the more recent proliferation of high power d.c. convertor installations, which are susceptible to the production of non-characteristic harmonic currents even with small unbalance, there is a renewed interest in the study of the causes of power system unbalance.

The quantitative analysis of unbalanced power systems operating in the presence of d.c. convertors, is a demanding task, which, until now has only been attempted in very restricted cases. This thesis describes a general method of analysis in which the unbalanced operation of the three phase system, including the influence of large three phase convertor installations, is analysed using an efficient steady state load flow technique. In addition to the study of the power frequency unbalanced operation of convertors, this thesis also deals with the related problem of harmonic current generation.

The methods presented are, in general, extensions of the most advanced and well proven single phase load flow techniques. In particular, the development of the three phase load flow algorithm is based on the fast decoupling principles which have proved so successful in the single phase case.

The emphasis in the thesis is on algorithmic formulation, with only brief discussions on the relevant computational details. Although it is acknowledged that the computational aspects are critical to the practicality of any load flow solution, methods for efficient programming of storage and solution routines have been extensively studied in the recent past and further effort in this area is unlikely to bring any significant advance. Therefore existing sparsity storage and solution routines have been used wherever practicable.

Symmetrical components is a well established method which provides immense simplification in the analysis of unbalanced operation of balanced transmission systems. However, when the system itself is unbalanced, the transformation provides no simplification and its use cannot be justified. The three phase system and the d.c. convertors are therefore represented directly in phase quantities. Symmetrical components are however, a valuable aid in the understanding and interpretation of results and they are used for this purpose where appropriate.

The material presented conveniently separates to form the individual chapters and each chapter is, for the most part, treated as a separate unit.

Chapter 2 presents a review of power system modelling for steady state analysis. The relationship of the well known symmetrical components to the steady state system modelling in phase components is discussed. Models for all the common three phase elements are presented and the methods for their derivation reviewed. Although the material in this chapter is largely a review of existing methods, it is essential to the formulation of the three phase load flow as well as being of considerable interest in itself.

Chapter 3 is a brief description of the basic Newton-Raphson solution method. This material, although well documented, forms an important basis for the application of the method to the less familiar situations of the three phase load flow and the steady state convertor models. It is therefore included as a chapter in its own right to reflect its importance to the remainder of this thesis.

Chapter 4 describes the development of a three phase fast decoupled load flow for the unbalanced a.c. system. The three phase version is an extension of the well known single phase fast decoupled load flow. The original aspects of the three phase version and their relationships to the single phase case are discussed in detail. The performance of the developed algorithm is investigated and it is demonstrated that the three phase version retains the computational efficiency and reliability of the single phase version.

Chapter 5 describes the formulation of a model of the balanced operation of the d.c. convertors which is suitable for integration into single phase load flow studies of combined a.c. and d.c. systems. Various sequential and unified (simultaneous) integrations with the single phase fast decoupled load flow are discussed and compared. The primary motivation for the work described in this chapter is to provide a basis for the development of a three phase convertor model and to enable selection of the best algorithm for the subsequent integration of that model into the three phase fast decoupled load flow.

Chapter 6 describes the formulation of a model of the unbalanced three phase convertor with sufficient generality to incorporate a wide range of convertor control modes including the effect of symmetrical firing and the more traditional phase angle firing controllers. The sequential integration of the unbalanced model

into the three phase load flow is presented and the performance of the three phase integration compared to the corresponding single phase version. The steady state unbalanced convertor model forms a basis for the investigation of the harmonic current generation during unbalanced steady state operation as discussed in chapter 8.

Chapter 7 deals with the extension of the techniques for power frequency modelling of the three phase system to the more general case of harmonic frequency modelling. In addition, this chapter introduces the nature of some of the problems caused by harmonic power flows and also discusses the degree of representation required if an analysis is to be attempted. This chapter is an introduction to the topic only and is intended to form a basis for further investigation. The material presented provides the necessary background to the final chapter.

Finally, chapter 8 is concerned with the steady state harmonic generation of d.c. convertors under unbalanced conditions when the system harmonic impedances cannot be assumed zero. Features such as the harmonic interaction of a convertor and the a.c. system and also the effect of system resonances are considered on a general three phase basis. The limitations of the steady state analysis are discussed and illustrative examples are studied in detail.

Several papers[2 - 6] have been written in connection with the work in this thesis and where appropriate they are referenced or included as appendices.

CHAPTER 2

REVIEW OF POWER SYSTEM MODELLING FOR STEADY STATE LOAD FLOW ANALYSIS

2.1 INTRODUCTION

To enable a load flow analysis to be performed, be it three phase or single phase, it is necessary to form a mathematical representation of the power system. The most successful load flow techniques to date are based upon the nodal admittance formulation. This chapter describes the formulation of the admittance parameters for the various three phase elements.

A three phase power system consists of the interconnection of a number of relatively simple physical elements such as generators, transformers, transmission lines and loads. However, the electrical characteristics of these interconnected elements are extremely complex. By making as many simplifying assumptions as the purpose of the study will allow, methods have been developed to enable engineers to cope with this complexity.

The elements of the power system are inevitably unbalanced and some unbalance will also exist in the system loading and generation. To study features associated with this unbalance it is necessary to perform a three phase load flow analysis. In this analysis each phase is independently modelled as are all inductive and capacitive mutual couplings between phases and between circuits. No transformations yield any simplification to this analysis although symmetrical components are a valuable aid in the interpretation of results.

For many studies on the electrical power system the unbalance itself is not of any particular interest and may be ignored. The parameters of the system are then assumed to be balanced as are the system loads and generation. In such cases a steady state analysis is possible with a single phase (positive sequence) load flow. The system modelling for the single phase case is relatively simple and is well documented and will not be discussed further here.

This chapter firstly reviews the relationship of the well known symmetrical component theory to the three phase system modelling. The development of models for the various three phase elements is discussed and a systematic procedure for the formation of the system admittance matrix is developed.

2.2 SYMMETRICAL COMPONENTS

The symmetrical component transformation is a general mathematical technique developed by Fortescue whereby any "system of n vectors or quantities may be resolved, when n is prime, into n different symmetrical n phase systems."[7] Any set of three phase voltages or currents may therefore be transformed into three symmetrical systems of three vectors each. This, in itself, would not commend the method. However, consider the equation describing the system operation,

$$[I_{abc}] = [Y_{abc}][V_{abc}] \tag{2.1}$$

where abc indicates the actual phase quantities. The transformed quantities (indicated by subscripts 012 for the zero, positive and negative sequences respectively) are related to the phase quantities by:

$$[V_{012}] = [T_s]^{-1} [V_{abc}] \tag{2.2}$$

$$[I_{012}] = [T_s]^{-1} [I_{abc}] \tag{2.3}$$

where $[T_s]$ is the transformation matrix.

Substitution into (2.1) yields:

$$[I_{012}] = [T_s]^{-1} [Y_{abc}][T_s][V_{012}] \tag{2.4}$$

The transformed voltages and currents are related by the transformed admittance matrix,

$$[Y_{012}] = [T_s]^{-1} [Y_{abc}][T_s] \tag{2.5}$$

If the original phase admittance matrix $[Y_{abc}]$ is in its' natural unbalanced state then the transformed admittance matrix $[Y_{012}]$ is full. Therefore current flow of one sequence will give rise to voltages of all sequences, i.e. the equivalent circuits for the sequence networks are mutually coupled. The problem of analysis is no simpler in sequence components than in the original phase components and, in this case, symmetrical components should not be used.

However, when the unbalance is small, or of no particular interest, then it may be ignored and $[Y_{abc}]$ becomes, upon transformation, a diagonal matrix. That is, the mutually coupled three phase system has been replaced by three uncoupled symmetrical systems. In addition, if the generation and loading are balanced, or may be assumed balanced, then only one system, the positive sequence system, has any current flow and the other two sequences may be ignored. This is essentially the situation with the single phase load flow.

2.3 NETWORK SUBDIVISION

To enable the system to be modelled in a systematic, logical and convenient manner the system must be subdivided into more manageable units. These units, called subsystems, are defined as follows: A SUBSYSTEM is the unit into which any part of the system may be divided such that no subsystem has any mutual couplings between its constituent branches and those of the rest of the system. This definition ensures that the subsystems may be combined in an extremely straightforward manner.

The system is first subdivided into the most convenient subsystems consistent with the definition above. An example of this process is illustrated in Appendix 1.

The smallest unit of a subsystem is a single network element. In the following sections the nodal admittance matrix representation of all common elements is derived. More complex subsystems must be defined because of mutual coupling between three phase system elements and because many connections between busbars consist of a number of elements in series. Methods are presented for deriving the nodal admittance matrix for these subsystems.

The subsystem unit is retained for input data organisation. The data for any subsystem is input as a complete unit, the subsystem admittance matrix is formulated and stored and then all subsystems are combined to form the total system admittance matrix.

2.4 SYNCHRONOUS MACHINE MODELLING FOR LOAD FLOW ANALYSIS

Synchronous machines are designed for maximum symmetry of the phase windings and are therefore adequately modelled by their sequence parameters. The sequence impedances contain all the information that is required to analyse the steady state unbalanced

behaviour of the synchronous machine.

The admittance representation of the generator in phase components may be derived from the sequences impedances (Z_0, Z_1, Z_2). The generator sequence impedance matrix $[Z_{gen}]_{012}$ is first transformed to phase components, $[Z_{gen}]_{abc}$ is given by,

$$[Z_{gen}]_{abc} = [T_s][Z_{gen}]_{012}[T_s]^{-1} \tag{2.6}$$

$$= [T_s][Z_{gen}]_{012}[T_s]^{*} \tag{2.7}$$

where $[T_s]^*$ is the complex conjugate of matrix $[T_s]$, where

$$[T_s] = \begin{bmatrix} 1 & 1 & 1 \\ 1 & a^2 & a \\ 1 & a & a^2 \end{bmatrix} \tag{2.8}$$

and a is the complex operator $e^{j2\pi/3}$.

The phase component impedance matrix is thus,

$$[Z_{gen}]_{abc} = \begin{array}{|c|c|c|} \hline Z_0 + Z_1 + Z_2 & Z_0 + aZ_1 + a^2Z_2 & Z_0 + a^2Z_1 + aZ_2 \\ \hline Z_0 + a^2Z_1 + aZ_2 & Z_0 + Z_1 + Z_2 & Z_0 + aZ_1 + a^2Z_1 \\ \hline Z_0 + aZ_1 + a^2Z_2 & Z_0 + a^2Z_1 + aZ_2 & Z_0 + Z_1 + Z_2 \\ \hline \end{array} \tag{2.9}$$

The phase component model of the generator is illustrated in Fig 2.1 (a). The machine excitation acts symmetrically on the three phases and the voltages at the internal or excitation busbar form a balanced three phase set, i.e.,

$$E_k^a = E_k^b = E_k^c \tag{2.10}$$

and

$$\theta_k^a = \theta_k^b + \frac{2\pi}{3} = \theta_k^c - \frac{2\pi}{3} \tag{2.11}$$

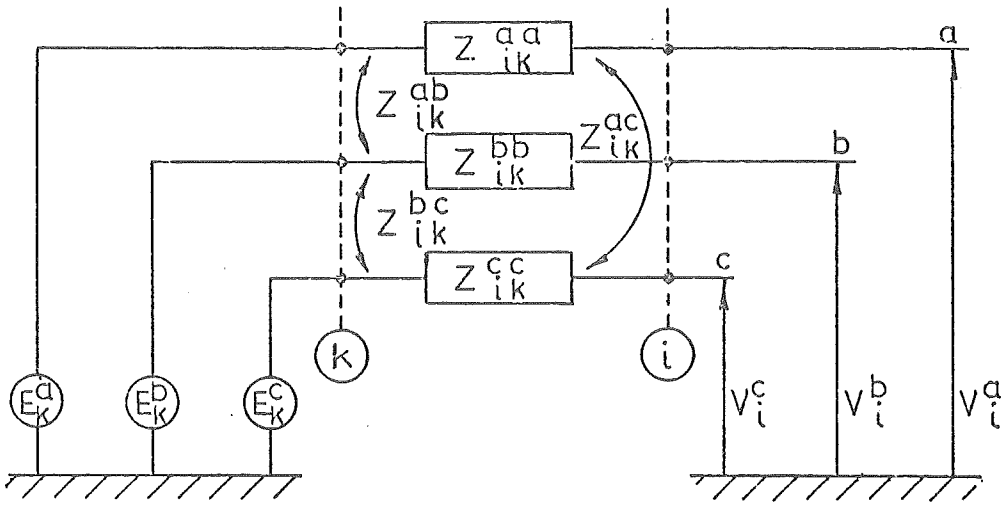

(a) Phase component representation

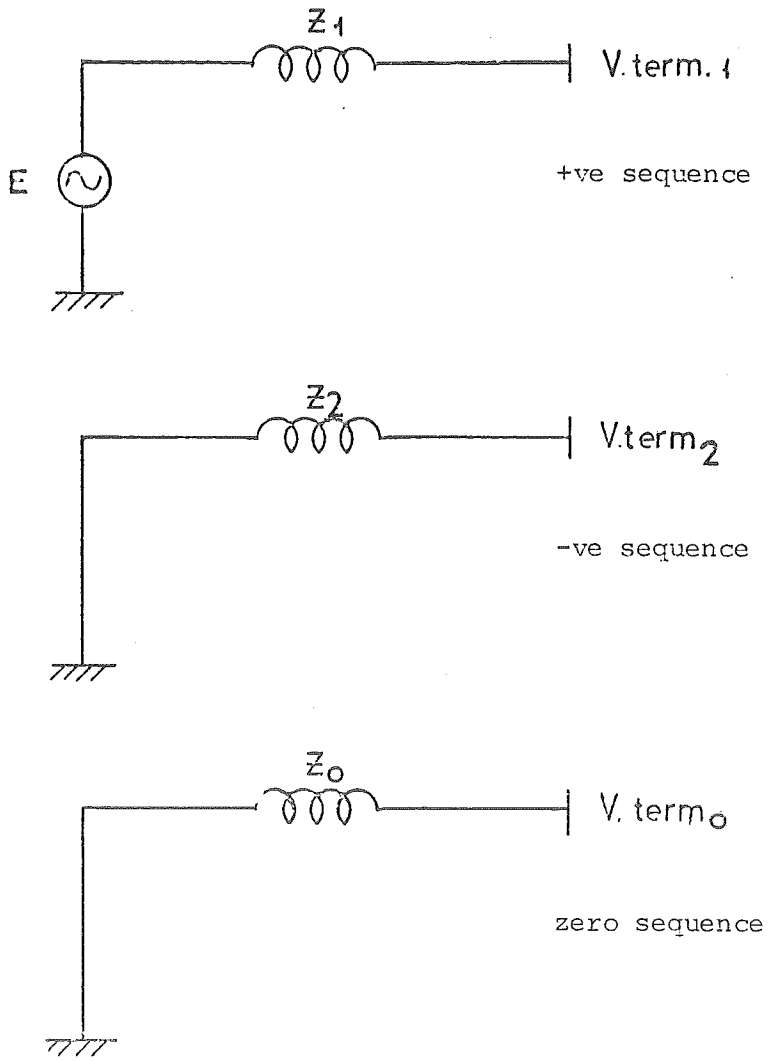

(b) Symmetrical component representation

Fig. 2.1 Synchronous Machine Models

For three phase load flow the voltage regulator must be accurately modelled as it influences the machine operation under unbalanced conditions. The voltage regulator monitors the terminal voltages of the machine and controls the excitation voltage according to some predetermined function of the terminal voltages. Some common examples are:

(i) The voltage on one phase is maintained.

(ii) One phase to phase voltage is maintained.

In general the voltage regulator constraint may be written as some function of the terminal voltages.

Before proceeding further it is instructive to consider the generator modelling from a symmetrical component frame of reference. The sequence network model of the generator is illustrated in Fig. 2.1 (b). As the machine excitation acts symmetrically on the three phases positive sequence voltages only are present at the internal busbar.

The influence of the generator upon the unbalanced system is known if the voltages at the terminal busbar are known. In terms of sequence voltages, the positive sequence voltage may be obtained from the excitation and the positive sequence voltage drop caused by the flow of positive sequence currents through the positive sequence reactance. The negative and zero sequence voltages are derived from the flow of their respective currents through their respective impedances. It is important to note that the negative and zero sequence voltages are not influenced by the excitation or positive sequence impedance.

There are infinite combinations of machine excitation and machine positive sequence reactance which will satisfy the conditions at the machine terminals and give the correct positive sequence volt-

age. Whenever the machine excitation must be known (as in fault studies) the actual positive sequence impedance must be used. For load flow however, the excitation is not of any particular interest and the positive sequence impedance may be arbitrarily assigned to any value. This feature has been recognised by previous researchers[8] for load flow studies on unbalanced systems when the system has been modelled using coupled sequence networks. The positive sequence impedance is usually set to zero for these studies. With regard to three phase load flow in phase co-ordinates, the practice of setting the positive sequence reactance to a small value is equally valid. The advantage to the three phase load flow is that the excitation voltage is reduced to the same order as the usual system voltages and there is a corresponding reduction in the angle between the internal busbar and the terminal busbar. Both these features are important when a fast decoupled algorithm is used.

Therefore, in forming the phase component generator model using equation (2.9), an arbitrary value may be used for Z_1 but the actual values are used for Z_0 and Z_2. There is no loss of relevant information as the influence of the generator upon the unbalanced system is accurately modelled.

The nodal admittance matrix, relating the injected currents at the generator busbars to their nodal voltages, is given by the inverse of the series impedance matrix derived from equation (2.9).

2.5 TRANSMISSION LINES

Transmission line parameters are calculated from the line geometrical characteristics. The calculated parameters are expressed as a series impedance and shunt admittance per unit length of line.

The effect of ground currents and earth wires are included in the calculation of these parameters[7,9,10].

The usual single phase transmission line model represents the electrically short line by a nominal-π network. Half of the total shunt admittance is connected to earth at each terminal and the series impedance for the total line is placed in series between the busbars as shown in Fig. 2.2.

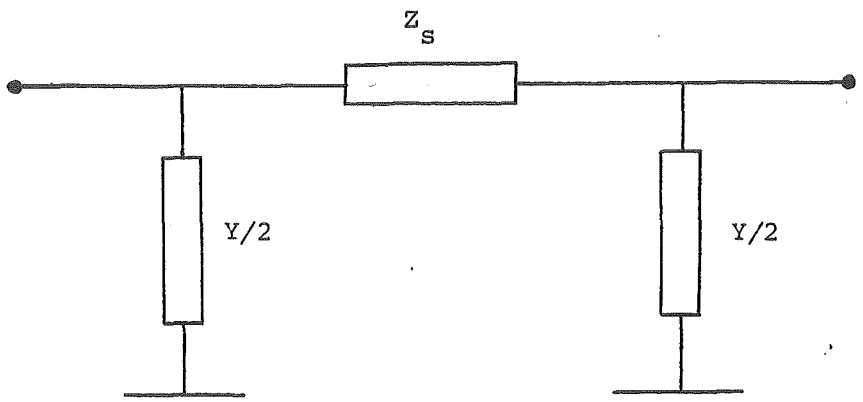

Fig. 2.2 Nominal-π Model: Single Phase Transmission Line

The same nominal-π model can be used in the three phase case. The process by which Z_s and Y become 3 × 3 matrix quantities is illustrated in Fig. 2.3. In part (i) of the figure the full circuit representation is shown. This consists of three nominal-π circuits (one for each phase) which are coupled together. The mutual coupling is lumped in a similar manner to the other parameters. Parts (ii) and (iii) show alternative and more concise circuit representations where $[Z_s]$ and [Y] are written as 3 × 3 matrices and corresponding three phase compound coils.

Kron[11] refers to these matrix quantities as compound tensors and states

Fig. 2.3 Nominal π Model: Three phase transmission line

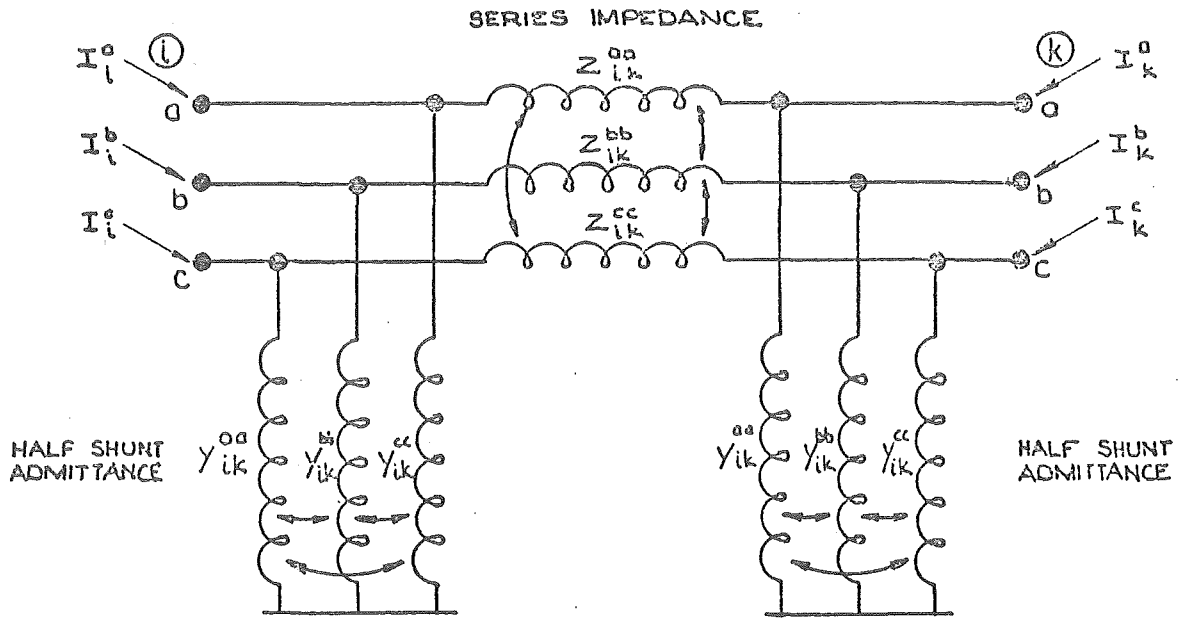

(i) FULL CIRCUIT REPRESENTATION.

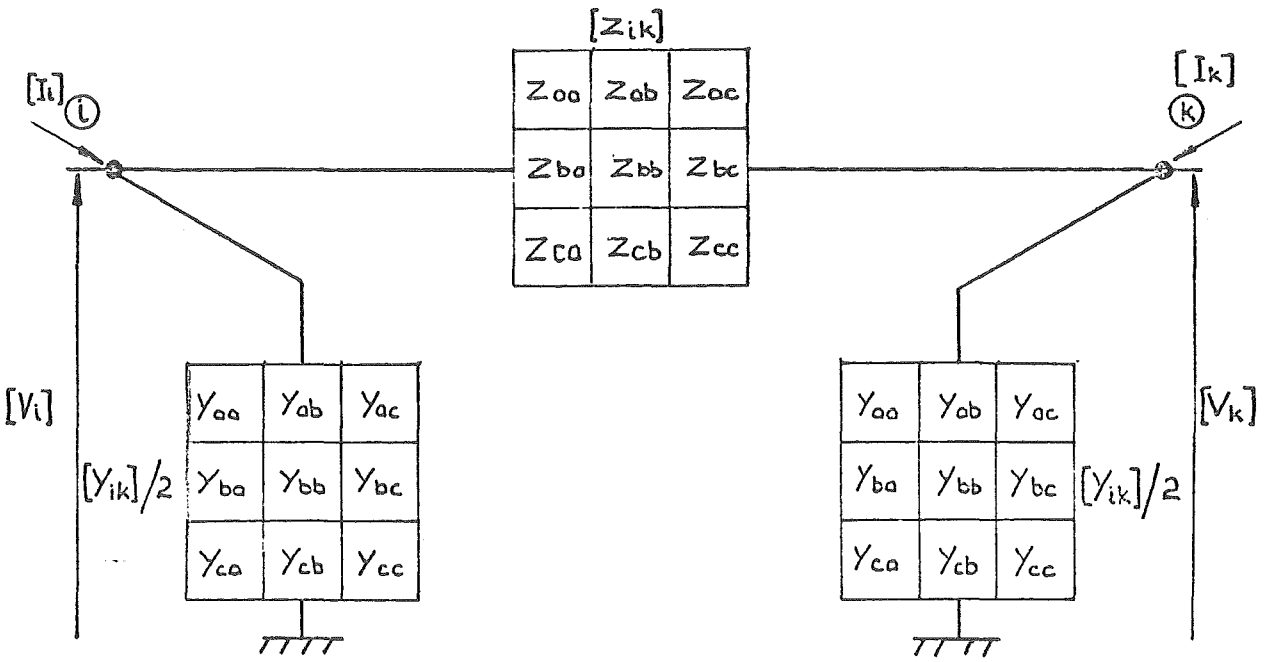

(ii) MATRIX EQUIVALENT.

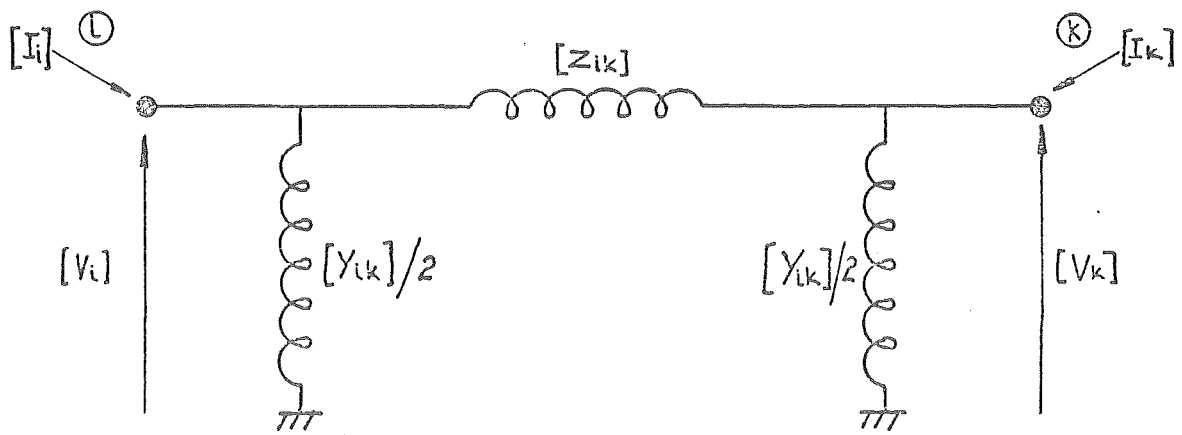

(iii) USING THREE PHASE COMPOUND COILS.

> "the whole impedance terminology of ordinary networks can be transferred to compound networks by replacing ordinary numbers with appropriate tensors" and also the "theories, laws, equations etc ... for ordinary networks are all valid for compound networks by simply replacing single quantities by appropriate tensors and single tensors by appropriate compound tensors."

The representation of three phase elements by the use of compound coils will be used extensively. The formation of both the primitive and actual network admittance matrices using three phase compound coils is covered in detail in Appendix 2. The admittance matrix for the three phase element can now be written. (This is done following the rules which are developed in Appendix 2 for the formation of the admittance matrix using compound coils.)

The element admittance matrix relates the nodal injected currents illustrated in Fig.2.3 (iii) to the nodal voltages by the equation,

$$\begin{array}{c|c} [I_i] \\ \hline [I_k] \end{array} = \begin{array}{c|c} [Z]^{-1} + [Y]/2 & -[Z]^{-1} \\ \hline -[Z]^{-1} & [Z]^{-1} + [Y]/2 \end{array} \begin{array}{c|c} [V_i] \\ \hline [V_k] \end{array} \qquad (2.12)$$

$6 \times 1 \qquad\qquad 6 \times 6 \qquad\qquad 6 \times 1$

This forms the element admittance matrix representation for the short line between busbars i and k in terms of 3 × 3 matrix quantities.

This representation is often not accurate enough for electrically long lines. The physical length at which a line is no longer electrically short depends on the wavelength, therefore if harmonic frequencies are being considered, this physical length may be quite small. Using transmission line and wave propagation theory[12,13] more exact models may be derived. However, for normal mains frequency analysis, it is considered sufficient to model a long line as a

series of 2 or 3 nominal-π sections. If many sections are taken an exact representation is approached.

2.6 TRANSFORMER MODELLING

2.6.1 Introduction

Traditionally, three phase transformers have been represented by their equivalent sequence networks. The inherent assumption, that the transformer is a balanced three phase device, is justified in the majority of practical situations. More recently, however, methods have been developed[9,14,15] to enable all three phase transformer connections to be accurately modelled in phase coordinates. In phase coordinates no assumptions are necessary although the physically justifiable assumptions are usually introduced in order to simplify the modelling. The basis of the derivation of the phase coordinate transformer models, is the primitive admittance matrix which is derived from the primitive or unconnected network for the transformer windings. The method of linear transformation (Appendix 2) enables the admittance matrix of the actual connected network to be found.

This section describes the primitive admittance matrix for a basic two winding three phase transformer in the most general case. The usual simplifying assumptions are introduced and models for the common connections are derived.

2.6.2 Primitive Admittance Model of Three Phase Transformers

Many three phase transformers are wound on a common core and all windings are therefore coupled to all other windings. Therefore, in general, a basic two winding three phase transformer has a primitive or unconnected network consisting of six coupled coils. If a

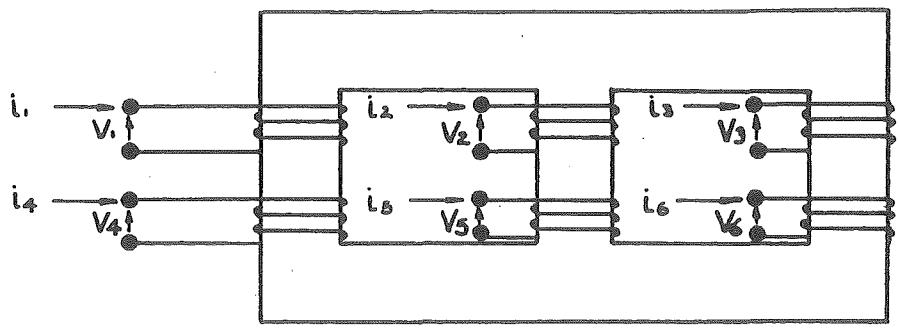

(a) Diagramatic representation of two winding transformer

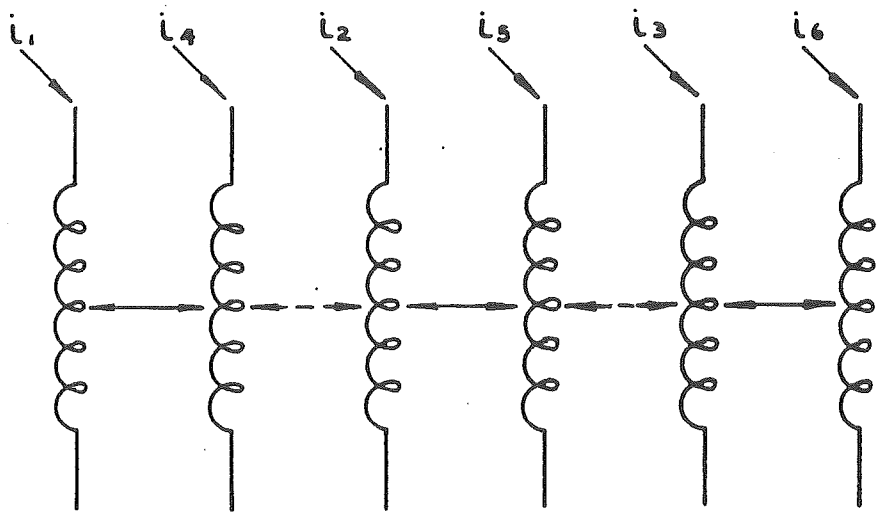

(b) Six coupled coil primitive network

NOTE: the dotted coupling represents parasitic coupling between phases.

Fig. 2.4 Primitive Network of Two Winding Transformer

tertiary winding is also present the primitive network consists of nine coupled coils. The basic two winding transformer only will be considered; the addition of further windings is a simple but cumbersome extension of the method.

The primitive network, Fig. 2.4, can be represented by the primitive admittance matrix which has the general form of equation 2.13.

$$\begin{bmatrix} i_1 \\ i_2 \\ i_3 \\ i_4 \\ i_5 \\ i_6 \end{bmatrix} = \begin{bmatrix} y_{11} & y_{12} & y_{13} & y_{14} & y_{15} & y_{16} \\ y_{21} & y_{22} & y_{23} & y_{24} & y_{25} & y_{26} \\ y_{31} & y_{32} & y_{33} & y_{34} & y_{35} & y_{36} \\ y_{41} & y_{42} & y_{43} & y_{44} & y_{45} & y_{46} \\ y_{51} & y_{52} & y_{53} & y_{54} & y_{55} & y_{56} \\ y_{61} & y_{62} & y_{63} & y_{64} & y_{65} & y_{66} \end{bmatrix} \begin{bmatrix} v_1 \\ v_2 \\ v_3 \\ v_4 \\ v_5 \\ v_6 \end{bmatrix} \qquad (2.13)$$

Assuming the reciprocal nature of the mutual couplings in equation 2.13, twenty one short circuit measurements would be necessary to complete the admittance matrix. Such a detailed representation is seldom required.

By assuming the flux paths to be symmetrically distributed between all windings then equation 2.13 may be simplified to equation 2.14.

$$\begin{bmatrix} i_1 \\ i_2 \\ i_3 \\ i_4 \\ i_5 \\ i_6 \end{bmatrix} = \begin{bmatrix} y_p & y'_m & y'_m & -y_m & y''_m & y''_m \\ y'_m & y_p & y'_m & y''_m & -y_m & y''_m \\ y'_m & y'_m & y_p & y''_m & y''_m & -y_m \\ -y_m & y''_m & y''_m & y_s & y''' & y'''_m \\ y''_m & -y_m & y''_m & y'''_m & y_s & y'''_m \\ y''_m & y''_m & -y_m & y'''_m & y'''_m & y_s \end{bmatrix} \begin{bmatrix} v_1 \\ v_2 \\ v_3 \\ v_4 \\ v_5 \\ v_6 \end{bmatrix} \qquad (2.14)$$

where y'_m is the mutual admittance between primary coils.

y''_m is the mutual admittance between primary and secondary coils on different cores.

y'''_m is the mutual admittance between secondary coils.

For three separate single phase units all the primed values are effectively zero. In three phase units the primed values, representing parasitic inter-phase coupling, do have a noticeable effect. This effect can be interpreted through the symmetrical component equivalent circuits as discussed in detail in references (9) and (14).

Normally, the only parameters which are available are from the standard short circuit and open circuit transformer tests. These give the leakage impedance (Z_{sc}) and the magnetising admittance (Y_{oc}) for each pair of primary and secondary windings. The magnetising admittances are conveniently removed from the transformer model; if required these may be added later as small shunt connected admittances at the transformer terminals.[15,16]

In order to model three phase transformers it is necessary to derive the primitive admittance matrix in terms of the standard parameters. Equation 2.14, with all primed values ignored, forms the primitive admittance matrix. The coupling between coils is modelled as for a single phase unit, with an appropriate allowance for both primary and secondary off nominal tap ratios. An equivalent p.u. representation is shown in Fig. 2.5.

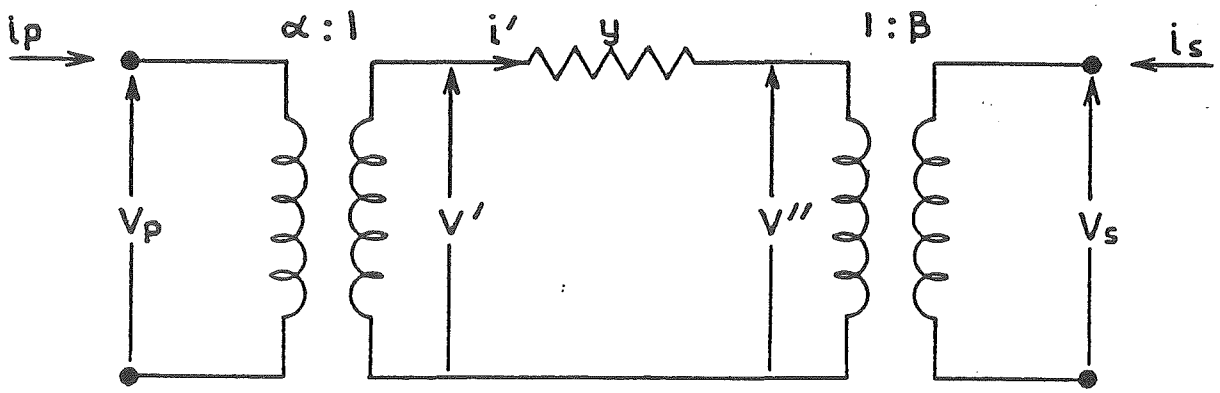

Fig. 2.5 Equivalent Circuit in p.u. for Coupled Transformer Windings

Primary and secondary off nominal tap ratios are designated α and β respectively. Solving for the terminal currents in terms of the terminal voltages yields:

$$\begin{bmatrix} i_p \\ i_s \end{bmatrix} = \begin{bmatrix} y/\alpha^2 & -y/\alpha\beta \\ -y/\alpha\beta & y/\beta^2 \end{bmatrix} \begin{bmatrix} v_p \\ v_s \end{bmatrix} \qquad (2.15)$$

The primitive network and corresponding primitive admittance matrix can be derived in terms of equation 2.15. Allowing for independent parameters for each coupled winding the primitive network of Fig. 2.6 (i) is applicable. The primitive admittance

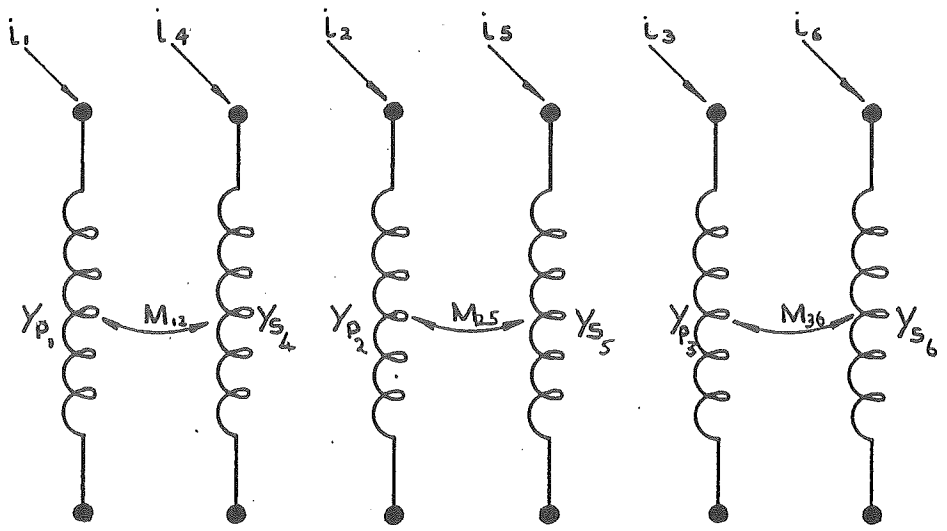

where $Y_{p_i} = Y/\alpha_i^2$, $Y_{s_j} = Y/\beta_j^2$ and $M_{ij} = Y/\alpha_i\beta_i$

(i) Primitive network

$$\begin{bmatrix} i_1 \\ i_2 \\ i_3 \\ i_4 \\ i_5 \\ i_6 \end{bmatrix} = \begin{bmatrix} Y_{p_1} & & & M_{14} & & \\ & Y_{p_2} & & & M_{25} & \\ & & Y_{p_3} & & & M_{36} \\ M_{41} & & & Y_{s_4} & & \\ & M_{52} & & & Y_{s_5} & \\ & & M_{63} & & & Y_{s_6} \end{bmatrix} \begin{bmatrix} V_1 \\ V_2 \\ V_3 \\ V_4 \\ V_5 \\ V_6 \end{bmatrix} \quad (2.16)$$

(ii) Primitive admittance matrix.

Fig. 2.6 Primitive Network of Two Winding Transformer in Terms of Standard Parameters

matrix (equation 2.16 in Fig. 2.6 (ii)), forms the basis for deriving the models of the common transformer connections.

2.6.3 Models for Common Transformer Connections

The network admittance matrix for any two winding three phase transformer can now be formed by the method of linear transformation. This method is described in Appendix 2.

As an example consider the formation of the admittance matrix for the star-star connection with both neutrals solidly earthed. This example is chosen as it is the simplest computationally.

The connection matrix is derived from consideration of the actual connected network. For the star-star transformer this is illustrated in Fig. 2.7. The connection matrix [C] relating the branch voltages (i.e. voltages of the primitive network) to the node voltages (i.e. voltages of the actual network) is given by equation 2.17 which is illustrated in Fig. 2.8.

The nodal admittance matrix $[Y]_{NODE}$ is given by

$$[Y]_{NODE} = [C]^t [Y]_{PRIM} [C] \tag{2.18}$$

Substituting for [C] yields,

$$[Y]_{NODE} = [Y]_{PRIM} \tag{2.19}$$

as the connection matrix for this example is a 6 × 6 identity matrix.

The models for the other common connections can be derived following a similar procedure. A further example of the star-g/delta connection is given in Appendix 3.

In general, any two winding three phase transformer may be represented using two coupled compound coils. The network and admittance matrix for this representation is illustrated in Fig. 2.9.

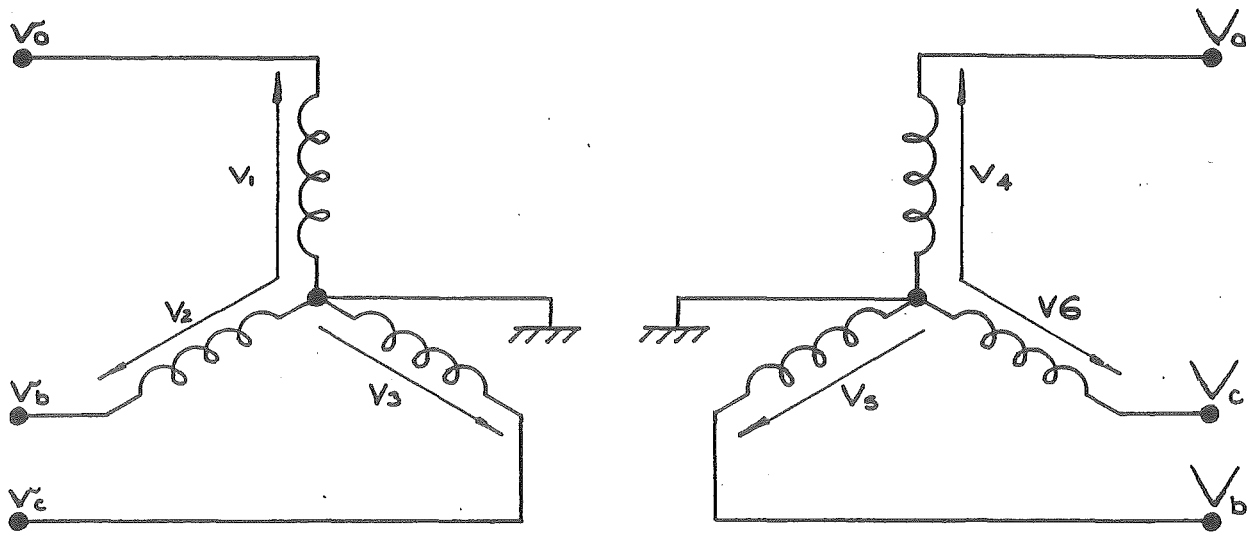

Fig. 2.7 Connection Diagram for Star-Star Transformer

$$\begin{bmatrix} V_1 \\ V_2 \\ V_3 \\ V_4 \\ V_5 \\ V_6 \end{bmatrix} = \begin{bmatrix} 1 & & & & & \\ & 1 & & & & \\ & & 1 & & & \\ & & & 1 & & \\ & & & & 1 & \\ & & & & & 1 \end{bmatrix} \begin{bmatrix} V'_a \\ V'_b \\ V'_c \\ V_a \\ V_b \\ V_c \end{bmatrix} \quad (2.17)$$

Fig. 2.8 The Connection Matrix for Star-Star Transformer

$$\begin{bmatrix} i_p \\ i_s \end{bmatrix} = \begin{bmatrix} Y_{pp} & Y_{ps} \\ Y_{sp} & Y_{ss} \end{bmatrix} \begin{bmatrix} V_p \\ V_s \end{bmatrix}$$

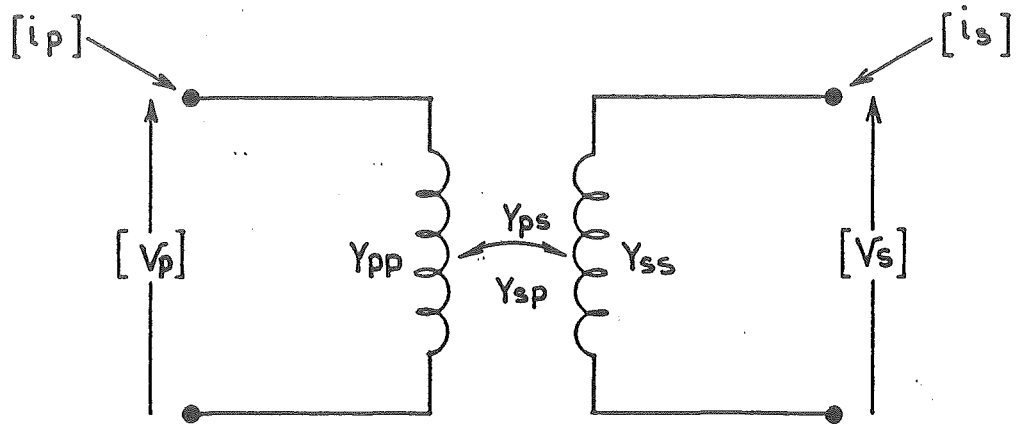

Fig. 2.9 Two winding three phase transformer as two coupled compound coils.

It should be noted that,

$$[Y_{sp}] = [Y_{ps}]^T \qquad (2.20)$$

as the coupling between the two compound coils is bilateral.

Often, because more detailed information is not required, the parameters of all three phases are assumed balanced. In this case the common three phase connections are found to be modelled[9] by three basic submatrices.

The submatrices, $[Y_{pp}]$, $[Y_{ps}]$ etc., are given in Table 2.1 for the common connections.

Finally these submatrices must be modified to account for off nominal tap ratios as follows:

Table 2.1 Characteristic submatrices used in forming the transformer admittance matrices

TRANSF. CONNECTION		SELF ADMITTANCE		MUTUAL ADMITTANCE
BUS P	BUS S	Y_{pp}	Y_{ss}	Y_{ps}, Y_{sp}^{T}
Wye-G	Wye-G	Y_{i}	Y_{i}	$-Y_{i}$
Wye-G	Wye	$Y_{ii/3}$	$Y_{ii/3}$	$-Y_{ii/3}$
Wye-G	DELTA	Y_{i}	Y_{ii}	$+Y_{iii}$
Wye	Wye	$Y_{ii/3}$	$Y_{ii/3}$	$-Y_{ii/3}$
Wye	DELTA	$Y_{ii/3}$	Y_{ii}	Y_{iii}
DELTA	DELTA	Y_{ii}	Y_{ii}	$-Y_{ii}$

where

$$Y_{i} = \begin{bmatrix} Y_t & & \\ & Y_t & \\ & & Y_t \end{bmatrix}$$

$$Y_{ii} = \begin{bmatrix} 2Y_t & -Y_t & -Y_t \\ -Y_t & 2Y_t & -Y_t \\ -Y_t & -Y_t & 2Y_t \end{bmatrix}$$

$$Y_{iii} = \begin{bmatrix} -Y_t & Y_t & \\ & -Y_t & Y_t \\ Y_t & & -Y_t \end{bmatrix}$$

(i) Divide the self admittance of the primary by α^2.

(ii) Divide the self admittance of the secondary by β^2.

(iii) Divide the mutual admittance matrices by $(\alpha\beta)$.

It should be noted that in the p.u. system a delta winding has an off nominal tap of $\sqrt{3}$.

For transformers with ungrounded Wye connections, or with neutrals connected through an impedance, an extra coil is added to the primitive network for each unearthed neutral and the primitive admittance matrix increases in dimension. By noting that the injected current in the neutral is zero, these extra terms can be eliminated from the connected network admittance matrix[14].

Once the admittance matrix has been formed for a particular connection it represents a simple subsystem composed of the two busbars interconnected by the transformer.

2.7 SHUNT ELEMENTS

Shunt reactors and capacitors are used in a power system for reactive power control. The data for these elements are usually given in terms of their rated MVA and rated kV, the equivalent phase admittance in p.u. is calculated from this data.

The admittance matrix for shunt elements is usually diagonal as there is normally no coupling between the components of each phase.

This matrix is then incorporated directly into the system admittance matrix, contributing only to the self admittance of the particular bus. It represents the simplest subsystem, being composed of only one busbar.

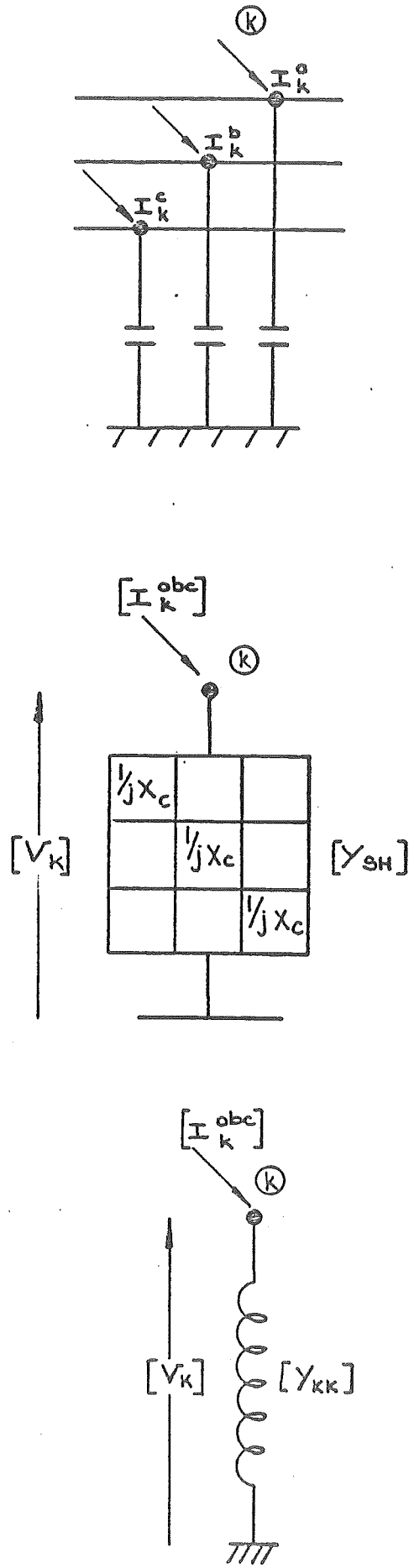

Fig. 2.10 Representation of a Shunt Capacitor Bank

A three phase capacitor bank is illustrated in Fig. 2.10 as an example.

2.8 MUTUALLY COUPLED THREE PHASE ELEMENTS

2.8.1 Mutually Coupled Three Phase Lines

Significant coupling exists between some three phase system elements. Transmission lines will be considered here as they are a common example.

When transmission lines occupy the same right of way for a considerable length, the electrostatic and electromagnetic coupling between those lines must be considered.

In the simplest case of two mutually coupled three phase lines the two coupled lines are considered to form one subsystem composed of four system busbars. The coupled lines are illustrated in Fig. 2.11.

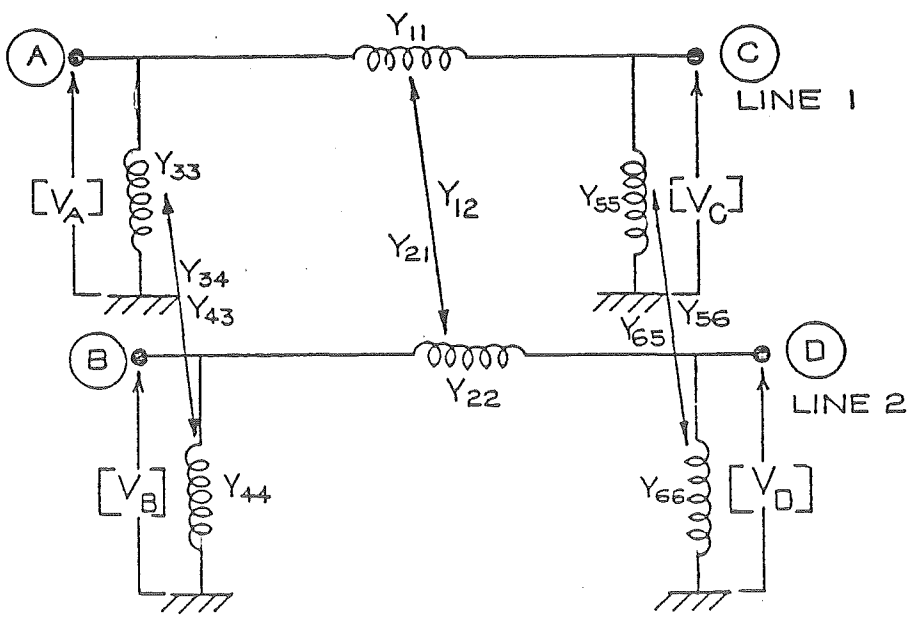

Fig. 2.11 Mutually Coupled Transmission Lines

In Fig. 2.11 each coil is a 3 × 3 compound coil and all voltages and currents are 3 × 1 vectors.

The coupled series elements represent the electromagnetic coupling while the coupled shunt elements represent the capacitive or electrostatic coupling. These coupled parameters are lumped in a similar way to the standard line parameters discussed in section 2.5.

With the admittances labelled as in Fig. 2.11 and applying the rules of linear transformation for compound coils (see Appendix 2) the admittance matrix for the subsystem is defined as follows:

$$\begin{array}{c} \begin{bmatrix} I_A \\ I_B \\ I_C \\ I_D \end{bmatrix} \\ 12 \times 1 \end{array} = \begin{array}{c} \begin{bmatrix} y_{11} + y_{33} & y_{12} + y_{34} & -y_{11} & -y_{12} \\ y_{12}^T + y_{34}^T & y_{22} + y_{24} & -y_{12}^T & -y_{22} \\ -y_{11} & -y_{12} & y_{11} + y_{55} & y_{12} + y_{56} \\ -y_{12}^T & -y_{22} & y_{12}^T + y_{56}^T & y_{22} + y_{66} \end{bmatrix} \\ 12 \times 12 \end{array} \begin{array}{c} \begin{bmatrix} V_A \\ V_B \\ V_C \\ V_D \end{bmatrix} \\ 12 \times 1 \end{array} \tag{2.21}$$

It is assumed here that the mutual coupling is bilateral. Therefore $y_{21} = y_{12}^T$ etc.

The subsystem may be redrawn as Fig. 2.12. The pairs of coupled 3 × 3 compound coils are now represented as a 6 × 6 compound coil. The matrix representation is also shown. Following this representation and the labelling of the admittance blocks in the figure, the admittance matrix may be written in terms of the 6 × 6 compound coils as,

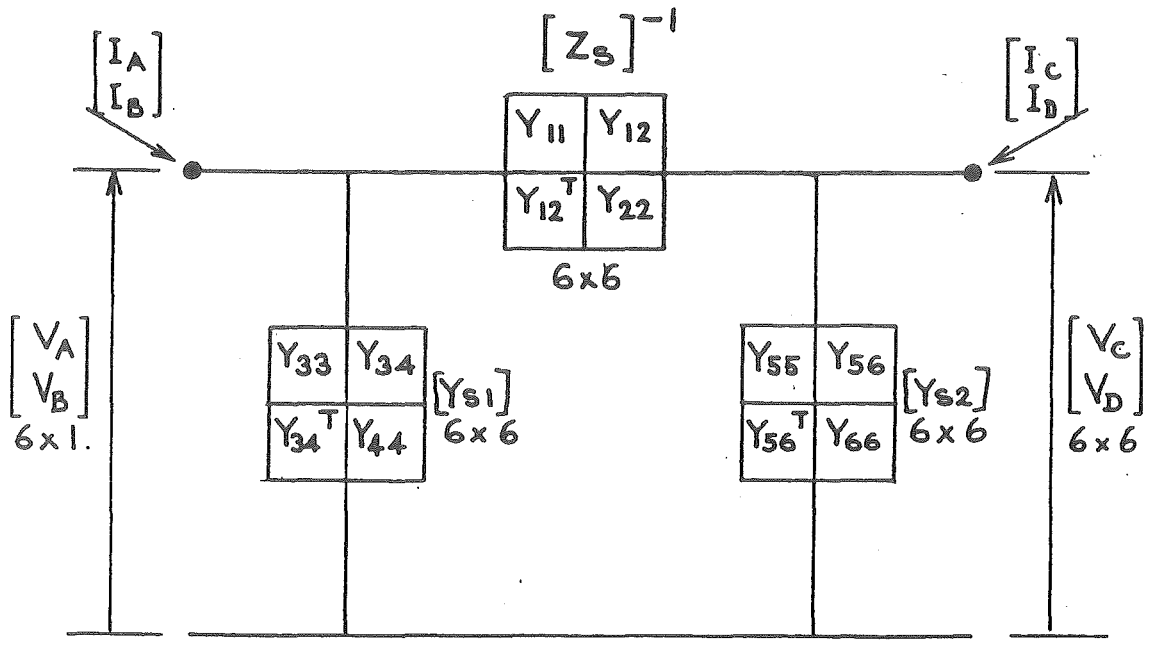

(i) 6 × 6 matrix representation

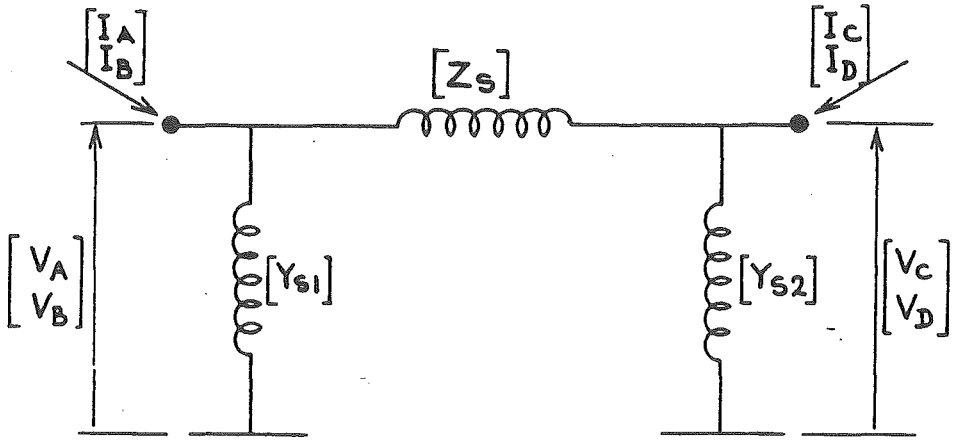

(ii) 6 × 6 compound coil representation

Fig. 2.12 6 × 6 Compound Coil Representation of Two Coupled Three Phase Lines

$$\begin{array}{c} \left[\begin{array}{c} \left[\begin{array}{c} I_A \\ I_B \end{array}\right] \\ \hline \left[\begin{array}{c} I_C \\ I_D \end{array}\right] \end{array}\right] \\ 12 \times 1 \end{array} = \begin{array}{c} \left[\begin{array}{c|c} [Z_s]^{-1} + [Y_{s1}] & -[Z_s]^{-1} \\ \hline -[Z_s]^{-1} & [Z_s]^{-1} + [Y_{s2}] \end{array}\right] \\ 12 \times 12 \end{array} \begin{array}{c} \left[\begin{array}{c} \left[\begin{array}{c} V_A \\ V_B \end{array}\right] \\ \hline \left[\begin{array}{c} V_C \\ V_D \end{array}\right] \end{array}\right] \\ 12 \times 1 \end{array} \qquad (2.22)$$

This is identical to equation 2.21 with the appropriate matrix partitioning.

The representation of Fig. 2.12 is more concise and the formation of equation 2.22 from this representation is straight forward, being exactly similar to that which results from the use of 3 × 3 compound coils for the normal single three phase line as discussed in section 2.5.

The data which must be input to the programme, to enable coupled lines to be treated in a similar manner to single lines, is the series impedance and shunt admittance matrices. These matrices are of order 3 × 3 for a single line, 6 × 6 for two coupled lines, 9 × 9 for three and 12 × 12 for four coupled lines.

Once the matrices $[Z_s]$ and $[Y_s]$ are available, the admittance matrix for the subsystem is formed by application of equation 2.22.

When all the busbars of the coupled lines are distinct, the subsystem may be combined directly into the system admittance matrix. However, if the busbars are not distinct then the admittance matrix as derived from equation 2.22 must be modified. This is considered in the following section.

2.8.2 Consideration of Terminal Connections

The admittance matrix as derived above must be reduced if there are different elements in the subsystem connected to the same busbar. As an example consider two parallel transmission lines illustrated in Fig. 2.13:

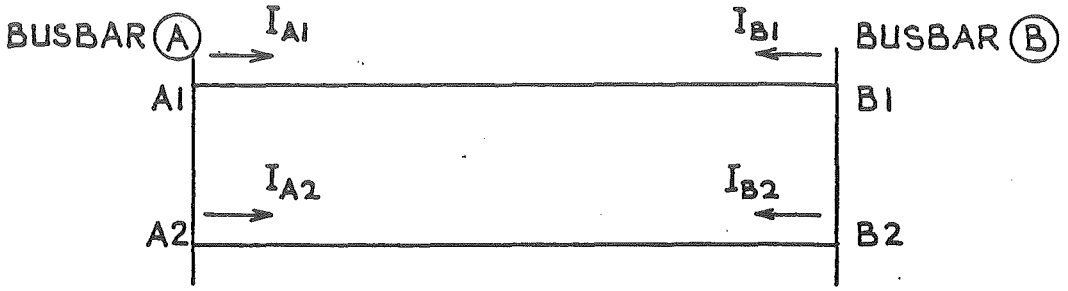

Fig. 2.13 Mutually coupled parallel transmission lines

The admittance matrix derived previously, related the currents and voltages at the four busbars A1, A2, B1 and B2. This relationship is given by:

$$\begin{bmatrix} I_{A1} \\ I_{A2} \\ I_{B1} \\ I_{B2} \end{bmatrix} = \begin{bmatrix} Y_{A1A2B1B2} \end{bmatrix} \begin{bmatrix} V_{A1} \\ V_{A2} \\ V_{B1} \\ V_{B2} \end{bmatrix} \qquad (2.23)$$

The nodal injected current at busbar A, (I_A), is given by

$$I_A = I_{A1} + I_{A2}$$

similarly

$$I_B = I_{B1} + I_{B2}$$

Also from inspection of Fig. 2.13

$$V_A = V_{A1} = V_{A2}$$

$$V_B = V_{B1} = V_{B1}$$

The required matrix equation relates the nodal injected currents, I_A and I_B, to the voltages at these busbars. This is readily derived from equation 2.23 and the conditions specified above. This is simply a matter of adding appropriate rows and columns and yields,

$$\begin{bmatrix} I_A \\ \hline I_B \end{bmatrix} = \begin{bmatrix} \quad \\ [Y_{AB}] \\ \quad \end{bmatrix} \begin{bmatrix} V_A \\ \hline V_B \end{bmatrix} \qquad (2.24)$$

This matrix $[Y_{AB}]$ is the required nodal admittance matrix for the subsystem.

It should be noted that the matrix in equation 2.23 must be stored in full as it is required in the calculation of the individual line power flows (after the solution of the load flow).

2.9 LINE SECTIONALISATION

A line may be divided into sections to account for features such as the following:

- Transposition of line conductors.
- Change of type of supporting towers.
- Variation of soil permittivity.
- Improvement of line representation. (Series of two or more equivalent π networks.)
- Series capacitors for line compensation.

- Lumping of series elements not central to a particular study.

An example of a line divided into a number of sections is shown in Fig. 2.14.

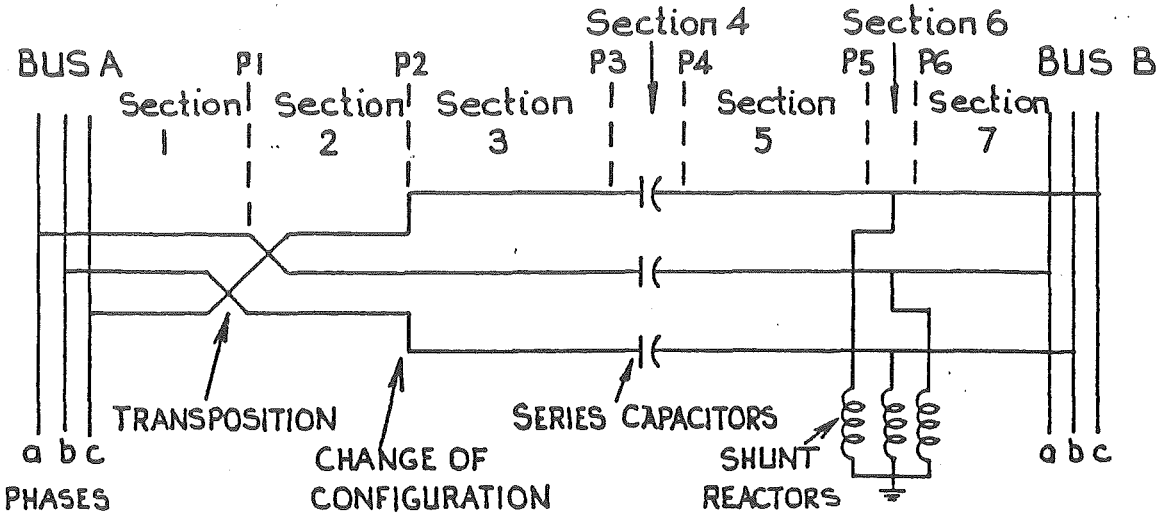

Fig. 2.14 Transmission line sectionalisation

The network of Fig. 2.14 is considered to form a single subsystem. The resultant admittance matrix between bus A and bus B may be derived by finding, for each section, the ABCD or transmission parameters, then combining these by matrix multiplication to give the resultant transmission parameters. These are then converted to the required admittance parameters.

This procedure involves an extension of the usual two port network theory to multi-two-port networks. Currents and voltages are now matrix quantities and are defined in Fig. 2.15. The ABCD matrix parameters for the common sections are given in Table 2.2

The dimensions of the parameter matrices correspond to those of the section being considered, i.e. 3, 6, 9 or 12 for 1, 2, 3 or 4 mutually coupled three phase elements respectively. All sections

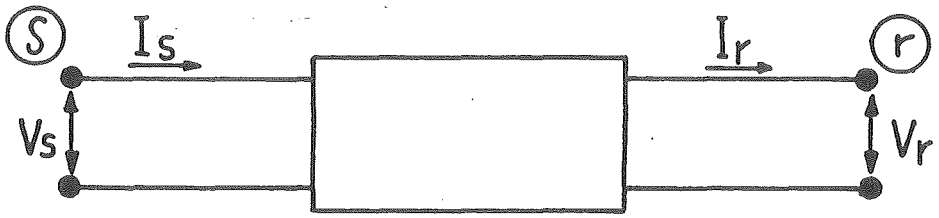

(i) Normal two port network

$$\begin{bmatrix} V_s \\ I_s \end{bmatrix} = \begin{bmatrix} A & B \\ C & D \end{bmatrix} \begin{bmatrix} V_r \\ I_r \end{bmatrix}$$

(ii) Transmission parameters

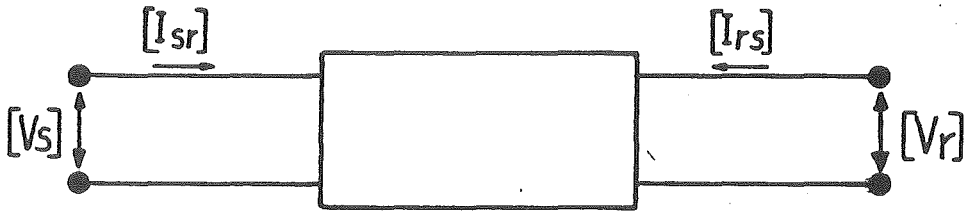

(iii) Multi-two port network

$$\begin{bmatrix} [V_s] \\ [I_{sr}] \end{bmatrix} = \begin{bmatrix} [A] & [B] \\ [C] & [D] \end{bmatrix} \begin{bmatrix} [V_r] \\ [I_{rs}] \end{bmatrix}$$

(iv) Matrix transmission parameters

Fig. 2.15 Two Port Network Transmission Parameters

must contain the same number of mutually coupled three phase elements, ensuring that all the parameter matrices are of the same order and that the matrix multiplications are executable. To illustrate this feature, consider the example of Fig. 2.16. This example shows the need to consider uncoupled elements as coupled ones with zero coupling to ensure correct dimensions for all matrices.

TABLE 2.2

ABCD PARAMETER MATRICES FOR THE COMMON SECTION TYPES

Transmission Line	$[u] + [Z][Y]/2$	$-[Z]$
	$[Y]\{[u] + [Z][Y]/4\}$	$-\{[u]+[Y][Z]/2\}$
Transformer	$-[Y_{SP}]^{-1}[Y_{SS}]$	$[Y_{SP}]^{-1}$
	$[Y_{PS}]-[Y_{PP}][Y_{SP}]^{-1}[Y_{SS}]$	$[Y_{PP}][Y_{SP}]^{-1}$
Shunt Element	$[u]$	$[0]$
	$[Y_{SH}]$	$-[u]$
Series Element	$[u]$	$-[Y_{SE}]^{-1}$
	$[0]$	$-[u]$

In the table [u] is the unit matrix, [0] is a matrix of zeros, and all other matrices have been defined in their respective sections.

It should be noted that all the above matrices have dimensions corresponding to the number of coupled three phase elements in the section.

Fig. 2.16 Sample system to illustrate line sectionalisation

Features of interest:

(a) As a matter of programming convenience an ideal transformer is created and included in section 1.
(b) The dotted coupling represents coupling which is zero. It is included to ensure correct dimensionality of all matrices.
(c) In the p.u. system the mutual coupling between the 220 kV and 66 kV lines is expressed to a voltage base given by [7] the geometric mean of the base line-neutral voltages of the two parallel circuits.

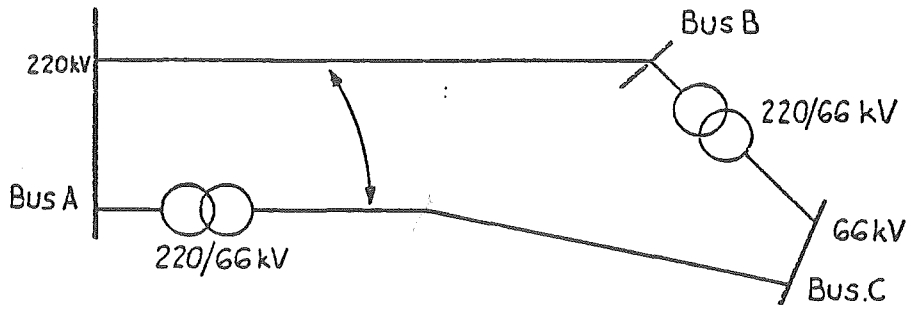

(i) System Single Line Diagram

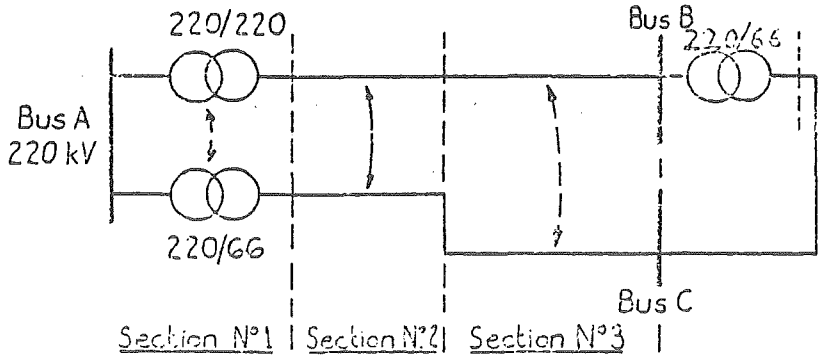

(ii) System redrawn to illustrate line sectionalisation.

Once the resultant ABCD parameters have been found the equivalent nodal admittance matrix for the subsystem can be calculated from equation 2.25.

$$[Y] = \begin{array}{|c|c|} \hline [D]\ [B]^{-1} & [C] - [D]\ [B]^{-1}\ [A] \\ \hline [B]^{-1} & -[B]^{-1}\ [A] \\ \hline \end{array} \qquad (2.25)$$

2.10 FORMING THE SYSTEM ADMITTANCE MATRIX

It has been shown that the element (and subsystem) admittance matrices can be derived and manipulated efficiently if the three nodes at a busbar are associated together. This association proves equally helpful when forming the admittance matrix for the total system.

The subsystem, as defined in section 2.3, may have common busbars with other subsystems, but may not have mutual coupling terms to the branches of other subsystems. Therefore the subsystem admittance matrices can be combined to form the overall system admittance matrix as follows:

(a) The self admittance of any busbar is the sum of all the individual self-admittance matrices at that busbar.

(b) The mutual admittance between any two busbars is the sum of the individual mutual admittance matrices from all the subsystems containing those two nodes.

2.11 CONCLUSION TO CHAPTER 2

This chapter has described the nature of three phase system modelling in phase co-ordinates with emphasis on the essential features which must be present in the input routine for any three phase load flow analysis.

In contrast to single phase load flow investigations the complexity of three phase system modelling requires the load flow programmer to devote a comparable effort on the formulation of the system model as on the solution routine itself.

Methods have been presented to enable the various system elements to be modelled in as much detail as the purpose of the study demands.

CHAPTER 3

BASIC NEWTON-RAPHSON SOLUTION METHOD

3.1 PROBLEM FORMULATION

The Newton-Raphson method is a general mathematical technique which enables the solution of a set of simultaneous algebraic equations.

To apply the technique it is necessary to formulate n independent algebraic equations, $\bar{F}$, in terms of the n variables, $\bar{x}$, which describe the system. The solution of the problem is the vector $\bar{x}$ for which the constraint equations $\bar{F}$ are all satisfied.

For any physical system the minimum number of variables required to define the state of the system is the number of independent variables. For a.c. load flow problems this minimum set is invariably used. However, for combined a.c. and d.c. load flows it is often more convenient to use an enlarged set of variables.

Once the equations have been formulated as,

$$\bar{F}(\bar{x}) = 0 \tag{3.1}$$

the Newton-Raphson process may be applied.

3.2 NEWTON-RAPHSON SOLUTION METHOD

The Newton-Raphson method is an iterative procedure which enables the vector $(\bar{x})$, which satisfies equation 3.1, to be found. The method is presented here with reference to a single equation and single variable. The problem is to find x such that,

$$f(x) = 0 \tag{3.2}$$

Let x^p be an approximation to the solution, with an error Δx^p from the solution, at any iteration p[17]. Then,

$$f(x^p + \Delta x^p) = 0 \tag{3.3}$$

Expanding (3.3) by Taylor's Theorem[18] yields,

$$f(x^p + \Delta x^p) = 0$$
$$= f(x^p) + \frac{(\Delta x^p)^1}{1!} f(\dot{x}^p) + \frac{(\Delta x^p)^2}{2!} f(\ddot{x}^p) + \ldots \tag{3.4}$$

If the estimate x^p is near the solution value, Δx^p will be small and all terms where Δx^p is raised to a power greater than 1 may be neglected[19]. Hence,

$$f(x^p) + \Delta x^p \cdot f(\dot{x}^p) = 0 \tag{3.5}$$

or

$$\Delta x^p = - \frac{f(x^p)}{f(\dot{x}^p)} \tag{3.6}$$

A new value for the variable is then obtained from

$$x^{p+1} = x^p + \Delta x^p \tag{3.7}$$

Equation (3.7) may be written as

3.6 ?

$$f(x^p) = -J \Delta x^p \tag{3.8}$$

The method is readily extended to a set of N equations in N unknowns. J becomes the square jacobian matrix of first order partial differentials of the functions $\bar{F}(\bar{x})$. Elements of [J] are defined by,

$$J_{km} = \frac{\partial F_k}{\partial x_m} \tag{3.9}$$

The jacobian represents the slopes of the tangent hyperplanes which approximate the function $\bar{F}(\bar{x})$ at each iteration point[20]. In the multivariable case the method involves the selection of estimates for all variables ($\bar{x}^p$) and then evaluation of,

$$\bar{F}[\bar{x}^p]$$

followed by solution of,

$$[\Delta\bar{x}^p] = - [J]^{-1} \bar{F}[\bar{x}^p]$$

for $\Delta\bar{x}^p$. A new and hopefully better estimate of the solution vector is then obtained from,

$$[\bar{x}^{p+1}] = [\bar{x}^p] + [\Delta\bar{x}^p]$$

The process continues until the equations $\bar{F}$ can be considered to be solved.

A large number of derivations from the basic method have been applied to the particular problem of load flow analysis and many of these methods have proved more successful than the general technique described here. However, these methods use the same problem formulation as the standard Newton-Raphson method and are, in general, derived from the equations presented above.

3.3 CONVERGENCE PROPERTIES

The Newton-Raphson algorithm will converge if; the functions have continuous first derivatives in the neighbourhood of the solution[21], the Jacobian matrix is non-singular, and the initial

approximations of $\bar{x}$ are close to the actual solutions. However the method is sensitive to the behaviours of the functions $\bar{F}[\bar{x}]$ and hence to their formulation[20]. The more linear they are, the more rapidly and reliably Newton's method converges. Non-smoothness, i.e. humps, in any one of the functions in the region of interest, can cause convergence delays, total failure or misdirection to a non-useful solution.

CHAPTER 4

THREE PHASE FAST DECOUPLED LOAD FLOW FOR A.C. SYSTEMS.

4.1 INTRODUCTION

With the increasing use of long untransposed high voltage transmission lines there has been a corresponding increased interest in the analysis of power system unbalance. Early techniques[22-25] for analysing the unbalance were restricted to the case of isolated unbalanced lines operating from known terminal conditions. In order to investigate the unbalanced operation of an interconnected system, including the influence of any significant load unbalance, it is necessary to perform a three phase load flow analysis[8,26,27,28].

The storage and computational requirements of a three phase load flow analysis are greater than those of the corresponding single phase case. The need for efficient algorithms is therefore significant even though, in contrast to single phase analysis, the three phase load flow is likely to remain a planning, and not an operational, exercise.

Of the numerous load flow techniques which have been proposed[20], the general Newton-Raphson algorithm[29], combined with efficient programming techniques has proved the most successful.

This method has been improved by the application of 'decoupling' techniques[30,31,32]. The fast decoupled Newton-Raphson algorithm[30] is now widely accepted as the best general load flow method available and is currently being applied to many associated power system problems[33].

A review of the single phase load flow problem and the application of the Newton-Raphson technique to its solution, is presented in Appendix 4. Also in the Appendix, the single phase fast decoupled algorithm, as developed by Stott[30], is derived from the Newton-Raphson formulation. This derivation forms the basis upon which the three phase fast decoupled algorithm is developed.

The formulation of the three phase load flow problem is significantly different to the single phase case. Three phase line and transformer models are more complex than the single phase ones. Moreover, the three phase load flow includes detailed representation of the generators as they have considerable influence on the system unbalance. The inclusion of the generators creates a need to depart from the usual load flow specification of busbar types. It is therefore necessary to examine the formulation of the load flow problem in some detail.

A basic belief which influenced the derivation of the three phase load flow algorithm was that as single phase and three phase load flows are solving the same physical system, the three phase representation simply being more detailed, then the behaviour of the algorithms adopted for a solution of the system equations should be basically similar in both cases. This has been reinforced by the results obtained.

This chapter describes the formulation of the three phase load flow problem and the derivation of a fast decoupled algorithm for its solution. The convergence properties are investigated and compared with those of the single phase algorithm. A concise summary of this chapter is contained in a paper[3] published in the I.E.E. and reproduced in Appendix 5.

4.2 NOTATION

To enable three phase vector and matrix elements to be clearly and unambiguously identified a system of superscripts and subscripts is required. Three phase system notation is complex and clearly defined bus numbering and scripting is essential for the mathematical statement of the load flow problem and for the subsequent development of a solution technique.

The a.c. system is considered to have a total of n busbars where;

$$n = nb + ng$$

and nb is the number of actual system busbars

ng is the number of synchronous machines.

Subscripts i,j etc refer to system busbars as shown in the following examples:

$i = 1, nb$ identifies all actual system busbars. ie. all load busbars and all generator terminal busbars.

$i = nb + 1, nb + ng - 1$ identifies all generator internal busbars with the exception of the slack machine.

$i = nb + ng$ identifies the internal busbar at the slack machine.

In addition the following subscripts are used as an aid to clarity;

reg - refers to a voltage regulator

int - refers to an internal busbar at a generator

gen - refers to a generator.

Superscripts p,m identify the three phases at a particular busbar.

4.3 FORMULATION OF THE THREE PHASE LOAD FLOW PROBLEM

The object of the three phase load flow is to find the state of the three phase power system under the specified conditions of load, generation and system configuration.

The set of variables required to define the operation of the three phase system is similar to that which is required for the usual single phase load flow with the exception of the variables associated with the description of the generator busbars. A polar co-ordinate representation is used throughout this development.

The generator model, as discussed in section 2.4, includes a balanced set of internal (excitation) voltages acting behind the synchronous impedances. The voltage regulator controls the magnitude of the internal voltages according to some function of the three terminal voltages. In addition, the total real power output from each generator will be specified although the distribution amongst the three phases will not be known.

The following variables form a minimum and sufficient set to define the operating state of the three phase system under steady state operation:

- The slack generator internal busbar voltage magnitude $V_{int\,j}$ where $j = nb + ng$. (The angle $\theta_{int\,j}$ is taken as a reference.)
- The internal busbar voltage magnitudes $V_{int\,j}$ and angles $\theta_{int\,j}$ at all other generators. ie $j = nb + 1,\ nb + ng - 1$
- The three voltage magnitudes (V_i^p) and angles (θ_i^p) at every

load busbar in the system ie. i = 1,nb and p = 1,3.

Only two variables are associated with each generator internal busbar as all three phase voltages are balanced and symmetrical. There is no justification for retaining the redundant voltages and angles as variables for the solution of the load flow. However, for ease of programming these are retained as variables for the calculation of the real and reactive power mismatches.

A knowledge of all the variables listed above completely defines the steady state operation of the three phase system. In order to solve for these state variables using a Newton-Raphson based technique it is necessary to formulate a similar number of independent equations. These equations are derived from the specified operating conditions, ie. from apriori knowledge about the system operation.

The specified three phase system conditions may be summarised as:

(i) The individual phase real and reactive power loading at every system busbar.

(ii) The voltage regulator specification for every synchronous machine.

(iii) The total real power generation of each synchronous machine, with the exception of the slack machine.

The usual load flow specification of a slack machine is applicable to the three phase load flow.

4.3.1 Derivation of Equations

The three phase system behaviour is described by,

$$[I] - [Y][V] = 0 \tag{4.1}$$

where the system admittance matrix [Y], as developed in chapter 2, represents each phase independently and models all inductive and capacitive mutual couplings between phases and between circuits. The mathematical statement of the specified conditions is derived in terms of the system admittance matrix

$$[Y] = [G] + j[B]$$

as follows;

(i) For each of the three phases (p) at every load and generator terminal busbar (i),

$$\Delta P_i = (P_i^p)^{sp} - P_i^p$$

$$= (P_i^p)^{sp} - V_i^p \sum_{k=1}^{n} \sum_{m=1}^{3} V_k^m \left[G_{ik}^{pm} \cos \theta_{ik}^{pm} + B_{ik}^{pm} \sin \theta_{ik}^{pm}\right] \tag{4.2}$$

and

$$\Delta Q_i^p = (Q_i^p)^{sp} - Q_i^p$$

$$= (Q_i^p)^{sp} - V_i^p \sum_{k=1}^{n} \sum_{m=1}^{3} V_k^m \left[G_{ik}^{pm} \sin \theta_{ik}^{pm} - B_{ik}^{pm} \cos \theta_{ik}^{pm}\right] \tag{4.3}$$

where, when k refers to a generator internal busbar,

$$V_k^1 = V_k^2 = V_k^3 = V_{int\,k}$$

and

$$\theta_k^{\,1} = \theta_k^{\,2} - \frac{2\pi}{3} = \theta_k^{\,3} + \frac{2\pi}{3} = \theta_{int\,k}$$

(ii) For every generator j,

$$(\Delta V_{reg})_j = f(V_k^{\,1}, V_k^{\,2}, V_k^{\,3}) \qquad (4.4)$$

where k is the bus number of the j^{th} generator's terminal busbar.

(iii) For every generator j, with the exception of the slack machine, ie. $j \neq nb + ng$

$$(\Delta P_{gen})_j = (P_{gen}^{\,sp})_j - (P_{gen})_j$$

$$= (P_{gen}^{\,sp})_j - \sum_{p=1}^{3} (V_{int})_j \sum_{k=1}^{n} \sum_{m=1}^{j} V_k^{\,m} [G_{jk}^{\,pm} \cos \theta_{jk}^{\,pm} + B_{jk}^{\,pm} \sin \theta_{jk}^{\,pm}] \qquad (4.5)$$

where, although the summation for k is over all system busbars, the mutual terms G_{jk} and B_{jk} are non zero only when k is the terminal busbar of the j^{th} generator.

It should be noted that the real power which is specified for the generator is taken as the total real power which is leaving the generator internal or excitation busbar. In actual practice the specified quantity is the power leaving the terminal busbar. In effect, the real power losses are ignored.

The real power losses in the generators or synchronous

compensators are small and they have an insignificant influence on the system operation. If the losses are of particular interest they may be calculated from the sequence impedances after the solution of the unbalanced load flow when all generator sequence currents are known.

The reason for writing the mismatch at the internal busbar is primarily one of conceptual simplicity and programming convenience. Any other method requires the real power mismatch to be written at busbars remote from the variable in question, that is, the angle at the internal busbar. In addition, inspection of equations (4.2) and (4.5) will show that the equations are identical except for the summation over the three phases at the generator internal busbar.

That is, the generator power mismatches may be calculated in exactly the same way and by the same subroutines as are used for the power mismatches at other system busbars. This is possible as the generator is the only element connected to each internal busbar. Inspection of the jacobian submatrices derived later will show that this feature is retained throughout the study. In terms of programming, the generators present no additional complexity. Equations (4.2) to (4.5) form the mathematical formulation of the three phase load flow as a set of independent algebraic equations in terms of the system variables.

The solution to the load flow problem is the set of variables which, upon substitution, make the left hand side mismatches in equations (4.2) to (4.5) equal to zero.

4.4. FAST DECOUPLED THREE PHASE LOAD FLOW ALGORITHM

The standard Newton-Raphson algorithm (chapter 3) may be applied to enable solution of equations (4.2) to (4.5). This involves successive solutions of;

$$\begin{bmatrix} \Delta P \\ \Delta P_{gen} \\ \Delta Q \\ \Delta V_{reg} \end{bmatrix} = \begin{bmatrix} A & E & I & M \\ B & F & J & N \\ C & G & K & P \\ D & H & L & R \end{bmatrix} \begin{bmatrix} \Delta\theta \\ \Delta\theta_{int} \\ \Delta V/V \\ \Delta V_{int}/V_{int} \end{bmatrix} \qquad (4.6)$$

for the right hand side vector of variable updates. The right hand side matrix is the usual jacobian matrix of first order partial derivatives.

Following decoupled single phase load flow practice (Appendix 4) the effects of $\Delta\theta$ on reactive power flows and ΔV on real power flows are ignored. Equation (4.6) may therefore be simplified by assigning,

$$[I] = [M] = [J] = [N] = 0$$

and

$$[C] = [G] = 0$$

In addition, the voltage regulator specification is assumed to be in terms of the terminal voltage magnitudes only and therefore,

$$[D] = [H] = 0$$

Equation (4.6) may be written in the decoupled form as;

$$\begin{bmatrix} \Delta P_i^p \\ \Delta P_{gen\ j} \end{bmatrix} \begin{bmatrix} A & E \\ B & F \end{bmatrix} \begin{bmatrix} \Delta\theta_k^m \\ \Delta\theta_{int\ \ell} \end{bmatrix} \qquad (4.7)$$

for i,k = 1,nb and j,ℓ = 1, ng - 1 (ie. excluding the slack generator), and

$$\begin{bmatrix} \Delta Q_i^p \\ \Delta V_{reg\ j} \end{bmatrix} = \begin{bmatrix} K & P \\ L & R \end{bmatrix} \begin{bmatrix} \Delta V_k^m \\ \Delta V_{int\ \ell} / V_{int\ \ell} \end{bmatrix} \qquad (4.8)$$

for i,k = 1,nb and j,ℓ = 1, ng (ie. including the slack generator).

4.4.1 Jacobian Submatrices

To enable further development of the algorithm it is necessary to consider the jacobian submatrices in more detail.

In deriving these jacobians from equations (4.2) to (4.5) it must be remembered that,

$$V_\ell^{\,1} = V_\ell^{\,2} = V_\ell^{\,3} = V_{int\ \ell}$$

$$\theta_\ell^{\,1} = \theta_\ell^{\,2} - \frac{2\pi}{3} = \theta_\ell^{\,3} + \frac{2\pi}{3} = \theta_{int\ \ell}$$

when ℓ refers to a generator internal busbar. The coefficients of matrix equation (4.7) are;

$$-[A_{ik}^{pm}] = [\partial\ \Delta P_i^{\,p} / \partial\ \theta_k^m]$$

where

$$A_{ik}^{pm} = V_i^p\ V_k^m\ [G_{ik}^{pm} \sin\theta_{ik}^{pm} - B_{ik}^{pm} \cos\theta_{ik}^{pm}]$$

except

$$A_{kk}^{mm} = -B_{kk}^{mm}\ (V_k^m)^2 - Q_k^m$$

$$-[B_{jk}^m] = [\partial\ \Delta P_{gen\ j} / \partial\ \theta_k^m]$$

$$= \sum_{p=1}^{3} V_{int\ j}\ V_k^m\ [G_{jk}^{pm} \sin\theta_{jk}^{pm} - B_{jk}^{pm} \cos\theta_{jk}^{pm}]$$

$$- [E^{p}_{i\ell}] = [\partial P_i{}^{p} / \partial \theta_{int\,\ell}]$$

$$= \sum_{m=1}^{3} V_{int\,\ell} V_i{}^{p} [G^{pm}_{i\ell} \sin \theta^{pm}_{i\ell} - B^{pm}_{i\ell} \cos \theta^{pm}_{i\ell}]$$

$$- [F_{j\ell}] = [\partial P_{gen\,j} / \partial \theta_{int\,\ell}]$$

where $[F_{j\ell}] = 0$ for all $j \neq \ell$ because the j^{th} generator has no connection with the ℓ^{th} generator's internal busbar.

and
$$[F_{\ell\ell}] = \sum_{p=1}^{3} \left(- B^{pp}_{\ell\ell} \left(V_{int\,\ell} \right)^2 - Q^{p}_{\ell} \right)$$

$$+ \sum_{\substack{m=1 \\ m \neq p}}^{3} \sum_{p=1}^{3} (V_{int\,\ell})^2 [G^{pm}_{\ell\ell} \sin \theta^{pm}_{\ell\ell} - B^{pm}_{\ell\ell} \cos \theta^{pm}_{\ell\ell}]$$

The coefficients of matrix equation (4.8) are;

$$- [K^{pm}_{ik}] = V^{m}_{k} [\partial \Delta Q_i{}^{p} / \partial V^{m}_{k}]$$

where

$$K^{pm}_{ik} = V^{m}_{k} V^{p}_{i} [G^{pm}_{ik} \sin \theta^{pm}_{ik} - B^{pm}_{ik} \cos \theta^{pm}_{ik}]$$

except

$$K^{mm}_{kk} = - B^{mm}_{kk} (V^{m}_{k})^2 + Q^{m}_{k}$$

$$- [L^{m}_{jk}] = V^{m}_{k} [\partial \Delta V_{reg\,j} / \partial V^{m}_{k}]$$

let

$$[L^{m}_{jk}] = V^{m}_{k} [L^{m}_{jk}]'$$

where k is the terminal busbar of the j^{th} generator

$$L^{m}_{jk} = 0 \quad \text{otherwise.}$$

$$- [P^{p}_{\ell\ell}] = V_{int\,\ell} [\partial \Delta Q^{p}_{i} / V_{int\,\ell}]$$

$$= V_{int\,\ell} \sum_{m=1}^{3} V_i^p \left[G_{i\ell}^{pm} \sin \theta_{i\ell}^{pm} - B_{i\ell}^{pm} \cos \theta_{i\ell}^{pm}\right]$$

$$-[R_{j\ell}] = [\partial \Delta V_{reg\,j} / \partial V_{int\,\ell}]$$

$= 0$ for all j,ℓ as the voltage regulator specification does not explicitly include the variables V_{int}.

Although the above expressions appear complex, their meaning and derivation are similar to the usual single phase jacobian elements.

4.4.2 Jacobian Approximations

Approximations similar to those applied to the single phase load flow are applicable to the jacobian elements as follows;

(i) at all nodes (ie all phases of all busbars)

$$Q_k^m << B_{kk}^{mm} (V_k^m)^2$$

(ii) between connected nodes of the same phase,

$$\cos \theta_{ik}^{mm} \approx 1 \qquad \text{ie} \quad \theta_{ik}^{mm} \text{ is small}$$

and

$$G_{ik}^{mm} \sin \theta_{ik}^{mm} << B_{ik}^{mm}$$

(iii) An additional assumption which is applicable to the three phase system is that the phase angle unbalance at any busbar will be small and hence;

$$\theta_{kk}^{pm} \approx \pm 120^{o} \text{ for } p \neq m$$

(iv) As a consequence of approximation (ii) and (iii) the angle between different phases of connected

busbars will be approximately 120° * ie

$$\theta_{ik}^{pm} \approx \pm 120^{\circ} \quad \text{for } p \neq m$$

or $$\cos \theta_{ik}^{pm} \approx -0.5$$

and $$\sin \theta_{ik}^{pm} \approx \pm 0.866$$

The final approximation (iv), which is necessary if the jacobians are to be approximated to constants, is the least valid of those listed as the cosine and sine values change rapidly with small changes in angle around 120 degrees. This approximation probably accounts for the relatively slow convergence of the unbalance at a busbar compared to the convergence of the average voltage magnitudes and angles at the busbar.

It should be emphasised that these approximations apply to the jacobian elements only, they do not prejudice the accuracy of the solution nor do they restrict the type of problem which may be attempted.

Applying approximations (i) to (iv) to the jacobians and substituting into equations (4.7) and (4.8) yields,

$$\begin{bmatrix} \Delta P_i^p \\ \Delta P_{gen\ j} \end{bmatrix} = \begin{bmatrix} \begin{bmatrix} V_i^p & M_{ik}^{pm} & V_k^m \end{bmatrix} & \begin{bmatrix} \sum_{m=1}^{3} V_i^p & M_{i\ell}^{pm} & V_{int\ \ell} \end{bmatrix} \\ \begin{bmatrix} \sum_{p=1}^{3} V_{int\ j} & M_{jk}^{pm} & V_k^m \end{bmatrix} & \begin{bmatrix} \sum_{m=1}^{3} \sum_{p=1}^{3} V_{int\ j} & M_{j\ell}^{pm} & V_{int\ \ell} \end{bmatrix} \end{bmatrix} \begin{bmatrix} \Delta\theta_k^m \\ \Delta\theta_{int\ \ell} \end{bmatrix}$$

(4.9)

---

* This assumption is modified for the $\pm 30^{\circ}$ phase shift inherent in the star-delta connection of three phase transformers.

and

$$\begin{bmatrix} \Delta Q_i^p \\ \\ \Delta V_{reg\ j} \end{bmatrix} \quad \begin{bmatrix} \left[V_i^p\ M_{ik}^{pm}\ V_k^m\right] & \left[\sum_{m=1}^{3} V_i^p\ M_{i\ell}^{pm}\ V_{int\ \ell}\right] \\ V_k^m\ [L'] & [0] \end{bmatrix} \quad \begin{bmatrix} \Delta V_k^m / V_k^m \\ \\ \Delta V_{int\ \ell} / V_{int\ \ell} \end{bmatrix} \tag{4.10}$$

where $M_{ik}^{pm} = G_{ik}^{pm} \sin \theta_{ik}^{pm} - B_{ik}^{pm} \cos \theta_{ik}^{pm}$

with $\theta_{kk}^{mm} = 0$

$\theta_{ik}^{mm} = 0$

$\theta_{ik}^{pm} = \pm 120^{\circ}$ for $p \neq m$.

All terms in the matrix [M] are constant, being derived solely from the system admittance matrix.

Matrix [M] is the same as matrix [-B] except for the off-diagonal terms which connect nodes of different phases. These are modified by allowing for the nominal 120° angle and also including the $G_{ik}^{pm} \sin \theta_{ik}^{pm}$ terms. The similarity in structure of all jacobian submatrices reduces the programming complexity which is a feature of many three phase load flows. This uniformity has been achieved primarily through the method of implementing the three phase generator constraints.

The above derivation closely parallels the single phase fast decoupled algorithm although this tends to become obscured by the added complexity of the notation. At the present stage the jacobian elements in equations (4.9) and (4.10) are identical except for those terms which involve the additional features of the generator modelling.

Equations (4.9) and (4.10) are then modified as follows:

(i) The left hand side defining functions are redefined as $[\Delta P^p_i/V^i_p]$, $[\Delta P_{gen\ j}/V_{int\ j}]$ and $[\Delta Q^p_i/V^p_i]$.

These functions are more linear in terms of the voltage magnitude [V] than are the functions $[\Delta\bar{P}]$ and $[\Delta\bar{Q}]$. In both the Newton-Raphson and related constant jacobian methods, the reliability and convergence rate is improved with more linearity in the defining functions[34].

(ii) In equation (4.9) the remaining right hand side V terms are set to 1 p.u.

(iii) In equation (4.10), the remaining right hand side V terms are cancelled by the corresponding terms in the right hand side vector.

This yields,

$$\begin{bmatrix} \Delta P^p_i/V^p_i \\ \Delta P_{gen\ j}/V_{int\ j} \end{bmatrix} \quad \begin{bmatrix} M^{pm}_{ik} & \sum_{m=1}^{3} M^{pm}_{i\ell} \\ \sum_{p=1}^{3} M^{pm}_{jk} & \sum_{p=1}^{3}\sum_{m=1}^{3} M^{pm}_{j\ell} \end{bmatrix} \quad \begin{bmatrix} \Delta\theta^p_k \\ \Delta\theta_{int\ \ell} \end{bmatrix}$$

$$[B'] \qquad (4.11)$$

$$\begin{bmatrix} \Delta Q^p_i/V^p_i \\ \Delta V_{reg\ j} \end{bmatrix} \quad \begin{bmatrix} M^{pm}_{ik} & \sum_{m=1}^{3} M^{pm}_{i\ell} \\ [L^m_{jk}]' & 0 \end{bmatrix} \quad \begin{bmatrix} \Delta V^m_k \\ \Delta V_{int\ \ell} \end{bmatrix}$$

$$[B''] \qquad (4.12)$$

Recalling that $[L'^{m}_{jk}] = \partial \Delta V_{reg\,j} / \partial V^{m}_{k}$ it is clear that if V_{reg} is a simple function of the terminal voltages then [L'] will be a constant matrix. For example, the voltage regulator may hold one phase voltage constant (eg phase 1) or it may monitor the phase to phase voltage at the terminal. In the first case the equation is,

$$\Delta V_{reg\,j} = V^{sp}_{gen} - V^{1}_{k} = 0$$

and in the second case

$$V_{reg\,j} = V^{sp}_{gen} - V^{1}_{k} + V^{2}_{k}$$

for the phase to phase voltage between phases 1 and 2. In either case, the partial derivatives with respect to V^{m}_{k} will be constants.

Therefore, both the jacobian matrices [B'] and [B"] in equations (4.11) and (4.12) have been approximated to constants.

Zero diagonal elements in equation (4.12) result from the ordering of the equations and variables. This feature causes no problems if these diagonals are not used as pivots until the rest of the matrix has been factorised (by which time, fill in terms will have occurred on the diagonal). There is a minor loss of efficiency as a result of inhibiting the optimal ordering for the complete matrix. This could be avoided by a reordering of the equations, however, this reordering is programmatically and conceptually difficult and the extra complexity is not justified.

4.4.3 Final Jacobian Approximations

The use of equations (4.11) and (4.12) gave varied results. Although only a small number of systems were tested it was clear that the use of these equations was not satisfactory. Fortunately

the same systems, under the assumption of balanced conditions, had been investigated by Bodger[35] using a fast decoupled load flow both with the standard algorithm[30] and with various single [B] matrix versions. The single [B] matrix version where [B"] is effectively used for both jacobians, gave very similar convergence to the use of (4.11) and (4.12) for the three phase case. This feature is not unexpected as the algorithms are similar except for the inclusion of the generator model. It was therefore decided to modify the jacobians (4.11) and (4.12) based on the reasoning of Stott and Alsac[30], which proved successful in the single phase load flow.

The [B'] matrix is modified by omitting the representation of those elements that predominantly effect MVAR flows. The implementation of this general intention is not as obvious for the three phase system representation. The line shunt capacitance matrices as discussed in chapter 2, represent phase to phase as well as phase to earth capacitance.

The capacitance matrix and the physical significance of the values is shown in Fig. 4.1 for a single three phase line. For capacitively coupled parallel lines the matrix will be $3n \times 3n$, where n is the number of lines involved; the equivalent circuit for the shunt capacitance will be correspondingly altered.

From a consideration of the equivalent circuit it was decided that the phase to earth capacitances solely affect MVAR conditions while the phase to phase values affect MVAR and also MW conditions to some extent. Therefore, the phase to earth capacitances only were removed in the formation of the [B'] matrix.

Convergence was reliable but somewhat slow. The influence of the shunt capacitance matrix on real power flows was therefore

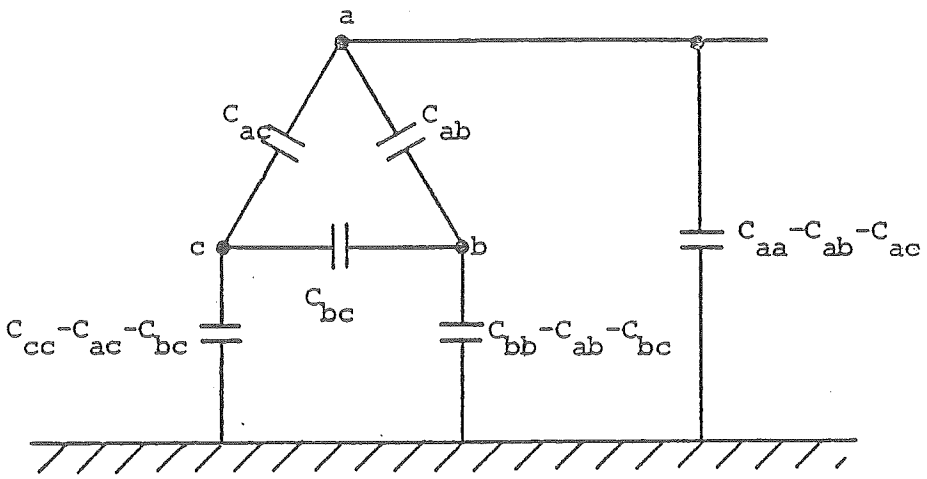

(i) Physical Significance of Shunt Capacitances.

Caa	-Cab	-Cac
-Cba	Cbb	-Cbc
-Cca	-Ccb	Ccc

(ii) Capacitance Matrix

Fig. 4.1 Shunt capacitance matrices

re-examined. The single phase modelling was used as an aid to this re-examination.

In single phase load flows the shunt capacitance is the positive sequence capacitance which is determined from both the phase to phase and the phase to earth capacitances of the line. It therefore appears that the entire shunt capacitance matrix predominantly affects MVAR flows only. Thus, following single phase fast decoupling practice, it was decided to omit the representation of the entire shunt capacitance matrix in the formulation of [B']. The rate of real power convergence increased and, as a result, the number of iterations to convergence was approximately halved.

With capacitively coupled three phase lines the implementation of this procedure requires further clarification as the interline capacitance influences the positive sequence shunt capacitance. However, the values of interline capacitances are small in comparison with the self capacitance of the phases and investigations have shown that it does not make any noticeable difference whether these values are included or not.

Off-nominal transformer taps are straightforward except it should be noted that the effective tap of $\sqrt{3}$ introduced by the star-delta transformer connection is interpreted as a nominal tap and is therefore included when forming the [B'] matrix.

A further difficulty arises from the modelling of the star-g/delta transformer connection. The equivalent circuit, illustrated in Appendix 3, shows that large shunt admittances are effectively introduced into the system. Initially these were excluded from [B'] as for a normal shunt element; divergence resulted in all cases attempted. When they are included in [B'] excellent

convergence results. The most appropriate explanation is that, viewing the transformer as an element, then, on nominal turns ratio, it does not affect MVAR conditions any more than MW conditions. The entire transformer model, must, therefore be included in both [B'] and [B"].

With the modifications described above the two final algorithmic equations may be concisely written,

$$\begin{bmatrix} \Delta P/V \\ \Delta P_{gen}/V_{int} \end{bmatrix} = \begin{bmatrix} B'_M \end{bmatrix} \begin{bmatrix} \Delta\theta \\ \Delta\theta_{int} \end{bmatrix} \tag{4.13}$$

$$\begin{bmatrix} \Delta Q/V \\ \Delta V_{reg} \end{bmatrix} = \begin{bmatrix} B''_M \end{bmatrix} \begin{bmatrix} \Delta V \\ \Delta V_{int} \end{bmatrix} \tag{4.14}$$

The constant approximated Jacobians $[B'_M]$ and $[B''_M]$ correspond to fixed approximated tangent slopes to the multidimensional surfaces defined by the left hand side defining functions.

The equations (4.13) and (4.14) are then solved according to the iteration sequence illustrated in Fig. 4.2. The solutions of equations (4.13) and (4.14) are carried out using sparsity techniques and near optimal ordering, as embodied in Zollenkopf's bifactorisation technique[36,37]. The sparsity storage is structured in 3 × 3 matrix blocks, which are assumed to be full, to take full advantage of the inherent block structure of the three phase system matrices.

The jacobian matrices in equation (4.13) and (4.14) are readily assembled from the system admittance matrix. Once assembled,

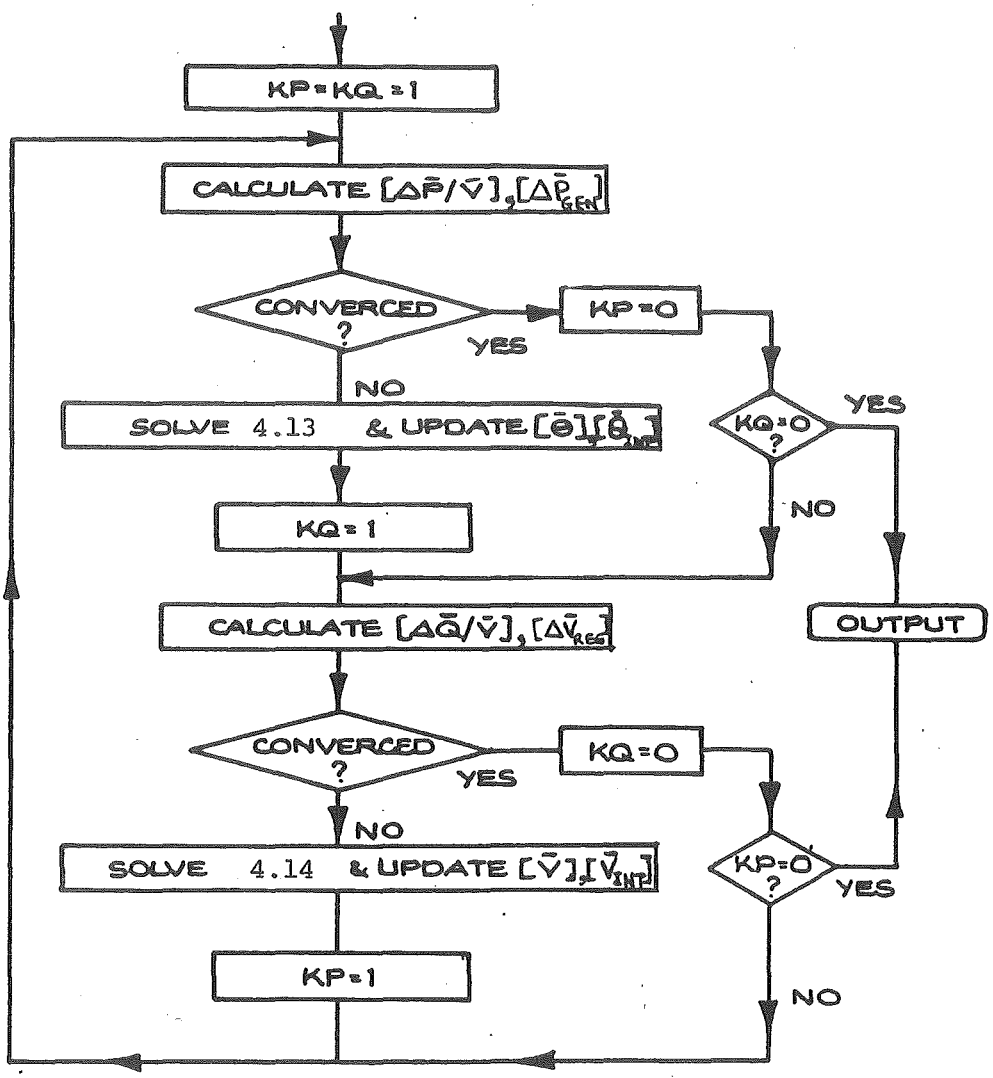

Fig. 4.2 Iteration sequence for three phase a.c. load flow

they are factorised before the iteration sequence is initiated. The solution of each equation within the iterative procedure is relatively fast, consisting only of the forward reduction and back substitution processes.

The three phase fast decoupled algorithm enjoys all the computational advantages of the single phase version when compared to alternative load flow algorithms.

4.4.4 Generator Models and the Fast Decoupled Algorithm

The derivation of the fast decoupled algorithm involves the use of several assumptions to enable the jacobian matrices to be approximated to constants. The same assumptions have been applied to the excitation busbars associated with the generator model as are applied to the usual system busbars. The validity of the assumptions regarding voltage magnitudes and the angles between connected busbars depends upon the machine loading and positive sequence reactance. As discussed in section 2.4 this reactance may be set to any value without altering the load flow solution and a value may therefore be selected to give the best algorithmic performance.

When the actual value of positive sequence reactance is used the angle across the generator and the magnitude of the excitation voltage both become comparitively large under full load operation. Angles in excess of forty five degrees and excitation voltages greater than 2.0 p.u. are not uncommon. Despite this considerable divergence from assumed conditions, convergence is surprisingly good. The only convergence difficulties have occured at the slack generator and then only when it is modelled with a high synchronous reactance (1.5 p.u. on machine rating) and with greater than 70%

full load power. Under these conditions the convergence becomes slow and, on increased loading, divergence may occur. All other system generators, under the same conditions, converge reliably but somewhat slowly.

This deterioration in convergence rate may be avoided by the simple practice of setting the generator positive sequence reactance to a low value. The value is not critical and an arbitrary value of 0.01 p.u. has been found satisfactory in all cases.

4.4.5 Starting values

Starting values are assigned as the three phase parallel of flat voltage and angle values as follows:

- All non-voltage controlled busbars are assigned 1 p.u. on all phases.
- At generator terminal busbars all voltages are assigned values according to the voltage regulator specification.
- All system busbar angles are assigned, 0, -120, +120 degrees for the three phases respectively.
- The generator internal voltages and angles are calculated from the specified real power and by assuming zero reactive power. For the slack machine the real power is estimated as the difference between total load and total generation plus 8% of the total load to allow for losses.

For cases where convergence is excessively slow or difficult it is possible to use the results of a single phase load flow to establish starting values. The values will, under normal steady state unbalance, provide excellent estimates for all voltages and angles including generator internal conditions which are calculated

from the single phase real and reactive power generations.

Moreover, as a three phase iteration is more costly than a single phase iteration, the overall cost of all studies will often be reduced by the use of single phase starting values. In practice therefore it is recommended that a single phase load flow is used for starting values for all cases. Although not necessary this will often provide more efficient overall convergence and it will also enable the more obvious data errors to be detected at an early stage.

For the purpose of investigating the load flow performance flat voltage and angle values will be used throughout.

4.5 PERFORMANCE OF THE ALGORITHM

4.5.1 Introduction

Exhaustive testing of the three phase load flow algorithm with a large number of practical systems is difficult owing to the unavailability of reliable data. Instead, this section attempts to identify and study those features which influence the convergence with particular reference to several small to medium sized test systems. General conclusions are then inferred from these results. Considerable justification for this course of action is provided by the fact that, under balanced conditions, the performance of the three phase fast decoupled load flow is virtually identical to that of the standard single phase fast decoupled load flow.

The performance of the three phase algorithm, under both balanced and unbalanced conditions, is examined in the following sections. Where applicable, comparisons are made with the performance of the single phase fast decoupled algorithm.

4.5.2 Performance under Balanced Conditions

A symmetrical three phase system, operating with balanced loading, is accurately modelled by the positive sequence system and either a three phase or a single phase load flow may be used.

Under these conditions it is possible to compare the three phase and single phase fast decoupled algorithms.

For the three phase system all transmission lines are represented by balanced full 3 × 3 matrices. All transformers are modelled with balanced parameters on all phases and all generators are modelled by their phase parameter matrices as derived from their sequence impedances.

The number of iterations to convergence for both the single phase and three phase algorithms are given in table 4.1. The algorithms behave identically. Features such as the transformer connection and the negative and zero sequence generator impedances have no effect on the convergence rate of the three phase system under balanced conditions. This is not unexpected as, under these conditions, only the positive sequence network has any power flow and there is no coupling between sequence networks for the balanced system. The negative and zero sequence information inherent in the three phase model of the balanced system, has no influence on system operation and this is reflected into the performance of the algorithm.

4.5.3 Performance With Unbalanced Systems

The number of iterations to converge several three phase systems, under realistic steady state unbalanced operation, are given in Table 4.1. The convergence rate deteriorates as compared with the balanced case and between six to eight iterations are

Table 4.1 Convergence Results.

Case	Number of busbars	Single phase load flow	Balanced three phase load flow		Typical three phase unbalance
1	5	4,3	4,3	4,3	6,6
2	6	3,3	3,3	3,3	8,8
3	14	3,3	3,3	3,3	6,5
4	17	3,3	3,3	3,3	8,7
5	30	3,3	3,3	3,3	6,6

Convergence tolerance is 0.1 MW/MVAR.

The numerical results, (i,j) should be interpreted as follows:

i - refers to the number of real power - angle update iterations

j - refers to the number of reactive power - voltage update iterations.

required. The cause of this deterioration is examined in this section.

The convergence patterns of real and reactive power mismatches for a corresponding single phase and unbalanced three phase load flow are compared in Figs 4.3 (a) and (b). The mismatches are in p.u. (100 MVA base for single phase and 33.33 MVA base for three phase) and are taken at the busbar which is the slowest to converge.

The initial convergence of the three phase mismatches is very close to that of the single phase load flow. However as the solution is approached the three phase convergence becomes slower. It appears that, although the voltage and angle unbalance are introduced from the first iteration, they have only a secondary effect on the convergence until the positive sequence power flows are approaching convergence. That is, the positive sequence power flows, which predominate the actual system operation, also predominate the initial convergence of the three phase load flow.

This feature is illustrated in Fig. 4.4 where the convergence pattern of the three phase voltages is shown. The convergence pattern of the positive sequence component of the unbalanced voltages is also given as is the convergence pattern of the voltage at the same busbar for the corresponding single phase load flow. The positive sequence voltage of the three phase unbalanced load flow has an almost identical convergence pattern to the corresponding single phase fast decoupled load flow.

The final convergence of the system unbalance is somewhat slow but is reliable.

The following features are peculiar to a three phase load flow and their influence on convergence is of interest:

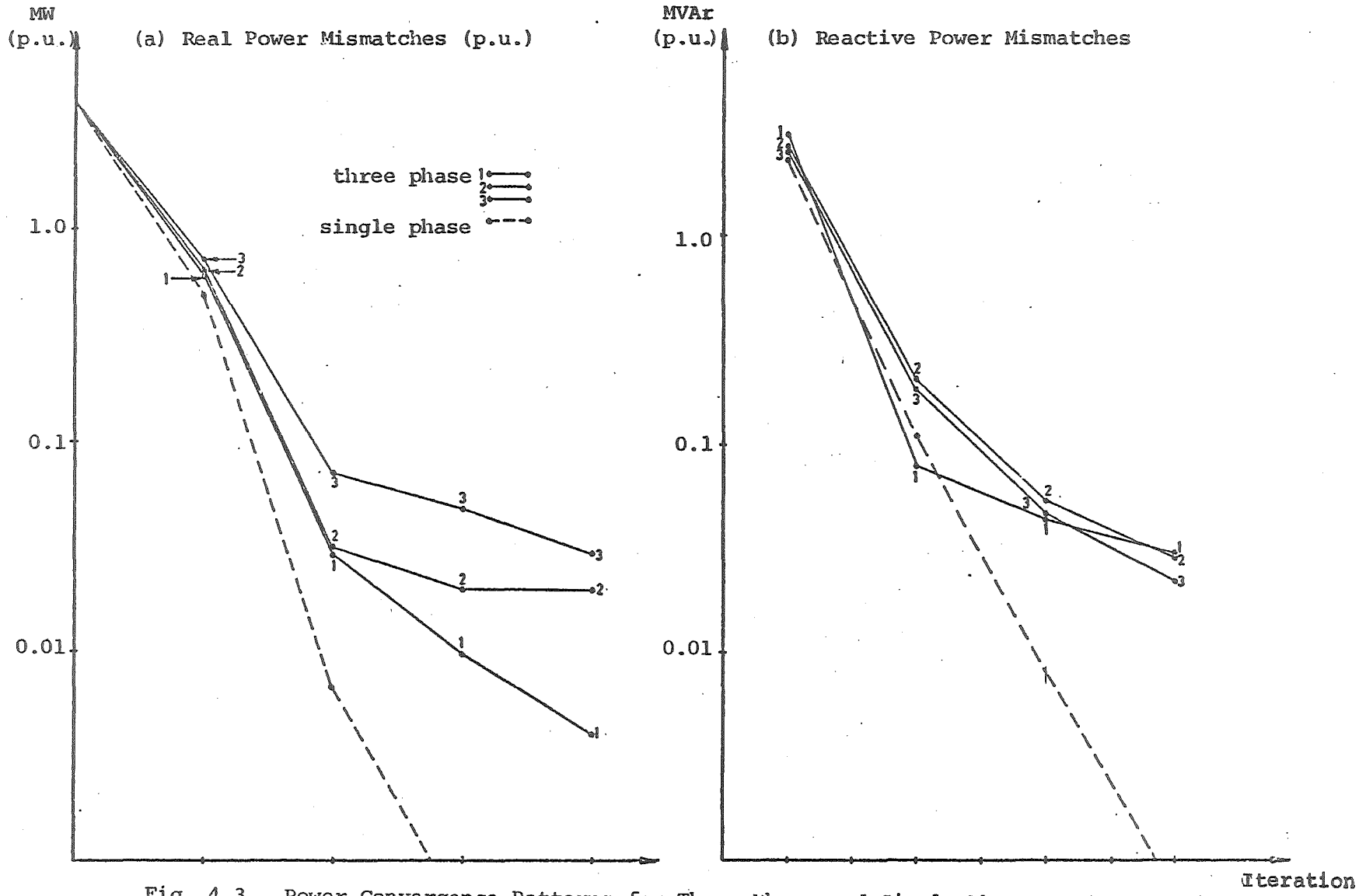

Fig. 4.3 Power Convergence Patterns for Three Phase and Single Phase Load Flow

(i) Three phase voltages

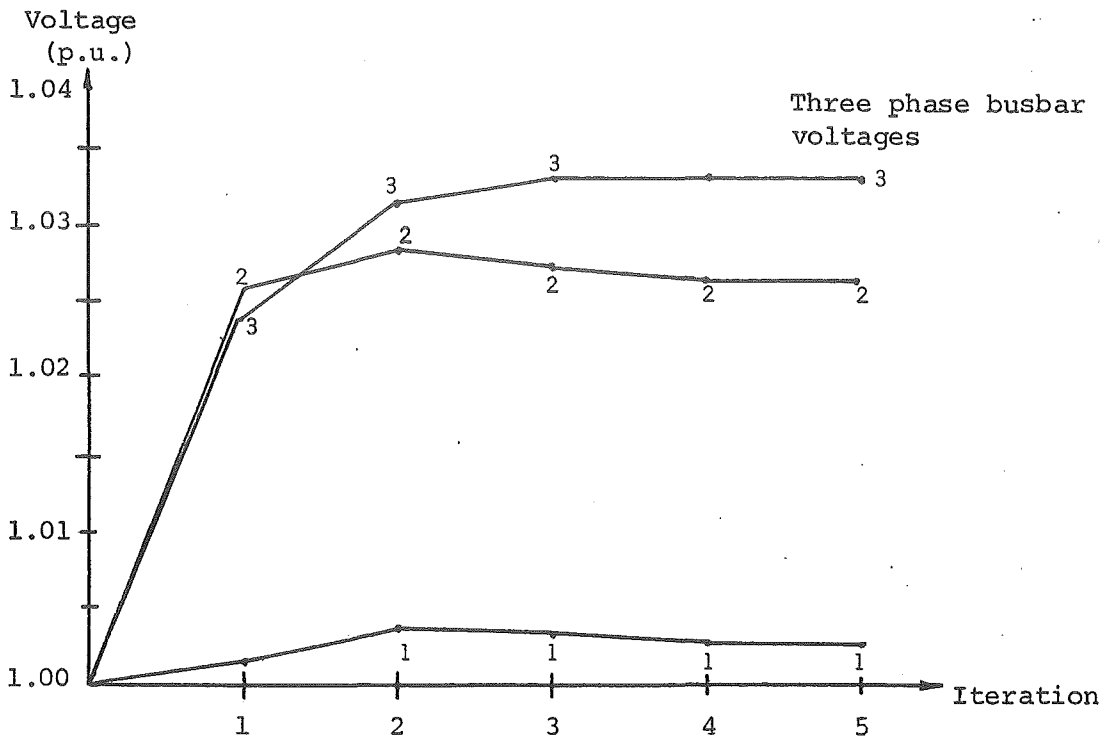

(ii) Single phase and three phase positive sequence voltages

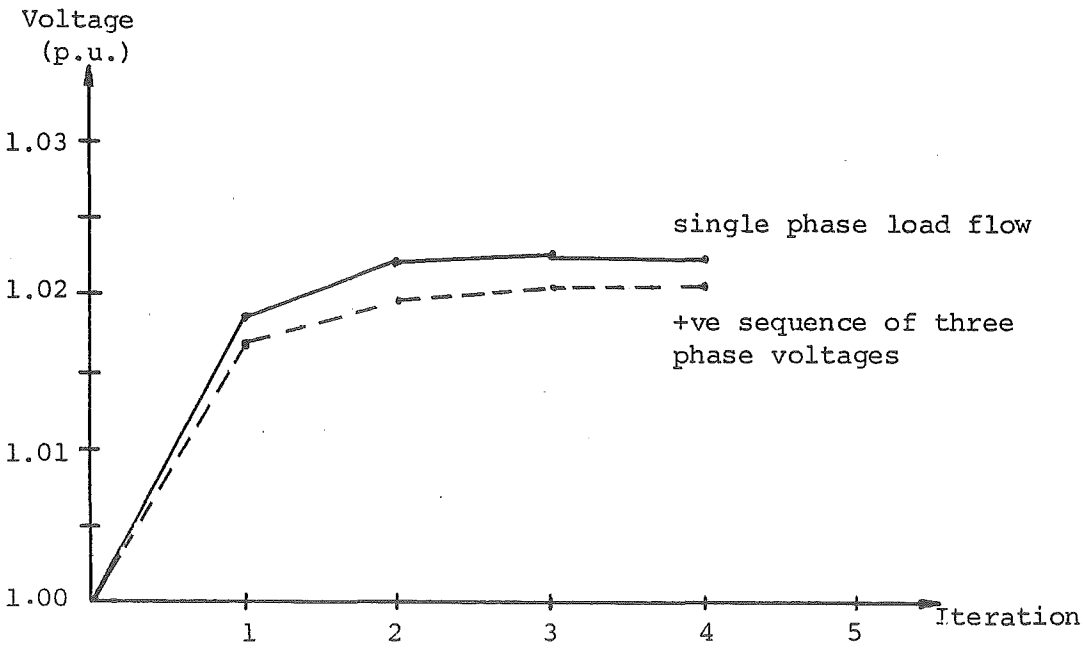

Fig. 4.4 Voltage convergence patterns for three phase and single phase load flows.

- Asymmetry of the system parameters.
- Unbalance of the system loading.
- The influence of the transformer connection.
- Mutual coupling between parallel transmission lines.

These features have been examined with reference to the small 6 bus test system illustrated in Fig. 4.5.

The system includes synchronous generators, three phase lines, transformers and a section of four mutually coupled parallel three phase lines. A description of the system and a set of case specifications are given in sections 6 and 7 of Appendix 5. The Appendix also discusses the modelling of synchronous compensators and the resulting system power flows with unbalanced system voltages.

The system illustrated in Fig. 4.5 is used here to investigate the three phase system parameters which influence convergence.

The following cases have been examined:

(i) Balanced system with balanced loading and no mutual coupling between parallel three phase lines.

(ii) As for case (i) but with balanced mutual coupling introduced for all parallel three phase lines as indicated in Fig. 4.5.

(iii) As for case (ii) but with unbalanced loading.

(iv) As for case (ii) but with system unbalance introduced by line capacitance unbalance only.

(v) As for case (ii) but with system unbalance introduced by line series impedance unbalance only.

(vi) Combined system capacitance and series impedance unbalance with balanced loading.

(vii) As for case (vi) but with unbalanced loading.

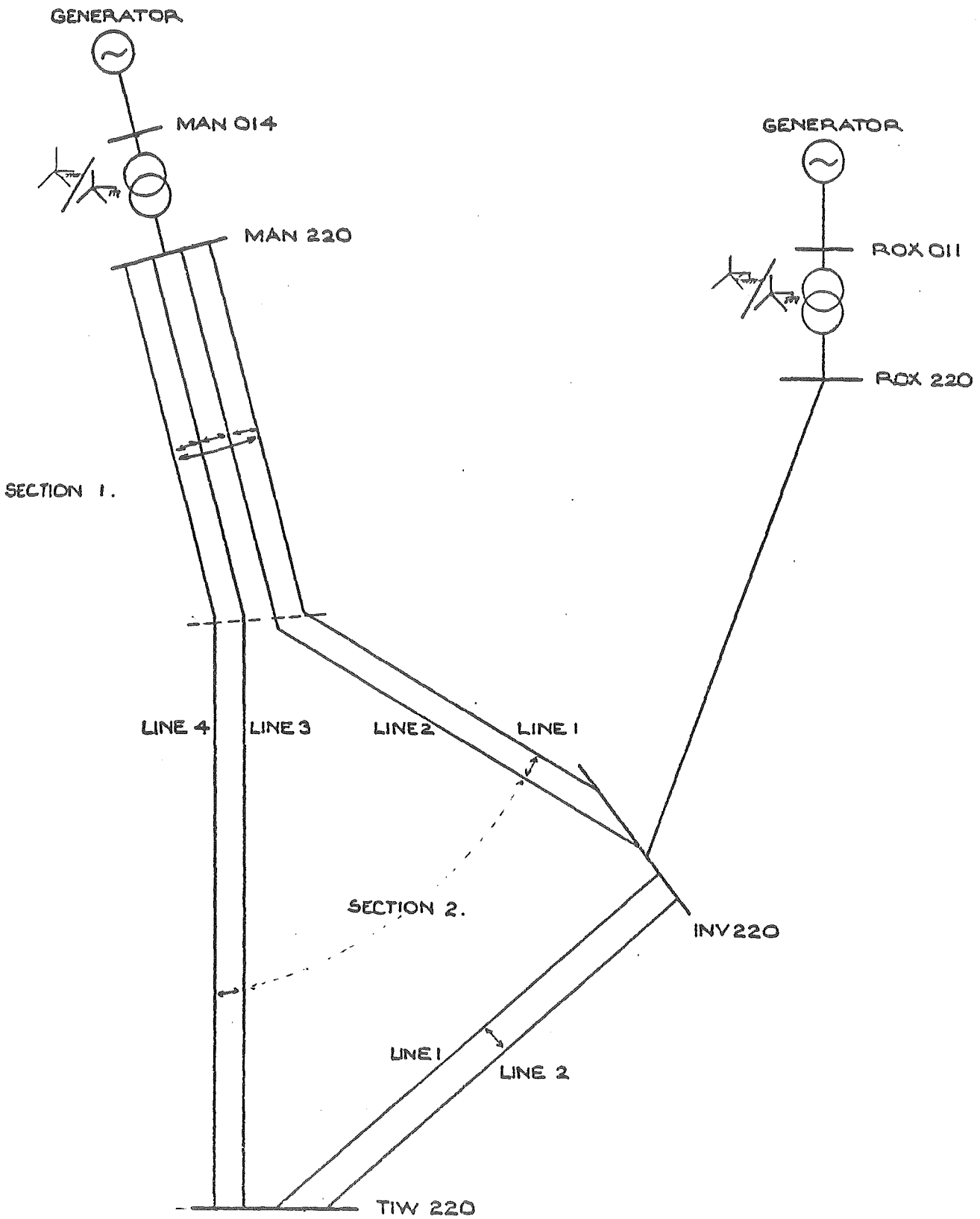

Fig. 4.5 Three phase test system

(viii) As for case (vii) but with Delta/Star-g for the generator transformers.

(ix) As for case (viii) but with large unbalanced real power loading at INV220.

(x) As for case (viii) but with large unbalanced reactive power loading at INV220.

Table 4.2 Number of iterations to convergence for 6 bus test system.

Case	Convergence tolerance (MW/MVAR)		
	10.0	1.0	0.1
i	2,1	2,2	3,3
ii	2,1	2,2	3,3
iii	2,1	6,5	10,10
iv	2,1	5,4	8,8
v	2,1	5,4	9,9
vi	2,1	5,4	9,9
vii	2,1	4,3	10,9
viii	2,1	3,3	8,7
ix	4,3	11,9	17,16
x	4,3	10,10	16,16

The numbers of iterations to convergence, given in Table 4.2, clearly indicates that system unbalance causes a deterioration in convergence. Such deterioration is largely independent of the source of the unbalance although it is dependent on the severity of the unbalance.

The degree of unbalance may be assessed from the sequence components of the busbar voltages, which are given in Table 4.3 for cases (vii), (viii) and (x). The degree of unbalance is considerable in all cases, particularly in case (x) which is included only to demonstrate the convergence properties of the algorithm.

It is noteworthy that the initial convergence of the algorithm is fast even in cases of extreme steady state unbalance. The reliability of the algorithm is not prejudiced by significant unbalance although convergence to small tolerances becomes slow.

The influence of the three phase transformer connection maybe seen in the sequence voltages of cases (vii) and (viii). The star-g/delta connection provides no through path for zero sequence currents and the zero sequence machine current is zero. This is reflected in the zero sequence voltages at the machine terminal voltages.

The sequence voltages also illustrate the position of angle reference at the slack generator internal busbar. In addition it may be seen that at all generator internal busbars the negative and zero sequence voltages are zero reflecting the balanced and symmetrical nature of the machine excitations.

Table 4.3 Sequence Components of Busbar Voltages

Case (vii)

Busbar	+ ve sequence		- ve sequence		zero sequence	
	V_1	θ_1	V_2	θ_2	V_0	θ_0
INV220	1.020	-0.16	0.028	2.42	0.021	-0.85
RQX220	1.037	-0.13	0.028	2.37	0.025	-1.13
MAN220	1.058	-0.09	0.015	1.84	0.014	-0.77
MAN014	1.039	-0.01	0.008	1.85	0.012	-0.76
TIW220	1.015	-0.17	0.028	2.40	0.021	-0.74
RQX011	1.055	-0.03	0.019	2.39	0.019	-1.12
MAN.GN	1.056	0.03	0.0	-	0.0	-
RQX.GN	1.066	0.0	0.0	-	0.0	-

Case (viii)

Busbar	+ ve sequence		- ve sequence		zero sequence	
	V_1	θ_1	V_2	θ_2	V_0	θ_0
INV220	1.034	0.36	0.023	-3.12	0.004	0.23
RQX220	1.049	0.40	0.023	3.04	0.005	-0.80
MAN220	1.071	0.43	0.015	2.39	0.001	0.20
MAN014	1.050	-0.01	0.006	2.93	0.0	-
TIW220	1.029	0.36	0.023	3.11	0.005	0.69
RQX011	1.064	-0.02	0.016	-2.70	0.0	-
MAN.GN	1.067	0.03	0.0	-	0.0	-
RQX.GN	1.074	0.0	0.0	-	0.0	-

Case (x)

Busbar	+ ve sequence		- ve sequence		zero sequence	
	V_1	θ_1	V_2	θ_2	V_0	θ_0
INV220	1.011	0.37	0.100	-2.69	0.083	-2.62
RQX220	1.043	0.40	0.086	-2.70	0.031	-2.36
MAN220	1.065	0.44	0.058	-2.65	0.017	-2.50
MAN014	1.061	-0.01	0.032	-2.11	0.0	-
TIW220	1.007	0.36	0.098	-2.68	0.080	-2.59
RQX011	1.081	-0.02	0.060	-2.16	0.0	-
MAN.GN	1.086	0.03	0.0	-	0.0	-
RQX.GN	1.096	0.0	0.0	-	0.0	-

4.5.4 Conclusion On Algorithmic Performance

This section has investigated the performance of the three phase algorithm under various degrees of steady state unbalance. It has been demonstrated that the algorithm behaves identically to a standard single phase fast decoupled load flow when the three phase system is symmetrical and has balanced loading. The initial convergence pattern with unbalanced systems is very similar to the single phase fast decoupled version, and, therefore, the three phase algorithm possesses similar reliability as the single phase algorithm.

Final convergence of the three phase algorithm is determined by the degree of unbalance but does not depend upon the source of that unbalance. In all practical cases of steady state unbalanced system operation the convergence rate has been acceptable.

As the initial convergence is fast and reliable starting values are not critical and flat voltage and angle values have proved adequate in all cases.

CHAPTER 5

FAST DECOUPLED LOAD FLOW ALGORITHMS FOR BALANCED A.C./D.C. SYSTEMS

5.1 INTRODUCTION

The relatively small number of h.v.d.c. transmission schemes in existance has not encouraged sufficient development of a.c./d.c. load flow programmes to ensure that the integration of the d.c. equations is most efficient and reliable. However, an increasing interest in the potential application of h.v.d.c. schemes, both point to point and multiterminal, has highlighted the need for efficient incorporation of the d.c. system into modern load flow techniques.

The computational efficiency and reliability of the fast decoupled a.c. load flow[30] is well documented and programmes based on this technique are being gradually adopted for general purpose load flow studies.

The incorporation of the d.c. system models into the fast decoupled load flow is therefore of considerable interest.

The aim of including the d.c. system model into the load flow analysis is to enable solution for the operating state of the combined a.c. and d.c. systems under the specified conditions of load, generation and d.c. system control strategy.

The formulation of suitable d.c. system models and the integration of the models into the fast decoupled load flow is discussed in this chapter.

Two basic approaches have been used to integrate the d.c. system model into a.c. load flows, ie sequential and unified approaches.

The sequential approach [38,39], enables integration into existing load flow programmes without significant modification or restructuring of the a.c. solution technique. The a.c. and d.c. equations are solved separately. For the a.c. iterations each convertor is modelled simply by the equivalent real or reactive power injection at the terminal busbar. The terminal busbar voltages obtained from the a.c. iteration are then used to solve the d.c. equations and consequently, new power injections are obtained. This process continues iteratively to convergence.

Alternatively, the more sophisticated unified methods [34,40,41,42] give full recognition to the interdependence between a.c. and d.c. system equations and simultaneously solve the complete set of equations.

In the absence of comparative studies the discussions on the relative merits of the alternative techniques have been vague.

The aim of this chapter is to develop efficient unified and sequential fast decoupled a.c./d.c. load flows which are suitable for multiple and/or multiterminal d.c. systems. Several variations of the algorithms are described and a detailed assessment of the relative merits presented.

5.2 FORMULATION OF THE SINGLE PHASE A.C./D.C. LOAD FLOW PROBLEM

The aim of the single phase a.c./d.c. load flow is to solve for the state of the combined a.c. and d.c. systems, under the specified conditions of load, generation and d.c. system control strategy.

The operating state of the combined power system is defined by:

$$[\bar{V},\ \bar{\theta},\ \bar{x}]^T$$

where $\bar{V}$ is a vector of voltages at all a.c. system busbars

$\bar{\theta}$ is a vector of angles at all a.c. system busbars (except one, which is assigned $\theta = 0$ ie. taken as a reference)

$\bar{x}$ is a vector of d.c. variables.

The selection of $\bar{V}$ and $\bar{\theta}$ as a.c. system variables is straightforward and is well documented. However, the selection of d.c. variables $\bar{x}$ is more complex and is discussed in depth in section 5.3.

To enable the use of a Newton-Raphson based technique it is necessary to formulate a set of n independent algebraic equations in terms of the n variables.

The equations which relate to the a.c. system variables are derived from the specified a.c. system operating conditions. The only modification to the usual real and reactive power mismatches (Appendix 4) occurs with those equations derived from the specified injected powers at the convertor terminal busbar. These equations become:

$$P^{sp}_{term} - P_{term}(ac) - P_{term}(dc) = 0 \qquad (5.1)$$

$$Q^{sp}_{term} - Q_{term}(ac) - Q_{term}(dc) = 0 \qquad (5.2)$$

where $P_{term}(ac)$ is the injected power at the terminal busbar as a function of the a.c. system variables.

$P_{term}(dc)$ is the injected power at the terminal busbar as a function of the d.c. system variables

and similarly for $Q_{term}(dc)$ and $Q_{term}(ac)$.

The injected powers $Q_{term}(dc)$ and $P_{term}(dc)$ are functions of the a.c. convertor source voltage (taken as the a.c. terminal busbar voltage; see section 5.3.1 for basic assumptions) and of the d.c. system variables, i.e.

$$P_{term}(dc) = f(V_{term}, \bar{x}) \tag{5.3}$$

$$Q_{term}(dc) = f(V_{term}, \bar{x}) \tag{5.4}$$

The equations derived from the specified a.c. system conditions may therefore be summarised as:

$$\begin{bmatrix} \Delta\bar{P} & (\bar{V},\bar{\theta}) \\ \Delta\bar{P}_{term} & (\bar{V},\bar{\theta},\bar{x}) \\ \Delta\bar{Q} & (\bar{V},\bar{\theta}) \\ \Delta\bar{Q}_{term} & (\bar{V},\bar{\theta},\bar{x}) \end{bmatrix} = 0 \tag{5.5}$$

where the mismatches at the convertor terminal busbars are indicated separately.

A further set of independent equations is derived from the d.c. system conditions. These are designated,

$$\bar{R}(V_{term}, \bar{x})_k = 0 \tag{5.6}$$

for k = 1, number of convertors present.

It should be noted that the d.c. system equations (5.6) are independent of the a.c. system angles $\bar{\theta}$. This is achieved by using a separate angle reference for the d.c. system variables as defined in Fig. 5.2. This mathematical contrivance has been found to give improved algorithmic performance by effectively decoupling the angle dependence of a.c. and d.c. systems.

Equations 5.3, 5.4 and 5.6 mathematically model the steady state operation of the d.c. system. Their formulation is discussed in section 5.3.

The general a.c./d.c. load flow problem may therefore be summarised as the solution of:

$$\begin{bmatrix} \Delta\bar{P} & (\bar{V},\bar{\theta}) \\ \Delta\bar{P}_{term} & (\bar{V},\bar{\theta},\bar{x}) \\ \Delta\bar{Q} & (\bar{V},\bar{\theta}) \\ \Delta\bar{Q}_{term} & (\bar{V},\bar{\theta},\bar{x}) \\ \bar{R} & (V_{term},\bar{x}) \end{bmatrix} = 0 \qquad (5.7)$$

for the variables $\bar{V},\bar{\theta}$ and $\bar{x}$.

5.3 D.C. SYSTEM MODEL

The mathematical model of the d.c. system (equations 5.3, 5.4 and 5.6) is developed in this section. The formulation of the equations and selection of variables $\bar{x}$ requires several basic assumptions.

5.3.1 Basic Assumptions

The following assumptions are made in the formulation of the d.c. convertor model:

(i) The three a.c. voltages at the terminal busbar are perfectly balanced and perfectly sinusoidal.

(ii) The convertor operation is perfectly balanced.

(iii) The direct current and voltage are smooth.

(iv) The convertor transformer is lossless and the magnetising admittance may be ignored.

These assumptions are generally accepted[43] for balanced steady

state analysis of d.c. convertor operation and no further justification will be given here.

5.3.2 Convertor Model

The assumptions listed enable each convertor in the d.c. system to be modelled as shown in Fig. 5.1. The variables illustrated, representing every fundamental frequency or d.c. quantity, fully describe the system operation.

An equivalent circuit for the convertor is shown in Fig. 5.2. A trivial modification to the angles has been performed as regards the position of angle reference.

The variables are defined with reference to Fig. 5.2, as follows:

$V_{term} \angle\phi$	convertor terminal busbar nodal voltage (phase angle referred to convertor reference).
$E \angle\psi$	fundamental frequency component of the voltage waveform at the convertor transformer secondary.
I_p, I_s	fundamental frequency component of the current waveshape on the primary and secondary respectively.
α	firing delay angle.
a	transformer off-nominal tap ratio.
Vd	average d.c. voltage.
Id	convertor direct current.

These ten variables, nine associated with the convertor plus the a.c. terminal voltage magnitude V_{term}, form a possible choice

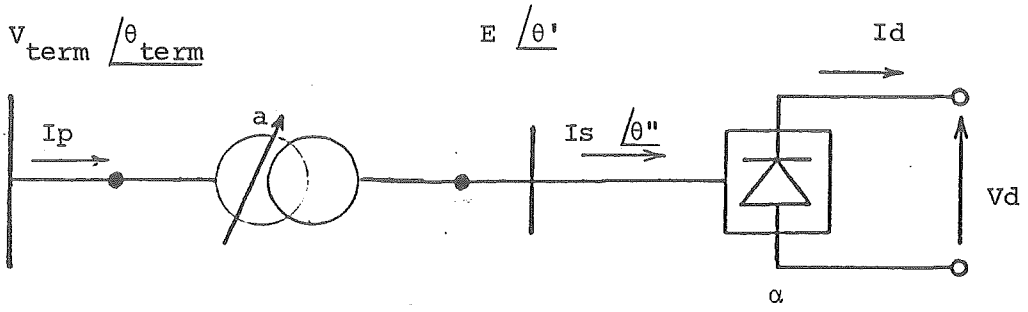

Fig. 5.1 Basic d.c. convertor (Angles referred to a.c. system reference)

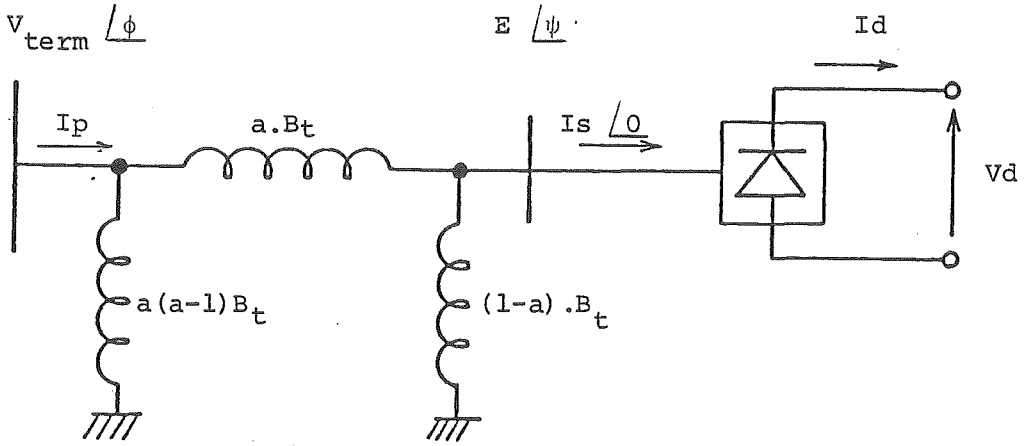

Fig. 5.2 Single phase equivalent circuit for basic convertor. (Angles referred to d.c. reference)

of $\bar{x}$ for the formulation of equations 5.3, 5.4 and 5.6.

For efficiency, the smallest number of variables, consistant with the need for convenient incorporation of a wide range of control modes, should be used.

This clearly involves a compromise and the number of variables used by different researchers has varied[39-41].

As mentioned in chapter 3 the minimum number of variables required to define the operation of any system is the number of independent variables. These completely define the operating state of the system and any other system variable or parameter (eg. P_{dc} and Q_{dc}) may be written in terms of these variables.

A d.c. convertor, operating under balanced conditions, from a known terminal voltage, has two independent variables. The use of two variables yields a d.c. convertor model of the smallest dimension. However, the control requirements of the d.c. convertors are such that a range of variables, or functions of them (eg. constant power), are the specified conditions. If the minimum number of variables are used then the control specifications must be translated into equations in terms of these two variables. These equations often contain complex non-linearities, which are difficult to derive and include in programme implementation. In addition, the equations for P_{dc} and Q_{dc} may be complex and this will make the programming of a unified solution more difficult.

For these reasons, a non minimal set of variables is used. This is in contrast to a.c. load flows where, due to the restricted nature of the control specifications, a minimum set is convenient. Therefore all variables which are influenced by control action are retained in the study.

The following set of variables enable simple relationships to be written for all control strategies.

$$[\bar{x}] = [V_d, I_d, a, \cos\alpha, \phi]^T$$

Variable ϕ is included to ensure that a simple equation for Q_{dc} may be written. This is important in the formulation of a unified solution method; for sequential methods this variable may be omitted as it is not essential in the formulation of any control specification. The variable cos α is used rather than α as the equations are more linear and this has a favourable influence on convergence as discussed in chapter 3. Before developing the equations it is necessary to discuss the per unit system, if any, which should be used for the d.c. system.

5.3.2.1 D.C. Per Unit System

No per unit system is necessary to enable the modelling of the d.c. system. For the d.c. system equations the p.u. a.c. terminal voltage can be translated into kV. All d.c. equations could then be written in actual values. The injected powers $P_{term}(dc)$ and $Q_{term}(dc)$ would simply be divided by the a.c. system power base before inclusion in equations (5.1) and (5.2).

However, to avoid any per unit to actual value translations and to enable comparable convergence tolerances to be obtained for both a.c. and d.c. system mismatches, a per unit system is used for the d.c. quantities.

Computational simplicity is achieved by using common power and voltage base parameters on both sides of the convertor ie. a.c. and d.c. sides. To preserve constancy of power in per unit, the direct current base, obtained from $(MVA_B)/V_B$, is $\sqrt{3}$ times

larger than the a.c. current base.

This has the effect of changing the coefficients involved in the a.c./d.c. current relationships. For a perfectly smooth direct current and neglecting the commutation overlap, the r.m.s. fundamental component of the phase current is related to I_d by the expression:

$$I_s = \frac{\sqrt{6}}{\pi} \cdot I_d \tag{5.8}$$

To improve the accuracy of this approximation a factor of 0.995 is often introduced. For clarity this minor addition will be omitted from the equations presented here.

Translating equation 5.8 to per unit yields:

$$I_s(\text{p.u.}) = \frac{\sqrt{6}}{\pi} \cdot \sqrt{3} \cdot I_d(\text{p.u.})$$

ie.
$$I_s(\text{p.u.}) = \frac{3\sqrt{2}}{\pi} \cdot I_d(\text{p.u.}) \tag{5.9}$$

5.3.2.2 Consideration of Series and Parallel Bridges

Under balanced conditions similar convertor bridges attached to the same a.c. terminal busbar will operate identically regardless of the transformer connection. All such bridges may therefore be replaced by an equivalent single bridge for the purpose of single phase load flow analysis.

5.3.2.3 Derivation of Equations

The following relationships may be derived for the variables defined in Fig. 5.2. The equations are in p.u.

(i) The fundamental current magnitude on the secondary of the convertor may be approximated to,

$$I_s = \frac{3\sqrt{2}}{\pi} \cdot I_d \qquad (5.10)$$

(ii) The fundamental current magnitude on the primary may be found by referring the secondary current across the lossless transformer,

$$I_p = a \cdot I_s \qquad (5.11)$$

(iii) The d.c. voltage may be expressed in terms of the convertor source voltage* referred to the transformer secondary as,

$$V_d = \frac{3\sqrt{2}}{\pi} \cdot a \cdot V_{term} \cos \alpha - \frac{3}{\pi} \cdot I_d \cdot X_c \qquad (5.12)$$

(iv) The d.c. current and voltage are related by the d.c. system configuration,

$$f(V_d, I_d) = 0 \qquad (5.13)$$

eg.

$$V_d - I_d \cdot R_d = 0$$

for a simple rectifier supplying a passive load.

(v) The assumptions listed previously ensure that there is no real power in the harmonic frequencies at both the primary and secondary busbars. Therefore the d.c. real power may be equated to the a.c. real power at the transformer secondary in terms of the fundamental components alone, ie.

$$V_d \cdot I_d = E \cdot I_s \cdot \cos \psi \qquad (5.14)$$

(vi) As the transformer is lossless a similar equation may be written equating the primary real power to the d.c. power ie.

* From the assumptions listed previously the source voltage is simply the a.c. terminal busbar voltage V_{term}.

$$V_d \cdot I_d = V_{term} \cdot I_p \cdot \cos \phi \qquad (5.15)$$

(vii) The final independent equation may be written in terms of the fundamental component of current flow across the convertor transformer, ie.

$$I_s = B_t \cdot E \cdot \sin \psi - B_t \cdot a \cdot V_{term} \sin \phi \qquad (5.16)$$

where $jB_t = Y_t$ the transformer leakage admittance.

No other independent equations may be written relating the total set of nine convertor variables. A total of seven equations have been derived.

The variables, I_p,I_s,E and ψ are not included as d.c. convertor variables $\bar{x}$ and these are eliminated from the equations to yield,

$$V_d - K_1 \cdot a \cdot V_{term} \cos \alpha + \frac{3}{\pi} I_d \cdot X_c = 0 \qquad (5.17)$$

$$V_d - K_1 \cdot a \cdot V_{term} \cos \phi = 0 \qquad (5.18)$$

$$f(V_d, I_d) = 0 \qquad (5.19)$$

where $K_1 = \frac{3\sqrt{2}}{\pi}$.

The final two independent equations which are required are derived from the specified control mode. Two equations are required as the convertor has two degrees of freedom (ie. two independent variables) which must be restrained in order to define an operating state.

The d.c. model may thus be summarised as follows:

$$\bar{R}(\bar{x}, V_{term})_k = 0 \qquad (5.20)$$

where

$$R(1) = V_d - K_1 \cdot a \cdot V_{term} \cdot \cos \phi$$

$$R(2) = V_d - K_1 \cdot a \cdot V_{term} \cdot \cos \alpha + \frac{3}{\pi} \cdot I_d \cdot X_c.$$

$$R(3) = f(V_d, I_d)$$

$$R(4) = \text{Control equation}$$

$$R(5) = \text{Control equation}$$

and

$$\bar{x} = [V_d, I_d, a, \cos \alpha, \phi]^T$$

It should be noted that V_{term} is either known, (i.e. specified) or it is an a.c. system variable.

The equations for P_{dc} and Q_{dc} may be written as:

$$Q_{dc} = V_{term} \cdot I_p \cdot \sin \phi$$

$$= V_{term} \cdot K_1 \cdot a \cdot I_d \cdot \sin \phi \qquad (5.21)$$

and

$$P_{dc} = V_{term} \cdot I_p \cdot \cos \phi$$

$$= V_{term} \cdot K_1 \cdot a \cdot I_d \cdot \cos \phi \qquad (5.22)$$

or

$$P_{dc} = V_d \cdot I_d. \qquad (5.23)$$

Several simple equations for P_{dc} may be written; the equation may be chosen to give the most convenient algorithmic implementation.

The equation for Q_{dc} is written as the fundamental reactive power load of the convertor, the reactive power of the harmonics is zero as perfect filtering has been assumed.

5.3.3 Clarification of an Anomaly in Previous D.C. Models

Several earlier d.c. models used by this author and others [4,5,34,41,42] retained the variables E and ψ in their formulation.

This was necessary as the equation for d.c. voltage was written in terms of E and not the convertor source voltage referred to the secondary of the convertor transformer. These variables could not, therefore, be conveniently removed. As a result the regulation due to the commutation reactance was effectively included twice. The form of the algorithms is not significantly altered although the accuracy of the solutions is affected.

5.3.4 Incorporation of Control Equations

Each convertor in the d.c. system provides two additional independent variables to the system. Two further constraint equations must therefore be derived from the control strategy of the system to ensure a defined operating state. For example a classical two-terminal d.c. link has two convertors and therefore requires four control equations. The four equations must be written in terms of the ten d.c. variables (five for each convertor).

Any function of the ten d.c. system variables is a valid (mathematically) control equation so long as each equation is independent of all other equations. In practice there are restrictions limiting the number of alternatives. Some control strategies refer to the characteristics of power transmission (eg. constant power or constant current), others introduce constraints such as minimum delay or extinction angles.

Examples of valid control specifications are:

(i) Specified convertor transformer tap,

$$a - a^{sp} = 0$$

(ii) Specified d.c. voltage

$$V_d - V_d^{sp} = 0$$

(iii) Specified d.c. current

$$I_d - I_d^{sp} = 0$$

(iv) Specified minimum firing angle,

$$\cos \alpha - \cos \alpha_{min} = 0$$

(v) Specified d.c. power transmission

$$V_d \cdot I_d - P_{dc}^{sp} = 0$$

The control equations are simple and are easily incorporated into the solution algorithm. In addition to the usual control modes, non standard modes such as specified convertor power factor or specified a.c. terminal voltage may also be included as convertor control equations (see section 5.5).

5.3.5 Invertor Operation

All the equations presented are equally applicable to invertor operation. However, during inversion it is the extinction advance angle (γ) which is the subject of control action and not the firing angle (α). For convenience therefore equation R(2) may be rewritten as:

$$V_d - K_1 \cdot a \cdot V_{term} \cdot \cos(\pi - \gamma) - \frac{3}{\pi} X_c \cdot I_d = 0 \qquad (5.24)$$

This equation is valid for rectification or inversion. Under inversion, V_d, as calculated by 5.24, will be negative.

To specify operation with constant extinction angle the following equation is used:

$$\cos(\pi - \gamma) - \cos(\pi - \gamma^{sp}) = 0$$

where γ^{sp} is usually γ minimum for minimum reactive power consumption of the invertor.

5.3.6 Convertor Control Strategies

During the iterative solution procedure the uncontrolled convertor variables may go outside prespecified limits. When this occurs the offending variable is usually held to its' limit value and an appropriate control variable is freed.[34]

Each time a control equation is altered a small discontinuity occurs and convergence will usually be delayed for one or two iterations.

This process is common to both the unified and sequential techniques. For the purposes of this chapter, which is to compare the two techniques, the control strategy is a further and unneccessary complication. For this reason the specified convertor controls are appropriately selected to ensure that limit violations do not occur.

It should be noted also that, upon final convergence the tap ratio may need to be adjusted to the nearest discrete tap ratio available. This reconvergence will usually be very fast.

5.4 SOLUTION TECHNIQUES

The aim of this section is to develop a solution procedure for equation (5.7) which fully retains the computational advantages of the fast decoupled a.c. load flow method. The standard fast decoupled a.c. load flow algorithm (Appendix 4) involves the iterative solution of the following equations in a block successive iteration scheme.

$$[\Delta\bar{P}/\bar{V}] = [B'][\Delta\bar{\theta}] \tag{5.25}$$

$$[\Delta\bar{Q}/\bar{V}] = [B''][\Delta\bar{V}] \tag{5.26}$$

where [B'] and [B"] are the constant approximated jacobian matrices.

Any method of solution for equation (5.7), which involves the fast decoupled algorithm, should possess all, or at least most, of the following features:

(i) The jacobian matrices [B'] and [B"] must remain constant and symmetrical for the a.c. network solution and must be able to be factorised before the iterative solution process.

(ii) The speed and reliability of the a.c. load flow algorithm is, in part, due to the block successive iteration scheme which is initiated with a real power - angle update iteration. Except with evidence to the contrary this practice should be retained.

(iii) The minimum modification to any existing fast decoupled algorithm is a desirable feature.

(iv) The integration of the convertor equations should not increase the number of solutions of (5.25) and (5.26) that are required for convergence. The dimension of these equations (and hence their solution time) will, in general, be many times greater than the dimension of the d.c. equations. The number of solutions of the d.c. equations is therefore of relatively minor importance.

These features provide an indication of the variations which are worthy of investigation.

All methods are discussed with reference to a single convertor connected to an a.c. busbar. The extension to multiple or multi-terminal d.c. systems is relatively trivial and is discussed in section 5.7.

5.4.1 Unified Methods

The unified methods give recognition to the interdependence of a.c. and d.c. system equations and simultaneously solve the complete system. Several variations of the unified technique are investigated in this section.

The a.c./d.c. load flow problem, as formulated in (5.7), may be written for a single convertor d.c. system, as:

$$\begin{bmatrix} \Delta\bar{P} \quad (\bar{V},\bar{\theta}) \\ \Delta P_{term}(\bar{V},\bar{\theta},\bar{x}) \\ \Delta\bar{Q} \quad (\bar{V},\bar{\theta}) \\ \Delta Q_{term}(\bar{V},\bar{\theta},\bar{x}) \\ \bar{R}(V_{term},\bar{x}) \end{bmatrix} = 0 \tag{5.27}$$

where the subscript term indicates the value at the convertor terminal busbar.

Recalling that,

$$\Delta P_{term} = P^{sp}_{term} - P_{term}(ac) - P_{term}(dc) \tag{5.28}$$

$$\Delta Q_{term} = Q^{sp}_{term} - Q_{term}(ac) - Q_{term}(dc) \tag{5.29}$$

and,

$$P_{term}(dc) = f(V_{term},\bar{x}) \tag{5.30}$$

$$Q_{term}(dc) = f(V_{term},\bar{x}) \tag{5.31}$$

the standard Newton-Raphson algorithm may be applied (see chapter 3). Essentially, this method involves repeat solutions of,

$$\begin{bmatrix} \Delta\bar{P} \quad (\bar{V},\bar{\theta}) \\ \Delta P_{term}(\bar{V},\bar{\theta},\bar{x}) \\ \Delta\bar{Q} \quad (\bar{V},\bar{\theta}) \\ \Delta Q_{term}(\bar{V},\bar{\theta},\bar{x}) \\ \bar{R}(V_{term},\bar{x}) \end{bmatrix} = \begin{bmatrix} \\ J \\ \\ \end{bmatrix} \begin{bmatrix} \Delta\bar{\theta} \\ \Delta\theta_{term} \\ \Delta\bar{V} \\ \Delta V_{term} \\ \Delta\bar{x} \end{bmatrix} \tag{5.32}$$

where J is the matrix of first order partial derivatives.

Applying the usual a.c. fast decoupled assumptions to all jacobian elements related to the a.c. system equations, yields:

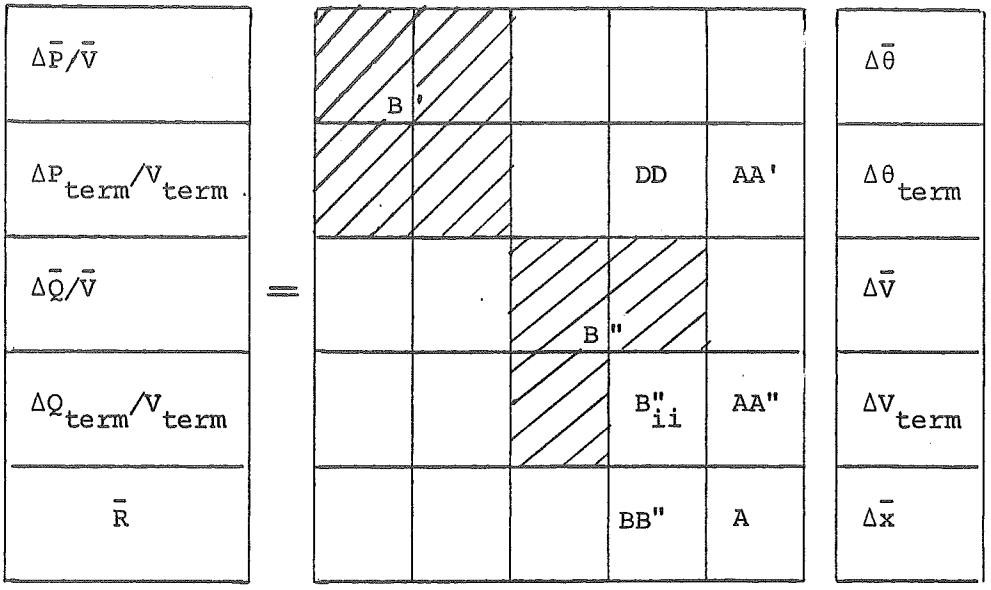

(5.33)

where all matrix elements are zero unless otherwise indicated. The matrices [B'] and [B"] are exactly the usual single phase fast decoupled jacobians. These matrices are constant in value. The other matrices indicated, vary at each iteration in the solution process.

The only element of [B"] which becomes modified is indicated as B''_{ii} in equation (5.33). This element varies at each iteration ie. it is a function of the system variables.

The advantage of an independent angle reference for the d.c. equations is demonstrated in the equation where it may be seen that:

$$\partial P_{term}(d.c.)/\partial\theta_{term} = 0$$

ie. the diagonal jacobian element for the real power mismatch at the convertor terminal busbar depends on the a.c. equations only and

is therefore the usual fast decoupled B' element.

In addition,

$$\partial\bar{R}/\partial\theta_{term} = 0$$

which is an aid to the subsequent decoupling of the equation.

In order to maintain the block successive iteration sequence of the usual fast decoupled a.c. load flow it is necessary to decouple equation (5.33). The jacobian submatrices must be examined in more detail.

The jacobian submatrices are:

$$DD = \frac{1}{V_{term}} \partial\Delta P_{term}/\partial V_{term}$$

$$= \frac{1}{V_{term}} \left[\partial P_{term}(ac)/\partial V_{term}\right] + \frac{1}{V_{term}} \left[\partial P_{term}(dc)/\partial V_{term}\right]$$

$$= 0 + \frac{1}{V_{term}} \left[\partial P_{term}(dc)/\partial V_{term}\right]$$

by the usual decoupled load flow practice.

$$AA' = \frac{1}{V_{term}} \left[\partial\Delta P_{term}/\partial\bar{x}\right]$$

$$= \frac{1}{V_{term}} \left[\partial P_{term}(ac)/\partial\bar{x}\right] + \frac{1}{V_{term}} \left[\partial P_{term}(dc)/\partial\bar{x}\right]$$

$$= 0 + \frac{1}{V_{term}} \left[\partial P_{term}(dc)/\partial\bar{x}\right]$$

$$AA'' = \frac{1}{V_{term}} \left[\partial\Delta Q_{term}/\partial\bar{x}\right]$$

$$= \frac{1}{V_{term}} \left[\partial Q_{term}(dc)/\partial\bar{x}\right]$$

$$BB'' = \partial\bar{R}/\partial V_{term}$$

$$[A] = \partial\bar{R}/\partial\bar{x}$$

$$B''_{ii} = \frac{1}{V_{term}}\left[\partial\Delta Q_{term}/\partial V_{term}\right]$$

$$= \frac{1}{V_{term}}\,\partial Q_{term(ac)}/\partial V_{term} + \frac{1}{V_{term}}\left[\partial Q_{term(dc)}/\partial V_{term}\right]$$

$$= B''_{ii(ac)} + B''_{ii(dc)}$$

Now, taking

$$P_{term(dc)} = V_d \cdot I_d$$

then,

$$\partial P_{term(dc)}/\partial V_{term} = 0$$

and therefore,

$$DD = 0$$

The derivation to this point is common to the unified solution methods which utilise the fast decoupled a.c. load flow. These methods are described in the following sections.

5.4.1.1 Unified Method 1

Without further assumptions the d.c. variables $\bar{x}$ are coupled to both the real and reactive power a.c. mismatches. However, equation (5.33) may be separated to enable a block successive iteration scheme to be used. The following two equations result:

$$\begin{bmatrix} \Delta\bar{P}/\bar{V} \\ \Delta P_{term}/V_{term} \\ \bar{R} \end{bmatrix} = \begin{bmatrix} B' & \\ & AA' \\ & A \end{bmatrix} \begin{bmatrix} \Delta\bar{\theta} \\ \Delta\theta_{term} \\ \Delta\bar{x} \end{bmatrix} \qquad (5.34)$$

$$\begin{bmatrix} \Delta\bar{Q}/\bar{V} \\ \Delta Q_{term}/V_{term} \\ \bar{R} \end{bmatrix} = \begin{bmatrix} B'' & & \\ & B''_{ii} & AA'' \\ & BB'' & A \end{bmatrix} \begin{bmatrix} \Delta\bar{V} \\ \Delta V_{term} \\ \Delta\bar{x} \end{bmatrix} \qquad (5.35)$$

The a.c. mismatches and variables are appended to both the usual fast decoupled a.c. equations.

These equations are solved according to the iteration sequence illustrated in Fig. 5.3. This iteration scheme is referred to as - PDC, QDC - where the significance of the mnemonic is clear.

The results for a number of test cases are given in section 5.8.

5.4.1.2 Unified Method 2

The algorithm of method 1 may be further simplified by recognising the following characteristics of the a.c. and d.c. systems:

(i) The coupling between d.c. variables and the a.c. terminal voltage is strong.

(ii) There is no coupling between d.c. mismatches and a.c. system angles.

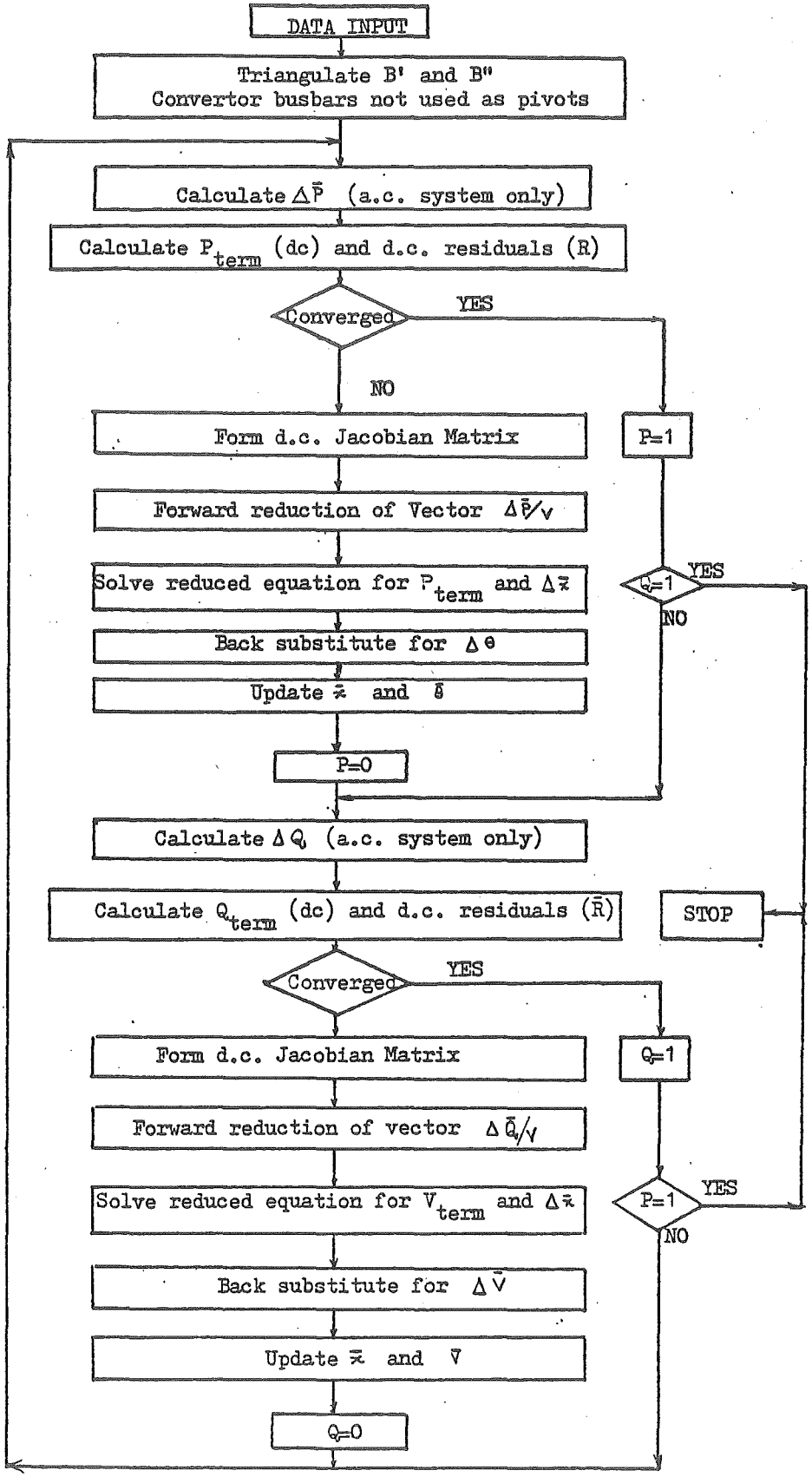

Fig. 5.3 Flow Chart for Unified Single Phase A.C./D.C. Load Flow

(iii) Under all practical control strategies the d.c. power is well constrained and this implies that the changes in d.c. variables $\bar{x}$ do not greatly affect the real power mismatches at the terminals. This coupling, embodied in matrix AA' of equation (5.34) can therefore be justifiably removed.

These features justify the removal of the d.c. equations from equation (5.34) to yield the following two algorithmic equations:

$$[\Delta\bar{P}/\bar{V}] = [B'][\Delta\bar{\theta}] \tag{5.36}$$

$$\begin{bmatrix} \Delta\bar{Q}/\bar{V} \\ \Delta Q_{term}/V_{term} \\ \bar{R} \end{bmatrix} = \begin{bmatrix} B'' & & \\ & B''_{ii} & AA'' \\ & BB'' & A \end{bmatrix} \begin{bmatrix} \Delta\bar{V} \\ \Delta V_{term} \\ \Delta\bar{x} \end{bmatrix} \tag{5.37}$$

The block successive iteration scheme - P,QDC - is used.

For the solution of equation (5.36) the d.c. variables are considered constant and the convertors are therefore modelled simply as the appropriate real power load at the terminal busbars.

5.4.1.3 Programming Considerations for the Unified Algorithms

In order to retain the efficiency of the fast decoupled load flow, the B' and B" matrices must be factorised only once, before the iterative process begins.

The method of solving equations (5.34) and (5.35) is therefore

the key to the feasibility of any unified method utilising the fast decoupled a.c. algorithm.

The jacobian elements related to the d.c. variables are non-constant and must be re-evaluated at each iteration. It is therefore necessary to separate the constant and non-constant parts of the equations for the solution routine.

By manipulation of the factorisation process, Bodger[35] developed a method to enable the constant and non-constant parts to be factorised and processed separately. The constant part is factorised only once, before the iteration process as in the usual fast decoupled a.c. load flow. The method requires a trivial modification to the existing a.c. load flow algorithm.

The technique is explained here with reference to a single d.c. convertor. It is however, equally applicable for any number of convertors.

Initially, the a.c. fast decoupled equations are formed with the d.c. link ignored (except for the minor addition of the filter reactance at the appropriate a.c. busbar). The reactive power mismatch equation for the a.c. system is:

$$\begin{bmatrix} \Delta\bar{Q}/\bar{V} \\ \Delta Q'_{term}/V_{term} \end{bmatrix} = \begin{bmatrix} B'' \end{bmatrix} \begin{bmatrix} \Delta\bar{V} \\ \Delta V_{term} \end{bmatrix} \qquad (5.38)$$

where $\Delta Q'_{term} = Q^{sp}_{term} - Q_{term(ac)}$ is the mismatch calculated in the absence of the d.c. convertor

and $[B'']$ is the usual constant a.c. fast decoupled jacobian.

After triangulation down to, but excluding the busbars to

which d.c. convertors are attached, equation (5.39) results:

$$\begin{bmatrix} (\Delta\bar{Q}/\bar{V})'' \\ (\Delta Q_{term}/V_{term})'' \end{bmatrix} = \begin{bmatrix} B''' & \\ & B'''_{ii} \end{bmatrix} \begin{bmatrix} \Delta\bar{V} \\ \Delta V_{term} \end{bmatrix} \qquad (5.39)$$

$(\Delta\bar{Q}/\bar{V})''$ and $(\Delta Q_{term}/V_{term})''$ signify that the left hand side vector has been processed. Matrix [B'''] is the matrix [B"] after triangulation.

This triangulation (performed before the iterative process) may be achieved simply by inhibiting the terminal busbars being used as pivots during the optimal ordering process.

The processing of $\Delta\bar{Q}$ indicated in the equation is actually performed by the standard forward reduction process used at each iteration.

The d.c. convertor equations may then be combined with equation (5.39) as follows:

$$\begin{bmatrix} (\Delta\bar{Q}/\bar{V})'' \\ \left(\frac{\Delta Q_{term}}{V_{term}}\right)'' + \frac{\Delta Q_{term(dc)}}{V_{term}} \\ \bar{R} \end{bmatrix} = \begin{bmatrix} 0 & B''' & 0 \\ 0 & B'''_{ii}+B''_{ii(dc)} & AA'' \\ 0 & BB'' & A \end{bmatrix} \begin{bmatrix} \Delta\bar{V} \\ \Delta V_{term} \\ \Delta\bar{x} \end{bmatrix} \qquad (5.40)$$

where $B''_{ii(dc)} = \frac{1}{V_{term}} \left[\partial Q_{term(dc)}/\partial V_{term}\right]$.

The unprocessed section, ie,

$$\begin{array}{|c|} \hline \left(\frac{\Delta Q_{term}}{V_{term}}\right)'' + \frac{\Delta Q_{term(dc)}}{V_{term}} \\ \hline \bar{R} \\ \hline \end{array} \quad \begin{array}{|c|c|} \hline B'''_{ii} + B''_{ii(dc)} & AA'' \\ \hline BB'' & A \\ \hline \end{array} \quad \begin{array}{|c|} \hline \Delta V_{term} \\ \hline \Delta\bar{x} \\ \hline \end{array}$$

(5.41)

may then be solved by any method suitable for non-symmetric matrices.

The values of $\Delta\bar{x}$ and ΔV_{term} are obtained from this equation. The value of ΔV_{term} is then used to enable the usual back substitution process for the remaining $\Delta\bar{V}$ to be completed, ie. equation (5.39) is solved for $\Delta\bar{V}$.

The most efficient method for solving equation (5.41) depends on the number of convertors. For six convertors or more the use of sparsity storage and solution techniques are justified; otherwise all elements should be stored. Bodger[35] found that the best method was a modified form of gaussian elimination where all elements were stored but only non-zero elements processed.

It is important to note that the unified solution of equation (5.34) or (5.35) is performed retaining all the computational advantages of the constant and symmetric a.c. system jacobians and that this is achieved with only minor modification to the a.c. solution procedure. Matrix and vector elements are simply withdrawn and replaced after the standard forward reduction and back substitution processes.

The only computational difference between a unified and a comparable sequential iteration is that the d.c. jacobian equation (ie. 5.41 for the unified method) is slightly larger for the unified method. The difference is one additional row and column for each

convertor present. In terms of computational cost per iteration the corresponding unified and sequential algorithms are virtually identical.

5.4.2 Sequential Methods

The sequential methods are a further simplification of the unified method 2. The a.c. system equations are solved with the d.c. system modelled simply as a real or reactive power injection at the appropriate terminal busbar. For a d.c. solution the a.c. system is modelled simply as a constant voltage at the convertor a.c. terminal busbar.

The following three equations are solved iteratively to convergence.

$$[\Delta\bar{P}/\bar{V}] = [B'][\Delta\theta] \tag{5.42}$$

$$[\Delta\bar{Q}/\bar{V}] = [B''][\Delta\bar{V}] \tag{5.43}$$

$$[\bar{R}] = [A][\Delta\bar{x}] \tag{5.44}$$

The appeal of this method is its' simplicity. The a.c. load flow is not modified; a further iterative loop is simply added.

As mentioned in section 5.3.2 the variable ϕ may be removed from $\bar{x}$ for the sequential solutions. The sequential approach has been investigated with both ϕ included (5 variable model) and ϕ excluded (4 variable model).

Several iteration schemes have been investigated.

5.4.2.1 Sequential Method 1

The iteration sequence is illustrated in the flow chart of Fig. 5.4 and may be summarised as follows:

(i) Calculate $\Delta\bar{P}/\bar{V}$, solve equation (5.42) and update $\bar{\theta}$.

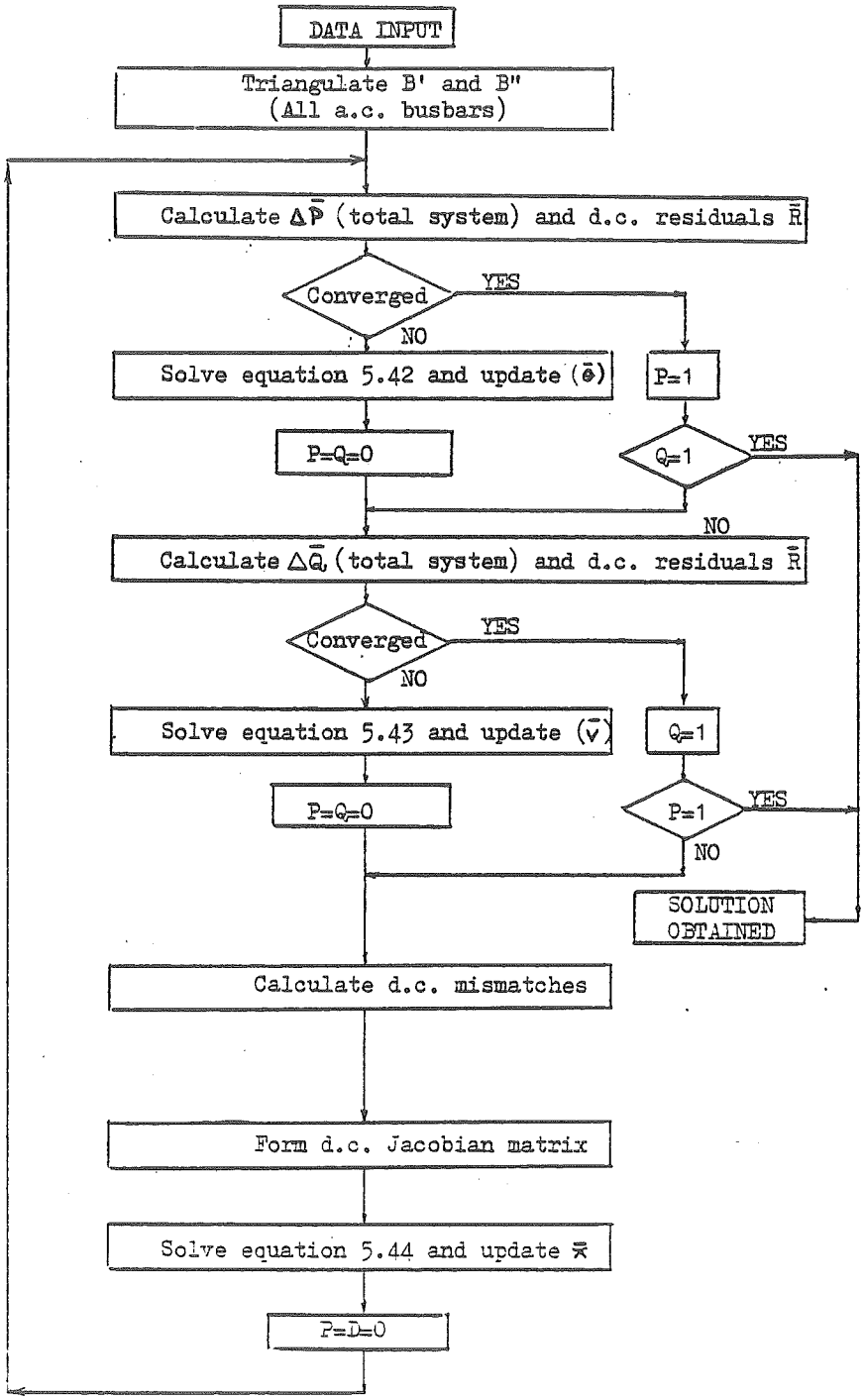

Fig. 5.4 Flow Chart for Sequential Single Phase A.C./D.C. Load Flow

(ii) Calculate $\Delta\bar{Q}/\bar{V}$, solve equation (5.43) and update $\bar{V}$.

(iii) Calculate d.c. residuals, $\bar{R}$, solve equation (5.44) and update $\bar{x}$.

(iv) Return to (i).

This sequence is referred to as P,Q,DC.

With reference to Fig. 5.4 the following features are noteworthy:

(i) To enable the number of iterations required for corresponding unified and sequential algorithms to be compared directly the convergence testing for the sequential algorithm is identical to that used in the unified case.

(ii) The d.c. equations are continued to be solved until both a.c. and d.c. systems have converged. This ensures that the sequential technique is an exact parallel of the corresponding unified algorithm.

These features are common to all the sequential algorithms presented in this chapter. It should, however, be noted that an advantage of the sequential method is that the d.c. equations need not be solved for the entire iterative process. Once the d.c. residuals have converged the d.c. system may be modelled simply as fixed real and reactive power injections at the appropriate convertor terminal busbar. The d.c. residuals must still be checked after each a.c. iteration to ensure that the d.c. system remains converged. However the computational cost of a d.c. iteration is, in any practical situation, only a fraction of the cost of an a.c. iteration and this advantage is therefore not considered significant.

5.4.2.2 Sequential Method 2

The iteration sequence differs from that of method 1 in that the

d.c. equations are solved after each real power as well as after each reactive power iteration. This sequence is summarised as P,DC,Q,DC. As in the previous method the d.c. equations are solved until all mismatches are within tolerance.

5.5 CONTROL OF CONVERTOR A.C. TERMINAL VOLTAGE

A convertor terminal voltage may be specified in two ways. Firstly by local reactive power injection at the terminal. In this case no reactive power mismatch equation is necessary for that busbar and the relevant variable (ie. ΔV_{term}) is effectively removed from the problem formulation. This is the situation where the convertor terminal busbar is a P.V busbar. Two control specifications are required for each d.c. convertor.

Alternatively the terminal voltage may be specified as a d.c. system constraint. That is, the d.c. convertor must inject the correct amount of reactive power so that the terminal voltage is maintained constant. This constraint is usually applicable in cases where the d.c. convertor model is extended to include additional items of plant[44] such as synchronous machines which are operated as an integral part of the convertor control. In such cases the convertor model may produce or absorb reactive power. For the basic convertor unit the terminal voltage may be controlled over a small range by altering the reactive power absorbed by the convertor.

With the unified method the equation,

$$V^{sp}_{term} - V_{term} = 0$$

is written as one of the two control equations. This would lead

to a zero row in equation (5.34) and therefore during the solution of equation (5.34) some other variable (eg. tap ratio) must be specified instead. The d.c. convergence is therefore marginally slowed for the PDC,QDC iteration. However the d.c. is overconverged by this iteration scheme and the slowing of the d.c. convergence does not have any noticeable effect on the overall convergence rate.

With the sequential method this control equation cannot be written. The terminal busbar is specified as a P.V busbar and the control equation

$$Q^{sp}_{term(dc)} - Q_{term(dc)} = 0$$

is used, where $Q^{sp}_{term(dc)}$ is taken as the reactive power required to maintain the voltage constant. The specified reactive power varies at each iteration and this discontinuity slows overall convergence.

This case is discussed for completeness; results are not given as, with the basic convertor model, the control of the terminal voltage by the d.c. system, is not a practical proposition.

5.6 CONSTANT D.C. JACOBIAN METHODS

With both the unified and sequential methods the jacobian elements related to the d.c. variables undergo only slight numerical change at each iteration; especially so, if good starting values are used. This prompted examination of the following algorithmic variations:

(i) The d.c. related jacobians are held constant at their initial values.

(ii) With assumptions for the values of the d.c. variables the jacobian may be approximated to a constant.

With the d.c. related jacobians constant all matrices, in

both the unified and sequential methods, may be factorised before the iterative procedure.

However, the dimension of the a.c. system is normally much greater than that of the d.c. system and the small savings in computing time per d.c. iteration are outweighed by an occasional deterioration in overall convergence. The advantages of these methods are therefore questionable and they were not pursued further.

5.7 EXTENSION TO MULTIPLE AND/OR MULTI-TERMINAL D.C. SYSTEMS

The basic algorithms have been developed for a single d.c. convertor. Each additional convertor adds a further five d.c. variables and a corresponding set of five equations. The number of a.c. system jacobian elements which become modified in the unified solutions is equal to the number of convertors.

As an example, consider the system shown in Fig. 5.5. The system represents the North and South Islands of the New Zealand Electricity Division's 220Kv a.c. system. At present convertors 1, 2 and 3 are in operation. Convertors 1 and 2 form the 600 MW, 500 Kv d.c. link between the two Islands. Convertor 3 represents a 420 MW aluminium smelter. The South Island may have some surplus hydro power in the future and the possibility of a further d.c. link to carry such power from the remote hydro generation in the South to two load centres, one in each Island, is under consideration. To this end, a further three terminal d.c. interconnection has been added. (Convertors 4,5 and 6.)

Normally, convertor 4 will operate in the rectifier mode with convertors 5 and 6 in the inversion mode.

The reactive power-d.c. jacobian for the unified method has the structure illustrated in equation (5.45).

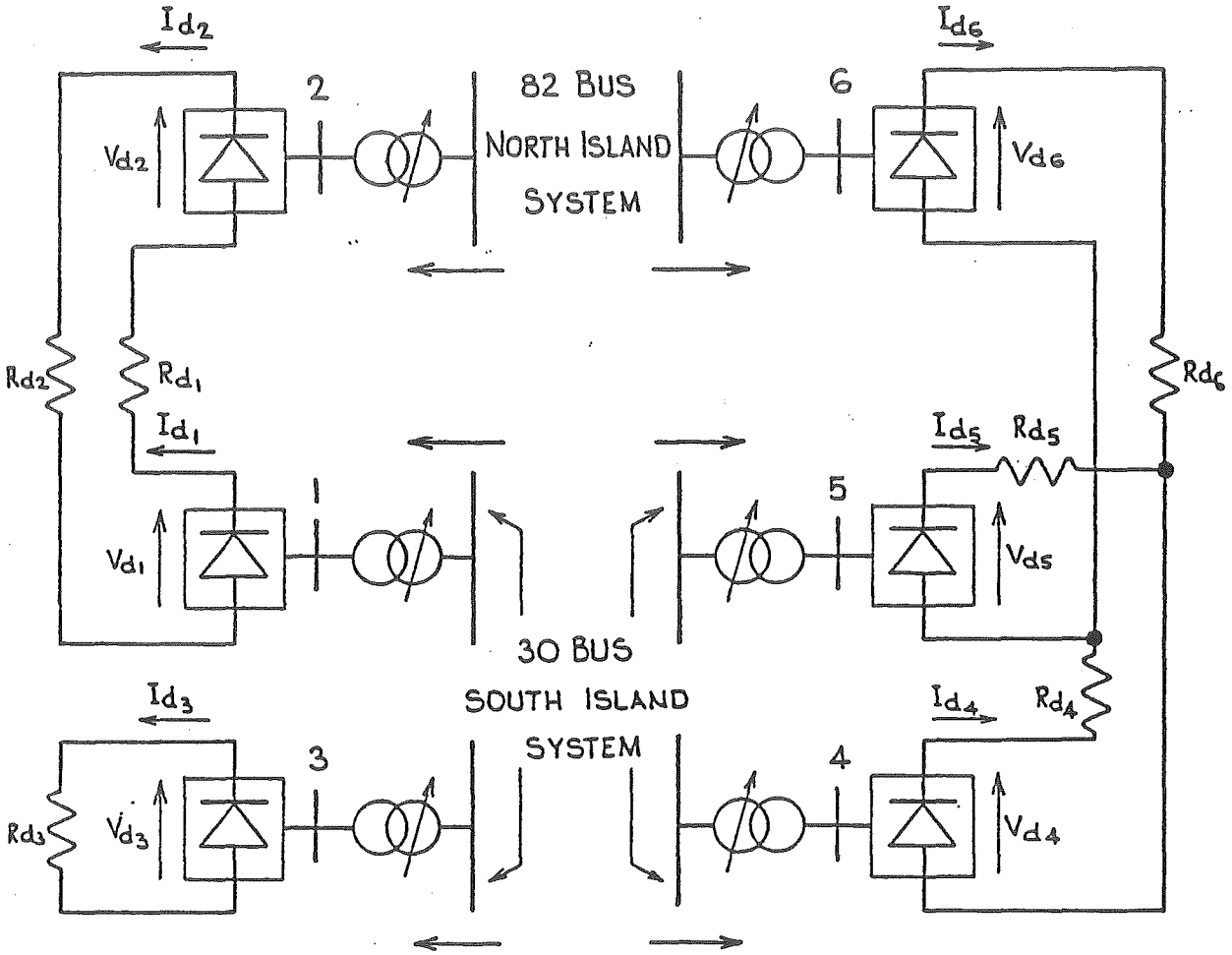

Fig. 5.5 Multiterminal D.C. System

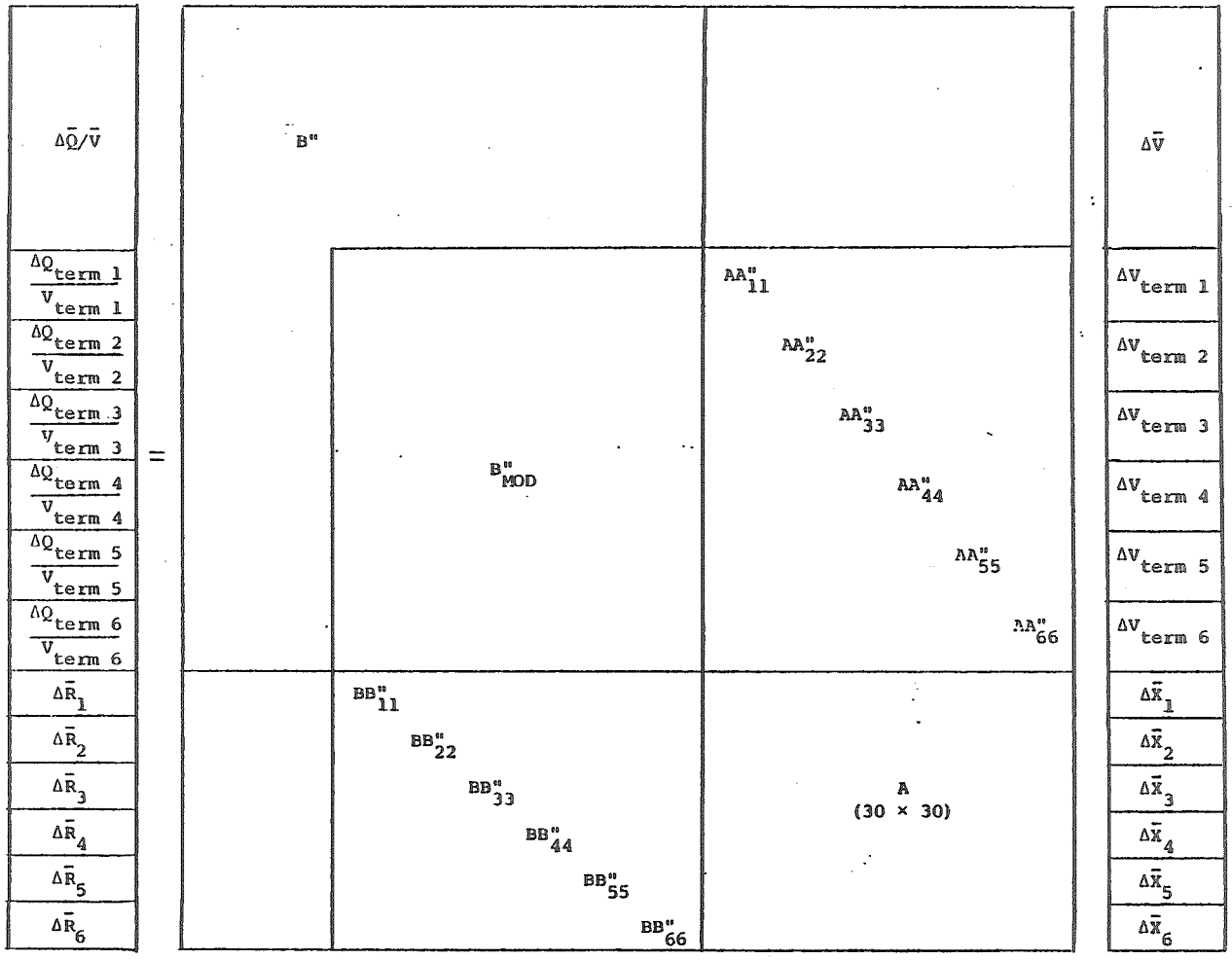
$\Delta\bar{Q}/\bar{V}$
$\Delta Q_{term\ 1}/V_{term\ 1}$
$\Delta Q_{term\ 2}/V_{term\ 2}$
$\Delta Q_{term\ 3}/V_{term\ 3}$
$\Delta Q_{term\ 4}/V_{term\ 4}$
$\Delta Q_{term\ 5}/V_{term\ 5}$
$\Delta Q_{term\ 6}/V_{term\ 6}$
$\Delta\bar{R}_1$
$\Delta\bar{R}_2$
$\Delta\bar{R}_3$
$\Delta\bar{R}_4$
$\Delta\bar{R}_5$
$\Delta\bar{R}_6$
=
B"
$B"_{MOD}$
$AA"_{11}$
$AA"_{22}$
$AA"_{33}$
$AA"_{44}$
$AA"_{55}$
$AA"_{66}$
$BB"_{11}$
$BB"_{22}$
$BB"_{33}$
$BB"_{44}$
$BB"_{55}$
$BB"_{66}$
A
(30 × 30)
$\Delta\bar{V}$
$\Delta V_{term\ 1}$
$\Delta V_{term\ 2}$
$\Delta V_{term\ 3}$
$\Delta V_{term\ 4}$
$\Delta V_{term\ 5}$
$\Delta V_{term\ 6}$
$\Delta\bar{X}_1$
$\Delta\bar{X}_2$
$\Delta\bar{X}_3$
$\Delta\bar{X}_4$
$\Delta\bar{X}_5$
$\Delta\bar{X}_6$

(5.45)

where B''_{MOD} is the part of B" which becomes modified. Only the diagonal elements become modified by the presence of the convertors.

Off diagonal elements will be present in B''_{MOD} if there is any a.c. connection between convertor terminal busbars.

Note: All off diagonal elements of BB" and AA" are zero.
In addition, matrix A is block diagonal in 5 × 5 blocks with the exception of the d.c. interconnection equations.

Equation R(3) in each set of d.c. equations is derived from the d.c. interconnection. For the six convertor system shown in Fig. 5.5 the following equations are applicable.

$$V_{d1} + V_{d2} - I_{d1}(R_{d1} + R_{d2}) = 0$$

$$V_{d3} - I_{d3} \cdot R_{d3} = 0$$

$$I_{d1} - I_{d2} = 0$$

$$V_{d4} + V_{d6} - I_{d4} \cdot R_{d4} - I_{d6} \cdot R_{d6} = 0$$

$$V_{d5} - V_{d6} - I_{d5} \cdot R_{d5} + I_{d6} \cdot R_{d6} = 0$$

$$I_{d4} - I_{d5} - I_{d6} = 0$$

This example indicates the ease of extension to the multiple convertor case.

5.8 INITIAL CONDITIONS

Initial values for the d.c. variables $\bar{x}$ are assigned from estimates for the d.c. power and d.c. voltage and assuming a power factor of 0.9 at the convertor terminal busbar. The terminal busbar voltage is set at 1.0 p.u. unless it is a voltage controlled busbar.

This procedure gives adequate initial conditions in all practical cases as good estimates of P_{dc} and V_{dc} are obtainable.

The effect of initial conditions on the convergence is examined in section 5.10.

5.9 D.C. CONVERGENCE TOLERANCE

A feature which is common to all methods is the requirement of a convergence tolerance for the d.c. residuals $\bar{R}$.

The aim of the combined a.c. d.c. load flow is to give information regarding power flows, line losses and voltage magnitudes for both the a.c. and d.c. systems. In addition, the requirements of the d.c. convertors in regard to reactive power demand and convertor transformer tap ranges may be studied.

The accepted tolerance for a.c. load flow is 0.1 MW or MVAR for the maximum power mismatch at any busbar. Similar power tolerances are acceptable for the d.c. system.

The d.c. p.u. system is based upon the same power base as the a.c. system and on the nominal open circuit a.c. voltage at the convertor transformer secondary. The p.u. tolerances required for d.c. powers, voltages and currents are therefore comparable with those adopted in the a.c. system.

The only d.c. residual equations not in terms of these quantities are some of the control equations. With reference to section 5.3.4 and 5.3.5 it may be seen that these equations are of the form,

$$X - X^{sp} = 0$$

where X may be the tap or cosine of the firing angle. It is important to note that these equations are linear and are solved exactly in one

d.c. iteration. The question of an appropriate tolerance for these mismatches is therefore irrelevant.

An acceptable tolerance for the d.c. residuals which is compatible with the a.c. system tolerance is therefore 0.001 p.u. on a 100 MVA base ie. the same as that adopted for the a.c. system.

5.10 TEST SYSTEM AND RESULTS

The A.E.P. standard 14 bus test system has been used to investigate the convergence properties of the proposed algorithms. The a.c. transmission line between busbars 5 and 4 has been replaced by a two terminal h.v.d.c. link. Neither bus is a voltage controlled busbar and the iteraction between a.c. and d.c. systems will therefore be considerable.

A comprehensive range of control strategies have been applied to the link and the convergence results for the various algorithms are given in Table 5.1. The number of iterations (m,n) should be interpreted as follows.

- m is the number of reactive power-voltage updates required
- n is the number of real power-angle updates.

The number of d.c. iterations varies for the different sequences, however this is of secondary importance and may, if required, be assessed in each case from the number of a.c. iterations. In terms of computational cost a unified QDC iteration is equivalent to a Q iteration and a DC iteration executed separately.

The d.c. link data and specified controls for case 1 are given in Table 5.2. The link operation is illustrated in Fig. 5.6. The specified conditions for all cases are derived from the results of

Table 5.1 Convergence Results

Case Specification		Number of iterations to convergence (0.1 MW/MVAR)					
Specified d.c. link constraints m-rectifier end n-invertor end		Unified Methods (5 variables)		Sequential Methods (5 variables)		(4 variables)	
		^{1}PDC,QDC	^{2}P,QDC	^{1}P,Q,DC	^{2}P,DC,Q,DC	^{1}P,Q,DC	^{2}P,DC,Q,DC
1	α_m P_{dm} γ_n V_{dn}	4,3	4,3	4,3	4,3	4,4	4,3
2	α_m P_{dm} a_n V_{dn}	4,3	4,3	4,4	5,5	4,4	failed
3	a_m P_{dm} a_n V_{dn}	4,3	4,3	4,4	5,5	4,4	failed
4	a_m P_{dm} γ_n V_{dn}	4,3	4,3	4,4	4,4	4,4	4,4
5	a_m P_{dm} γ_n a_n	4,3	4,3	4,4	4,4	4,4	4,4
6	a_m P_{dm} α_m γ_n	4,3	4,3	4,3	4,3	4,4	4,3
7	α_m I_d γ_n V_{dn}	4,3	4,3	4,3	4,3	4,4	4,3
8	a_m V_{dm} γ_n P_{dn}	4,3	4,3	4,4	4,4	4,4	4,4
	Case 1 with initial condition errors						
9	50% error	4,3	4,3	4,4	4,3	4,4	4,3
10	80% error	5,4*	6,5*	7,6*	5,4*	4,4	4,3

where * indicates a false solution

Table 5.2 Characteristics of d.c. link

	Convertor 1	Convertor 2
A.C. Busbar	Bus 5	Bus 4
D.C. Voltage base	100 kV	100 kV
Transformer Reactance	0.126	0.0728
Commutation Reactance	0.126	0.0728
Filter admittance Bf*	0.478	0.629
D.C. link resistance	0.334 ohms	
Control parameters for Case 1		
D.C. link power	58.6 MW	-
Rectifier firing angle (deg)	7	-
Invertor extinction angle (deg)	-	10
Invertor d.c. voltage	-	-128.87 kV

* Filters are connected to a.c. terminal busbar.

Note: All reactances are in p.u. on a 100 MVA base.

case 1. All cases therefore yield the same d.c. operation.

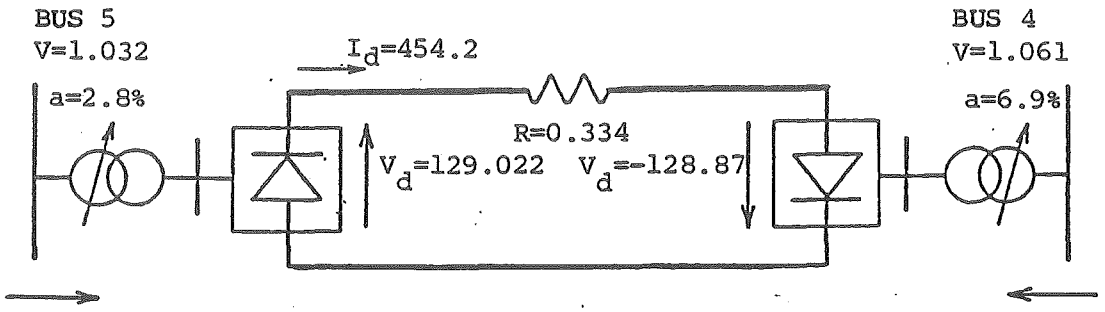

P = 58.60	α = 7.0	γ = 10.0	P = -58.31
Q = 18.79	μ = 17.32	μ 10.33	Q = 16.78

All angles are in degrees. D.C. voltages and current are in kV and Amps respectively. D.C. resistance is in ohms. A.C. powers (P,Q) are in MW and MVARs.

Fig. 5.6 D.C. Link Operation

The a.c. system in isolation (i.e. with the d.c. system modelled by the equivalent a.c. loads) requires (4,3) iterations.

The d.c. system in isolation (i.e. operating from fixed terminal voltages) requires 2 iterations under all control strategies. A typical convergence pattern for the terminal power flows, P_{term} and Q_{term}, is illustrated in Fig. 5.7. The example given has poor starting values.

The additional iterations required for the combined a.c./d.c. systems by many of the sequential versions is therefore due to the interaction between the two systems.

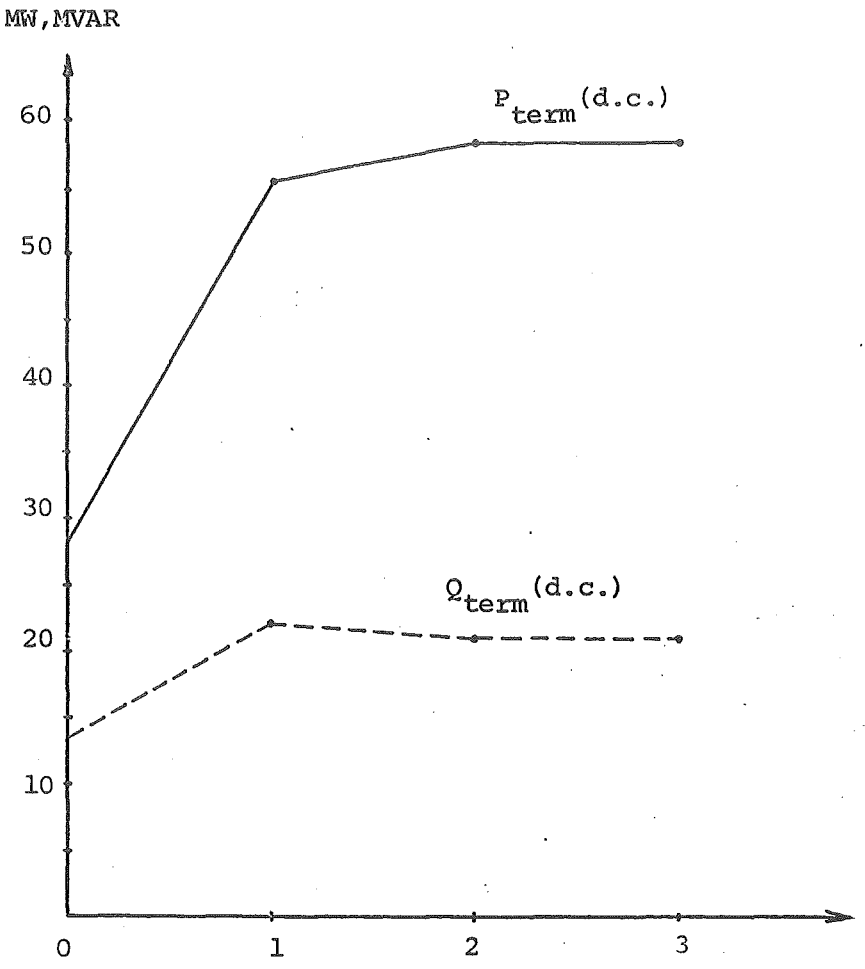

Fig. 5.7 Convergence Pattern For D.C. System In Isolation

5.11 DISCUSSION OF RESULTS

The convergence results shown in Table 5.1 expose several significant features of the a.c./d.c. load flow algorithms which have been developed. These features are discussed in the following sections.

5.11.1 Unified Methods

The unified methods provide fast and reliable convergence in all cases.

For the unified methods 1 and 2 the number of iterations did not exceed the number required for the a.c. system alone.

5.11.2 Sequential Method 1 (- P,Q,DC -)

Convergence was fast and reliable although the reactive power convergence was slower than for the a.c. system alone. This caused an extra Q iteration to be required in many cases.

The removal of the variable ϕ caused a slight deterioration in performance. An investigation of the mismatches at each iteration showed that $Q_{term}(dc)$ actually converges faster when ϕ is removed. However, the faster convergence pattern is also more oscillatory and these oscillations are reflected in a slowing of overall voltage convergence in the a.c. system.

5.11.3 Sequential Method 2 (- P,DC,Q,DC -)

The occasional deterioration in performance (cases 2 and 3) has been traced to the first d.c. iteration when the a.c. terminal voltage is at the initial value of 1.0 p.u. The feature common to cases 2 and 3 is that both the transformer tap and d.c. voltage are specified at the invertor end. In order to maintain the specified

d.c. voltage from a fixed a.c. terminal voltage of 1 p.u. and with a fixed tap, the firing angle must decrease. In order to satisfy the equation,

$$V_d = K_1 \cdot a \cdot V_{term} \cdot \cos(\pi - \gamma) + \frac{3}{\pi} \cdot X_c \cdot I_d$$

the control variable $\cos(\pi - \gamma)$ is actually updated to be less than -1. Although physically unobtainable this presents no mathematical problem unless the variable γ is explicitly required.

Similarly, with the five variable version, the equation

$$V_d = K_1 \cdot a \cdot V_{term} \cdot \cos \phi$$

causes the variable ϕ to be updated for minimum $\cos \phi$ (i.e. approaching -1). $Q_{term}(dc)$ is therefore in considerable error.

The next d.c. iteration follows a reactive power voltage update and the d.c. is converged to be compatible with a better (in this case higher) a.c. terminal voltage and convergence to the correct solution is subsequently obtained. The variations in the reactive power which occur do, however, slow the overall convergence.

In the 4 variable version, ϕ is absent. The calculation of $Q_{(dc)}$ by equation 5.21 requires a value for ϕ which may be calculated from

$$\phi = \cos^{-1}\left(\frac{V_d}{K_1 \cdot a \cdot V_{term}}\right)$$

when both a and V_d are specified and with a value of V_{term} of 1 p.u., the inverse cosine argument is greater than 1 and ϕ cannot be calculated. The 4 variable version is recorded as having failed in these cases although it should be noted that with appropriate limits on the inverse cosine argument convergence may be obtained.

5.11.4 Dependence on Starting Values

The starting value for the a.c. terminal voltages is 1 p.u. as this is usually the best estimate available. The d.c. starting values are calculated from an estimate of the d.c. power and d.c. voltage. These estimates determine the initial values for the real and reactive power mismatches at the convertor terminal busbars. They are therefore relevant to the variation in the a.c. terminal voltage.

With starting values for d.c. real and reactive powers within ± 50%, which are available in all practical situations, all algorithms converged rapidly and reliably (see case 9).

For completeness it is instructive to consider a rather impractical case, such as 10, which has initial estimates for the d.c. variables such that the terminal powers are in error by - 80%. All methods which retain the variable ϕ converged to an incorrect solution. The convertor is generating, rather than absorbing, reactive power, i.e. the variable cos ϕ is correct, and equation (5.15) is satisfied, but this occurs with ϕ being negative instead of positive. This problem cannot occur with the 4 variable versions. It should also be noted that with limits placed on ϕ the correct solution may be obtained.

5.12 OTHER ITERATION SCHEMES

The iteration schemes reported have all begun with a real power-angle update iteration. As the operation of the d.c. convertors is strongly related to the voltage magnitudes the idea of initiating the solution sequence with a reactive power-voltage update iteration is appealing. This was tested with both the unified and sequential

methods. Rapid and reliable convergence was obtained in all cases.

However, Stott and Alsac[30] reported generally improved performance of the a.c. load flow by initiating the iterative process with a real power iteration.

Moreover, from the results obtained it is clear that for the best a.c./d.c. methods, convergence depends on the a.c. system itself i.e. the overall convergence rate does not suffer with integration of the d.c. equations.

Therefore, although the iteration schemes which begin with a reactive power iteration improve the reliability of the sequential integration, it is not recommended.

5.13 DISCUSSION OF CONVERGENCE PROPERTIES

The overall convergence rate of the algorithms depends on the successful interaction of the two distinct parts. The a.c. system equations are solved using the well behaved constant tangent fast decoupled algorithm; the d.c. system equations are solved using the more powerful, but somewhat more erratic, full Newton-Raphson approach.

In general, the solution times for the d.c. equations will be small compared to the solution time of the a.c. equations. The relative efficiencies of the alternative algorithms may therefore be assessed by comparing the number of a.c. voltage and angle updates which are required.

Comparing corresponding unified and sequential schemes the unified method gives more robust and dependable performance. The unified method 2 (i.e. P,QDC) is the best algorithm which has been been investigated. The performance of the unified method 1 (PDC,QDC)

is comparable but the d.c. equations are effectively solved twice as often and this method is therefore slightly less efficient. Of the sequential methods, the sequential method 1 (P,Q,DC) proved the best; being only marginally inferior to the unified method.

Those schemes which acknowledge the fact that the d.c. variables are strongly related to the terminal voltage give the fastest and most reliable performance. In these schemes the first d.c. iteration occurs alongside or following the first alteration of system voltages.

The powerful convergence of the Newton-Raphson process for the d.c. equations can cause overall convergence difficulties. If the first d.c. iteration occurs before the reactive power voltage update then the d.c. variables are converged to be compatible with the incorrect terminal voltage. This introduces an unnecessary discontinuity which may lead to convergence difficulties in the sequential method. In the unified approach the powerful convergence of the d.c. equations is dampened by the reflection of the a.c. mismatches onto the changes in d.c. variables. This gives faster and better behaved convergence.

When the busbar to which the convertors are attached is voltage controlled (as is often the case) the two approaches become virtually identical as the interaction between a.c. and d.c. systems is much smaller.

5.13.1 Generalisations On Convergence Properties

The unified and sequential algorithms have been investigated with reference to the well behaved 14 bus test system. If general conclusions are to be drawn regarding the performance of the algorithms then further investigation is required.

With reference to the results already presented and based on

experience with other systems, the performance of the a.c./d.c. load flow is dependent on the following:

(i) The initial values of the a.c. terminal voltage for the initial d.c. iteration (sequential method only).

(ii) The strength of the a.c. system at the terminal busbar. This gives a measure of how the changing real and reactive powers of the d.c. convertor influences the a.c. system convergence.

(iii) The convergence pattern of the a.c. terminal busbar voltage.

The initial value of a.c. terminal voltage for the first d.c. iteration is, in the sequential method, determined by a normal fast decoupled a.c. iteration. The maximum error in this voltage will be small. Stott[30] reported maximum errors of around 3% even with difficult a.c. systems. The error may be slightly different for a.c./d.c. systems depending on the initial values for the d.c. variables, however, this error will be small in all practical cases.

The overall convergence of the a.c./d.c. load flow is therefore primarily due to the manner in which the a.c. terminal voltage varies with changing convertor power flows and vice versa.

The nature of the a.c. system and the rate at which it converges is not relevant to the behaviour of the integrated a.c./d.c. load flows except in as much as it influences features (ii) and (iii) above.

In order to investigate the performance of the algorithms with a weak a.c. system the test system described earlier was modified by the addition of two a.c. lines as shown in Fig. 5.8.

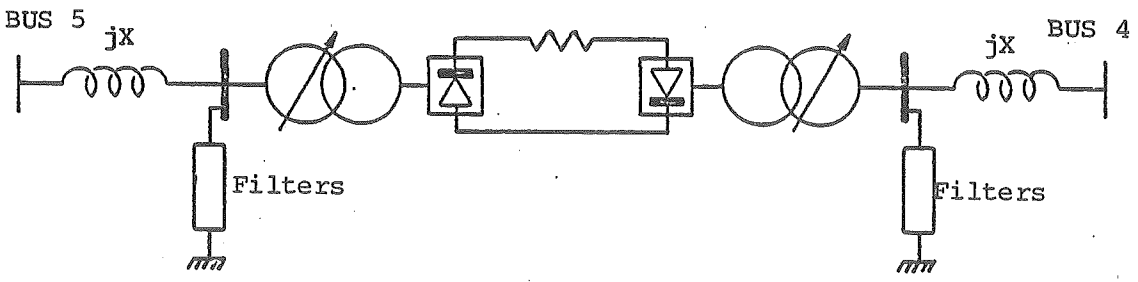

Fig. 5.8 D.C. Link Operating From Weak A.C. System

The reactive power compensation of the filters was adjusted to give similar d.c. operating conditions as previously.

The number of iterations to convergence for the most promising algorithms are shown in Table 5.3 for the control specifications corresponding to cases 1 to 5 in the previous results.

CASE	SPECIFICATION m-rectifier n-invertor	x = 0.3			x = 0.4		
		UNIFIED P,QDC	SEQUENTIAL P,Q,DC		UNIFIED P,QDC	SEQUENTIAL P,Q,DC	
			5V	4V		5V	4V
12	α_m P_{dm} γ_n V_{dn}	4,4	4,4	4,4	4,4	5,4	4,4
13	α_m P_{dm} a_n V_{dn}	4,4	9,8	10,12	4,4	>30	Diverges
14	a_m P_{dm} a_n V_{dn}	4,3	9,8	10,12	4,3	>30	Diverges
15	a_m P_{dm} γ_n V_{dn}	4,3	6,5	7,7	4,3	28,27	>30

Table 5.3 Numbers of Iterations for Weak A.C. Systems

The different nature of the sequential and unified algorithms is clearly demonstrated. The effect of the type of convertor control is also shown. For case 12 both the d.c. real power and the d.c. reactive powers are well constrained by the convertor control strategy. Convergence is rapid and reliable for all methods.

For all other cases, where the control angle at one or both convertors is free, an oscillatory relationship between a.c. terminal voltage and the reactive power of the convertor is possible. This leads to poor convergence of the sequential algorithms.

To illustrate the nature of the interaction the convergence pattern of the convertor reactive power demand and the a.c. system terminal voltage is plotted in Fig. 5.9 for the rectifier. The convergence patterns, under the same conditions, for the a.c. and d.c. systems in isolation are shown in Figs 5.10 and 5.11 respectively. The oscillatory interaction is clear in Fig. 5.8. Figs 5.9 and 5.10 demonstrate that this problem is purely due to the interaction and not due to any feature associated with either a.c. or d.c. system.

The nature of the problem is that when the firing angle is not specified and the d.c. voltage is effectively fixed, any increase in terminal voltage leads to an increase in firing angle and hence increase in the reactive power demand. The increased reactive power demand causes a subsequent decrease in terminal voltage during the following a.c. iteration and an ocsillatory pattern emerges. With a strong a.c. system the terminal voltage is well constrained and the oscillations are well damped.

It may be possible to alleviate some of the oscillatory problem by the use of acceleration factors or similar techniques. It is considered doubtful that the oscillation may be sufficiently dampened without detrimentally effecting convergence speed in well

(i) Sequential Method (P,Q,DC 5 Variable)

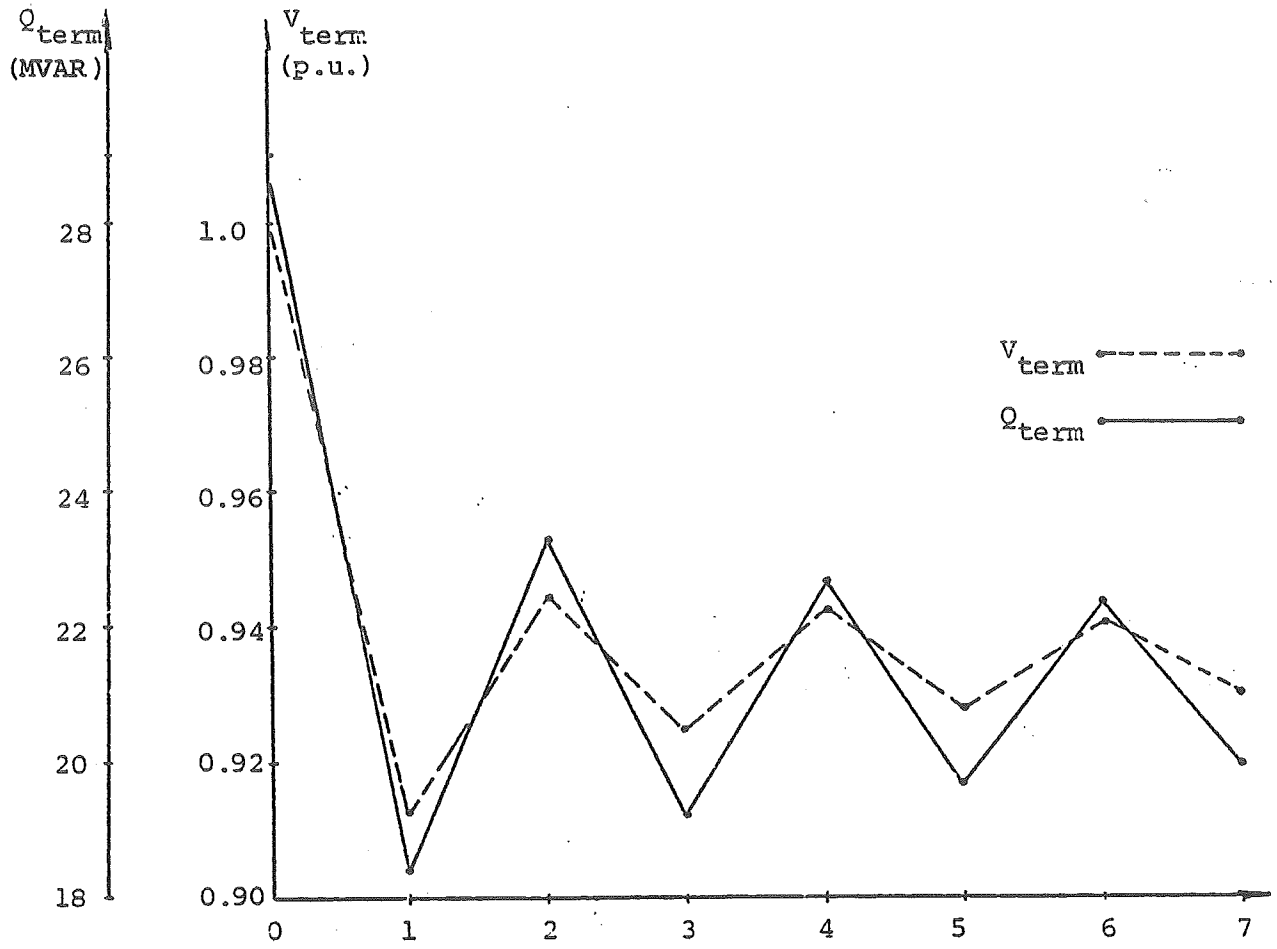

(ii) Unified Method (P,Q,DC)

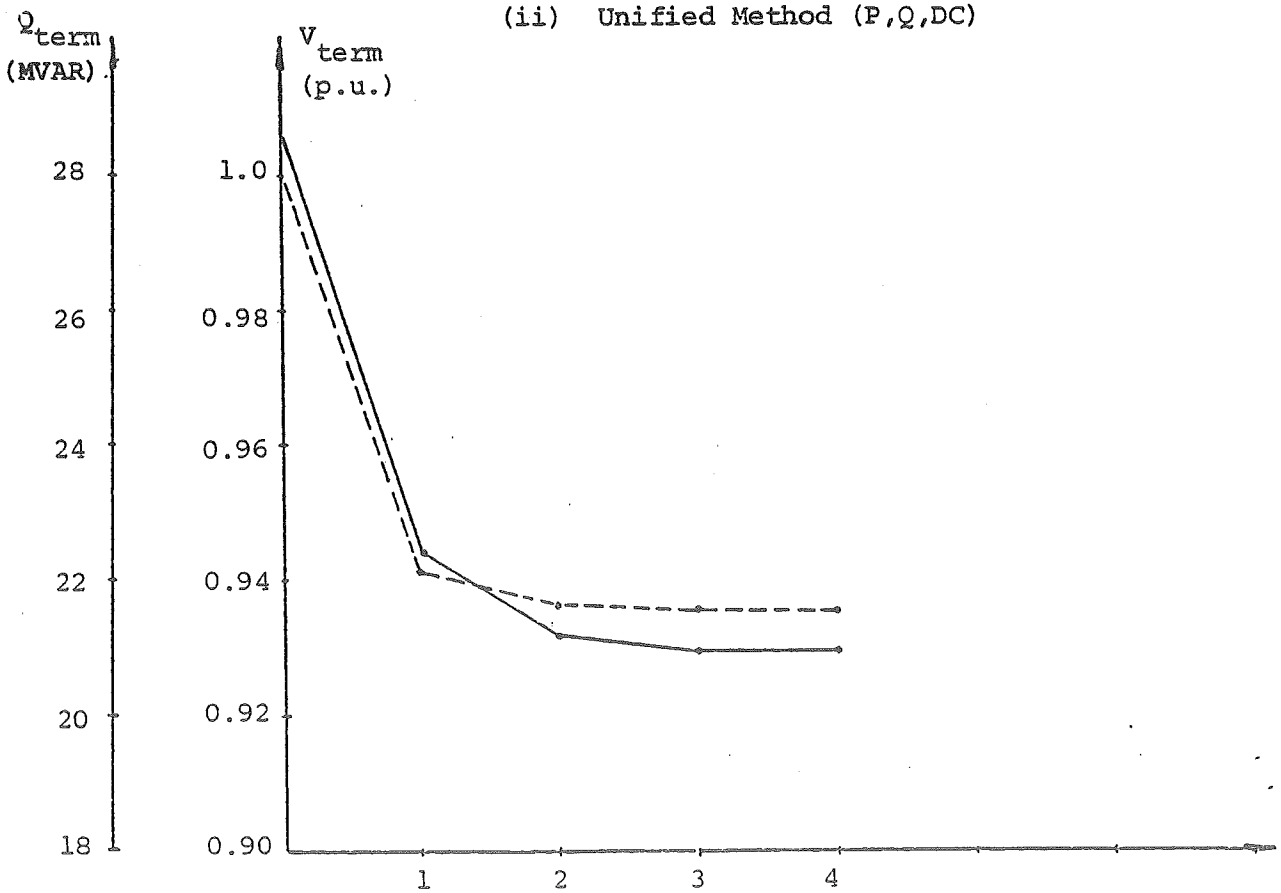

Fig. 5.9 Convergence Pattern for A.C./D.C. Load Flow with Weak A.C. System

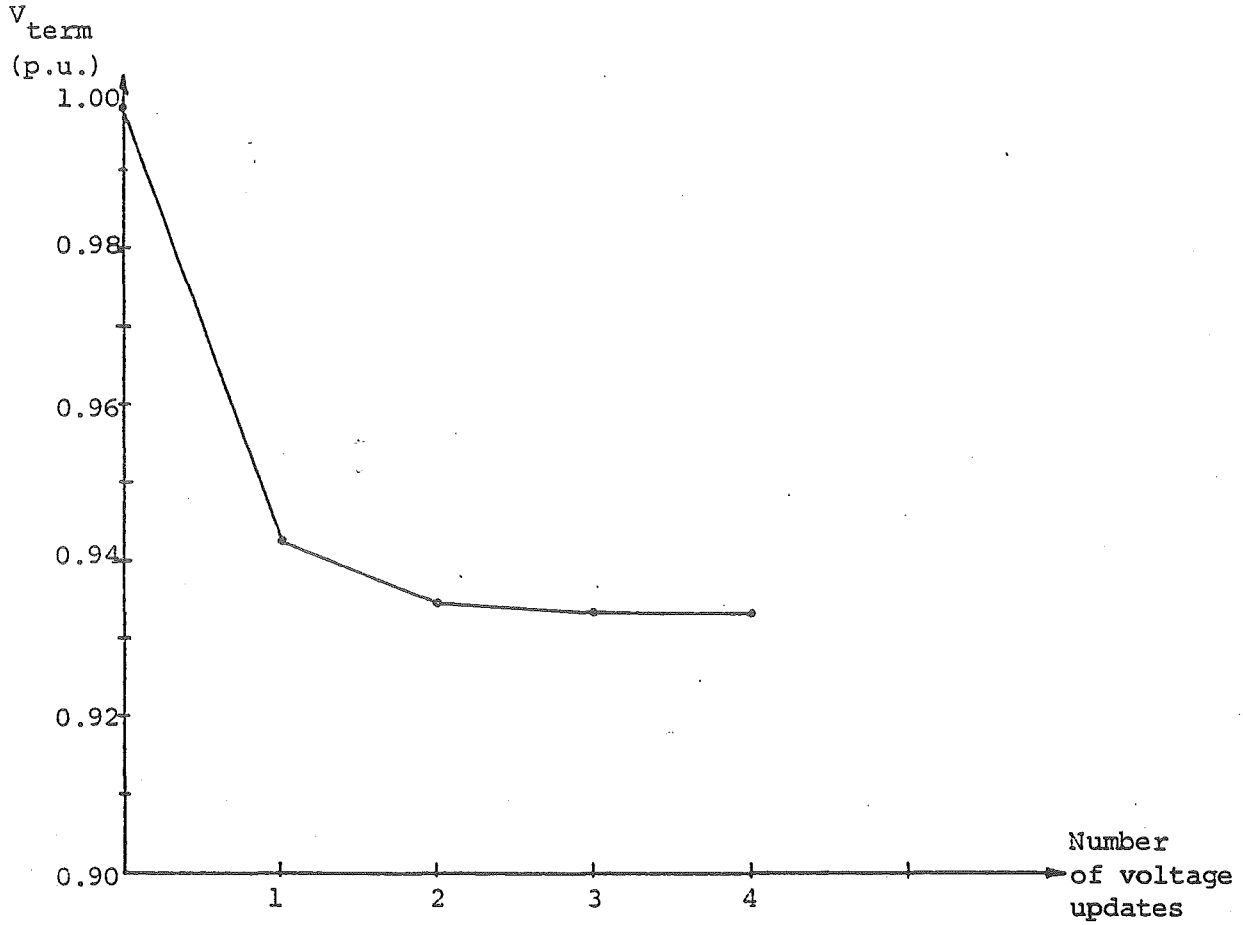

Fig. 5.10 Convergence Pattern of Terminal Voltage for Weak A.C. System

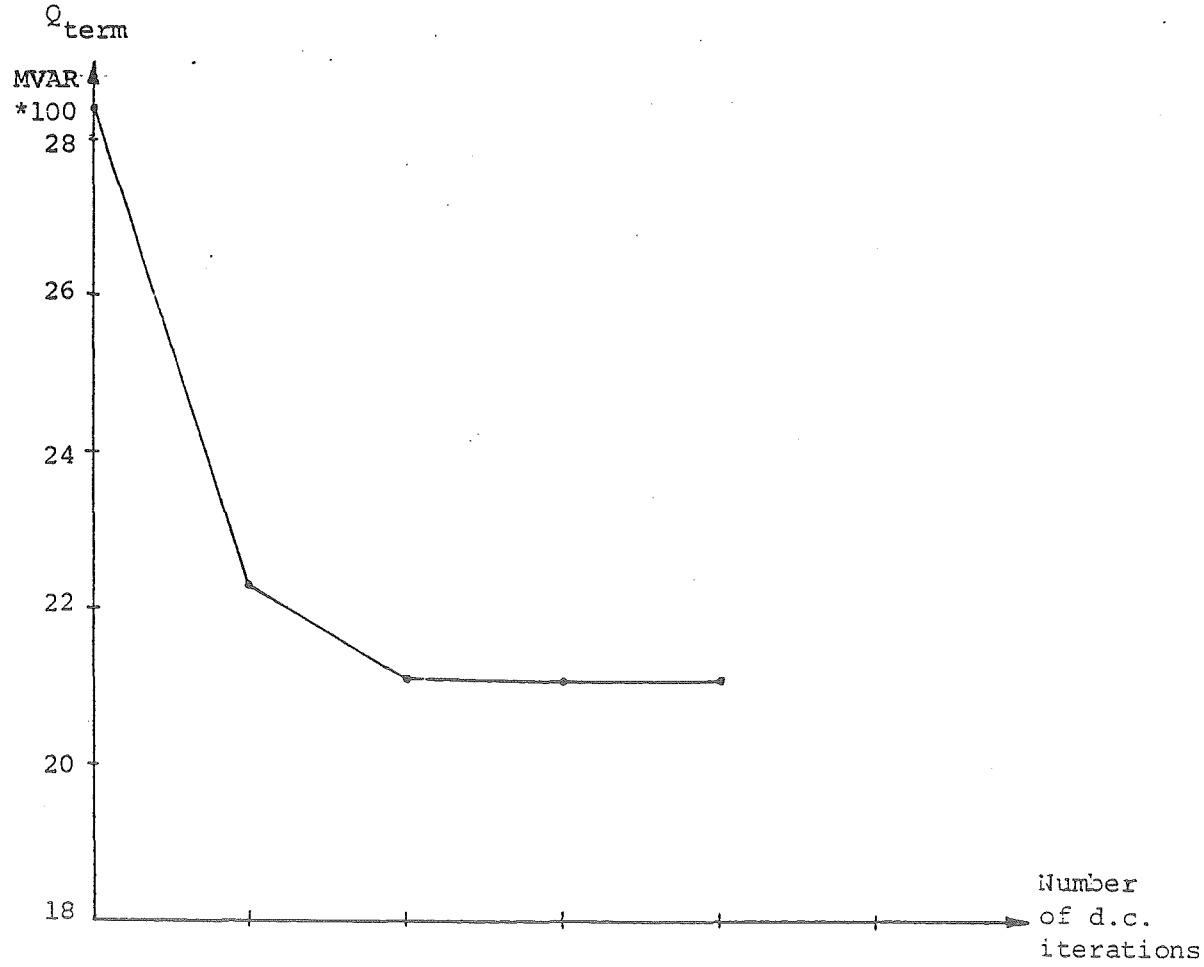

Fig. 5.11 Convergence Pattern of D.C. Reactive Power For D.C. in Isolation (i.e. fixed terminal voltage)

behaved cases.

5.13.2 General Conclusions on Convergence Properties

The features which influence the convergence of the unified and sequential algorithms have been discussed in some detail. The following general conclusions may be made:

- In cases where the a.c. system is strong both the unified and sequential algorithms may be programmed to give fast and reliable convergence.
- If the a.c. system is weak the sequential algorithm is susceptible to convergence problems.

A potential load flow user may assess the best method for their particular system.

The discussion on the strength of the a.c. system has been deliberately vague. The usual measure of the strength of an a.c. system containing a convertor installation is the short circuit ratio (SCR). The SCR is calculated from the fault MVA at the terminal busbar, and, as such, depends not only upon the lines and transformers but also on the machine transient or subtransient reactances. However, in load flow studies, these reactances are zero, that is, the machine terminal voltages represents an infinite busbar and the SCR does not therefore give an exact indication of the strength of the system. For example a small synchronous condensor attached to a busbar makes that busbar infinitely strong in a load flow sense while having a far smaller influence on the SCR.

A survey of existing schemes[43,46] indicates that, almost invariably, with systems of low SCR, some form of voltage control, often synchronous condensors, is an an integral part of the convertor

installation. These schemes are therefore often strong as far as the load flow is concerned.

A measure of the strength of a system in a load flow sense is the SCR calculated with all machine reactances set to zero. This short circuit ratio is invariably much higher than the usual value. It has been demonstrated in the previous section that the sequential load flow converges under all control strategies even down to a load flow SCR of around 3. In the usual sense the SCR of this system is considerably less than 3. Since SCR's below 3 are not encountered in practical convertor schemes it may be concluded that the sequential integration should converge in all practical situations although the convergence may become slow if the system is weak in a load flow sense.

The only disadvantage of the unified method is increased programming complexity; if this is not an important consideration then the unified method is to be preferred in all cases due to its greater inherent reliability. Experience with multiterminal d.c. systems has shown the features described here to be equally applicable.

CHAPTER 6

THREE PHASE A.C./D.C. LOAD FLOW ALGORITHM

6.1 INTRODUCTION

Any convertor which is operating from an unbalanced a.c. system will itself operate with unbalanced power flows and unsymmetric valve conduction periods. In addition any unbalance present in the convertor control equipment or any asymmetry in the convertor transformer will introduce additional unbalance.

Considerable interaction exists between the unbalanced operation of the a.c. and d.c. systems. The exact nature of this interaction depends on features such as the convertor transformer connection and the convertor firing controller.

One purpose of a detailed study of the unbalanced operation of a.c./d.c. systems is as an aid to system planning and development. Operation of high power convertors is being considered in situations of relatively low short circuit ratios. Unbalance effects are more likely to be significant under these conditions and may require additional consideration. The steady state unbalance and its' relevance to convertor harmonic current generation may also influence the consideration of possible transmission line transpositions and also the suitability of either synchronous or static reactive power compensation.

In addition the developed model and its' integration into the load flow provides an excellent basis for a thorough understanding of steady state convertor behaviour.

The fundamental frequency model derived here also provides a basis for an investigation of several features associated with the steady state harmonic interaction between d.c. convertors and the a.c. system. This subject is considered in the final chapters of this Thesis.

The present chapter is restricted to the study of the fundamental frequency unbalanced operation of integrated a.c./d.c. system.

Previous researchers[47] have developed coupled sequence representations to enable the convertor to be analysed in conjunction with the a.c. system. However the parameters of the coupled sequence impedances depend upon the operating conditions of the convertor; therefore they change at every iteration. In addition, the impedances are a mathematical artificiality and cannot be physically realised. These features make this approach unattractive.

Arrillaga et al[48] extended investigations into convertor unbalance and developed an equivalent sequence current generator concept for the unbalanced convertor.

The artificiality of modelling the convertor in terms of sequence components may be avoided simply by integrating the equations, in actual phase quantities, directly into a phase component, three phase load flow analysis.

The convertor model for unbalanced analysis is considerably more complex than that developed in the preceeding chapter for the balanced case. The additional complexity arises from the need to include the effect of the three phase convertor transformer connection and the different convertor firing control modes. Early h.v.d.c. control schemes were based on phase angle control, where the firing of each valve is timed individually with respect to the appropriate

crossing of the phase voltages. This control scheme has proved susceptible to harmonic stability problems when operating from a weak a.c. system. An alternative control, based on equidistant firings on the steady state, is generally accepted to provide greater inherent accuracy in the timing of firing pulses and also to provide more stable operation in the presence of weak a.c. systems.[49,50,51] Under normal steady state and perfectly balanced operating conditions there is no difference between these two basic control strategies. However, their effect on the a.c. system and d.c. voltage and current waveshapes during normal, but not balanced, operation, is quite different.

A three phase convertor model, with the flexibility to represent alternative control strategies, has been developed.

Although this chapter is restricted to considering the integration of the developed model with the three phase fast decoupled load flow described in chapter 4, the model may be used with any three phase load flow.

Similar techniques are available for the integration of the three phase convertor model into the load flow analysis as were discussed with respect to the balanced single phase analysis. Based upon the extensive investigations into the behaviour of single phase a.c./d.c. load flow described in chapter 5, the sequential approach is considered the most appropriate for the integration of the d.c. model into the three phase load flow. The complexity of the unified approach is not considered justified in the three phase case because, in cases of difficult convergence such as those involving very weak a.c. systems, it is possible to use starting values derived from single phase analysis.

This chapter describes the development of a model for the

unbalanced convertor and the subsequent integration of that model into the three phase fast decoupled load flow analysis. A summary of this chapter is contained in a paper[3] published in the Proc. IEE and reproduced in Appendix 6.

6.2 FORMULATION OF THE THREE PHASE A.C./D.C. LOAD FLOW PROBLEM

The aim of the three phase a.c./d.c. load flow is to solve for the unbalanced operating state of the combined a.c. and d.c. systems, under the specified conditions of load, generation and d.c. system control strategy.

The operating state of the combined system is defined by:

$$[\bar{V}_{int}, \bar{\theta}_{int}, \bar{V}, \bar{\theta}, \bar{x}]$$

where:

$\bar{V}_{int}/\bar{\theta}_{int}$ are the vectors of the balanced internal voltages at the generator internal busbars.

$\bar{V}/\bar{\theta}$ are vectors of the three phase voltages at every generator terminal busbar and every load busbar.

$\bar{x}$ is a vector of the d.c. variables (as yet undefined).

The significance of the three phase a.c. variables was discussed in chapter 4. The selection of d.c. variables $\bar{x}$ is discussed in the following section.

To enable a Newton-Raphson based technique to be used it is necessary to formulate a set of n independent equations in terms of the n variables describing the system. The equations which

relate to the a.c. system variables are derived from the specified a.c. system operating conditions. The only modification to these equations (described in chapter 4) which results from the presence of the d.c. system occurs at the convertor terminal busbars. These equations become,

$$\Delta P^{p}_{term} = (P^{p}_{term})^{sp} - P^{p}_{term}(ac) - P^{p}_{term}(dc) \qquad (6.1)$$

$$\Delta Q^{p}_{term} = (Q^{p}_{term})^{sp} - Q^{p}_{term}(ac) - P^{p}_{term}(dc) \qquad (6.2)$$

where $P^{p}_{term}(dc)$ and $Q^{p}_{term}(dc)$ are functions of the a.c. terminal conditions and the convertor variables, i.e.:

$$P^{p}_{term}(dc) = f(V^{p}_{term}, \theta^{p}_{term}, \bar{x}) \qquad (6.3)$$

$$Q^{p}_{term}(dc) = f(V^{p}_{term}, \theta^{p}_{term}, \bar{x}) \qquad (6.4)$$

The equations for the a.c. system may therefore be summarised as,

$$\begin{bmatrix} \Delta\bar{P} & (\bar{V}, \bar{\theta}) \\ \Delta\bar{P}_{term} & (\bar{V}, \bar{\theta}, \bar{x}) \\ \Delta\bar{P}_{gen} & (\bar{V}, \bar{\theta}) \\ \Delta\bar{Q} & (\bar{V}, \bar{\theta}) \\ \Delta\bar{Q}_{term} & (\bar{V}, \bar{\theta}, \bar{x}) \\ \Delta\bar{V}_{reg} & (\bar{V}) \end{bmatrix} = 0 \qquad (6.5)$$

where the mismatches at the convertor terminal busbars are indicated separately from the usual three phase a.c. system equations.

Further equations are derived from the d.c. system conditions. Let these equations be designated,

$$\bar{R}(V^{p}_{term}, \theta^{p}_{term}, \bar{x})_{k} = 0 \qquad (6.6)$$

That is, for each convertor, k, a set of equations is derived in terms of the terminal conditions and the convertor variables $\bar{x}$.

Equations 6.3, 6.4 and 6.6 form a mathematical model of the d.c. system suitable for inclusion into load flow analysis.

The three phase a.c./d.c. load flow problem may therefore be formulated as the solution of,

$$\begin{bmatrix} \Delta\bar{P} & (\bar{V}, \bar{\theta}) \\ \Delta\bar{P}_{term} & (\bar{V}_{term}, \bar{\theta}_{term}, \bar{x}) \\ \Delta\bar{P}_{gen} & (\bar{V}, \bar{\theta}) \\ \Delta\bar{Q} & (\bar{V}, \bar{\theta}) \\ \Delta\bar{Q}_{term} & (\bar{V}, \bar{\theta}, \bar{x}) \\ \Delta\bar{V}_{reg} & (\bar{V}) \\ \bar{R} & (\bar{V}_{term}, \bar{\theta}_{term}, \bar{x}) \end{bmatrix} = 0 \qquad (6.7)$$

for the set of variables $(\bar{V}, \bar{\theta}, \bar{x})$.

6.3 D.C. SYSTEM MODELLING

6.3.1 Introduction

The basic h.v.d.c. interconnection shown in Fig. 6.1 is used as a reference in the development of the model. The extension to other configurations is clarified throughout the development. Under unbalanced conditions the convertor transformer modifies the source voltages applied to the convertor and also affects the phase distribution of current and power. In addition, the a.c. system operation may be influenced (e.g. by a zero sequence current flow to a star-g/delta transformer) by the transformer connection. Each bridge in Fig. 6.1 will thus operate with a different degree of unbalance, due to the influence of the convertor transformer connections,

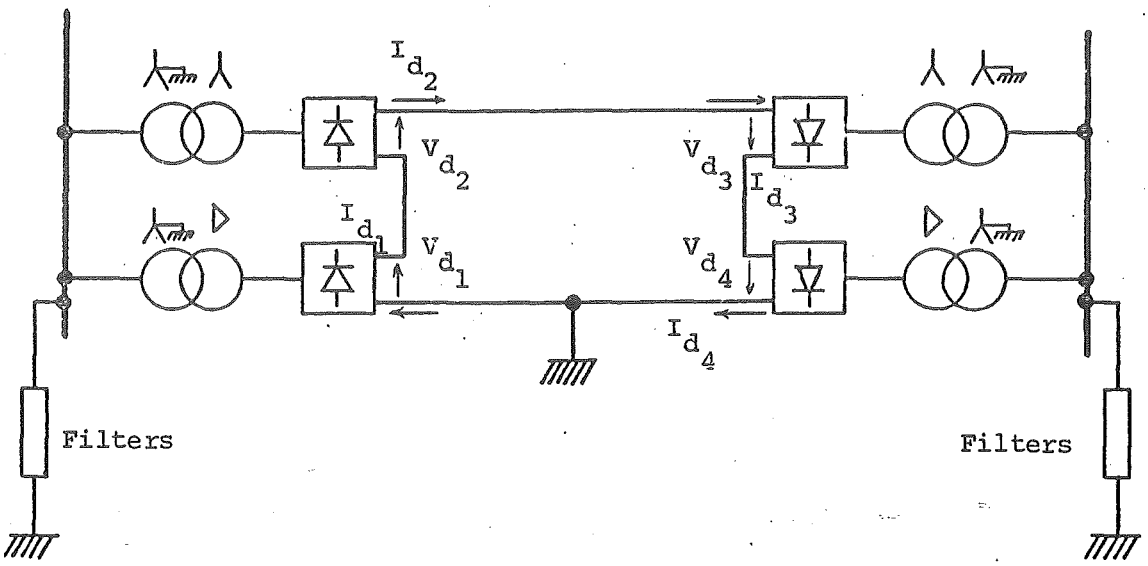

Fig. 6.1 Basic h.v.d.c. Interconnection

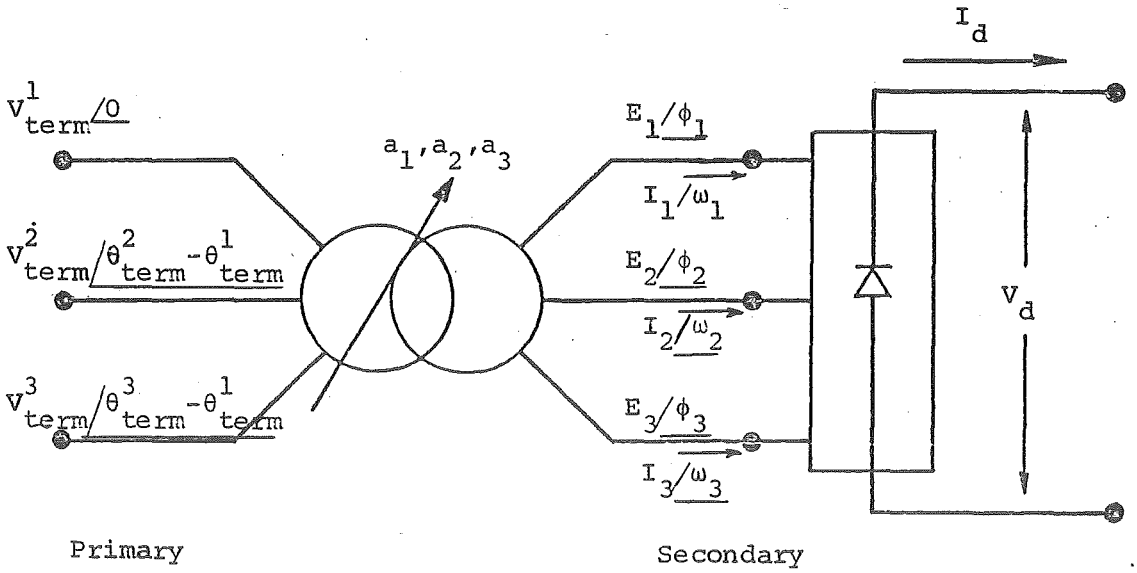

Fig. 6.2 Basic Three Phase Convertor Unit

and must be modelled independently. This feature is in contrast to the balanced d.c. model where it is possible to combine bridges in series and in parallel to form an equivalent single bridge. The dimensions of the three phase d.c. model, will, for this reason alone, be greater than the balanced d.c. model.

All convertors, whether rectifying or inverting, are represented by the same model (Fig. 6.2) and their equations are of the same form.

6.3.2 Basic Assumptions

To enable the formulation of equation (6.6) and to simplify the selection of variables $\bar{x}$ the following assumptions are made:

(i) The three a.c. phase voltages at the terminal busbar are sinusoidal.

(ii) The direct voltage and direct current are smooth.

(iii) The convertor transformer is lossless and the magnetising admittance is ignored.

Assumption (i) requires more critical examination for unbalanced study. Under balanced operation only characteristic harmonics are produced and, as filtering is normally provided at these frequencies, the level of harmonic voltages will be small. However, under even small amounts of unbalance, significant non-characteristic harmonics may be produced and the harmonic content at the terminal busbar may increase.

An investigation of the possible worst case influence of harmonic voltages up to the limits allowed by power authorities, is discussed in Appendix 7. The investigation concludes that although a rigorous justification is not possible, the assumption can be expected to be justified in all practical cases. A rigorous justification

requires an assessment of the possible harmonic levels and this is considered further in chapter 8. For the present, in line with other investigations[47,48], the assumption will be accepted with only heuristic justification.

Assumptions (ii) and (iii) are equally valid for three phase analysis as for single phase analysis and no further justification will be given here.

6.3.3 Selection of Convertor Variables

The philosophy governing the selection of convertor variables was discussed in detail in section 5.3 with regard to the balanced convertor model. The same considerations are relevant to the unbalanced three phase convertor model. The important features may be summarised as follows:

(i) For computing efficiency the smallest number of variables should be used.

(ii) To enable a wide range of control specifications to be readily incorporated all variables involved in their formulation should be retained.

An unbalanced convertor, operating from known three phase voltages, requires a knowledge of six independent variables to define the convertor operating state. For example if all three firing angles and all three transformer taps are known then the convertor operation is defined. The minimum number of convertor variables is therefore six. However to satisfy condition (ii) above additional variables are used.

The assumptions listed in section 6.3.2 justify the use of idealised voltage and current waveforms as illustrated in Fig. 6.3. The following variables are defined with reference to Figs 6.2 and

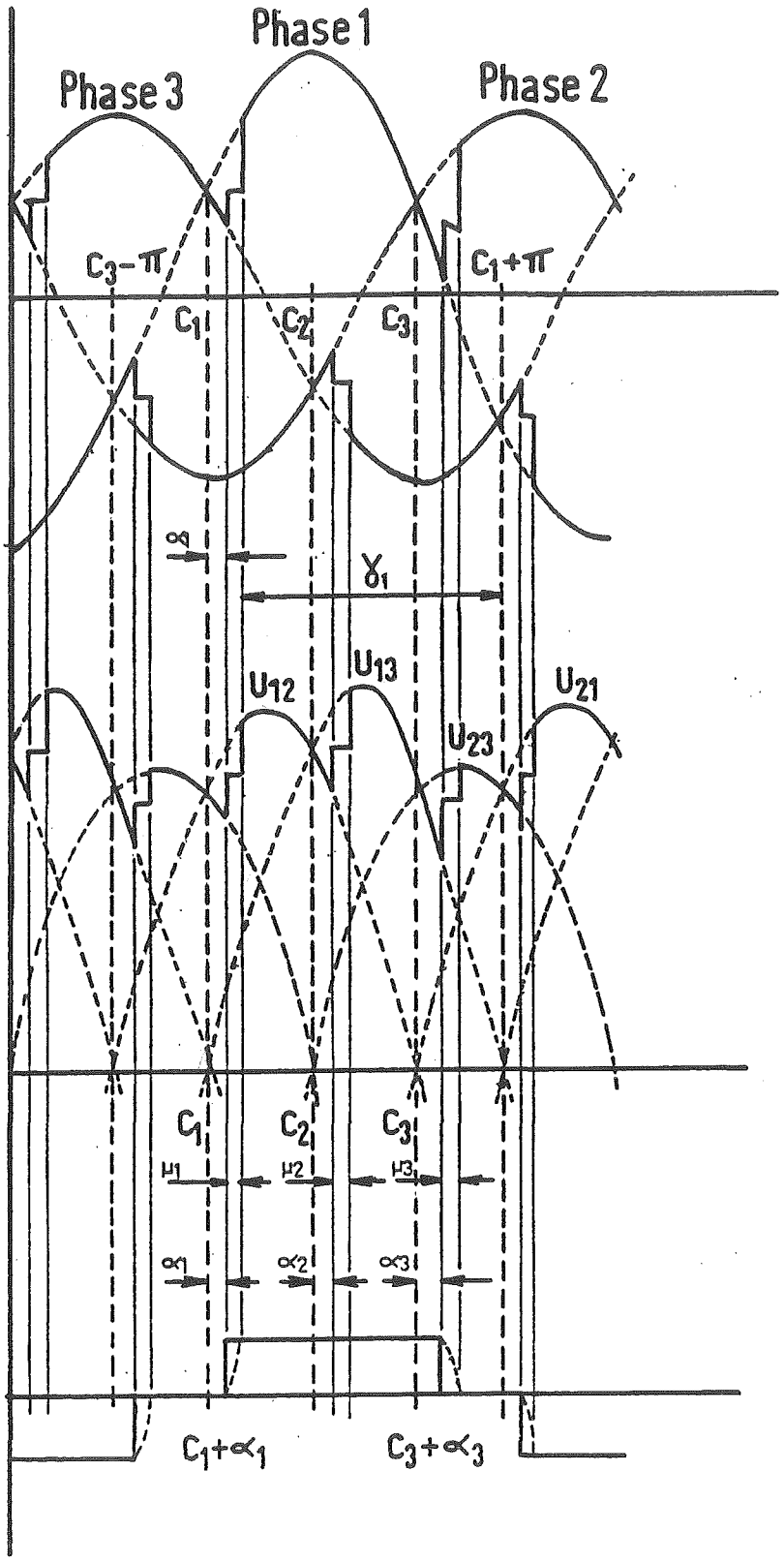

Fig. 6.3 Unbalanced Convertor Voltage and Current Waveform

(i) phase voltages
(ii) D.C. voltage waveform
(iii) assumed current waveshape for phase 1
(actual waveform is indicated by dotted line)

6.3.

a_i	Off-nominal tap ratios on the primary side.
$U_{12}\angle C_1$, $U_{23}\angle C_2$, $U_{21}\angle C_3$	Phase to phase source voltages for convertor referred to the transformer secondary. C_i are therefore the zero crossings for the timing of firing pulses.
α_i	Firing delay angle measured from the respective zero crossing.
V_d	Total average d.c. voltage from complete bridge.
I_d	Average d.c. current.

Where i = 1,2,3 for the three phases involved.

All of the above variables are required in the formulation of the control specifications for unbalanced convertor operation. The variables parallel those used in the balanced model except for the addition of the phase to phase source voltages at the secondary. In the single phase model the convertor source voltage is not included as a variable as its calculation is trivial and it is not required in the formulation of any control specification. In contrast the unbalanced phase to phase source voltages at the transformer secondary are more complex to calculate as they depend not only on the transformer taps but also on the transformer connection. In addition, the zero crossings, C_i, are explicitly required in the formulation of the symmetrical firing controller. For these reasons they are included as convertor variables.

Equation (6.6) may be conveniently formulated in terms of these

14 variables.

6.3.4 Derivation of Basic D.C. Equations

The previous discussion justifies the use of 14 variables to model each convertor. The vector $\bar{x}$ is

$$[U_i, C_i, \alpha_i, a_i, V_d, I_d]^T$$

where i = 1,3.

The convertor model requires the formulation of a corresponding number of independent algebraic equations in terms of these 14 variables. Following the preliminary development of a convertor angle reference and suitable per unit system, the derivation of these equations will be given.

6.3.4.1 Convertor Angle Reference

In the three phase a.c. load flow all angles are referred to the slack generators internal busbar. The angle reference for each convertor may be arbitrarily assigned. Similarly to the single phase a.c./d.c. load flow (chapter 5), by using one of the convertor angles (e.g. θ'_{term} in Fig. 2) as a reference the mathematical coupling between the equations describing the a.c. system and those describing the convertor, is weakened. This has a favourable effect on the rate of convergence, especially so, as a sequential solution technique is to be used.

6.3.4.2 Per Unit System

The application of a p.u. system to the single phase representation of the d.c. system was discussed in detail in section 5.3.2.1. Similar considerations apply to the three phase representation. The following p.u. system is adopted.

Computational simplicity is achieved by using common power and voltage bases on both sides of the convertor.

The three phase a.c. system base values are:

$$MVA_{base} = \text{Base power per phase}$$

$$V_{base} = \text{Phase - neutral voltage base.}$$

With common power and voltage bases the current base on the a.c. and d.c. sides are also equal and therefore no constants appear in the equations due to the p.u. system.

6.3.4.3 Convertor Source Voltages

The phase to phase source voltages referred to the transformer secondary are found by a consideration of the transformer connection and off-nominal turns ratio. For example consider the star-star transformer of Fig. 6.4.

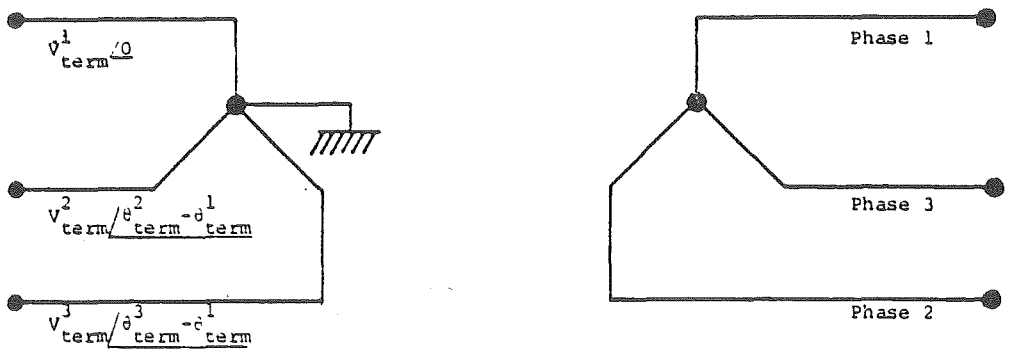

Fig. 6.4 Star-Star Transformer Connection

The phase to phase source voltages referred to the secondary are:

$$U_{13}\angle C_1 = \frac{1}{a_1} V^1_{term}\angle 0 - \frac{1}{a_3} V^3_{term}\angle\theta^3_{term} - \theta^1_{term} \quad (6.8)$$

$$U_{23}\angle C_2 = \frac{1}{a_2} V^2_{term}\angle\theta^2_{term} - \theta^1_{term} - \frac{1}{a_3} V^3_{term}\angle\theta^3_{term} - \theta^1_{term} \quad (6.9)$$

$$U_{21}\angle C_3 = \frac{1}{a_2} V^2_{term}\angle\theta^2_{term} - \theta^1_{term} - \frac{1}{a_1} V^1_{term}\angle 0 \qquad (6.10)$$

Taking real and imaginary parts yields a further six equations.

6.3.4.4 D.C. Voltage

The d.c. voltage is found by integration of the waveforms in Fig. 6.3 (ii) and may be written in the form:

$$\frac{V_d * \pi}{\sqrt{2}} = U_{21}\,[\mathrm{Cos}(C_1 + \alpha_1 - C_3 + \pi) - \mathrm{Cos}(C_2 + \alpha_2 - C_3 + \pi)] \qquad (6.11)$$

$$+ U_{13}\,[\mathrm{Cos}(C_2 + \alpha_2 - C_1) - \mathrm{Cos}(C_3 + \alpha_3 - C_1)]$$

$$+ U_{23}\,[\mathrm{Cos}(C_3 + \alpha_3 - C_2) - \mathrm{Cos}(C_1 + \alpha_1 + \pi - C_2)]$$

$$- I_d(XC_1 + XC_2 + XC_3)$$

where XC_i is the commutation reactance for phase i.

6.3.4.5 D.C. Interconnection

An equation is derived for each convertor, from the d.c. system topology relating the d.c. voltages and currents. In general, this equation is of the form:

$$f(V_d, I_d) = 0 \qquad (6.12)$$

For example the system shown in Fig. 6.1 provides the following four equations:

$$Vd_1 + Vd_2 + Vd_3 + Vd_4 - Id_1 \cdot Rd = 0$$

$$Id_1 - Id_2 = 0$$

$$Id_1 - Id_3 = 0$$

$$Id_1 - Id_4 = 0$$

where clearly some redundancy results. This is the cost of complete

generality in the d.c. interconnection.

6.3.4.6 Incorporation of Control Strategies

A further six equations are derived from the specified operating conditions. Any function of the variables is a valid (mathematically) control equation so long as the equation is independent of all the others.

In practice there are restrictions limiting the number of alternatives. Some control specifications refer to the characteristics of power transmission (e.g. constant power or constant current), others introduce constraints such as minimum delay or extinction angles.

As the consideration of the alternative firing controls is of particular interest their implementation is now discussed.

Symmetrical firing is considered as being applied individually for each six pulse bridge although, if required, the equations may be written to consider the firing controller operating on an integral twelve pulse bridge. For a six pulse unit the interval between firing pulses is specified as 60°. This provides two equations. The third equation results from the specification of minimum firing angle control, i.e.

$$\alpha_i - \alpha_{min} = 0 \qquad (6.13)$$

Where phase i is selected during the solution procedure such that the other two phases will have, in the unbalanced case, firing angles greater than α_{min}.

With conventional phase angle control the firing angle on each phase is specified as being equal to α_{min}, i.e.

$$\alpha_1 - \alpha_{min} = 0 \tag{6.14}$$

$$\alpha_2 - \alpha_{min} = 0 \tag{6.15}$$

$$\alpha_3 - \alpha_{min} = 0 \tag{6.16}$$

The remaining three control equations are derived from the operating conditions. Usually, the off-nominal taps are specified as being equal, i.e.

$$a_1 - a_2 = 0 \tag{6.17}$$

$$a_2 - a_3 = 0 \tag{6.18}$$

The final equation will normally relate to the constant current or constant power controller, e.g.

$$I_d - I_d^{sp} = 0 \tag{6.19}$$

or

$$V_d \cdot I_d - P_d^{sp} = 0 \tag{6.20}$$

The above examples illustrate the case with which the various control specifications are incorporated.

6.3.4.7 Invertor Operation with Specified Extinction Angle

In the single phase load flow the d.c. equations for invertor operation are written in terms of the extinction angle γ (instead of the firing delay angle α) and the equations for specifying the extinction angle may be written directly. For the three phase load flow this cannot be done as the variable α must be retained in the study as it is required in the formulation of the symmetrical firing control equations. Therefore the restriction upon the extinction advance angle γ requires the implicit calculation of the commutation angle for each phase.

Taking the specification for γ, as defined in Fig. 6.3, the following equation is used:

$$\text{Cos } \gamma_1^{sp} + \text{Cos } \alpha_1 - I_d \frac{(XC_1 + XC_3)}{\sqrt{2}\, U_{13}} = 0 \qquad (6.21)$$

Similar equations apply to the other two phases with a cyclic change of suffices.

6.3.5 Calculation of Terminal Power Flows

The mathematical model of the convertor includes the formulation of equations (6.3) and (6.4) for the individual phase real and reactive power flows on the primary of the convertor transformer. It is in connection with these equations that the three phase model deviates significantly from the single phase model developed in the previous chapter.

The calculation of the individual phase real and reactive powers at the terminal busbar requires the values of both the magnitude and angle of the fundamental components of the individual phase currents flowing to the convertor transformer.

In the single phase analysis of the balanced convertor the magnitude of the fundamental is obtained by approximating the fourier analysis for the current waveshape on the transformer secondary and then transferring the fundamental magnitude across the convertor transformer. In the single phase case this procedure is trivial and the equations are eliminated from the d.c. solution. The angle of the fundamental component is calculated by simply equating the total real power on a.c. and d.c. sides of the convertor.

A similar procedure may be applied to the three phase analysis of the unbalanced convertor, however, the transferance of secondary

currents to the primary is no longer a trivial procedure due to the influence of the three phase transformer connection. In addition, the three phase convertor transformer may influence the a.c. system operation, for example, a star-g/delta connection provides a zero sequence path for the a.c. system.

The simplist and most general method of accounting for the influence of the three phase convertor transformer connection is to extend the d.c. system model to include the nodal admittance model of the transformer. The nodal admittance model of the various transformer connections have been discussed in chapter 2 for the usual a.c. system transformers; the same models are applicable to the convertor transformers except these may be generalised to include the modelling of independent tap ratios on each phase winding. An example is given in Appendix 5 for the star-g/delta connection.

The inclusion of the fundamental frequency three phase model of the transformer necessitates the inclusion of the following variables, defined here with reference to Fig. 6.2:

- $E_i \angle\phi_i$ the fundamental component of the voltage waveshape at the transformer secondary busbar.
- $I_i \angle\omega_i$ the fundamental component of the secondary current waveshapes.

where i = 1,3 for the three phases.

A total of 12 extra variables are added to the original 14 to yield a final set of 26 variables for each convertor in the d.c. system.

The terminal real and reactive power flows on the primary of the convertor transformer may be calculated from the values of E_i and ϕ_i which are solved for as part of the Newton-Raphson procedure for

the d.c. system. These power flows are calculated at each real or reactive power a.c. iteration to form the real or reactive power mismatch at the terminal busbar. They are calculated by the usual a.c. equations for calculating the power flow leaving a busbar (the convertor terminal) and flowing to another busbar (the convertor transformer secondary) through a three phase element (the convertor transformer) when all voltages and angles are known.

The additional 12 variables which are added to the d.c. model require the formulation of an additional 12 independent equations. As these equations relate to the fundamental frequency three phase power flows across a system element it may therefore seem appropriate to apply the usual real and reactive power mismatch equations at the convertor secondary busbar. However, the calculation of the individual phase real and reactive power flows to the d.c. side from the transformer secondary is difficult and these mismatch equations are not suitable. Therefore the variables $I_i \underline{/\omega_i}$ are included and current mismatch equations are used. The inclusion of these variables enables all equations to have clear physical significance. The equations are formed in the following sections.

6.3.5.1 Current Relationships

Relationships are derived for the fundamental frequency real and imaginary current flows across the convertor transformer.

Off nominal taps (a_1 a_2 a_3) are modelled on the system (primary) side of the transformer; and are, for generality, assumed independently controllable.

The three-phase convertor transformer is represented by its nodal admittance model, i.e.

$$Y_{node} = \begin{array}{|c|c|} \hline Y_{pp} & Y_{ps} \\ \hline Y_{sp} & Y_{ss} \\ \hline \end{array} \qquad (6.22)$$

where p indicates the primary side

and s the secondary side of the transformer.

The 3 × 3 submatrices (Y_{pp}, etc.) for the various transformer connections, including modelling of the independent phase taps, may be derived using Kron's connection matrix technique; an example is illustrated in Appendix 3.

In terms of these submatrices and on the assumption of a lossless transformer (i.e. $Y_{pp} = jb_{pp}$, etc.) the currents at the convertor side busbar are expressed as follows:

$$I_i e^{j\omega_i} = -\sum_{k=1}^{3} [jb_{ss}^{ik} E_k e^{j\phi_k} + jb_{sp}^{ik} V_{term}^{k} e^{j(\theta_{term}^{k} - \theta_{term}^{1})}] \qquad (6.23)$$

By subtracting θ_{term}^{1} in the above equation the terminal busbar angles are related to the convertor angle reference.

Separating this equation into real and imaginary components the following six equations result:

$$I_i \cos\omega_i = \sum_{k=1}^{3} [b_{ss}^{ik} E_k \sin\phi_k + b_{sp}^{ik} V_{term}^{k} \sin(\theta_{term}^{k} - \theta_{term}^{1})] \qquad (6.24)$$

$$I_i \sin\omega_i = \sum_{k=1}^{3} [- b_{ss}^{ik} E_k \cos\phi_k - b_{sp}^{ik} V_{term}^{k} \cos(\theta_{term}^{k} - \theta_{term}^{1})] \qquad (6.25)$$

Three further equations are derived from approximate expressions for the fundamental rms components of the line current waveforms[48] as shown in Fig. 6.3, i.e.

$$I_i = 0.995^* \frac{4 \cdot I_d}{\sqrt{2}} \sin(T_i/2) \qquad (6.26)$$

where T_i is the assumed conduction period for phase i.

The accuracy of these approximations depends upon the magnitude of the commutation angles and also upon the imbalance between the incoming and outgoing commutation periods. Within the range of unbalance expected in steady state operation the error should be less than 1%. If greater accuracy is required this may be achieved by the procedure outlined in Appendix 8. Solutions to greater accuracy are, however, seldom required in the context of load flow investigations.

6.3.5.2 Equality of Real Power Flow

The sum of the real powers on the three phases of the transformer secondary may be equated to the total d.c. power, i.e.

$$\sum_{i=1}^{3} E_i \cdot I_i \cdot \cos(\phi_i - \omega_i) - V_d \cdot I_d = 0 \qquad (6.27)$$

6.3.5.3 Final Equations

A total of 10 equations have been derived so far and an additional 2 independent equations are required. Several versions have been developed for these equations which are applicable to specific transformer connections. The version presented here, is general to all transformer connections and is therefore considered the most satisfactory.

The equations are derived from the position of the fundamental frequency voltage reference for the secondary of the convertor transformer.

The voltage reference for the a.c. system is earth. In d.c.

transmission the actual earth is placed on one of the convertors d.c. terminal and this point is used as a reference to define the d.c. transmission voltages and the insulation levels of the convertor transformer secondary windings.

However for the load flow analysis arbitrary references can be used for each convertor unit to simplify the mathematical model. The actual voltages to earth, if required, can then be obtained from the particular configuration and earthing arrangements.

The transformer nodal admittance matrix relates the injected currents to the nodal voltages, where the nodal voltages must be with respect to a common reference. In the case of the convertor transformer secondary an arbitrary reference can be explicitly included.

With a star winding on the secondary an obvious reference is the star point itself. If the nodal admittance matrix is formed for a star-g/star-g connection, then this reference is implicitly present through the admittance model of the transformer. In this case however the convertor transformer does not restrict the flow of zero sequence currents and the following two equations may be written:

$$\sum_{i=1}^{3} I_i \angle \omega_i = 0 \qquad (6.28)$$

These two equations (real and imaginery parts) complete the set of 12 independent equations in terms of the 12 additional variables.

However, for a delta secondary winding no star point is available and some other reference must be used.

To obtain a reference which may be applied to all transformer secondary windings an artificial reference node is formulated. The

zero sequence secondary voltage is taken as a reference, this is conveniently implemented by the following two equations:

$$\sum_{i=1}^{3} E_i \cos \phi_i = 0 \qquad (6.29)$$

$$\sum_{i=1}^{3} E_i \sin \phi_i = 0 \qquad (6.30)$$

The nodal admittance matrix for a star connected transformer secondary is formed for an unearthed star winding. The restriction on the zero sequence current flowing on the secondary is therefore implicitly included in the transformer model for both star and delta connections.

Both alternatives for a star winding have been programmed and, not unexpectedly, yield exactly the same solution to the load flow problem.

6.3.6 Summary of Equations and Variables

The 26 equations ($\bar{R}$) which define the operation of each convertor are:

$$R(1) = \sum_{i=1}^{3} E_i \cos \phi_i = 0$$

$$R(2) = \sum_{i=1}^{3} E_i \sin \phi_i = 0$$

$$R(3) = \sum_{i=1}^{3} E_i I_i \cos(\phi_i - \omega_i) - V_d \cdot I_d$$

$$R(4) = I_1 - \frac{4}{\pi} \cdot \frac{I_d}{\sqrt{2}} \sin(T_1/2)$$

$$R(5) = I_2 - \frac{4}{\pi} \cdot \frac{I_d}{\sqrt{2}} \sin(T_2/2)$$

$$R(6) = I_3 - \frac{4}{\pi} \cdot \frac{I_d}{\sqrt{2}} \sin(T_3/2)$$

$$R(7) = I_1 \cdot \cos\omega_1 - \sum_{k=1}^{3} [b_{ss}^{1k} E_k \sin\phi_k + b_{sp}^{1k} \cdot V_{term}^{k} \sin(\theta_{term}^{k} - \theta_{term}^{1})]$$

$$R(8) = I_2 \cdot \cos\omega_2 - \sum_{k=1}^{3} [b_{ss}^{2k} E_k \sin\phi_k + b_{sp}^{2k} \cdot V_{term}^{k} \sin(\theta_{term}^{k} - \theta_{term}^{1})]$$

$$R(9) = I_3 \cdot \cos\omega_3 - \sum_{k=1}^{3} [b_{ss}^{3k} E_k \sin\phi_k + b_{sp}^{3k} \cdot V_{term}^{k} \sin(\theta_{term}^{k} - \theta_{term}^{1})]$$

$$R(10) = I_1 \cdot \sin\omega_1 + \sum_{k=1}^{3} [b_{ss}^{1k} E_k \cos\phi_k + b_{sp}^{1k} \cdot V_{term}^{k} \cos(\theta_{term}^{k} - \theta_{term}^{1})]$$

$$R(11) = I_2 \cdot \sin\omega_2 + \sum_{k=1}^{3} [b_{ss}^{2k} E_k \cos\phi_k + b_{sp}^{2k} \cdot V_{term}^{k} \cos(\theta_{term}^{k} - \theta_{term}^{1})]$$

$$R(12) = I_3 \cdot \sin\omega_3 + \sum_{k=1}^{3} [b_{ss}^{3k} E_k \cos\phi_k + b_{sp}^{3k} \cdot V_{term}^{k} \cos(\theta_{term}^{k} - \theta_{term}^{1})]$$

R(13)
.
.
.
R(18)

depend on transformer connection

R(19)
.
.
.
R(24)

depend on the control specifications

$$R(25) = V_d \cdot \pi - \sqrt{2}\, U_{21}[\cos(C_1+\alpha_1-C_3+\pi) - \cos(C_2+\alpha_2-C_3+\pi)]$$

$$- \sqrt{2}\, U_{13}[\cos(C_2+\alpha_2-C_1) - \cos(C_3+\alpha_3-C_1)]$$

$$- \sqrt{2}\, U_{23}[\cos(C_3+\alpha_3-C_2) - \cos(C_1+\alpha_1+\pi-C_2)]$$

$$+ I_d(XC_1 + XC_2 + XC_3)$$

$R(26) = f(V_{di}, I_{di})$ from d.c. system topology.

The 26 variables $\bar{x}$ are:

$$[E_1, E_2, E_3, \phi_1, \phi_2, \phi_3, I_1, I_2, I_3, \omega_1, \omega_2, \omega_3,$$

$$U_{12}, U_{13}, U_{23}, C_1, C_2, C_3, \alpha_1, \alpha_2, \alpha_3, a_1, a_2, a_3,$$

$$V_d, I_d]^T$$

6.4 SOLUTION TECHNIQUES

As discussed in the introduction, the simpler sequential solution technique has been adopted for the three phase a.c./d.c. load flow, the complexity of the unified approach not being justified for the three phase case. The sequential technique, using the three phase fast decoupled a.c. algorithm and a full Newton-Raphson algorithm for the d.c. equations, involves the block successive iteration of the following three equations,

$$\begin{bmatrix} \Delta\bar{P}(\bar{V},\bar{\theta})/\bar{V} \\ \Delta\bar{P}_{gen}/\bar{V}_{int} \end{bmatrix} = \begin{bmatrix} B' \end{bmatrix} \begin{bmatrix} \Delta\bar{\theta} \\ \Delta\theta_{int} \end{bmatrix} \tag{6.31}$$

$$\begin{bmatrix} \Delta\bar{Q}(\bar{V},\bar{\theta})/\bar{V} \\ \Delta\bar{V}_{reg}(\bar{V}) \end{bmatrix} = \begin{bmatrix} B'' \end{bmatrix} \begin{bmatrix} \Delta\bar{V} \\ \Delta\bar{V}_{int} \end{bmatrix} \tag{6.32}$$

$$\begin{bmatrix} \bar{R}(\bar{x}) \end{bmatrix} = \begin{bmatrix} J \end{bmatrix} \begin{bmatrix} \Delta\bar{x} \end{bmatrix} \tag{6.33}$$

where [B'] and [B''] are the three phase fast decoupled a.c. jacobian matrices as developed in chapter 4

and [J] is the d.c. jacobian of first order partial derivatives.

Equations (6.31) and (6.32) are the three phase fast decoupled algorithmic equations from chapter 4. For the solution of the a.c. equations, the d.c. variables $\bar{x}$ are treated as constants and, in effect, the d.c. system is modelled simply as the appropriate real and reactive power loads at the convertor terminal busbar. For the d.c. iteration, the a.c. variables at the terminal busbars are considered to be constant.

The selection of the sequential iteration sequence for the three sets of equations (i.e., (6.31), (6.32) and (6.33)) has been based upon the results of the investigation with the single phase fast decoupled a.c./d.c. load flow presented in chapter 5. The iteration sequence, illustrated in Fig. 6.5, parallels the single phase P,Q,DC sequence which proved the most successful in the single phase case.

This sequence acknowledges the fact that the convertor operation is strongly related to the magnitude of the terminal voltages and more weakly dependent on their phase angles. Therefore the convertor solution follows the update of the a.c. terminal voltages.

It should be noted, however, that for the final convergence of the system unbalance, the d.c. operation is dependent on the phase angle unbalance as much as on the voltage unbalance. The final convergence of the three phase load flow is comparatively slow and no convergence problems have occured from this dependence on terminal busbar phase angle unbalance.

6.5 PROGRAMMING ASPECTS

Equations (6.31) and (6.32) are solved using sparsity techniques and near optimal ordering.

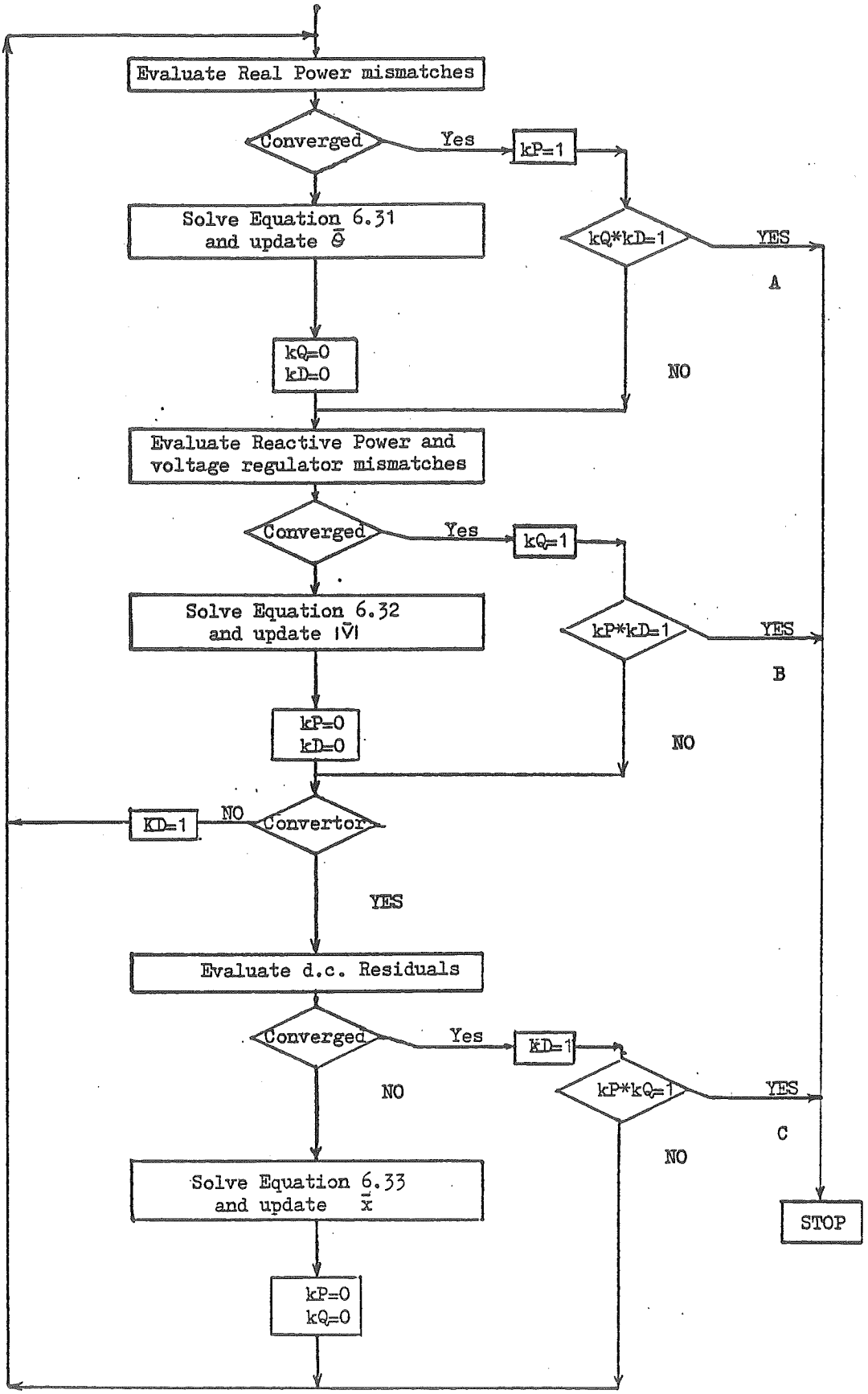

Fig. 6.5 Flow Chart for Three Phase A.C./D.C. Load Flow

The solution of equation (6.33) is carried out using a modified Gaussian Elimination routine. The equations for each convertor are separate except for those relating to the d.c. interconnection.

This feature may be utilized by appropriate ordering of variables to yield a block sparsity structure for the d.c. Jacobian. By placing the d.c. voltage variable last for each block of convertor equations and by placing all the d.c. current variables after all convertor blocks the d.c. Jacobian will have a structure as illustrated in Fig. 6.6.

By using row pivoting only during the solution procedure, the block sparsity of Fig. 6.6 is preserved. Each block containing non-zero elements is stored in full, but only non-zero elements are processed.

This routine requires less storage than a normal sparsity programme for non-symmetrical matrices and the solution efficiency is improved.

6.6 PERFORMANCE OF THE ALGORITHM AND SAMPLE RESULTS

6.6.1 Introduction

The performance of the sequential integration of the unbalanced convertor model into the three phase fast decoupled a.c. load flow is subject to the same considerations as the comparable single phase load flow discussed in chapter 5. That is, the convergence rate depends on the influence of the a.c. terminal voltages on the d.c. operation and the influence of the changing convertor real and reactive power flows on the a.c. system convergence.

This section investigates the performance of the three phase a.c./d.c. load flow and, where applicable, compares this with the

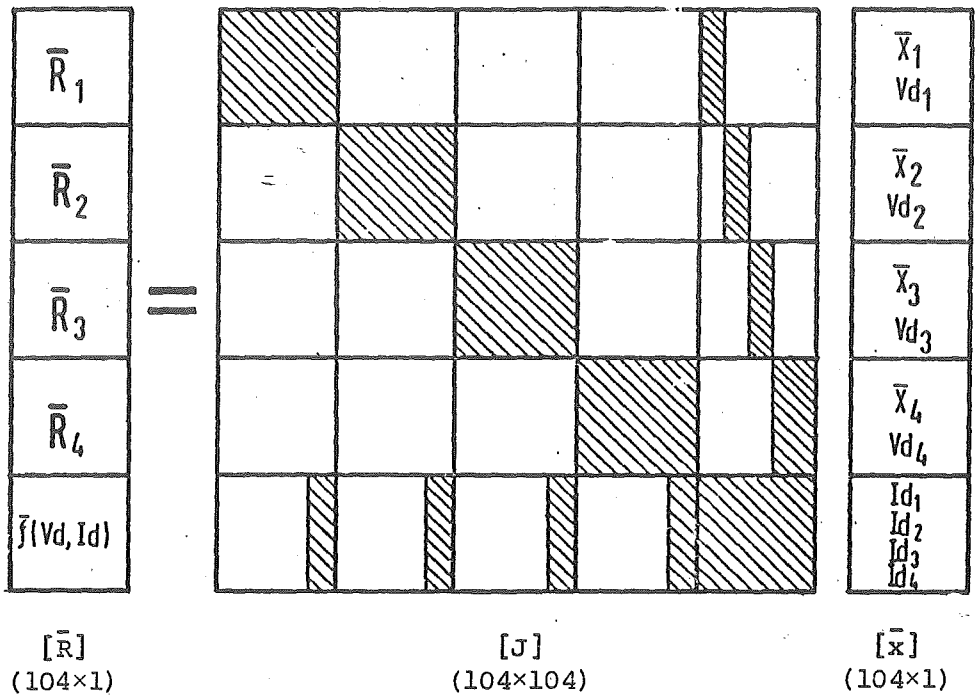

Fig. 6.6 Jacobian Structures for Multi Convertor D.C. System (Non zero elements indicated)

corresponding single phase sequential integration. The investigation is performed with reference to a particular test system which has been selected to illustrate the features which influence convergence and also to enable detailed results to be given.

The test system and d.c. convertor installations are described in the first part of this section. The convergence characteristics of the d.c. model when operating from fixed terminal conditions is examined and then the behaviour of the combined a.c./d.c. load flow is investigated.

6.6.2 Description of Test System

The developed algorithm has been investigated with reference to the test system illustrated in Fig. 6.7. The system consists of two a.c. systems interconnected by a 600 kv, 600 MW h.v.d.c. link.

The 20 bus system is a representation of the 220 kv a.c. network of the South Island of New Zealand. It includes mutually-coupled parallel lines, synchronous generators and condensers, star-star and star-delta connected transformers and has a total generation in excess of 2000 MW.

At the other end of the link a fictitious 5-bus system represents 800 MW of remote hydrogeneration connected to a convertor terminal and load busbar by long untransposed high voltage lines.

The small system is used to test the algorithm and to enable detailed discussion of results. The d.c. link should have considerable influence, as the link power rating is comparable to the total capacity of the small system. Relevant parameters for the a.c. system and d.c. link are given in Table 6.1.

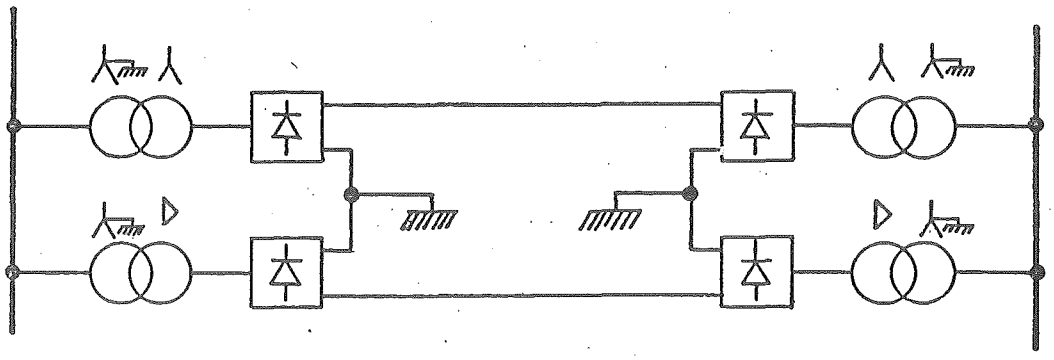

20 Bus System 5 Bus System

(a) H.V.D.C. interconnection

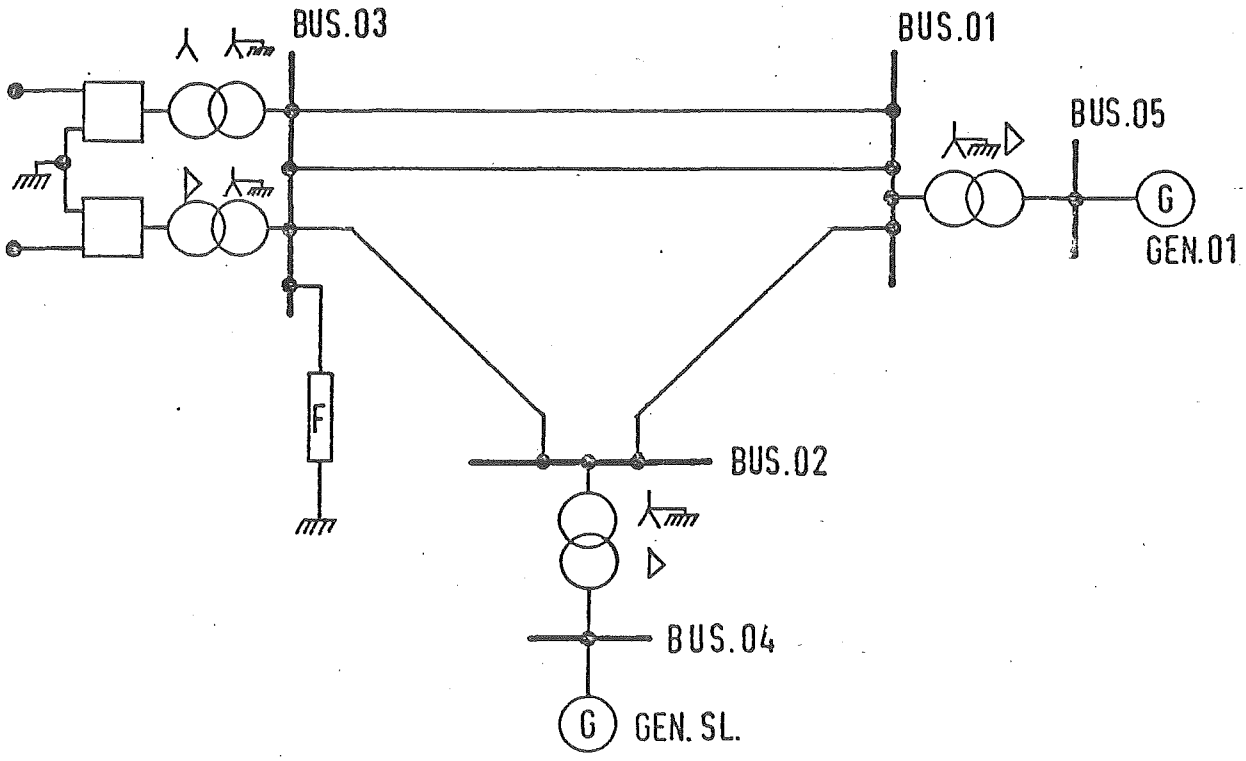

(b) 5 Bus a.c. system

Fig. 6.7 Three Phase A.C./D.C. Test System

Data for all lines

Z_s Series Impedance Matrix		
0.0066 +j0.056	0.0017 +j0.027	0.0012 +j0.021
0.0017 +j0.027	0.0045 +j0.047	0.0014 +j0.022
0.0012 +j0.021	0.0014 +j0.0220	0.0062 +j0.061

Y_s Shunt Admittance Matrix		
j0.15	-j0.03	-j0.01
-j0.03	j0.25	-j0.02
-j0.01	-j0.02	j0.125

Generator Data

Name	Sequence Reactances		Power (MW)	Voltage Regulator
	X_o	X_2		V^a
GEN.01	0.02	0.004	700.0	1.045
GEN.SL	0.02	0.004	SLACK	1.061

Data for generator transformers

Connection	Star-G/DELTA
Reactance	0.0016+j0.015
Off-nominal tap	+2.5% on Star

Busbar Loadings

BUS NAME	PHASE A		PHASE B		PHASE C	
	P-LOAD	Q-LOAD	P-LOAD	Q-LOAD	P-LOAD	Q-LOAD
BUS.01	20.000	10.000	20.000	10.000	20.000	10.000
BUS.02	66.667	26.667	66.667	26.667	66.667	26.667
BUS.03	0.000	0.000	0.000	0.000	0.000	0.000
BUS.04	0.000	0.000	0.000	0.000	0.000	0.000
BUS.05	0.000	0.000	0.000	0.000	0.000	0.000

Data for all convertors

	Phase 1	Phase 2	Phase 3
Transformer Reactances	0.0510	0.0510	0.0510
Commutation Reactances	0.0537	0.0537	0.0537
Minimum Firing Angle	7.0 deg		
Minimum Extinction Angle	10.0 deg		
Nominal Voltage	140 kV		

D.C. link resistance = 25.0 ohms.

Table 6.1 System Data

6.6.3 Convergence of D.C. Model from fixed Terminal Conditions

The set of equations $\bar{R}$ form a complete mathematical description of the steady state operation of the three phase d.c. convertor. These equations may be solved using a full Newton-Raphson procedure as discussed in section 6.4. If the terminal busbar voltages (V_{term}, θ_{term}) are fixed then the d.c. model may be solved in isolation. The convergence pattern of the real and reactive power flows from the a.c. busbar are of interest as this is the primary feature of the d.c. systems' influence on the convergence of the a.c. system. The convergence patterns for these terminal power flows for the three phase model, under both balanced and unbalanced terminal conditions, are shown in Fig. 6.8. Similar convergence patterns are obtained under all d.c. control strategies when the terminal conditions are fixed. The convergence pattern of the single phase representation of the same convertor, as developed in chapter 5, is also illustrated. To enable a comparison to be made, the total three phase powers are plotted for the balanced case. In all cases d.c. starting values were selected to give large initial errors in the terminal powers to better illustrate the convergence.

The d.c. equations require 2 iterations to converge for both the single and three phase models. The three phase terminal powers converge in a similar manner to the single phase powers under balanced conditions. With unbalanced terminal conditions the three phase convergence is rapid.

The influence of the changing three phase power flows on the a.c. system convergence is investigated in the following section.

6.6.4 Performance of the Integrated A.C./D.C. Load Flow

With reference to the test system illustrated in Fig. 6.7, the following control specifications are applied at the inverting

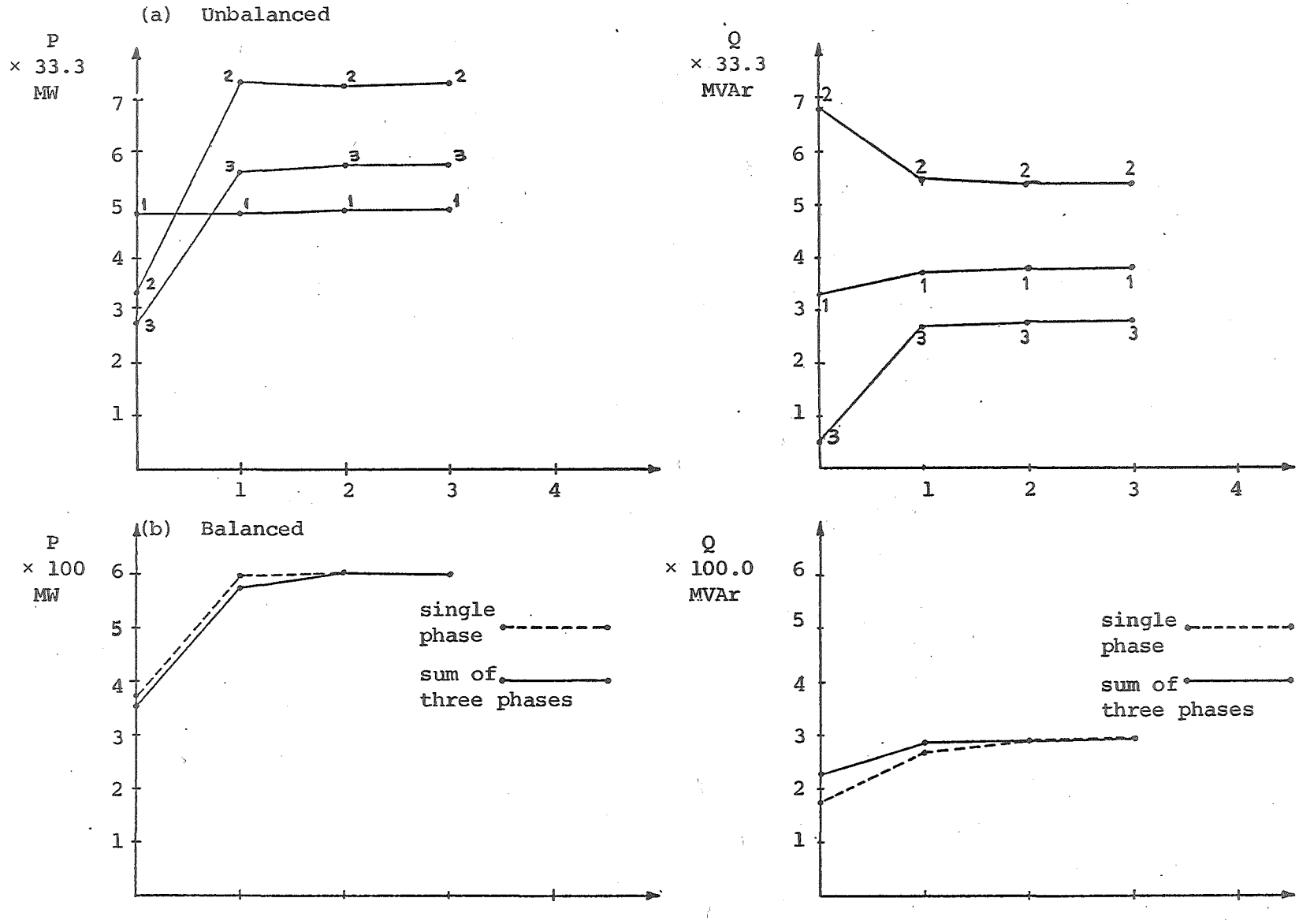

Fig. 6.8 Convergence of Terminal Powers for Three Phase Convertor Model

terminal for all cases which have been investigated;

- symmetrical firing control with the reference phase on minimum extinction angle.
- Off nominal tap ratios equal on all phases.
- D.C. voltage specified.

A variety of different control strategies have been applied at the rectifier terminal; the case descriptions and convergence results are given in Table 6.2. The Table also includes the results with the convertor installation modelled by equivalent a.c. loads at the terminal busbars and for cases where the system unbalance has been artificially increased with large unbalanced loads.

It should be noted that the iteration scheme illustrated in Fig. 6.5 does not allow for each individual a.c. system to be converged independently, therefore the number of iterations required is the larger of the two sets given in the Table.

It is clear that the integration of the d.c. convertor model does not cause any significant deterioration in performance. The only cases where convergence was slowed was for cases (viii) and (xi), where the system is weakened by the loss of one transmission line. This is not unexpected from the discussion of single phase sequential algorithms given in chapter 5.

The nature of the interaction between a.c. and d.c. systems is examined in more detail in the following section.

6.6.5 Interaction Between A.C. and D.C. Systems

The convergence pattern of the terminal voltages at BUS.03 is illustrated in Fig. 6.9 for the case where the convertor is modelled by the equivalent unbalanced real and reactive power loads. The deviation of the three phase angles from nominal balance (i.e.

Case	Case Description and Rectifier Specifications	Number of iterations to Convergence (0.1 MW/MVAR	
		20 Bus System	6 Bus System
a(i)	Convertor modelled by equivalent balanced loads*	8,7	6,5
(ii)	Convertor modelled by equivalent unbalanced loads*	8,7	6,5
b(i)	Phase angle control ; $\alpha_1=\alpha_2=\alpha_3=\alpha_{min}, a_1=a_2=a_3, P_{dc}=P_d^{sp}$	8,7	6,5
(ii)	Symmetrical firing ; $\alpha_i=\alpha_{min}$ " "	8,7	6,5
(iii)	Phase angle control ; $\alpha_1=\alpha_2=\alpha_3=\alpha_{min}, a_1=a_2=a_3, I_{dc}=I_{dc}^{sp} V_{d1}=V_{d2}$	8,7	6,5
(iv)	Symmetrical firing ; $\alpha_i=\alpha_{min}$ " " "	8,7	6,5
(v)	As for case b(i) ; with poor starting values. (P_{dc}, Q_{dc} in error by 70%)	8,7	8,7
(vi)	As for case b(i) ; with large unbalanced load at BUS.03	8,7	7,6
(vii)	As for case b(ii) ; with large unbalanced load at BUS.03	8,7	7,6
(viii)	As for case b(i) ; with loss of 1 line BUS.01 to BUS.03	8,7	9,9
(ix)	Symmetrical firing ; $\alpha_i=\alpha_{min}, a_1=-10\%, a_2=0, a_3=+10\%$	8,7	7,6
(x)	Phase angle control ; $a_1=a_2=a_3=a^{sp}, \alpha_1=\alpha_2=\alpha_3, P_{dc}=P_{dc}^{sp}$	8,7	7,6
(xi)	Case (x) loss of 1 line. BUS.01 to BUS.03	8,7	8,8

* loading for case a(i) and a(ii) derived from results for case b(i). See Table 3.

Table 6.2 Case Descriptions and Convergence Results

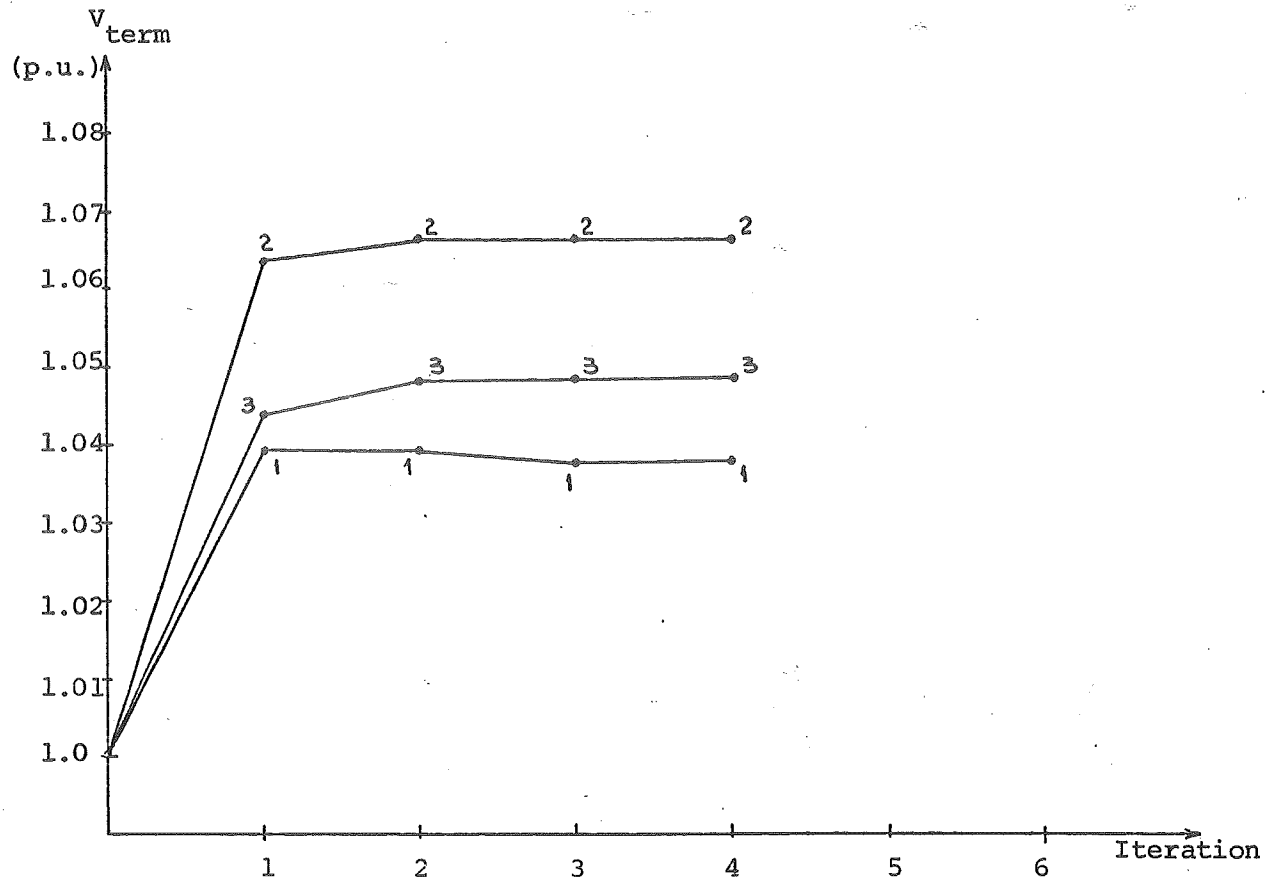

(a) Phase voltage magnitudes

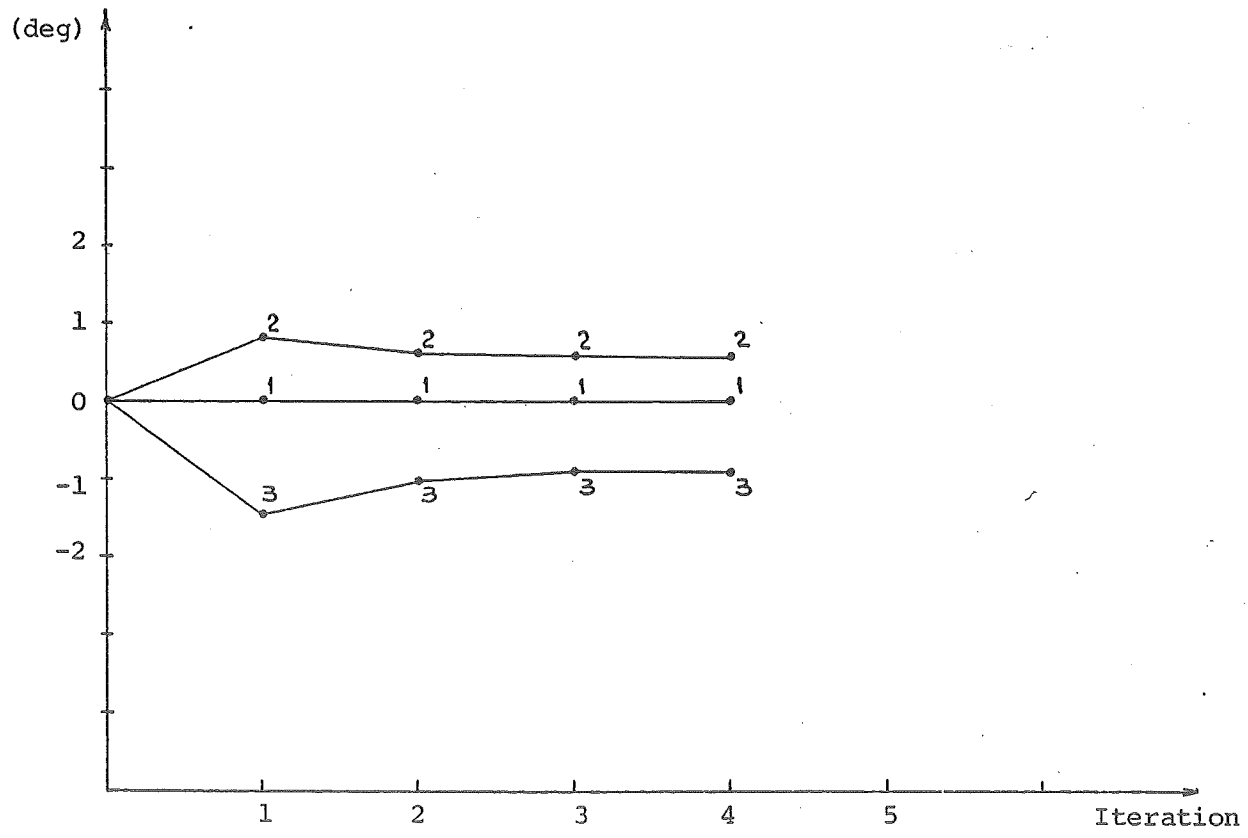

(b) Angle unbalance (deviation from nominal)

Fig. 6.9 Convergence Pattern of Phase Voltages at Terminal Busbar for the A.C. System in Isolation

0,-120,120) is also shown. The convergence of the three phase a.c. voltages for the a.c. system in isolation is well behaved and is very similar to the single phase case as discussed in chapter 4. The slower overall convergence of the three phase load flow occurs in a stable manner with the voltages and angles changing very little after the initial iterations. That is, the final unbalanced power mismatches require only very small changes in voltages and angles to enable final convergence to be obtained. As a result the d.c. terminal powers appear as virtually constant real and reactive power loads over the final convergence of the a.c. system and the d.c. convertor does not, except in the case of a weak a.c. system, influence the final convergence.

From the discussion thus far it has been shown that both the three phase d.c. convertor terminal power flows and the three phase a.c. voltages converge in virtually identical patterns to the corresponding single phase cases. The interaction between a.c. and d.c. systems in the three phase case can therefore be expected to closely parallel the single phase sequential integration discussed in chapter 5.

The most stringent test is therefore the case of a weak a.c. system when the convertor control angles are not specified, for example case (xi). In such cases it is possible to observe an oscillatory convergence pattern which slows the overall convergence.

To examine the effect of a weak system in the three phase case the convergence patterns for the terminal powers and voltages are shown for case (x) and (xi) in Figs 6.10 and 6.11 respectively. The following general features of the three phase a.c./d.c. load flow may also be seen:

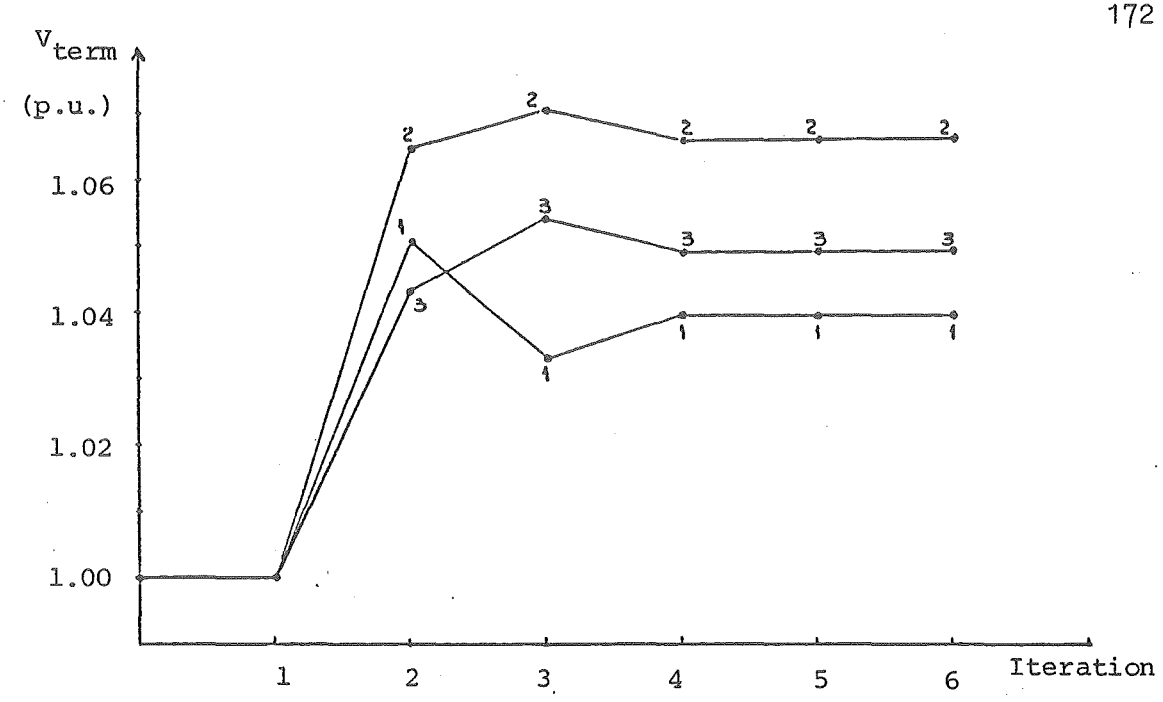

(a) A.C. Terminal Voltages

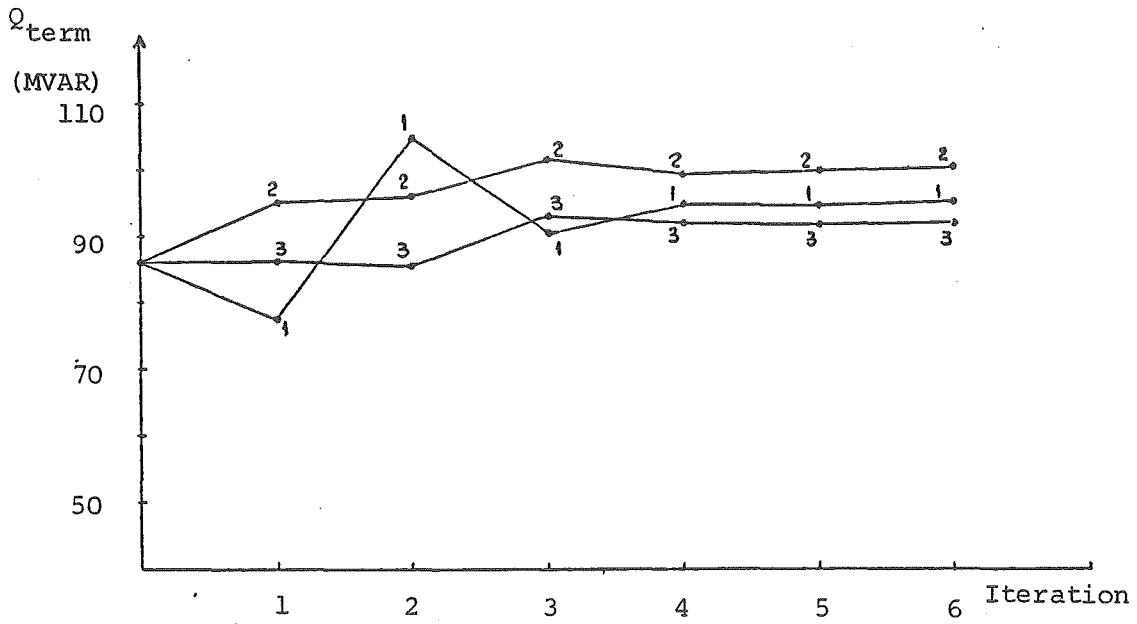

(b) Terminal Reactive Power Flows

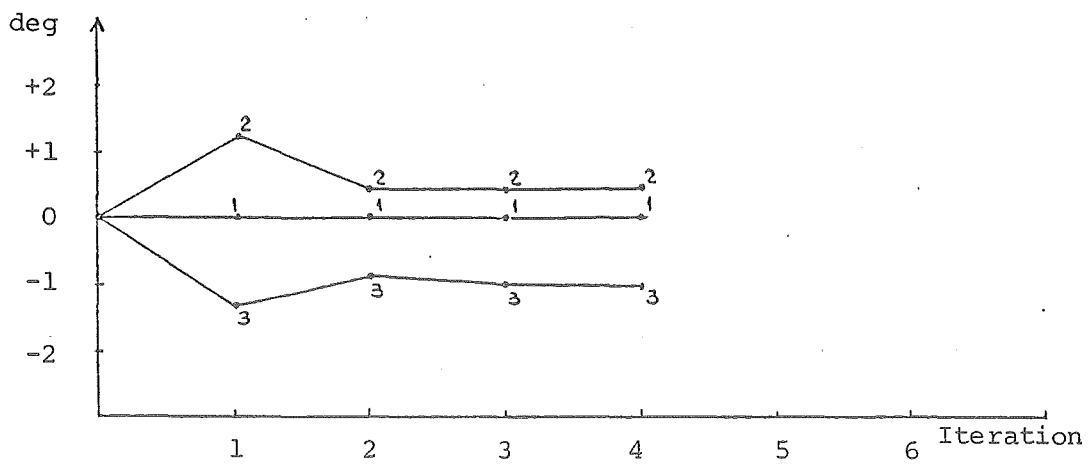

(c) A.C. Terminal Angle Unbalance (deviation from nominal)

Fig. 6.10 Convergence Patterns of Terminal Conditions for a Strong A.C. System

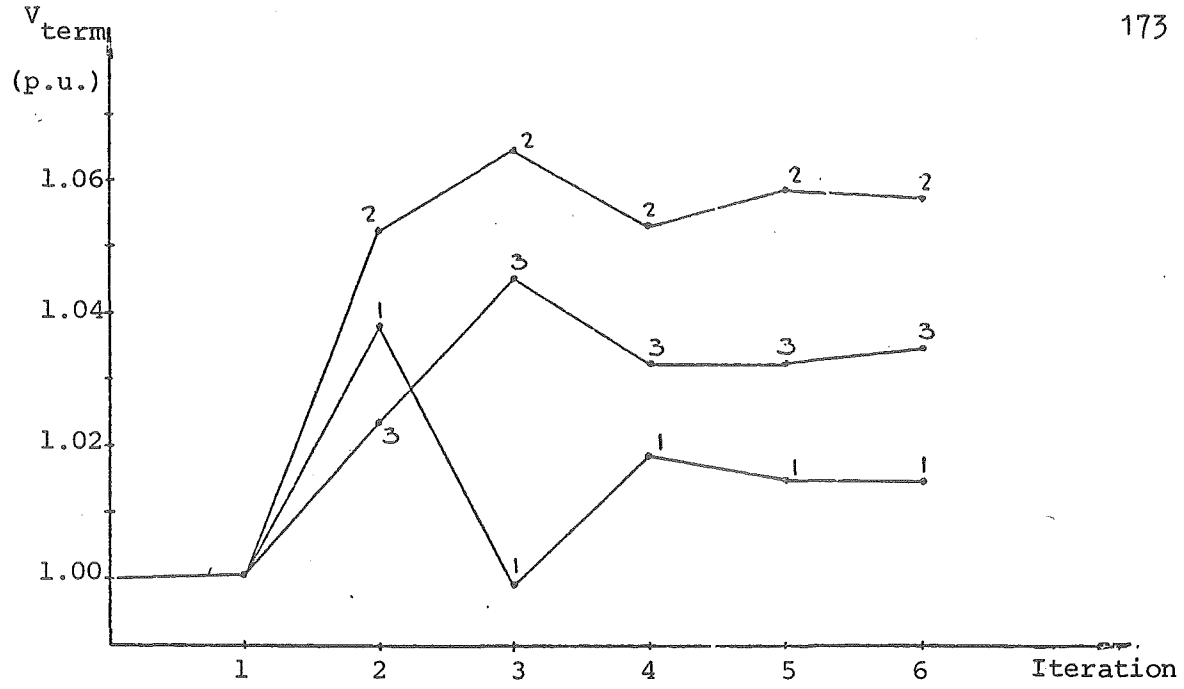

(a) A.C. Terminal Voltages

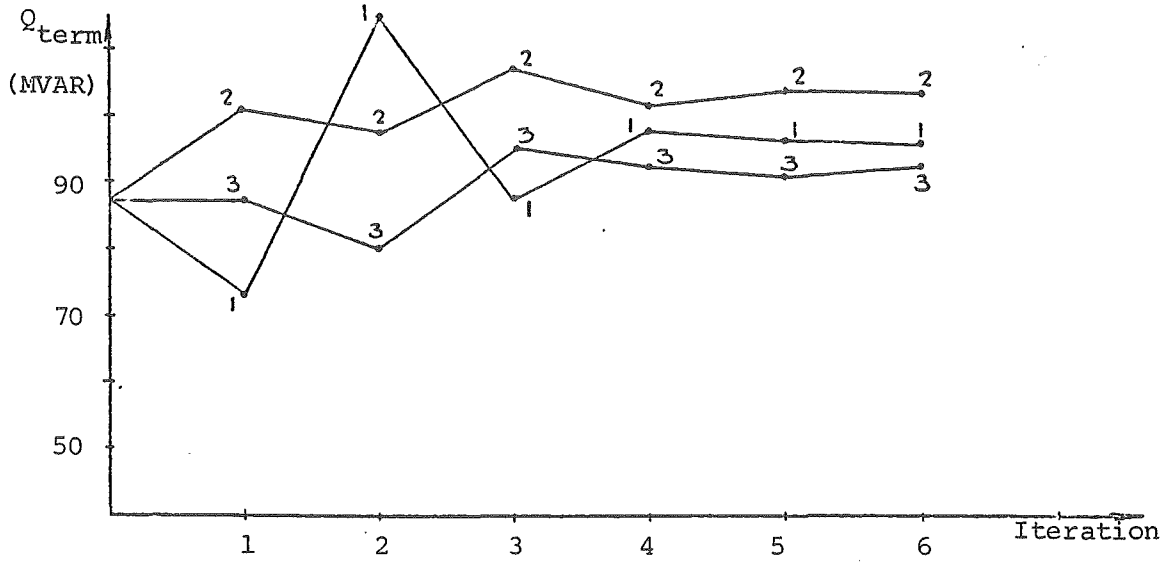

(b) Terminal Reactive Power Flows

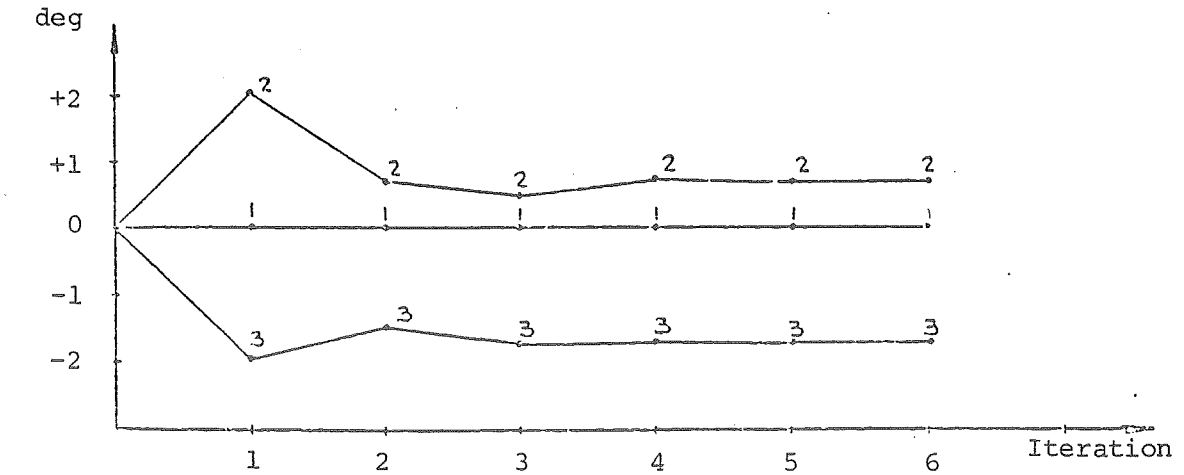

(c) A.C. Terminal Angle Unbalance (deviation from nominal)

Fig. 6.11 Convergence Patterns of Terminal Conditions for a Weak A.C. System

- for the first reactive power iteration the convertor reactive power demands are unbalanced. This unbalance is solely due to the terminal busbar phase angle unbalance and has, therefore, no definite relationship with the final reactive power unbalance.
- the terminal voltages resulting from the first reactive power iteration are due to a combination of the terminal reactive power, and the system unbalance.

As a consequence of these features the reactive power and voltage unbalance vary considerably over the first few iterations. Although this suggests that the d.c. convertor equations should not be solved until after one or two complete a.c. iterations, the initial variation in the unbalance does not cause any convergence problems and therefore alternative techniques, such as the one mentioned, have not been investigated.

Comparing Figs 6.10 and 6.11 it is clear that with the weaker system the unbalance is increased and also the convergence patterns are more oscillatory. Both these features cause a slowing of overall convergence. The corresponding convergence pattern for the single phase load flow for case (xi) is shown in Fig. 6.12 where a similar oscillatory pattern is observable. The sum of the three phase reactive powers and the +ve sequence voltage for the three phase case is also plotted in Fig. 6.12. The similarity is clear. In the three phase case it appears that the unbalance is virtually superimposed onto the behaviour of the single phase study.

6.6.6 Sample Results

The operating states for both convertors at BUS.03 are given for all cases in Tables 6.3(a) and (b). The corresponding a.c. system

(a) Three phase load flow

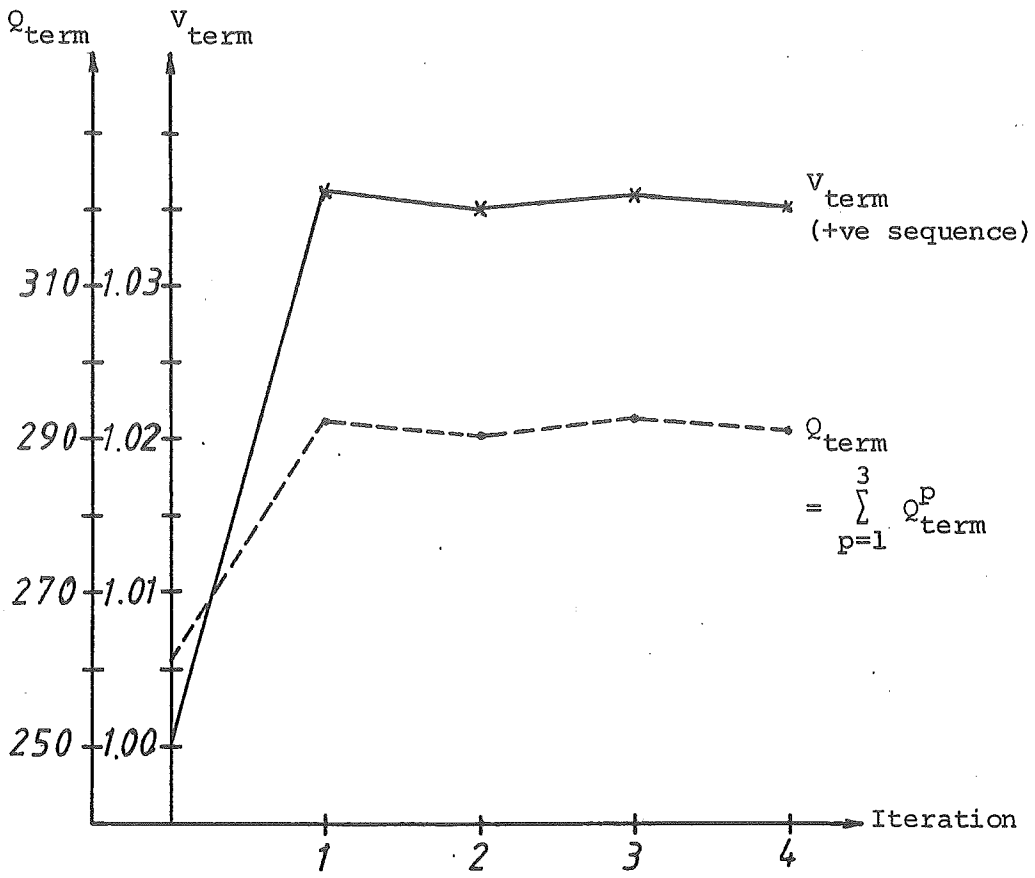

(b) Single phase load flow

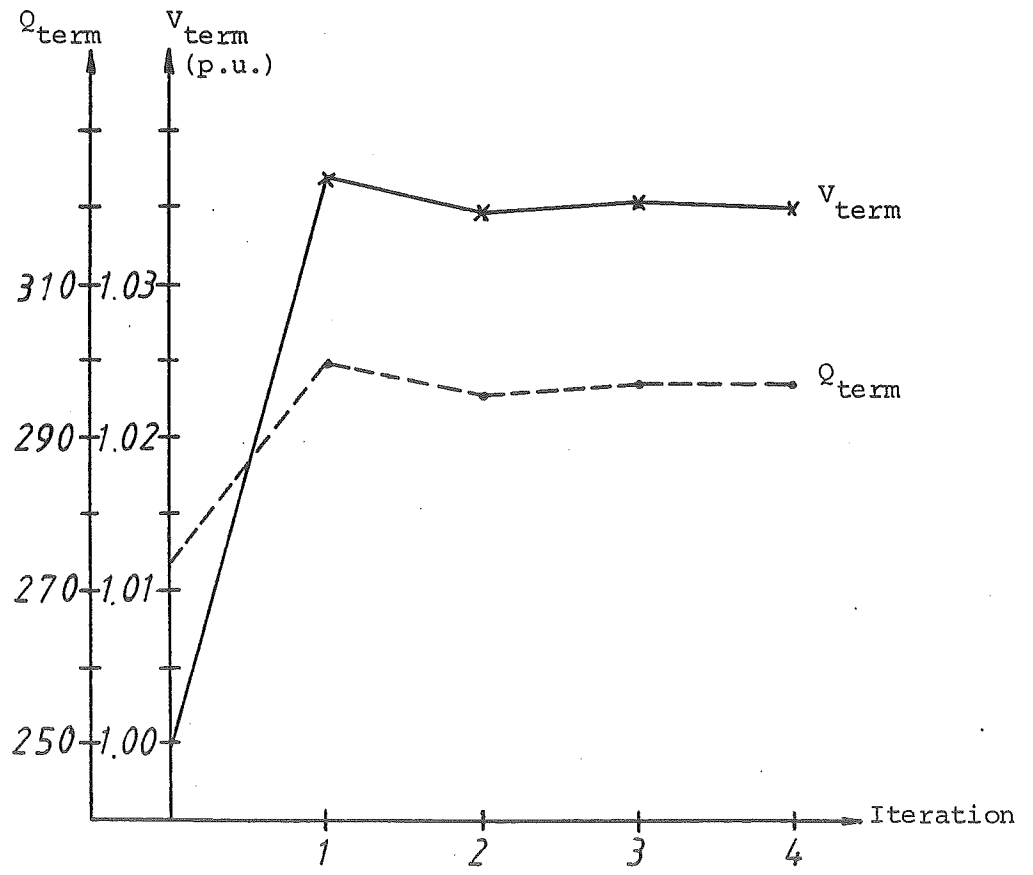

Fig. 6.12 Comparison of Single Phase and Three Phase Positive Sequence Convergence Patterns

Case	Phase	CONVERTOR 1 (STAR-STAR)						
		Firing Angle α_i (deg)	Tap Ratio a_i (%)	Commutation Angle μ_i (deg)	Terminal Powers		DC Conditions	
					Real P_i (MW)	Reactive Q_i (MVAr)	Voltage Vd_l (kV)	Current Id_l (kA)
b(i)	1	7.00	5.5	29.79	98.1	48.1	292.8	1.0246
	2	7.00	5.5	29.32	101.7	50.8	-	-
	3	7.00	5.5	29.61	100.3	48.3	-	-
b(ii)	1	7.00	5.3	29.78	98.6	49.0	292.8	1.0246
	2	7.20	5.3	29.14	100.9	51.3	-	-
	3	8.43	5.3	28.50	100.6	47.8	-	-
b(vi)	1	7.00	4.8	29.17	95.6	39.5	292.8	1.0246
	2	7.00	4.8	29.16	101.9	50.5	-	-
	3	7.00	4.8	30.43	102.44	57.2	-	-
b(vii)	1	7.00	3.9	29.03	97.6	39.1	292.8	1.0246
	2	11.64	3.9	25.63	101.8	54.7	-	-
	3	9.37	3.9	28.56	100.6	57.7	-	-
b(ix)	1	11.00	-10.0	24.32	104.6	49.4	314.1	0.9483
	2	7.00	0.0	27.76	101.1	45.4	-	-
	3	7.55	10.0	26.08	92.1	44.03	-	-

Table 6.3(a) Convertor 1 Results

Case	Phase	CONVERTOR 2 (STAR-G-DELTA)						
		Firing Angle α_i (deg)	Tap Ratio a_i (%)	Commutation Angle μ_i (deg)	Terminal Powers		DC Conditions	
					Real P_i (MW)	Reactive Q_i (MVAr)	Voltage Vd_2 (kV)	Current Id_2 (kA)
b(i)	1	7.00	5.5	29.80	97.3	49.2	292.8	1.0246
	2	7.00	5.5	29.60	102.6	53.2	-	-
	3	7.00	5.5	29.32	100.14	44.7	-	-
b(ii)	1	8.03	5.2	28.97	96.4	50.0	292.8	1.0246
	2	7.00	5.2	29.57	102.7	52.9	-	-
	3	8.55	5.2	28.08	100.87	45.66	-	-
b(vi)	1	7.00	4.3	30.63	67.9	13.0	292.8	1.0246
	2	7.00	4.3	28.92	95.5	89.4	-	-
	3	7.00	4.3	28.90	136.6	53.7	-	-
b(vii)	1	7.00	3.0	30.48	70.9	17.9	292.8	1.0246
	2	14.95	3.0	23.25	90.1	94.1	-	-
	3	13.41	3.0	24.25	138.9	52.2	-	-
b(ix)	1	8.08	-10.0	25.42	88.9	65.3	314.7	0.9483
	2	8.38	0.0	27.30	122.6	49.9	-	-
	3	7.00	10.0	26.96	86.9	24.2	-	-

Table 6.3(b) Convertor 2 Results

voltage profiles and generation results are given for cases a(i), b(i) and b(ii) in Table 6.4. The following discussion is with reference to these results.

Comparing cases a(i) and b(i) it may seem that the realistic three phase convertor model, which enables the unbalanced power demands of the convertor to be found, results in an identifiable alteration in the system voltages over the simple case of using balanced real and reactive loads at the terminal busbar.

The terminal power flows to the convertors are significantly unbalanced, especially in the case of the star-g/delta connection of the convertor transformer. The influence of these unbalanced loads on the a.c. operation depends on the strength of the a.c. system.

Comparing cases b(i) and b(ii) it may be seen that the symmetrical firing controller has only a small influence on the steady state fundamental power flows to the convertors. The main influence is, of course, on the harmonic generation and harmonic interaction which is considered further in the following chapters. Although small the following effects may be seen:

- there is a marginal increase in reactive power consumption due to two phases having greater than minimum firing angles.
- in the results given, a small increase in transformer tap boost was required to maintain the specified d.c. voltage. In actual practice the transformer taps are not infinitely variable and a small decrease in d.c. terminal voltage would occur for the same fixed tap.

The influence of the convertor transformer connection is significant. In addition to modifying the convertor source voltages it also

Case a(i)

BUS NAME	PHASE A VOLT.	PHASE A ANG.	PHASE B VOLT.	PHASE B ANG.	PHASE C VOLT.	PHASE C ANG.	GENERATION TOTAL	
BUS.01	1.067	27.294	1.067	-92.891	1.061	147.431	0.000	0.000
BUS.02	1.054	25.190	1.065	-94.670	1.057	144.915	0.000	0.000
BUS.03	1.038	23.185	1.071	-95.714	1.043	142.567	0.000	0.000
BUS.04	1.045	-3.566	1.046	-123.479	1.047	116.436	173.621	74.723
BUS.05	1.061	2.683	1.062	-117.367	1.061	122.628	700.000	113.920

Case b(i)

BUS NAME	PHASE A VOLT.	PHASE A ANG.	PHASE B VOLT.	PHASE B ANG.	PHASE C VOLT.	PHASE C ANG.	GENERATION TOTAL	
BUS.01	1.067	27.362	1.065	-92.955	1.062	147.437	0.000	0.000
BUS.02	1.055	25.232	1.064	-94.717	1.057	144.925	0.000	0.000
BUS.03	1.038	23.517	1.066	-95.965	1.049	142.543	0.000	0.000
BUS.04	1.045	-3.552	1.046	-123.483	1.047	116.438	173.570	74.706
BUS.05	1.061	2.690	1.062	-117.369	1.060	122.634	700.000	113.680

Case b(ii)

BUS NAME	PHASE A VOLT.	PHASE A ANG.	PHASE B VOLT.	PHASE B ANG.	PHASE C VOLT.	PHASE C ANG.	GENERATION TOTAL	
BUS.01	1.066	27.31	1.066	-92.942	1.062	147.421	0.000	0.000
BUS.02	1.054	25.238	1.064	-94.705	1.057	144.913	0.000	0.000
BUS.03	1.036	23.532	1.066	-95.947	1.049	142.506	0.000	0.000
BUS.04	1.045	-3.563	1.046	-123.479	1.047	116.439	173.593	75.949
BUS.05	1.061	2.690	1.062	-117.363	1.060	122.635	700.000	115.391

Table 6.4 Bus Voltages and Generation Results

modifies the phase distribution of power flows. The convertor transformer may also influence the a.c. operation directly which may be seen more clearly in Fig. 6.13 where the zero sequence voltages and currents are shown for case b(i).

It can be seen that under unbalanced conditions a zero sequence voltage may appear at system busbars. As the convertor has no zero sequence path, zero sequence current will only flow when the convertor transformer provides a path, as in the case of the star-G/delta transformer. Accurate convertor transformer models must therefore be included in the convertor modelling.

6.6.7 Conclusions On Performance of the Algorithm

It has been demonstrated that the fast decoupled three phase a.c./d.c. load flow behaves in a very similar manner to the corresponding single phase version. The following general conclusions on performance are applicable:

- the number of iterations to convergence is not significantly increased by the presence of the d.c. convertors.
- d.c. convergence is not dependent on the specific control specifications applied to each convertor.
- wide errors in initial conditions may be tolerated.
- for very weak a.c. systems the interaction of the convertor with the a.c. system is increased and the convergence is slowed.

Successful convergence can however, be expected in all practical cases.

- the algorithm exhibits good reliability even under conditions of extreme steady state unbalance.

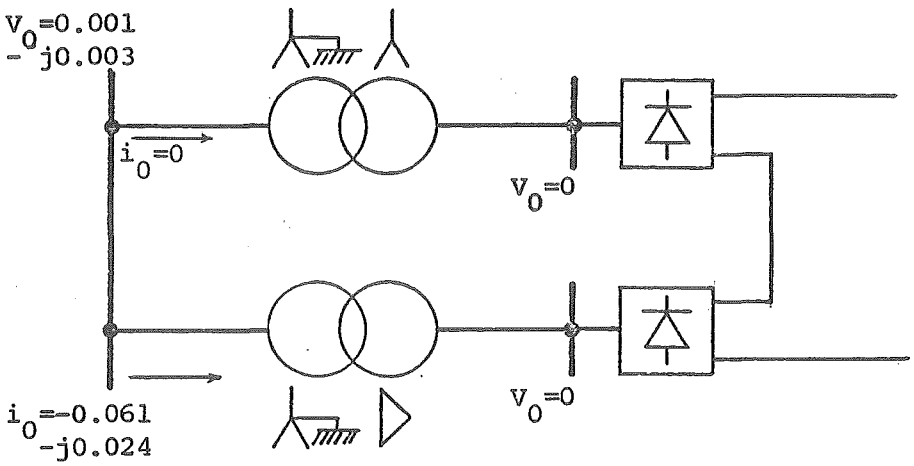

(a) Zero sequence potentials for case b(i)

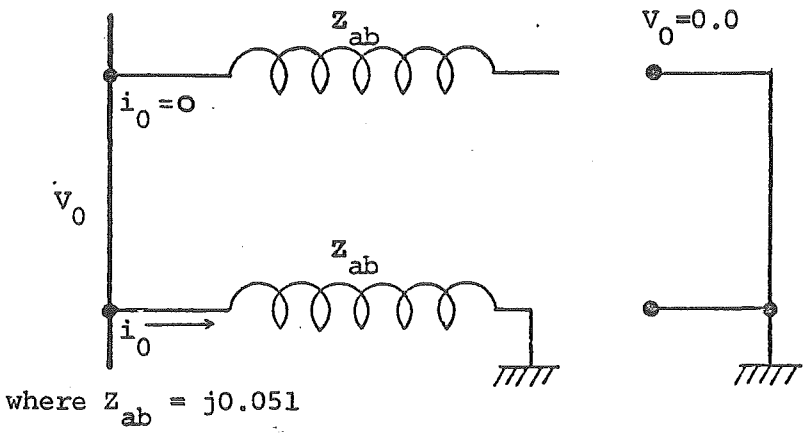

where Z_{ab} = j0.051

(b) Zero sequence network for convertor transformers

Note: Transformer secondary zero sequence reference is provided by equations

Fig. 6.13 Sequence Components and the Convertor Transformer Connection

6.7 CONCLUSION

A model of the steady state unbalanced operation of the three phase d.c. convertor has been formulated. The developed model is sufficiently general to enable convenient incorporation of the different firing controllers and also the various three phase convertor transformer connections. The sequential integration of the d.c. system model with the equations of a fast decoupled three phase load flow has been successfully implemented, without impairing the efficiency and convergence of the original fast decoupled algorithm.

CHAPTER 7

INTRODUCTION TO HARMONIC FREQUENCY POWER SYSTEM ANALYSIS

7.1 GENERAL CONSIDERATIONS

It is well known that any non-linear device operating from the power system will generate voltages and currents of harmonic frequencies. Common examples of such non-linear devices are the power transformer and d.c. power conversion equipment.

Harmonics in the power system cause many well documented[43] problems. In the New Zealand situation, the most significant problems experienced relate to Post Office communication and ripple control interference which result from the harmonic currents generated by high power d.c. conversion equipment. In the South Island of the New Zealand system up to 50% of the total generation is often used to supply the inter-island h.v.d.c. link and a large aluminium smelter. Early harmonic problems[52] and occasional recurring Post Office and ripple control interference have created a significant need for greater understanding of harmonic phenomena. In addition, overseas experience[53] suggests that the proliferation of non-linear solid state devices at domestic level, which generate both odd and even harmonic orders, are likely to be a source of future harmonic problems and there is a significant need to establish standards to limit harmonic generation levels at both domestic and industrial installations.

The use of ripple control equipment is widespread throughout New Zealand and many different frequencies and types of plant are

in use.[54]

A review of the ripple control characteristics shows that some systems are more susceptible to interference than others due to the wide frequency acceptance of the relay and the type of coding employed. The latest ripple control systems, employing fixed frequency solid state injection plant, allow better tuning of the relays and interference with this plant is unlikely. However, installed equipment is likely to remain in operation for a considerable time and the interference problem cannot be ignored.

In order to fully understand both harmonic generation and harmonic penetration into the power system, some means of analysis is required. Early techniques for harmonic frequency analysis were developed in connection with the design of ripple control systems[55,56,57]. These single phase harmonic penetration studies are used to determine the size of the injection plant, detect system resonances and identify locations with low signal levels. Apart from these studies very little has been done in the analysis of harmonic power flows. A notable exception is a detailed investigation into the flow of harmonics in transmission systems carried out in the 1940's by Whitehead and Radley[58].

Experience by New Zealand Electricity in extending the single phase analysis to the prediction of convertor generated harmonic levels on the h.v. transmission system has revealed significant deviations between calculated and monitored harmonic levels; this is thought to be due to the unbalanced nature of the harmonics at the point of generation and also the unbalanced and coupled nature of the three phase system.

It is the aim of this chapter to provide an introduction for further investigations into harmonic penetration studies on a three

phase basis. Although a detailed investigation of this topic is outside the scope of this thesis, many of the concepts and techniques involved are common to the steady state load flow analyses. In particular the steady state three phase convertor model developed in the previous chapter provides an excellent basis for the estimation of possible harmonic generation under unbalanced conditions, a subject discussed in the following chapter.

7.1.1 Harmonic Generation and Flow in the Transmission System

Any device which, when connected to a sinusoidal voltage supply, draws other than a sinusoidal current is a source of harmonics. Power transformers are a common example and some allowance is usually made for the zero sequence third harmonic currents which are required. Fifth and seventh harmonics also occur but these are generally small and do not cause operational problems.

The major source of harmonics which are troublesome in the a.c. system is the high power d.c. convertor. The harmonic currents injected into the a.c. system by the convertor are, in general, unbalanced between phases; the unbalance being more extreme for the case of non-characteristic harmonic orders. Measurements of the harmonic currents at Benmore[52] have shown deviations between phases of up to 56% (450 Hz) with an average deviation of 35%. The combined effect of the current unbalance and any system impedance unbalance is reflected in the phase voltages which are shown[52] in Table 7.1 for the Benmore 220 Kv busbar. All harmonic voltages are unbalanced with the most severe unbalance occurring at the non-characteristic third and ninth harmonics. Although unbalanced, the current injections at the convertor itself consist purely of positive and negative sequence components as there is no zero

Harmonic	400 A d.c. (one third full load current) Phase-to-neutral voltages At Benmore 220 kV		
	Red phase (%)	Yellow phase (%)	Blue phase (%)
1	100	100	100
2	0.5	0.7	1.0
3	2.9	0.3	1.0
4	0.6	0.3	0.4
5	0.25	0.15	0.25
6	0.25	0.30	0.35
7	0.15	0.15	0.1
8	0	0.05	0.1
9	0.05	0.05	0.15
10	0.05	0.05	0.05
11	0.1	0.15	0.1
12	0.15	0.05	0.15
13	0.05	0.05	0.05
14	0.05	0.05	0.05
15	0.15	0	0.2
16	0	0.1	0.15
17	0.3	0.3	0.3
18	0	0.05	0.1
19	0.3	0.3	0.7
20	-	-	-
21	-	-	-
22	0.2	0.2	0.5
23	0.4	0.2	0.3
25	0.2	0.2	0.15

Table 7.1 Harmonic Measurements during Back-to-back Testing.

sequence path for the convertor currents. This is discussed in more detail in the following chapter.

Moreover, with unbalanced conditions or with firing angle errors, both phase angle control and symmetrical firing control, give rise to uncharacteristic harmonics[59]. The advantage of symmetrical firing is the elimination of harmonic feedback effects[50] and the greater inherent accuracy of the firing controller.

Communication interference arising from harmonics in the a.c. system is usually caused by the flow of zero phase sequence components[43] of harmonic currents. If convertor generated harmonics are the source of the interference then the zero sequence currents arise solely because of the a.c. system unbalance. For long untransposed lines resultant zero sequence currents may be significant[58,60].

A series of tests have been carried out to investigate the importance of the mutual coupling between parallel transmission lines at harmonic frequencies. The harmonic voltages induced in an out of service 220 kv transmission line are shown in Table 7.2. The voltages, all of zero sequence, were caused by electromagnetic coupling with a parallel transmission line which was in service at the time of measurement. The zero sequence harmonic currents in the in service line are also given in Table 7.2.

Additional features which are illustrated in the Table are the high mutual coupling at 5th harmonic and the relatively high 9th harmonic current in the active line. Both these effects may be attributed to the transmission line length. The line is approximately 240 km long which corresponds to around a quarter of wavelength at 5th harmonic and approaches a half wavelength at 9th harmonic.

Harmonic Order	Zero Sequence Current (In Service Line) (Amps)	Induced Voltages (Volts) (Out of Service) VR	VY	VB
1	2.186	170	165	170
3	0.45	9	9	9
5	0.106	38	38	38
7	0.186	9	9	9
9	0.30	10	10	10

Table 7.2 - Measurements of Induced Voltages in Parallel Transmission

Zero sequence currents were measured using existing station CT's. The errors are small[60] at the frequencies measured (i.e. $< 1.5\%$).

Induced voltages were measured with a Plessey Audio Frequency Power Analyser.

Phase to Phase induced voltages were very small indicating that the induced voltages were of zero sequence.

From the preceding discussion it may be concluded that a realistic quantitive analysis of harmonic levels and their interference potential requires a detailed three phase representation of the power system. In addition, the major harmonic current injections must be accurately known.

The difficulties and uncertainty associated with harmonic investigations should not be underestimated. The major obstacles are:

(i) Three phase system data is not generally available at harmonic frequencies.

(ii) The values of both the characteristic and, more especially, the non-characteristic harmonic injections cannot be accurately assessed, except in the case of existing

schemes where measurements may be made. This difficulty is likely to remain insurmountable.

However, it is only by investigations into both the generation and propagation of harmonics on a three phase basis that a full appreciation of harmonic phenomena can be obtained. For this reason, research into both the calculation of harmonic current injections and the penetration of those harmonics into the a.c. system, is of considerable relevance.

The remainder of this chapter discusses the harmonic frequency system modelling.

7.2 COMPONENT MODELS FOR HARMONIC STUDIES

The formation of a mathematical model of the power system at harmonic frequencies is based on the fundamental frequency modelling discussed in chapter 2. However, more detailed consideration has to be given to the modelling of individual components at harmonic frequencies.

7.2.1 Transmission Lines

In general, the lumped parameter approximation commonly used for fundamental frequency analysis, where most lines may be considered electrically short (i.e., less than 1/20th of a wavelength long), can not be applied when higher harmonic frequencies are being considered. Accordingly, the exact representation[7], which takes full account of standing wave effects, must be used. The exact representation is most conveniently formed as an equivalent π or T circuit which gives the correct terminal conditions for the line under consideration. This technique is applicable to both three phase and single phase analysis.

The single phase equivalent pi and T circuits are shown in Fig. 7.1. The input impedance at any point along a line terminated with a load (Z_L) is,

$$Z_x = Z_0 \frac{Z_L + Z_0 \tanh\gamma.x}{Z_0 + Z_L \tanh\gamma.x} \qquad (7.1)$$

where

$$\gamma = \alpha + j\beta = \sqrt{ZY} \qquad \text{(propagation constant)}$$

and

$$Z_0 = \sqrt{\frac{Z}{Y}} \qquad \text{(characteristic impedance)}$$

For a short circuited lossless line:

$$Z_x = + j Z_0 \tan \beta.x \qquad (7.2)$$

For an open circuited lossless line:

$$Z_x = - j Z_0 \operatorname{cotan} \beta.x \qquad (7.3)$$

where

$\beta = 2\pi/\lambda$

λ is the wavelength

Therefore a line which is $\lambda/4$ long, will, when terminated in a short circuit, appear as a very high impedance, in a similar way to a parallel resonance of lumped capacitance and inductance. Under the same conditions a line $\lambda/2$ long will appear as a very low impedance, similarly to a series resonance.

For three phase models the series impedance and shunt admittance per unit length are 3 × 3 matrix quantities, as discussed in chapter 2, and matrix manipulations[12] are required to form the equivalent shunt and series matrices. Similar resonant effects are apparent, and, in addition, the influence of coupling between parallel circuits are included.

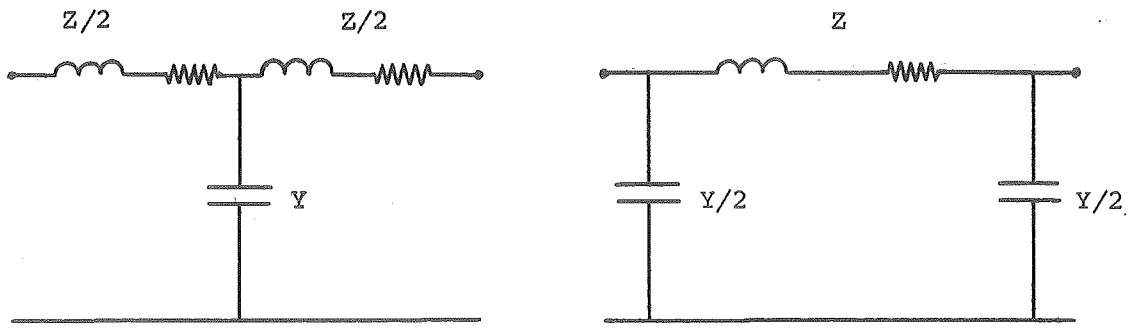

(a) Short line

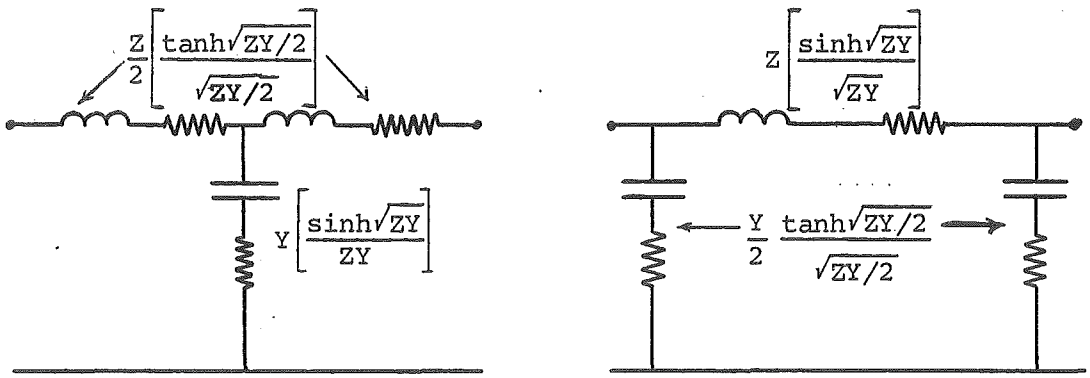

(b) Long line

where

$Z = \ell z = \ell(r + jx) = \ell(r + j2\pi fL)$

= total series impedance per phase

$Y = \ell y = \ell(g + jb) = \ell(g + j2\pi fC)$

= total shunt admittance per phase

where ℓ is length of line in miles; r,L,C, and g are resistance, inductance, capacitance, and leakance, respectively, per mile; f is frequency.

Fig. 7.1 Long Line Transmission Line Models

The methods of calculating the line parameters are well documented[7,61,62] and only the frequency dependent features will be considered further here.

7.2.2 Frequency Dependence of Transmission Line Parameters

7.2.2.1 Skin Effect

As the frequency increases the current concentrates at the outer circumference of the conductor or conductor bundle.

This effect is usually ignored in the calculation of reactance but it must be included in the calculation of a.c. resistance.

Detailed investigations[63] have shown that ACSR conductors may be considered as hollow tube conductors. The increase in a.c. resistance is strongly dependent on the ratio of inside to outside diameter as shown in Fig. 7.2.

7.2.2.2 The Effect of Ground Current Distribution

The effect of frequency on the ground currents and hence on the series impedance matrix, can be assessed by approximating the resistivity distributions of the earth. Carson[7] developed formulae which were based on the assumption of uniform earth resistivity.

The affect of variation of frequency and earth resistivity can be seen in Table 7.3 which was calculated[64] from Carson's equations for the line shown in Fig. 7.3. The increase in resistance with frequency due to skin effect and the increase in unbalance with increase in frequency is shown. The change in inductances may be understood by the concept of 'depth of penetration' of the earth currents. With increase in frequency or decrease in earth resistivity the currents do not penetrate so deeply and hence the inductance decreases.

More recent researchers[13] have developed techniques for considering the effect of multi layers of different conductivities.

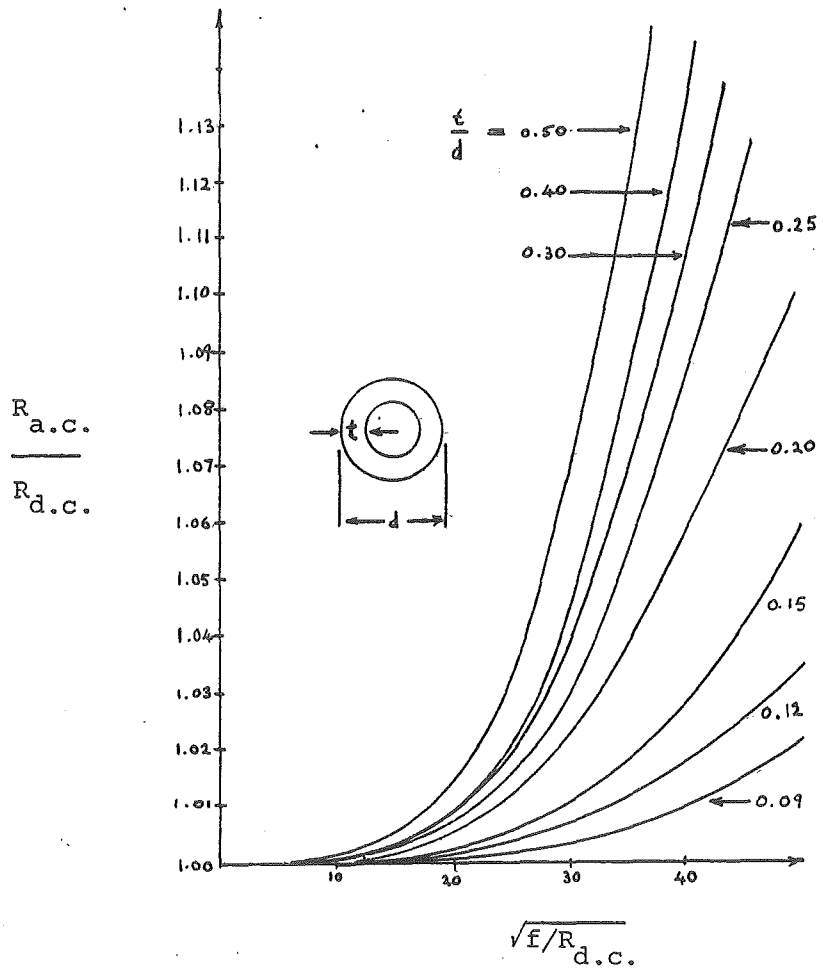

f - frequency cps

$R_{d.c.}$ - d.c. resistance in ohms/mile

Fig. 7.2 Skin Effect Curves for Tubular Conductors

	Earth Resistivity	Angular frequency ω rad/s					
		314		10^4		10^6	
	Ωm	Ω/mile	mH/mile	Ω/mile	mH/mile	Ω/mile	mH/mile
R_{11} L_{11}	20	0.075	2.831	1.925	2.338	61.62	1.962
	100	0.077	3.082	2.209	2.556	106.7	2.204
R_{12} L_{12}	20	0.074	1.321	1.794	0.845	49.58	0.518
	100	0.077	1.569	2.128	1.051	90.13	0.583
R_{13} L_{13}	20	0.073	1.102	1.680	0.641	41.41	0.353
	100	0.076	1.348	2.053	0.839	77.91	0.408
R_{22} L_{22}	20	0.073	2.841	1.680	2.381	41.42	2.092
	100	0.076	3.087	2.053	2.578	77.92	2.147
R_{23} L_{23}	20	0.071	1.330	1.580	0.885	35.54	0.625
	100	0.075	1.574	1.984	1.073	68.56	0.672
R_{33} L_{33}	20	0.070	2.850	1.491	2.419	31.11	2.184
	100	0.075	3.092	1.919	2.599	61.17	2.225

Table 7.3 Impedance of 275 kV Line

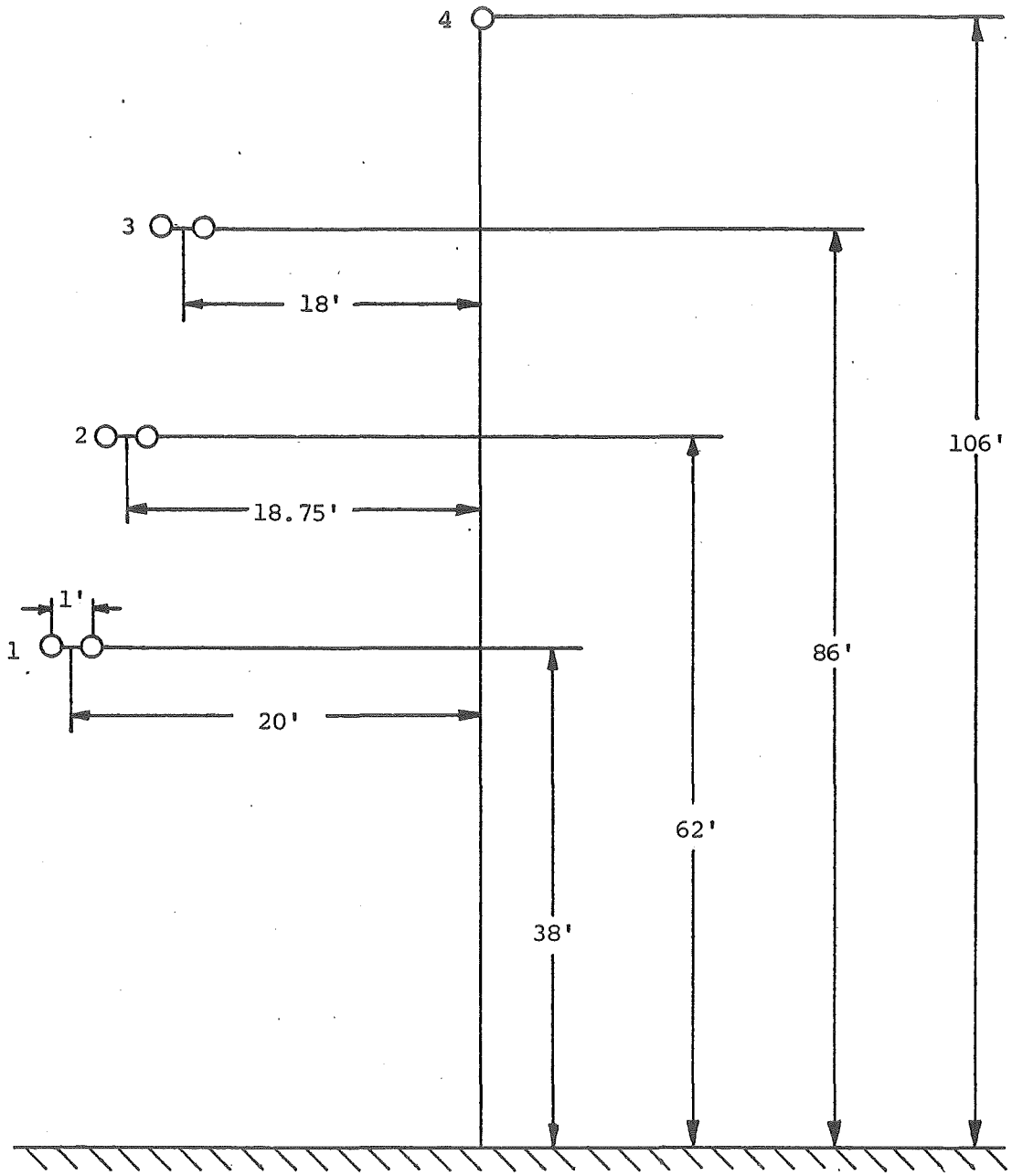

Fig. 7.3 Configuration for 275 kV Transmission Line

7.2.3 Transformer Modelling

The techniques discussed in chapter 2 for the modelling of various three phase connections are equally applicable to harmonic studies except for the values of leakage reactance and resistance, which must be modified. There is some disagreement in the literature[55,57] as to whether the full value or only 80% of the fundamental frequency reactance should be used. The resistance is taken as increasing with frequency and again there is some variation in the exact relationship. The exact values used are not critical unless the transformer forms part of a resonant circuit at a particular harmonic frequency.

A convenient model[57] to implement in an admittance formulation is shown in Fig. 7.4. A resistance, whose value is eighty times the fundamental leakage reactance in ohms, is placed in parallel with the transformer leakage inductance.

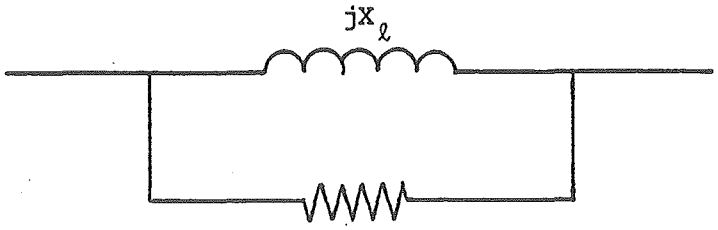

Fig. 7.4 Harmonic Frequency Transformer Model

The frequency variation of this model is shown in Fig. 7.5 where it may be seen that the resistance increases significantly with frequency while the leakage inductance decreases only slightly.

This model is applicable on a single phase basis or as part of

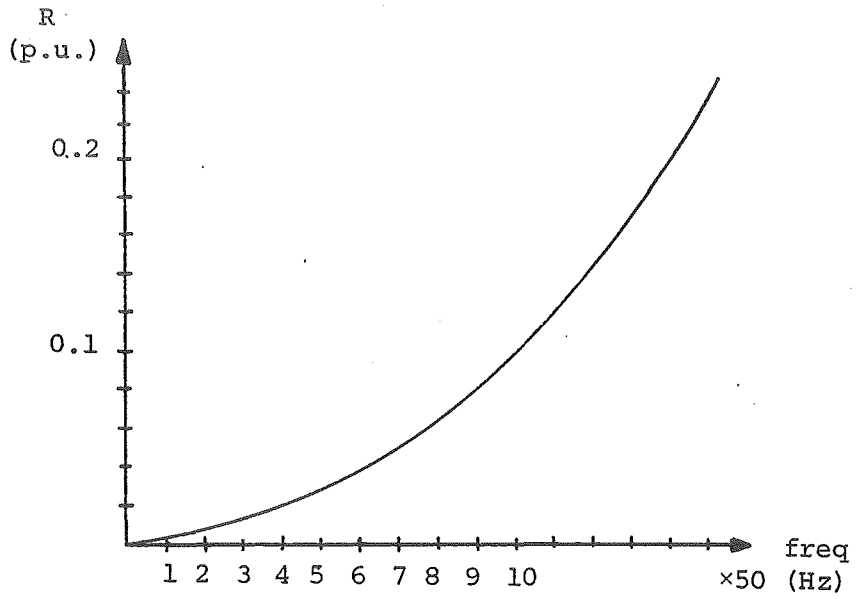

(a) p.u. resistance vs frequency

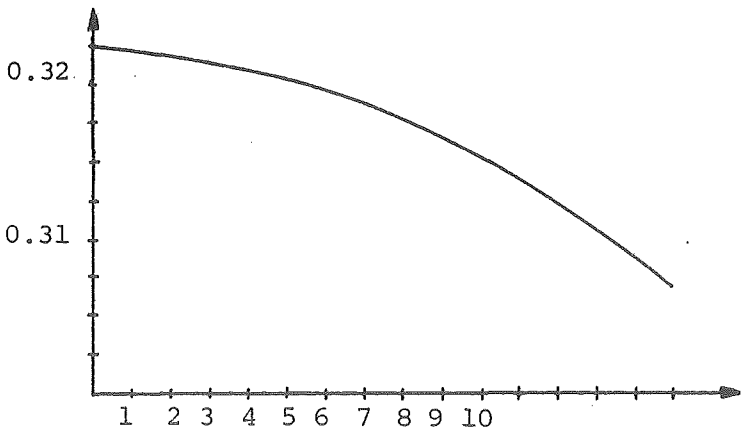

(b) p.u. inductance vs frequency
(note supressed zero of scale)

Fig. 7.5 Frequency Dependence of Transformer Model

the primitive network for the derivation of the three phase models.

7.2.4 Filter Modelling

In most high power d.c. convertor installations filters are provided for the characteristic harmonics.[43] Single tuned shunt filters are provided for the lower order harmonics. The higher order harmonics, usually 17th and above, are filtered using a second or third order high pass filter. It is not uncommon for additional filters to be required for abnormal harmonics which prove troublesome. For example at Benmore[52] an additional filter tuned to the 9th harmonic was found to be necessary. The filter types are illustrated in Fig. 7.6.

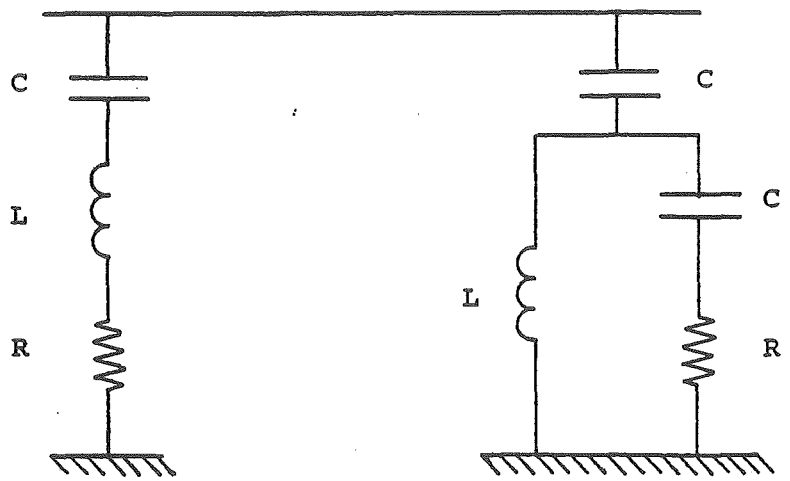

Fig. 7.6 H.V.D.C. Shunt Filter Types

The single tuned shunt filter impedance is,

$$Z_f = R + j\left(\omega L - \frac{1}{\omega C}\right) \tag{7.4}$$

and the third order high pass impedance with equal capacitors is,

$$Z_f = \frac{1}{j\omega C} + \left(\frac{1}{R + 1/j\omega C} + \frac{1}{j\omega L}\right)^{-1} \tag{7.5}$$

In an admittance formulation (where $Y_f = Z_f^{-1}$) the filters contribute

to the shunt admittance of the busbar to which they are connected.

7.2.5 Synchronous Machines

In general it may be assumed that the synchronous machines produce no harmonic voltages and they may therefore be modelled simply by a shunt connected impedance at their terminal busbar. A value of 80% of the subtransient inductance together with a power factor of 0.2 has been empirically determined to give satisfactory results.[55]

7.2.6 Loads

It is generally adequate to model loads by their equivalent parameters derived from the power frequency conditions.

7.3 CONCLUSION

This chapter has described the nature of the harmonic problems associated with transmission and distribution systems and has discussed the degree of system representation required for a quantitative analysis.

A brief introduction to three phase harmonic frequency power system modelling has been given and it is intended that this form a basis for further development.

CHAPTER 8

STEADY STATE HARMONIC GENERATION OF D.C. CONVERTORS.

8.1 INTRODUCTION

It is well known that, under unbalanced or distorted conditions (i.e. non sinusoidal supply), d.c. convertors produce abnormal a.c. current harmonics in addition to the expected characteristic harmonic orders. The unbalanced operation may be caused by the commutation reactances[65], the commutating voltages or the control system itself.[59,66,67]

Under normal steady state operation some minor unbalance is inevitably present and some uncharacteristic harmonic currents will be generated. These currents, together with the characteristic harmonic currents give rise to harmonic voltages at the convertor terminal busbar. The magnitude of the harmonic voltages is determined by the parallel combination of the system and filter impedances at each particular harmonic frequency.

The harmonic voltages may, depending on their magnitude and the control system in operation, give rise to an increased generation of harmonic currents of the same order. This feature of harmonic magnification[50], and in extreme cases instability, occurs due to a positive feedback loop between the terminal voltages and the harmonic current generation via the control system. It is usually only of importance for convertors connected to weak a.c. systems[51] or if the system harmonic impedance is high due to a.c. system resonances or resonances between the filters and the a.c. system.[67]

The use of control system filters to interupt this feedback loop has resulted in improved harmonic performance. However, several associated disadvantages[49] make the use of control system filters undesirable.

The symmetrical firing system, as proposed by Ainsworth[49], removes the feedback effect without the disadvantages of a control system filter. The symmetrical firing does not eliminate the generation of abnormal harmonics[59,69] under unbalanced conditions; it is however amenable to greater accuracy and it does eliminate many harmonic feedback effects.

The calculation of the harmonic currents produced by the convertor is complex due to the wide range of parameters which are involved and the difficulty of obtaining accurate values for those parameters. For these reasons it is difficult for the harmonic current generation to be calculated with reasonable accuracy. However, the features which influence harmonic generation and harmonic interactions can be studied and this provides valuable understanding of harmonic phenomena. This uncertainty introduces difficulties in assessing the assumptions which may be made without invalidating any particular study. As few assumptions as possible are therefore made and these are clearly stated.

Previous investigations[59,65,66,67] have assumed nominal conditions of unbalance (e.g. firing angle errors or voltage unbalance) or commutating voltage distortion and calculated the harmonic currents under those conditions. The results are usually presented as graphs of the percentages of positive and negative sequence harmonic current generation as a function of the unbalance or of the harmonic voltage distortion. The difficulty in presenting results is considerable and the thorough manner in which previous researchers have identified and quantified the various

features which cause harmonic production is commendable.

The aim of this chapter is not to reproduce those results but to develop a more general method to study the harmonic interaction between a convertor and the a.c. system, on the steady state.

Reeve et al[70] carried out harmonic interaction studies by means of dynamic simulation. Their analysis was restricted to a single convertor interacting with a reduced representation of the a.c. system. No attempt was made to include the effects of interaction between various convertors connected to the same a.c. system. While such extensions may be possible the computational costs become prohibitive and the use of dynamic analysis should be avoided whenever possible.

Steady state analysis can reduce the computational costs and still allow the investigation of many features associated with harmonic current generation. Although the dynamic response of the control system cannot be modelled, any steady state firing angle errors may be represented.

The steady state analysis presented here enables study of the harmonic interaction between separate convertor installations, the effectiveness of the filters and also the interaction of the filters and a.c. system. Computational efficiency is achieved by the use of a Fast Fourier Transform algorithm to calculate the fourier coefficients of the current waveshapes.

In common with previous investigations into the harmonic interaction of a convertor with the a.c. system, a knowledge of the system harmonic admittance is required. For the purpose of this chapter it is assumed that the harmonic frequency admittance matrices of the system elements are known. The calculation of these matrices and formation of the system admittance matrix for

each frequency was discussed in the previous chapter.

However, it is appropriate to restate here that, the formation of the harmonic system model is the area in which future efforts will need to be directed. The topic was introduced in the previous chapter and techniques for inclusion of the system model at harmonic frequency are discussed here. At present, the best data which is available is that derived from single phase studies and it is this data which has been used.

This chapter describes the calculation of the harmonic current injections of the d.c. convertors when operating from an a.c. system which contains unbalanced and distorted a.c. voltages. The harmonic interaction of the convertor and the a.c. system is studied with both symmetrical firing and phase angle control.

The basic method used to enable calculation of the harmonic voltages and currents generated by the d.c. convertor is illustrated in Fig. 8.1.

An important assumption, inherent in the method, is that the operating state of the convertors, as regards the d.c. current magnitude and the fundamental component of a.c. voltages at the terminal busbars, is not significantly altered by the presence of the harmonics. The validity of this assumption is considered in Appendix 7 where it is concluded that although intuitive reasoning suggests that harmonic voltages, up to the allowable limits, will not significantly affect the fundamental conditions, it is possible, under worst case conditions, for the fundamental operating state of the convertor, as calculated by the three phase load flow, to be significantly in error. The fundamental conditions which exist in the presence of harmonic distortion must therefore be compared with those originally calculated by the load flow. Lack of significant

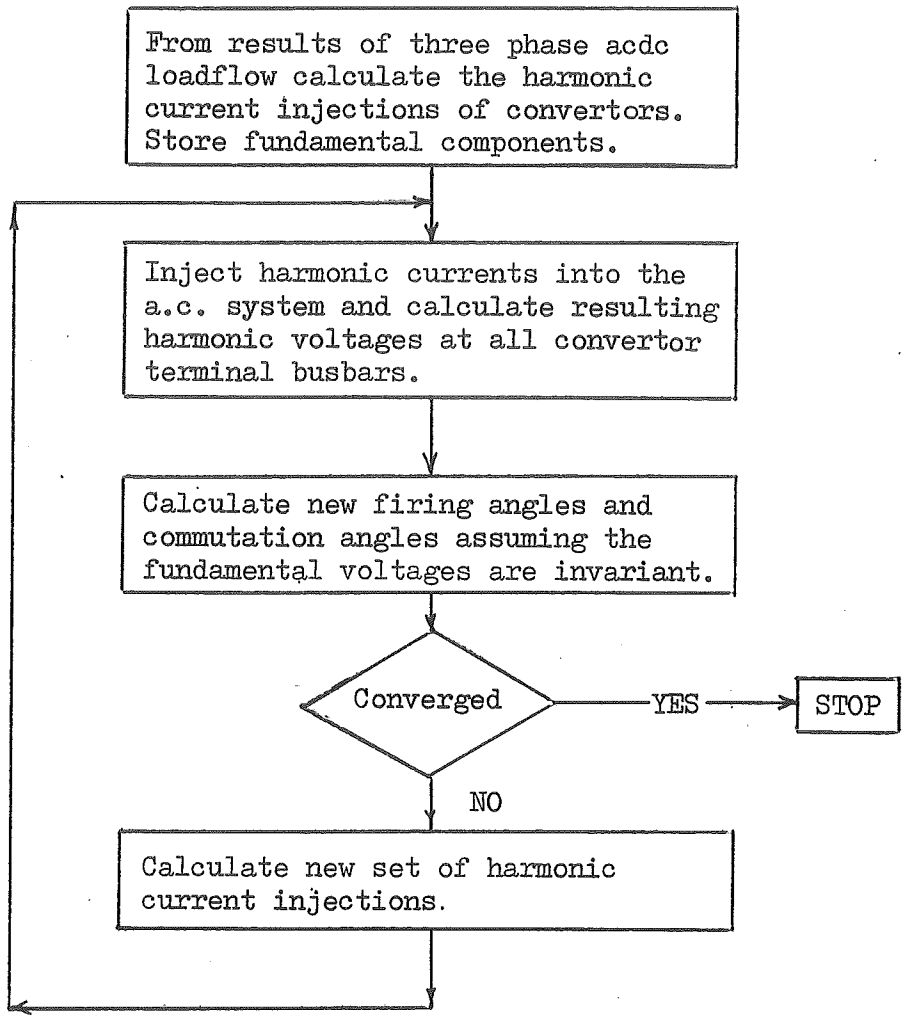

Fig. 8.1 Flow Chart of Harmonic Interaction Study

error confirms the validity of both the three phase a.c./d.c. load flow and of the harmonic study itself.

The details of the iterative solution technique, illustrated in Fig. 8.1, are discussed in the following sections.

8.2 CALCULATION OF HARMONIC VOLTAGES AT CONVERTOR TERMINAL BUSBARS.

8.2.1 A.C. System Modelling

It is assumed that the a.c. system is linear and therefore the principle of superposition may be applied to enable each harmonic to be considered separately. At each frequency of interest the system is modelled by its' harmonic admittance matrix. The harmonic voltages are related to the injected currents by the familiar equation:

$$[I] = [Y][V] \tag{8.1}$$

The development of the system harmonic admittance matrix was discussed in the previous chapter. For the present it is assumed that the system harmonic admittance matrix is known.

The method of solution for equation (8.1) is structured so that the harmonic admittance, as viewed from the convertor terminal, may be used if the complete system harmonic admittance matrix is not available.

8.2.2 Position of the Injected Currents

In the present investigation the only source of harmonic currents considered is d.c. convertor stations. The injected currents at most a.c. busbars will therefore be zero. For the convertors, the injected currents are calculated from the current waveshapes by fourier analysis.

Reeve et al[59] performed the Fourier analysis of the current

waveshapes at the convertor terminal busbar. This requires the transfer of the current waveshapes from the secondary (convertor) windings to the primary windings. While this is straightforward for a star-star unit it is considerably more complex for the star-delta connection, especially so as the transformer parameters and the commutation voltages may be unbalanced.

As models for all three phase transformers at the harmonic frequencies are available it is more convenient to include the convertor transformer into the system model and to simply calculate the harmonic currents on the transformer secondary. All units therefore have the same current waveshape and features such as phase shifts in the convertor transformer and the influence of the system unbalance are accurately included without the need for separate routines.

A further consideration influencing the convertor transformer modelling is the calculation of any zero sequence harmonic current flows in the a.c. system. Although the zero sequence voltage at the convertor terminal does not affect the convertor operation, it should be remembered that, in an unbalanced system, the magnitudes of the positive and negative sequence voltages are influenced by the flow of zero sequence currents. Therefore it is necessary to accurately model any zero sequence path in the convertor transformer.

8.2.3 Convertor Secondary Voltage Reference

The convertor transformer secondary is referenced to earth via the convertor to the d.c. earth. However, it is mathematically convenient to use a different reference for the purpose of analysis. As regards the position of a voltage reference, the considerations made in chapter 6 with reference to the fundamental frequency

modelling are applicable.

A reference may be provided by:

(i) Placing a large admittance to earth on one phase of the secondary. This effectively earths the phase concerned.

(ii) Placing a large resistance from each phase to a star point and earthing the star point. If the resistances are equal the reference is the zero sequence voltage as used in chapter 6.

Both methods have been tested and provide identical results. However, for consistency and ease of interpretation of results, method (ii) is used in the sections that follow.

8.2.4 Solution Technique

With reference to Fig. 8.1 it is clear that equation (8.1) must be solved repeatedly for the harmonic voltages at the convertor terminals. All other voltages are only required after the iterative solution procedure has converged. In addition, the system admittance matrix [Y] is constant at each frequency for each of the repeat solutions.

As an example consider the admittance matrix of the five bus test system used in chapter 6. Preserving the identity of each busbar in the system, including the convertor transformer secondarys (i.e. 6 and 7) equation (8.1) has the following form:

$$
\begin{bmatrix} I_1 \\ I_2 \\ I_3 \\ I_4 \\ I_5 \\ I_6 \\ I_7 \end{bmatrix} = \begin{bmatrix} 0 \\ 0 \\ 0 \\ 0 \\ 0 \\ I_6 \\ I_7 \end{bmatrix} = \begin{bmatrix} Y_{11} & Y_{12} & Y_{13} & & Y_{15} & & \\ Y_{21} & Y_{22} & Y_{23} & Y_{24} & & & \\ Y_{31} & Y_{32} & Y_{33} & & & Y_{36} & Y_{37} \\ & Y_{42} & & Y_{44} & & & \\ Y_{51} & & & & Y_{55} & & \\ & & Y_{63} & & & Y_{66} & \\ & & Y_{73} & & & & Y_{77} \end{bmatrix} \begin{bmatrix} V_1 \\ V_2 \\ V_3 \\ V_4 \\ V_5 \\ V_6 \\ V_7 \end{bmatrix}
$$

(8.2)

where all vectors are 3 × 1 and all matrix elements are 3 × 3.

The influence of the harmonic filters, if any, is inherently included in the calculation of the self admittances at the convertor terminal busbars as discussed in chapter 7.

In equation (8.2) the injected currents at all busbars except the convertor transformer secondaries (i.e. 6 and 7), have been set to zero.

Equation (8.2) retains the identity of every system busbar and its solution would yield the harmonic voltages at all system busbars. However in the iterative procedure only the voltages at the convertor terminal busbar are required. The a.c. system is therefore reduced to an equivalent system interconnecting all convertor a.c. terminal busbars. Considering the system of equations (8.2), the matrix may be re-ordered to ensure that the convertor terminal busbars, and all busbars where injected currents are present, are placed last. For example:

0		Y_{11}	Y_{12}		Y_{15}	Y_{13}			V_1
0		Y_{21}	Y_{22}	Y_{24}		Y_{23}			V_2
0			Y_{42}	Y_{44}					V_4
0	=	Y_{51}			Y_{55}				V_5
I_3=0		Y_{31}	Y_{32}			Y_{33}	Y_{36}	Y_{37}	V_3
I_6						Y_{63}	Y_{66}		V_6
I_7		=				Y_{73}		Y_{77}	V_7

(8.3)

The matrix may then be triangulated down to but excluding the convertor terminal busbars. The resulting matrix is:

0								V_1
0								V_2
0								V_4
0								V_5
I_3=0					Y^*_{33}	Y_{36}	Y_{37}	V_3
I_6					Y_{63}	Y_{66}		V_6
I_7					Y_{73}		Y_{77}	V_7

(8.4)

The 3 × 3 matrix elements $[Y_{33}]$ are modified but $[Y_{36}]$, $[Y_{37}]$, $[I_6]$ and $[I_7]$ are not.

In general the reduced matrix equation may be written:

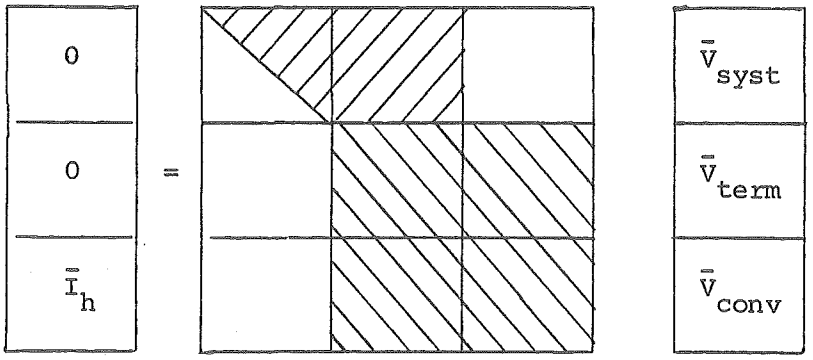

(8.5)

The lower part of the matrix, i.e.

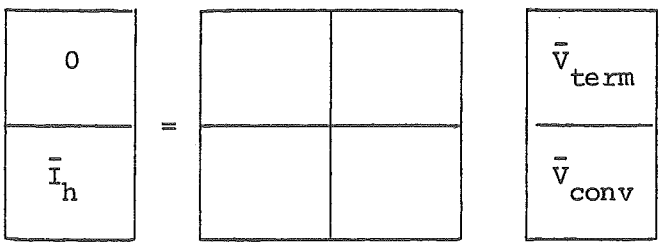

(8.6)

may be solved independently of the rest of the system. When data for the a.c. system elements are not available then the system admittance, as viewed from the convertor terminals, may be substituted into equation (8.6). The harmonic admittance may, in case of existing schemes, be from actual measurements or it may be estimated from single phase data or from the short circuit ratio and approximations for the phase angle of the short circuit impedance[68,70]. In these cases the system harmonic penetration and the harmonic interaction between convertors at separate a.c. busbars, cannot be studied.

In any case the reduced equation (8.6) is obtained. This is constant and need be factorised only once, before the iterative process. The vector of injected currents is then processed by the usual forward reduction and back substitution processes to yield the right hand side vector of harmonic voltages.

8.3 CALCULATION OF CURRENT WAVESHAPES

The calculation of the harmonic currents, in both magnitude and phase, requires a knowledge of the current waveshapes to a common phase reference. The angle reference for all quantities in the three phase load flow was arbitrarily taken as the phase 'a' voltage at the convertor terminal busbar. For convenience this reference is retained for the calculation of the current waveshapes.

When multiple convertor stations are present in a system it is necessary to ensure that all calculated harmonic currents are with respect to a common reference. The separate convertor references must therefore be related to a common reference.

The presence of harmonic voltages at the convertor terminal busbar will cause the actual zero crossing of the commutating voltages to be shifted from those calculated for the fundamentals alone. This shift has the effect of altering the time of valve firing with reference to the fundamental voltages. The commutation angles will therefore become altered.

The magnitude of these effects depends upon the control system. It is assumed that the control system, whether phase angle control or symmetrical firing, is presented with the actual zero crossings of the commutating voltages (i.e. there is no control system filter).

The process of calculating the new waveshapes involves:

(i) calculation of the actual crossing points of the commutation voltages

(ii) calculation of the new firing angles for the control system in operation

(iii) calculation of the new commutation angles.

These steps are discussed in the following sections.

8.3.1 Zero Crossing of the Commutating Voltage

The calculation of the zero crossings of the commutating voltages requires a knowledge of the magnitude and phase of all harmonic voltages at the convertor terminal. These voltages must then be referred across the transformer with consideration given to the transformer taps and transformer connection. Identical equations to those presented in chapter 6 for the fundamental, are applied to each harmonic.

An iterative process is used to determine the position of the zero crossings. A regula falsi method is used. As the crossing points of the fundamental voltages calculated by the load flow give excellent starting values, the iterative process converges rapidly.

It should be noted that, with harmonic voltages up to the allowable limits multiple zero crossings are extremely unlikely and therefore no procedures have been developed for this situation.

8.3.2 Derivation of Firing Angles

The firing angle refers to the angle between the actual zero crossing of the commutating voltage and the instant of subsequent valve firing.

With phase angle control it is assumed that the firing angles calculated by the three phase load flow are maintained. The firing angle need not be equal on each phase.

In the case of symmetrical firing control the firing angles become altered. Considering one phase as a reference and with the firing pulses delayed by sixty degrees for subsequent valve firings it is clear that, any shift in the zero crossing of the reference commutating voltage, will cause a similar shift in position of the valve firings on the other two phases. The actual firing angles on the other two phases are calculated from the shift in reference,

together with the shift in the respective zero crossing of the appropriate commutating voltage. With control system errors neglected the valve firings are constrained to be exactly sixty degrees apart.

In the context of the present investigation, which is to examine the nature of the harmonic interactions (not to attempt an exact analysis as this is considered impractical), the following assumptions are considered justified:

(i) The reference firing angle may be arbitrarily selected, e.g. phase 1.

(ii) Under inversion operation the extinction angle is the specified variable, however it is more convenient to assume that the firing angle is the control variable as for rectifier operation.

As a result of these approximations small errors between specified and actual control angles may occur however, this does not influence the nature of the harmonic interaction.

8.3.3 Calculation of Commutation Angles

Strictly speaking, the current waveform during commutation and the commutation angle should be calculated considering the harmonic voltages as well as the fundamentals. However, as the harmonic voltage magnitudes are generally small compared to the fundamental, the error in neglecting these is small[66]. Therefore all that is required for the calculation of the commutation current waveform and commutation angle is a knowledge of the effective firing delay from the zero crossing of the fundamental components of the commutating voltages. The equations used in the three phase load flow are then applicable.

8.4 FOURIER ANALYSIS OF CURRENT WAVESHAPES

The complexity of the Fourier analysis used in previous analyses[59,66] has been avoided here by the use of a Fast Fourier Transform (FFT) algorithm. The current waveshapes are simply sampled at regular intervals; the sampled data is then used by the FFT to yield the magnitude and phase of the Fourier coefficients.

With this technique, additional waveform complexity, such as the d.c. ripple, present no additional problems. In this chapter, however, the d.c. has simply been assumed constant.

The use of the FFT involves errors due to the numerical calculations themselves and the finite number of sample points used. To reduce computational cost a minimum number of sample points should be used, consistent with accuracy requirements. It has been found that for investigations of all harmonics up to the fiftieth, the use of 512 samples is adequate. With fewer samples the higher harmonics are subject to possible errors.

8.5 CONVERGENCE TEST

Convergence is obtained when a consistent self sustaining set of harmonic voltages and harmonic currents are found. Programmatically this is tested for by comparing the instant of valve firings from one iteration to the next. If the largest shift in valve firing is less than 0.001 radians, then convergence is accepted. A test related to the current waveshape is considered more appropriate than a test associated with the actual harmonic currents, largely due to the difficulty of assigning a realistic tolerance.

8.6 TEST SYSTEM AND SAMPLE RESULTS

8.6.1 Test System

The small six bus system described in chapter 4 has been modified by placing a large rectifier at bus TIW220. A single six pulse bridge rectifier is considered as this enables detailed results to be given whilst adequately demonstrating the nature of the harmonic study. The relevant convertor data and the results of the three phase a.c./d.c. load flow are given in Table 8.1. The results for both the symmetrical firing and the phase angle firing controllers are given.

8.6.2 Harmonic Study Under Normal Conditions

The initial values of the harmonic currents are calculated from the results of the three phase a.c./d.c. load flow which define the current waveshapes when fundamental voltages only are considered. These initial harmonic currents, given in Table 8.2, are then injected into the a.c. system and the resulting harmonic voltages at the terminal busbar are calculated from equation (8.6). This equation requires the harmonic admittances of the convertor transformer, filters and the a.c. system itself as viewed from the terminal busbar. The filter parameters[52] are given in Fig. 8.2 and typical system harmonic impedances are given in Table 8.3. The variation of filter impedance with frequency is indicated in Fig. 8.3.[52]

With reference to Fig. 8.1, the harmonic voltages, together with the existing fundamental voltages, must then be used to calculate new firing and commutation angles as discussed in section 8.3. A Fourier transform of the new current waveshapes yields a new set of harmonic injected currents. This process is repeated until a self sustaining consistent set of harmonic voltages and currents are obtained.

Table 8.1 Convertor Data and Load Flow Results

Convertor Data

Transformer type	star-g/delta
Transformer reactance (p.u.)	0.05
Commutation reactance (p.u.)	0.05
D.C. voltage base (kV)	0.44
D.C. load resistance (ohms)	0.0023
Filter susceptance (p.u.)	0.511

All values are equal on all phases.

Load Flow Results

	Phase Angle Control			Symmetrical Firing Control		
	Phase 1	Phase 2	Phase 3	Phase 1	Phase 2	Phase 3
Firing Angle (deg)	5.0	5.0	5.0	5.0	7.38	5.71
Interval between firing pulses*(deg)	119.2	118.4	122.4	120.0	120.0	120.0
Commutation Angle (deg)	33.2	33.1	33.8	33.2	31.1	33.1
Terminal Real Power (MW)	118.6	128.5	127.9	118.5	127.5	127.4
Terminal Reactive Power MVAR	59.8	64.0	57.5	60.3	64.8	57.5
Terminal Voltages						
Magnitude	1.0	1.031	1.028	1.0	1.031	1.028
Angle (deg)	0.0	-118.3	119.3	0.0	-118.3	119.3

* Interval is taken from firing instant of valve to the initiation of valve extinction. (See Fig. 6.3.)

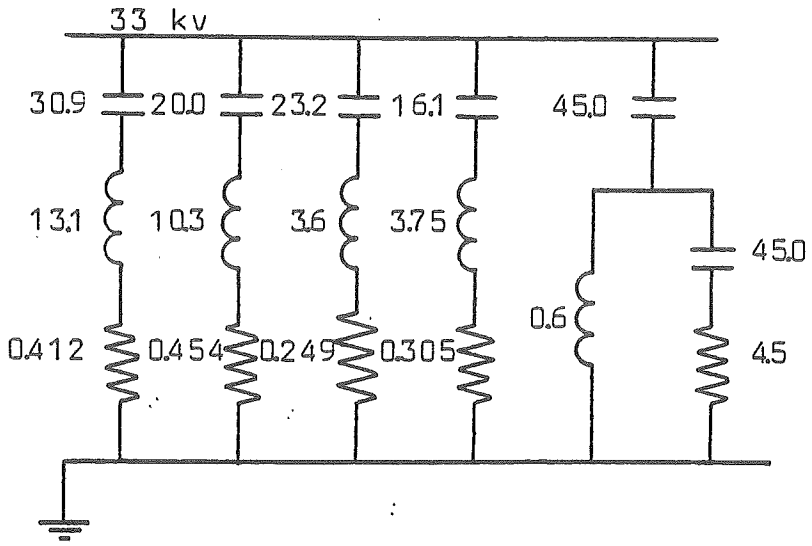

Fig. 8.2 Filter Parameters. (ohms, mH and μF)

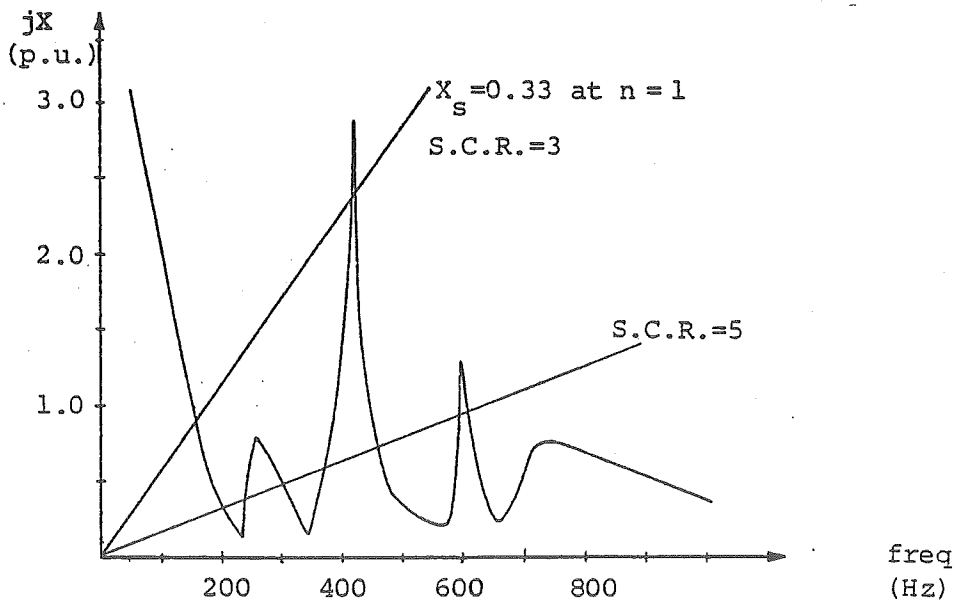

Fig. 8.3 Filter Impedance Diagram (p.u. to d.c. power base)

Table 8.2 Harmonic Currents When Harmonic Impedances Are Zero

(i) Symmetrical Firing Control

Order	Phase a		Phase b		Phase c	
	Mag.	Angle	Mag.	Angle	Mag.	Angle
1	4.075	2.16	4.047	0.08	4.115	-2.02
*3	0.006	-2.78	0.060	-3.01	0.066	0.15
5	0.617	1.33	0.645	-2.78	0.591	-0.68
7	0.322	-0.72	0.307	-2.67	0.352	1.48
*9	0.003	1.08	0.032	0.18	0.034	-2.89
11	0.084	-2.19	0.094	0.12	0.072	2.22
13	0.062	1.41	0.049	-0.47	0.066	-2.51
*15	0.001	-	0.015	2.46	0.015	-0.68

(ii) Phase Angle Control

Order	Phase a		Phase b		Phase c	
	Mag.	Angle	Mag.	Angle	Mag.	Angle
1	4.079	2.15	4.044	0.08	4.136	-2.01
*3	0.014	-2.77	0.077	-2.93	0.091	0.23
5	0.618	1.34	0.643	-2.75	0.576	-0.67
7	0.318	-0.72	0.296	-2.65	0.350	1.51
*9	0.005	1.03	0.033	0.32	0.036	-2.74
11	0.085	-2.20	0.093	0.11	0.072	2.20
13	0.062	1.42	0.051	-0.40	0.070	-2.51
*15	0.002	2.11	0.019	2.47	0.02	-0.70

Notes:
- rms values
- All angles are in radians relative to phase a terminal voltage
- * indicates non characteristic orders.

Table 8.3 Typical System Harmonic Impedances

Order	Impedance (ohms at 220 kV)
3	27.6 + j 84.0
5	200.3 + j 8.6
7	54.4 - j 59.7
9	11.7 - j 40.2
11	2.5 - j 3.8
13	2.2 + j 23.2
15	6.2 + j 57.6
17	28.1 + j122.3
19	79.7 - j 77.2
21	65.2 + j 66.6
23	111.3 - j 29.5
25	51.5 - j100.5

The values of the parameters which define the current waveshapes at each iteration are given in Table 8.4. The phase angle controller required four iterations and the symmetrical firing required three iterations. The final values of harmonic voltages and currents are given in Tables 8.5 and 8.6. The sequence components of the a.c. injected currents for the phase angle controller are given in Table 8.7.

8.6.3 Preliminary Discussion of Results

The results presented in the preceding tables demonstrate several aspects of harmonic current generation by d.c. convertors:

- small asymmetries in valve conduction periods produce significant non-zero sequence triplen harmonics.
- both firing controllers give rise to non-characteristic harmonic currents although the magnitudes are noticeably reduced with the symmetrical firing controller. The unbalance in commutating voltages causes a significant unbalance in the commutation angles which leads to the production of non-characteristic harmonics even with symmetrical firing. This feature is especially noticeable at small firing angles as in the example given.
- the predominant sequence of the characteristic harmonics is illustrated in Table 8.7.
- the unbalanced nature of the non-characteristic orders is clear.
- in this example both firing controllers are harmonically stable and this is reflected in the stability of the iteration procedure.
- with small values of α (5 degrees in the example), shifts in

Table 8.4 Values of Waveform Parameters at Each Iteration

(i) Phase Angle Control

Iteration	Shift in Zero Crossings			Commutation Angles			Period between Firings		
	SZC_1	SCZ_2	SZC_3	μ_1	μ_2	μ_3	T_1	T_2	T_3
0	0	0	0	33.22	33.15	33.78	119.26	118.37	122.36
1	1.10	-1.02	1.04	32.18	32.29	34.69	119.32	120.43	120.25
2	1.04	-0.79	0.92	34.12	32.48	34.59	119.38	120.08	120.53
3	1.05	-0.82	0.94	34.13	32.45	34.61	119.36	120.14	120.49
4	1.05	-0.82	0.94	34.13	32.45	34.61	119.36	120.14	120.49

- all firing angles are 5.00 degrees.

(ii) Symmetrical Firing

Iteration	Shift Zero Crossings			Commutation Angles			Firing Angles		
	SZC_1	SZC_2	SZC_3	μ_1	μ_2	μ_3	α_1	α_2	α_3
0	0	0	0	33.17	31.15	33.15	5.0	7.38	5.71
1	0.83	-0.83	0.89	33.94	31.86	33.89	5.0	5.68	5.72
2	0.95	-0.81	0.95	34.00	31.92	33.96	5.0	5.62	5.71
3	0.96	-0.81	0.96	34.01	31.92	33.96	5.0	5.62	5.71

- all periods between firings are 120.00 degrees.

Table 8.5 Harmonic Currents and Voltages for Symmetrical Firing

(i) Currents (p.u.)

Order	Phase a		Phase b		Phase c	
	Mag.	Angle	Mag.	Angle	Mag.	Angle
1	4.073	2.16	4.044	0.08	4.116	-2.01
3	0.007	-2.78	0.062	-2.99	0.069	0.17
5	0.612	1.35	0.641	-2.76	0.585	-0.66
7	0.317	-0.70	0.302	-2.65	0.348	1.49
9	0.003	1.07	0.032	0.23	0.034	-2.84
11	0.085	-2.20	0.094	0.12	0.072	2.21
13	0.063	1.45	0.051	-0.43	0.068	-2.48
15	0.001	-	0.014	2.46	0.015	-0.68

(ii) Voltages (p.u.)

Order	Phase a		Phase b		Phase c	
	Mag.	Angle	Mag.	Angle	Mag.	Angle
3	0.008	1.24	0.019	-1.86	0.011	1.31
5	0.022	0.72	0.021	2.89	0.02	-1.37
7	0.005	-1.19	0.006	3.11	0.006	0.88
9	0.001	2.46	0.012	1.62	0.013	-1.45
11	0.001	-	0.001	-	0.001	-
13	0.001	2.72	0.001	0.92	0.001	-1.39
15	0.001	-	0.015	2.49	0.016	-0.65

Table 8.6 Harmonic Voltages and Currents for Phase Angle Control

(i) Currents (p.u.)

Order	Phase a		Phase b		Phase c	
	Mag.	Angle	Mag.	Angle	Mag.	Angle
1	4.078	2.15	4.053	0.086	4.127	-2.011
3	0.132	-2.77	0.062	-2.98	0.075	0.19
5	0.614	1.354	0.638	-2.75	0.582	-0.66
7	0.315	-0.70	0.299	-2.64	0.347	1.50
9	0.004	1.01	0.031	0.23	0.034	-2.82
11	0.085	-2.21	0.094	0.11	0.072	2.2
13	0.063	1.45	0.052	-0.42	0.070	-2.49
15	0.002	2.15	0.015	2.51	0.017	-0.67

(ii) Voltages (p.u.)

Order	Phase a		Phase b		Phase c	
	Mag.	Angle	Mag.	Angle	Mag.	Angle
3	0.007	1.22	0.020	-1.84	0.013	1.34
5	0.022	0.73	0.021	2.89	0.020	-1.37
7	0.005	-1.19	0.006	3.12	0.006	0.88
9	0.001	1.93	0.002	-1.05	0.001	2.19
11	0.001	-	0.001	-	0.001	-
13	0.001	2.73	0.001	0.914	0.001	-1.39
15	0.001	-	0.002	-2.76	0.001	0.33

Table 8.7 Sequence Components of Harmonic Currents for Phase Angle Control

Order	Positive Seq.		Negative Seq.		Zero Seq.
	Mag.	Angle	Mag.	Angle	
3	0.041	3.12	0.039	1.91	0.0
5	0.032	-3.04	0.611	1.41	0.0
7	0.320	0.62	0.028	-2.41	0.0
9	0.020	1.78	0.018	-1.20	0.0
11	0.013	2.74	0.080	-2.06	0.0
13	0.063	1.61	0.009	0.18	0.0
15	0.009	-2.32	0.009	1.00	0.0

the position of zero crossings, and hence changes in firing angles, cause significant changes in the commutation angle. This change inhibits the alteration of the current waveshape and harmonic magnification is unlikely. Ainsworth[50] reported that with $\alpha = 0$ harmonic instability cannot occur.

- the presence of the harmonic voltages have little effect on the magnitude or phase of the fundamental currents in both cases given.

8.6.4 Investigation of Harmonic Instability

Harmonic magnification may occur with harmonic impedances above certain values. To illustrate this effect and to investigate the influence of a resonance phenomena, the third harmonic impedance of the system has been altered in order to form a resonant circuit with the filters. At third harmonic the filters appear capacitive and the system is invariably inductive. With typical filter parameters and a weak a.c. system parallel resonance at third harmonic is possible. This situation is illustrated in Fig. 8.3 where lines have been drawn on the filter impedance diagram indicating Short Circuit Ratios (S.C.R.) of around 3 and 5 respectively. A S.C.R. of around 3 gives a resonance at third harmonic.

The third harmonic system impedance has been arbitrarily selected as 94.0 + j 134.2 ohms to correspond to a S.C.R. of around 3. This yields a well damped resonant circuit whose resonant frequency is slightly off third harmonic.

In order to illustrate the harmonic interaction the study has been conducted as previously except with the nominal firing angles increased to 36.0 degrees.

The values of the parameters which define the waveform at each iteration are given for both cases in Tables 8.8 and 8.9 for the phase

	Shift in zero crossings (deg)			Commutation Angles (deg)			Periods between Firings (deg)			Third harmonic voltages (p.u.)		
	SZC_1	SZC_2	SZC_3	μ_1	μ_2	μ_3	T_1	T_2	T_3	Phase 1	Phase 2	Phase 3
0	0	0	0	14.34	14.29	14.75	119.23	118.17	122.60	0.015	0.047	0.032
1	-0.94	0.66	-1.23	14.12	14.15	14.44	119.61	116.17	124.21	0.036	0.078	0.042
2	-0.90	1.59	-1.74	14.13	14.68	14.35	120.06	114.84	125.09	0.051	0.097	0.046
3	-0.76	2.13	-1.92	14.16	14.82	14.31	120.4	114.11	125.49	0.060	0.106	0.046
4	-0.64	2.41	-1.99	14.19	14.89	14.29	120.60	113.80	125.65	0.065	0.111	0.046
5	-0.57	2.52	-2.02	14.20	14.92	14.28	120.68	113.61	125.70	0.066	0.112	0.046
. . .												
9	-0.52	2.58	-2.04	14.22	14.94	14.28	120.75	113.54	125.70	0.068	0.113	0.045

Table 8.8 Values of Waveform Parameters at each Iteration: Phase Angle Control

	Shift in crossings (deg)			Commutation Angles (deg)			Firing Angles (deg)			Third harmonic voltages (p.u.)		
	SZC_1	SZC_2	SZC_3	μ_1	μ_2	μ_3	α_1	α_2	α_3	Phase 1	Phase 2	Phase 3
0	0	0	0	14.14	13.52	14.40	36.00	38.67	36.71	0.006	0.008	0.002
1	-0.68	0.29	-0.94	13.98	13.38	14.24	36.00	39.06	36.45	0.006	0.008	0.002
2	-0.67	0.28	-0.90	13.98	13.38	14.25	36.00	39.06	36.48	0.006	0.008	0.002
3	-0.67	0.28	-0.90	13.98	13.38	14.25	36.00	39.06	36.48	0.006	0.008	0.002

Table 8.9 Values of Waveform Parameters at Each Iteration: Symmetrical Firing

angle and symmetrical firing controllers respectively. The phase angle controller required 9 iterations and the symmetrical firing controller 3.

The following features are noteworthy:

- at the larger value of α, the unbalance in commutation angles is less and the symmetrical firing controller gives rise to less non-characteristic harmonics.
- the symmetrical firing controller is harmonically stable where as the phase angle controller exhibits considerable harmonic interaction and harmonic magnification occurs. The harmonic stability or otherwise is directly reflected in the iterative process.

If the damping of the resonant circuit is reduced or if resonance is approached more closely the phase angle controller becomes harmonically unstable and the iteration process fails to converge.

8.7 CONCLUSION

A method has been developed to allow the investigation of many features associated with steady state harmonic phenomena in power systems. The penetration of harmonic currents into the power system may be studied on a three phase basis. In addition a wide range of features associated with d.c. convertor installations may be examined. In particular the harmonic interaction between convertors and the a.c. system may be studied including the influence of features such as the firing controller, a.c. system resonances, and the filter installations. The incomplete cancellation of characteristic six pulse harmonics with unbalanced operation of a twelve pulse bridge has also been studied.

As with all studies into harmonic phenomena associated with d.c. convertors, there is a significant uncertainty associated with any numerical solutions for the uncharacteristic orders, due to their sensitivity to a wide range of parameters, many of which either cannot be accurately known or are of a dynamic, rather than steady state nature. However, studies such as the one described here are a significant aid to the understanding of harmonic phenomena.

CHAPTER 9

CONCLUSION

This thesis has presented techniques for the general steady state analysis of integrated a.c. and d.c. power systems under normal, but not necessarily balanced, conditions.

Phase co-ordinate modelling of the unbalanced three phase system has been extensively reviewed. The nodal admittance representation in phase co-ordinates is suitable for the application of the most successful load flow analysis technique presently available, i.e. the fast decoupled algorithm.

The extension of single phase fast decoupling principles to the three phase load flow has been successfully attempted. Such extension is not straight forward due to the additional features associated with three phase system modelling. Further jacobian assumptions are required as regards the angle unbalance at a busbar and the angles across various three phase transformer connections. In addition, the modelling of the three phase synchronous generators requires a consideration of the voltage regulator. The most successful method developed is the inclusion of the voltage regulator specification directly in the formulation of the reactive power jacobian equation of the fast decoupled algorithm.

The developed three phase fast decoupled algorithm displays the same advantages, in terms of efficiency and reliability, as the original single phase version. The convergence patterns of the three phase version closely parallel those of the single phase version. The convergence of the system unbalance is, in effect, superimposed

on the convergence of the dominant positive sequence power flows. The rate of convergences decreases as the degree of system unbalance increases, but is acceptable even in cases of extreme steady state unbalance.

The three phase load flow is a necessary tool in the analysis of many features of steady state power system operation and the developed algorithm is currently being included in the suite of power system analysis programmes in use by New Zealand Electricity.

The development of d.c. convertor models, which are suitable for inclusion in single phase load flow analyses, have been discussed in detail. The most appropriate algorithm for the integration of such models into the single phase fast decoupled a.c. load flow has been investigated. The results of this investigation illustrated the superior convergence of the simultaneous or unified algorithms in difficult cases. For the vast majority of cases however, the simpler sequential algorithms proved equally efficient and reliable. In difficult cases, where the a.c. system is weak in a load flow sense, the convergence of the sequential algorithm is slower, but within the range of practical systems it is reliable.

The techniques developed for single phase a.c./d.c. load flow have been successfully extended to the three phase representation to enable the investigation of d.c. convertor performance under unbalanced conditions.

A phase co-ordinate model of d.c. convertor systems operating in an unbalanced state has been formulated with sufficient generality to allow representation of various control strategies such as predictive and symmetrical firing control. The sequential integration of the developed model into the three phase fast decoupled load flow analysis has been described. The results given illustrate the flexibility

and powerful convergence of the proposed integration. The similarity in performance to the corresponding single phase algorithm has also been demonstrated.

Using the unbalanced d.c. convertor model as a basis, the scope of the steady state analysis has been extended to the consideration of harmonic frequencies. Three phase a.c. system modelling at harmonic frequencies has been introduced. The harmonic current generation of d.c. convertors has been investigated including the influence of features such as the firing controller and system resonances. This investigation enables consideration of harmonic interaction between convertors, filters and the a.c. system. An important general conclusion regarding the calculation of harmonic current generation is the uncertainty in the numerical accuracy of any results due to the impracticability of including the large number of parameters involved. However, the harmonic study is of considerable value in that the possibility of harmonic problems and the effectiveness of the filters may be assessed. The harmonic study is suitable for extension to enable the assessment of even harmonic and d.c. components.

The development of harmonic frequency models of the power system and the subsequent realistic harmonic penetration studies is the area in which further study can be profitably directed.

REFERENCES

1. ROPER, R.D., and LEEDHAM, P.J.: 'A review of the causes and effects of distribution system three-phase unbalance', I.E.E. Conference on Sources and Effects of Power System Disturbances, no. 110, London, 1974.

2. ARRILLAGA, J., and HARKER, B.J.: 'Fast decoupled three-phase load flow', Proc. I.E.E., 1978, 125, (8) pp.734-740.

3. HARKER, B.J., and ARRILLAGA, J.: '3-phase a.c./d.c. load flow', Proc. I.E.E., 1979, 126(12), pp.1275-1281.

4. ARRILLAGA, J., HARKER, B.J. and BODGER, P.: 'Unified and sequential load flows for A.C. systems containing static convertors', Power Systems Computation Conference, Darmstatd, Germany, August, 1978. pp.719-729.

5. ARRILLAGA, J., HARKER, B.J. and BODGER, P.: 'Fast decoupled load flow algorithms for a.c./d.c. systems', I.E.E.E. PES Summer Meeting, Los Angeles, July, 1978, A78555-5.

6. ARRILLAGA, J. and HARKER, B.J.: 'Inclusion of a large convertor load into three phase load flow analysis'. Trans. I.E. (Aust), Vol. E.E. 16, No. 1, March, 1980, pp.6-13.

7. CLARKE, E.: 'Circuit Analysis of A.C. Power Systems - Vol. 1'. Wiley 1943.

8. EL-ABIAD, A.H., and TARSI, D.C.: 'Load flow solution of Untransposed EHV Networks'. Power Industry Computer Applications (PICA) Proceedings, Pittsburgh Pa, May 1967, pp.377-384.

9. CHEN, M.S., and DILLON, W.E.: 'Power System Modelling'. Proc. I.E.E.E., Vol. 62, No. 7, July 1974, pp.901-915.

10. STEVENSON, W.D., Jr: 'Elements of Power System Analysis'. McGraw Hill Book Company, 1962.

11. KRON, G.: 'Tensor Analysis of Networks'. MacDonald, London, republished 1965.

12. BOWMAN, K.I., and McNAMEE, J.M.: 'Development of Equivalent Pi and T Matrix Circuits for long Untransposed Transmission Lines'. I.E.E.E. PAS Vol. 84, June, 1964, pp.625-632.

13. WEDEPOHL, L.M., and WASLEY, R.G.: 'Wave Propagation in Multiconductor Overhead Lines'. Proc. I.E.E., Vol. 113, No. 4, April, 1966, pp.627-632.

14. DILLON, W.E., and CHEN, M.S.: 'Transformer Modelling in unbalanced Three Phase Networks'. I.E.E.E. Summer Power Meeting, Vancouver, July, 1972.

15. LAUGHTON, M.A.: 'Analysis of Unbalanced Polyphase Networks by the Method of Phase Co-ordinates. Part 1. System Representation in Phase Frame of Reference'. Proc. I.E.E., Vol. 115, No. 8, August, 1968, pp.1163-1172.

16. THE J & P Transformer Book. Johnson & Phillips Ltd, Ninth Edition, 1961.

17. LAUGHTON, M.A. and HUMPHREY DAVIES, M.W.: 'Numerical Techniques in Solution of Power System Load flow Problems'. Proc. I.E.E., Vol. III, No. 9, September, 1964, pp.1575-1588.

18. KREYSZIG, E.: 'Advanced Engineering Mathematics', 2nd Edition, N.Y., Wiley, 1967, pp.646.

19. STAGG, G.W. and EL-ABIAD, A.H.: 'Computer Methods in Power System Analysis'. McGraw Hill, 1968, pp.249.

20. STOTT, B.: 'Review of Load flow Calculation Methods'. Proc. I.E.E.E., Vol. 62, No. 7, July, 1974, pp.916-929.

21. WALLACH, Y., and EVEN, R.K.: 'Application of Newton's Method to Load flow Calculations'. Proc. I.E.E., Vol. 114, March, 1967, pp.372-374.

22. HOLLEY, H., COLEMAN, C. and SHIPLEY, R.B.: 'Untransposed ehv line computations'. I.E.E.E. Trans. on Power Apparatus and Systems, March, 1964, p.291.

23. HESSE, M.H.: 'Circulating currents in parallel untransposed, multicircuit lines: I - Numerical evaluations'. I.E.E.E. Trans. on Power Apparatus and Systems, July, 1966, p.802.

24. HESSE, M.H.: 'Circulating currents in parallel untransposed multicircuit lines: II - Methods of eliminating current unbalance', ibid., July, 1966, p.812.

25. KARAS, A.N.: Discussion on reference 23.

26. WASLEY, R.G. and SLASH, M.A.: 'Newton-Raphson algorithm for three-phase load flow'. Proc. I.E.E., Vol. 121, No. 7, July, 1974, p.630.

27. BIRT, K.A., GRAFFY, J.J., McDONALD, J.D. and EL-ABIAD, A.H.: 'Three phase load flow program'. I.E.E.E. Trans. on Power Apparatus and Systems, January, 1976, p.59.

28. KERSTING, W.H. and SEEKER, S.A.: 'A program to study the effects of mutual coupling and unbalanced loading on a distribution system'. I.E.E.E. PES Winter Meeting, N.Y., January, 1975, C75047-6.

29. TINNEY, W.F. and HART, C.E.: 'Power flow solution by Newton's Method'. I.E.E.E. Trans. on Power Apparatus and Systems, June, 1961, p.299.

30. STOTT, B. and ALSAC, O.: 'Fast decoupled load flow'. I.E.E.E. Trans. on Power Apparatus and Systems, May, 1974, p.859.

31. STOTT, B.: 'Decoupled newton load flow'. I.E.E.E. Trans. on Power Apparatus and Systems, September, 1972, p.1955.

32. DESPOTOVIC, S.T.: 'A new decoupled load flow method'. I.E.E.E. Trans. on Power Apparatus and Systems, May, 1974, p.884.

33. VERVLOET, F.G. and BRAEMELLER, A.: 'A.C. security assessment'. Proc. I.E.E., Vol. 122, No. 9, September, 1975, p.897.

34. STOTT, B.: 'Load flows for A.C. and integrated A.C./D.C. systems'. Ph.D. Thesis, University of Manchester Institute of Science and Technology, 1971.

35. BODGER, P.S.: 'Fast decoupled A.C. and A.C./D.C. load flows'. Ph.D. Thesis, University of Canterbury, 1977.

36. STOTT, B. and HOBSON, E.: 'Solution of large power system networks by ordered elimination: A comparison of ordering schemes'. Proc. I.E.E. Vol. 118, No. 1, January, 1971, pp.125-134.

37. ZOLENKOPF, K.: 'Bi-Factorisation - basic computational algorithm and programming techniques'. Conference on Large Sets of Sparse Linear Equations. Oxford, 1970, pp.75-96.

38. SATO, H. and ARRILLAGA, J.: 'Improved load flow techniques for integrated a.c./d.c. systems'. Proc. I.E.E., Vol. 116, no. 4, April, 1969, pp. 525-532.

39. REEVE, J., FAHMY, G. and STOTT, B.: 'Versatile load flow method for multiterminal h.v.d.c. systems'. I.E.E.E. PES Summer Power Meeting, Portland, July, 1976, F76 354-1.

40. BRAUNAGAL, D.A., KRAFT, L.A., and WHYSONG, J.L.: 'Inclusion of d.c. convertor and transmission equations directly in a Newton power flow. I.E.E.E. Trans. Power Apparatus and Systems, vol. 95, no. 1, January, 1976, pp.76-88.

41. ARRILLAGA, J., and BODGER, P.: 'Integration of h.v.d.c. links with fast decoupled load flow solutions'. Proc. I.E.E., Vol. 124, no. 5, May, 1977, pp.463-468.

42. EL-MARSAFANY, M.M., and MATHUR, R.M.: 'A new, fast technique for load flow solutions multiterminal D.C./A.C. systems'. I.E.E.E. PES Winter Meeting, New York, February, 1979, F79 174-4.

43. KIMBARK, E.W.: 'Direct current transmission'. New York, Wiley-Interscience, 1971.

44. ARRILLAGA, J. and BODGER, P.: 'A.C.-D.C. load flows with realistic representation of the convertor plant'. Proc. I.E.E., Vol. 125, no. 1, January, 1978, pp.41-46.

45. DANFORS, P.: 'Reactive Power', A.S.E.A. H.V.D.C. Transmission Study Course, Ludvika, 1962.

46. A GENERAL SURVEY OF A.C. HARMONIC FILTER AND REACTIVE POWER COMPENSATION FOR HVDC, Working Group 03, CIGRE Study Committee 14 (HVDC links), 1977.

47. PHADKE, A.G. and HARLOW, J.H.: 'Unbalanced convertor operation'. I.E.E.E. Trans. on Power Apparatus and Systems, Vol. 85, March, 1966, pp.233-239.

48. ARRILLAGA, J. and EFTHYMIADAS, A.F.: 'Simulation of Convertor Performance under unbalanced conditions'. Proc. I.E.E., Vol. 115, No. 12, December, 1968, pp.1809-1818.

49. AINSWORTH, J.D.: 'The phase locked oscillator - a new control system for controlled static convertors'. I.E.E.E. Trans. on Power Apparatus and Systems, Vol. 87, no. 3, March, 1968, pp.859-865.

50. AINSWORTH, J.D.: 'Harmonic instability between controlled static convertors and a.c. networks'. Proc. I.E.E., Vol. 114, No. 7, July, 1967, pp.949-957.

51. KÄUFERLE, J., MEY, R. and ROGOWSKY, Y.: 'H.V.D.C. stations connected to weak a.c. systems'. I.E.E.E. Trans. on Power Apparatus and Systems, Vol. 89, No. 7, September, 1970, pp. 1610-1617.

52. ROBINSON, G.H.: 'Harmonic phenomena associated with the Benmore-Haywards H.V.D.C. transmission scheme. N.Z. Engineering, January, 1966, pp.16-29.

53. INTERNATIONAL CONFERENCE ON SOURCES AND EFFECTS OF POWER SYSTEM DISTURBANCES. I.E.E., Vol. 110, London, 1974.

54. ROSS, N.W.: 'Harmonics and ripple control'. Conference on Harmonics in Power Systems, University of Canterbury, New Zealand, October, 1979.

55. ROSS, T.W. and SMITH, R.M.A.: 'Centralised ripple control on high voltage networks'. Proc. I.E.E. Vol. 95, part II, October, 1948, pp.470-479.

56. THE THEORETICAL DETERMINATION OF SIGNAL POWER REQUIRED FOR THE RIPPLE CONTROL OF A NETWORK. Strowger Journal, VIII, October, 1951, pp.30-35.

57. HILTON, A.P.: 'An outline of methods of evaluating the harmonic impedance of, and penetration into, A.C. power systems'. D.C. Transmission Department, English Electric Company Ltd. Report No. 5/NS y25, 1963.

58. WHITEHEAD, S. and RADLEY, W.G.: 'Generation and Flow of Harmonics in Transmission Systems'. Proc. I.E.E., Vol. 96, 1949, pp.22-48.

59. REEVE, J., and KRISHNAYYA, P.C.S.: 'Unusual current harmonics arising from high voltage d.c. transmission'. I.E.E.E. Trans. on Power Apparatus and Systems, Vol. 87, no. 3, March, 1968, pp.883-893.

60. KUUSSAARI, M., and PESONEN, A.J.: 'Measured power-line harmonic currents and induced telephone noise interference with special reference to statistical approach'. CIGRE International Conference on Large High Voltage Electric Systems, Paris 1976.

61. HESSE, M.H.: 'Electromagnetic and electrostatic transmission line parameters by digital computer'. I.E.E.E. Trans. on Power Apparatus and Systems, Vol. 82, June, 1963, pp.282-291.

62. COLEMAN, D., WATTS, F. and SHIPLEY, R.B.: 'Digital Calculation of overhead transmission line constants'. A.I.E.E. Trans. on Power Apparatus and Systems, Vol. 77, 1958, pp.1266-1268.

63. LEWIS, W.A. and TUTTLE, P.D.: 'The resistance and reactance of aluminium conductors, steel reinforced'. A.I.E.E. Trans. on Power Apparatus and Systems, Vol. 77, 1958, pp.1189-1215.

64. BATTISSON, M.J., DAY, S.J., MULLINEAUX, N., PARTON, K.C., and REED, J.R.: 'Some effects of the frequency dependence of transmission line parameters'. Proc. I.E.E., Vol. 116, No. 7, July, 1969, pp.1209-1216.

65. SUBBARAO, T., and REEVE, J.: 'Harmonics caused by imbalanced transformer impedances and imperfect twelve pulse operation in H.V.D.C. conversion'. I.E.E.E. Trans. on Power Apparatus and Systems, Vol. 95, No. 5, September, 1976, pp.1732-1735.

66. PHADKE, A.G., and HARLOW, J.H.: 'Generation of abnormal harmonics in high voltage A.C.-D.C. power systems'. I.E.E.E. Trans. on Power Apparatus and Systems, Vol. 87, No. 3, March, 1968, pp.873-882.

67. REEVE, J., BARON, J.A. and KRISHNAYYA, P.C.S.: 'A general approach to harmonic current generation by H.V.D.C. convertors'. I.E.E.E. Trans. on Power Apparatus and Systems, Vol. 88, No. 7, July, 1969, pp.989-995.

68. BOWLES, J.P.: 'A.C. system and transformer representation for H.V.-D.C. transmission studies'. I.E.E.E. Trans. on Power Apparatus and Systems, Vol. 89, No. 7, September, 1970, pp.1603-1609.

69. UHLMANN, E.: 'Power transmission by direct current'. Springer-Verlag, Berlin, 1975.

70. REEVE, J. and SUBBARAO, T.: 'Dynamic analysis of harmonic interaction between a.c. and d.c. power systems'. I.E.E.E. Trans. on Power Apparatus and Systems, Vol. 93, No. 2, March, 1972, pp.640-646.

71. LE CORBEILLER, P.: 'Matrix Analysis of Electric Networks'. John Wiley and Sons, Inc., 1950.

72. BRAEMELLER, A., JOHM, M.N. and SCOTT, M.R.: 'Practical Diakoptics for electrical networks'. Chapman and Hall Ltd, 1969.

73. LEWIS, W.E. and PRYCE, D.G.: 'The application of matrix theory to electrical engineering'. E. and F.N. Spon London, 1965.

74. LIMITS FOR HARMONICS IN THE U.K. ELECTRICITY SUPPLY SYSTEM. Engineering Recommendation G5.3, U.K. Electricity Council Chief Engineers' Conference.

APPENDIX 1

EXAMPLE OF SYSTEM MODELLING

The three phase power system illustrated in Fig. A 1.1 has been selected to illustrate the system modelling discussed in chapter 2. Some features of interest are:

- the presence of both synchronous generators and a synchronous condensor.
- an example of a line sectionalisation with one section containing four mutually coupled three phase lines.
- all lines are represented in their unbalanced mutually coupled state.
- the generator transformers are star-delta connected with the star neutrals earthed.

The system is redrawn in Fig. A 1.2 to illustrate the use of 3 × 3 compound coils to represent the three phase elements (see section A 2.2). An alternative representation is illustrated in Fig. A 1.3 using 3 × 3 matrix blocks to represent the various coupled elements.

For the purposes of input data organisation and the formation of the system admittance matrix, the system is divided into eight subsystems. These are illustrated in the exploded diagram of Fig. A 1.4.

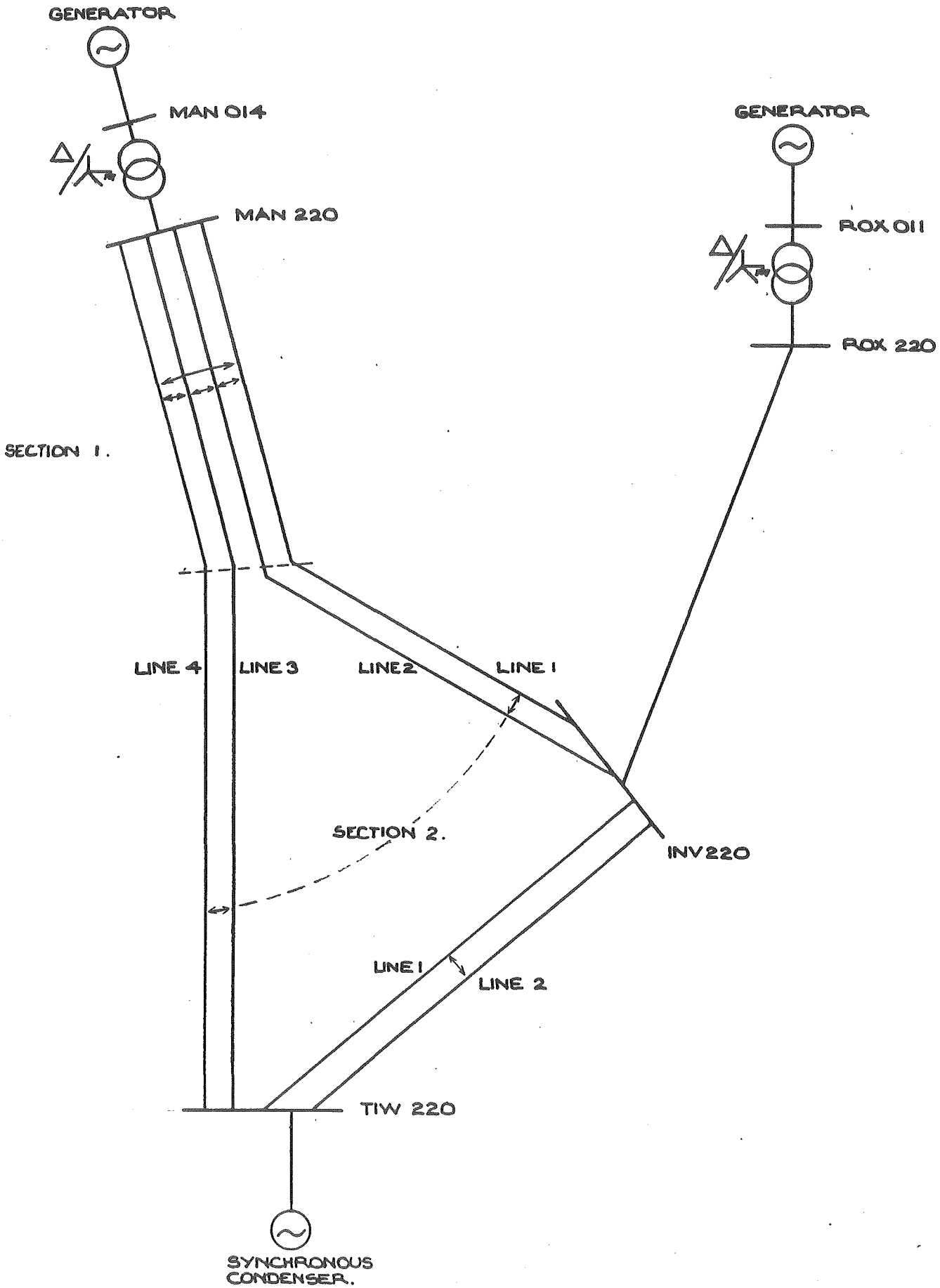

Fig. A1.1 Test System Single Line Diagram

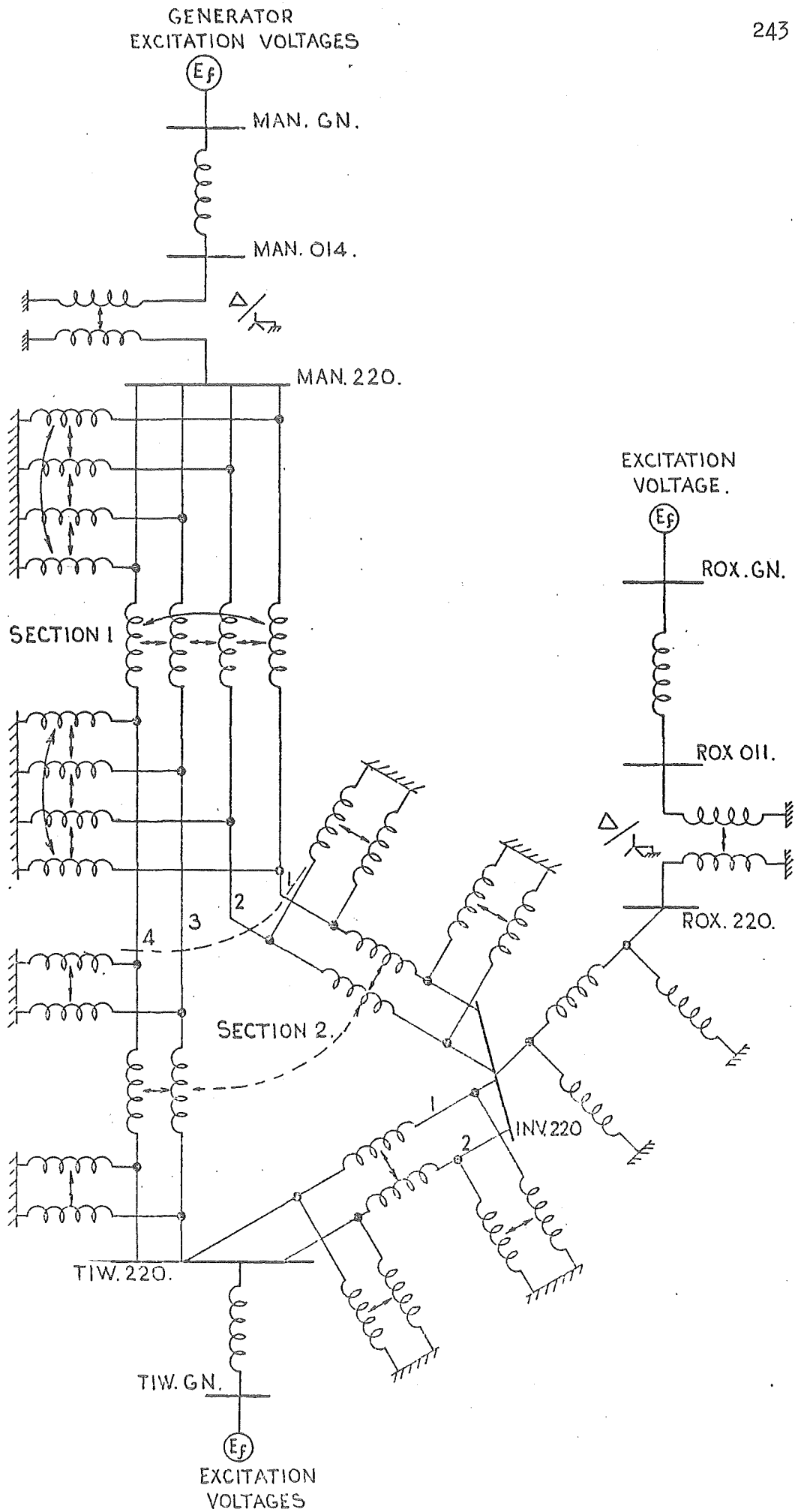

Fig. A1.2 Test System 3 × 3 Compound Coil Representation

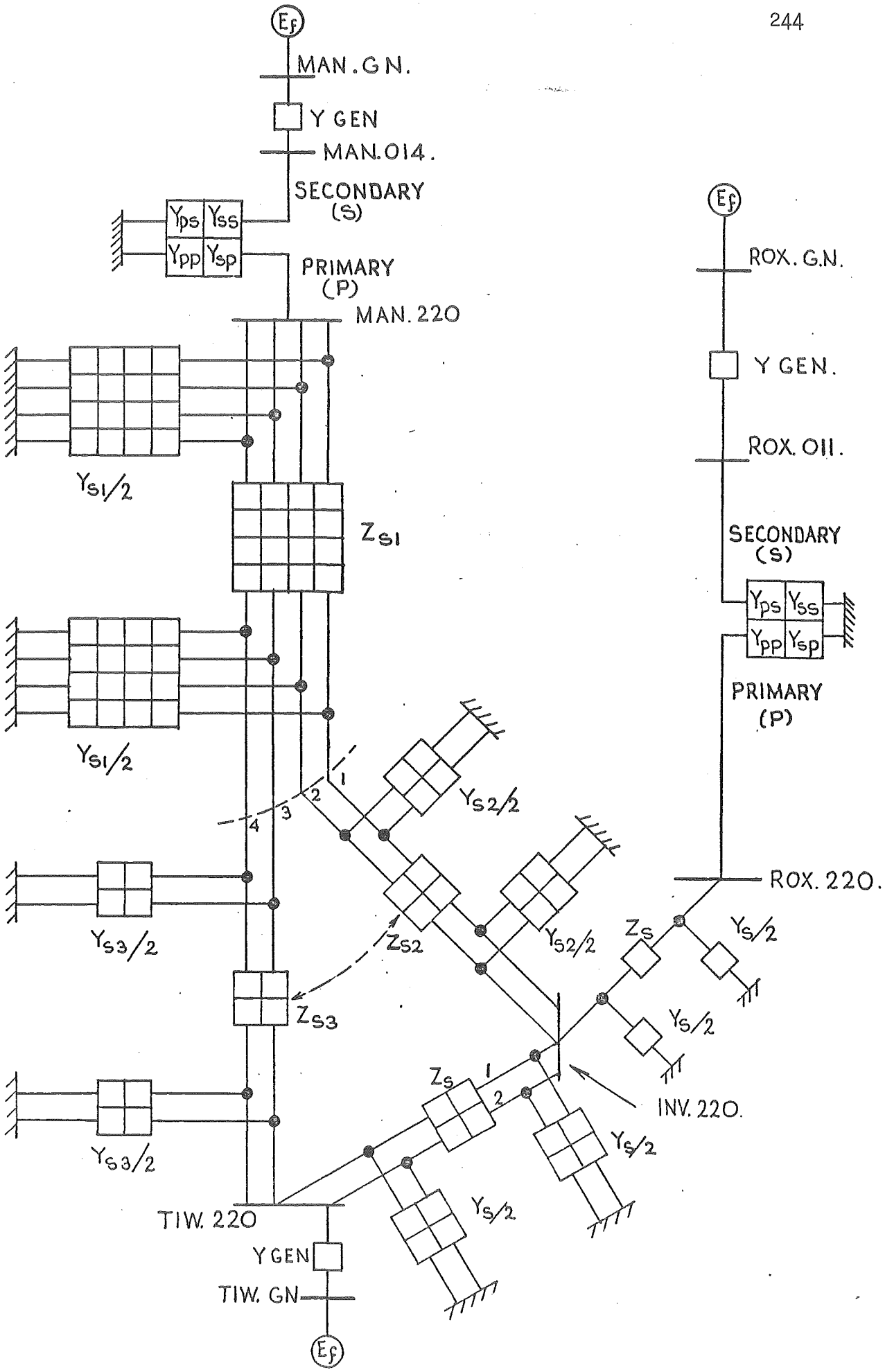

Fig. A1.3 Test System 3 × 3 Matrix Representation

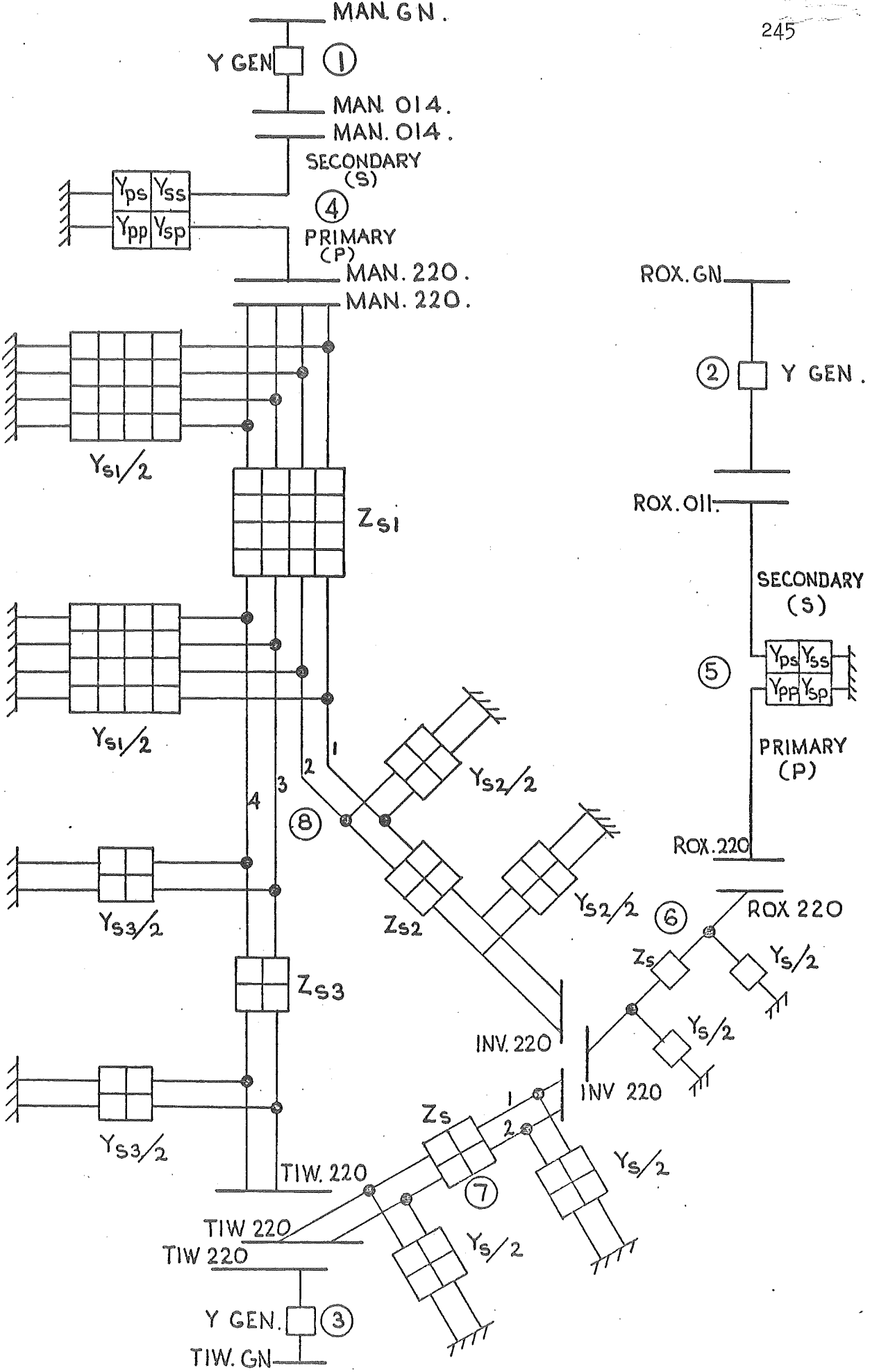

Fig. A1.4 Test System Exploded into Eight Subsystems

APPENDIX 2

LINEAR TRANSFORMATION AND THE USE OF COMPOUND COILS IN THE FORMATION OF NETWORK ADMITTANCE MATRICES

A 2.1 LINEAR TRANSFORMATION

The use of linear transformation techniques enables the admittance matrix of any network to be found in a systematic manner.[11,71-73]

Consider for the purposes of illustration, the network shown in Fig. A 2.1.

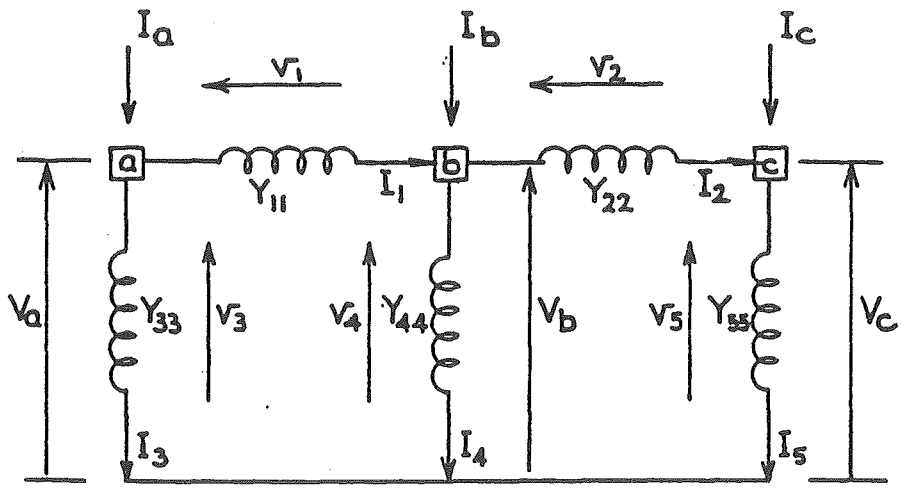

Fig. A2.1 Connected Network

The steps to form the network admittance matrix, by linear transformation, are listed below:

(1) Label the nodes in the original network.

(2) Number, in any order, the branches and branch admittances.

(3) Form the primitive network admittance matrix by inspection.

This matrix relates the nodal injected currents to the node voltages of the primitive network. The primitive network is also drawn by inspection of the actual network. It consists of the unconnected branches of the original network with a current equal to the original branch current injected into the corresponding node of the primitive network. The voltages across the primitive network branches then equal those across the same branch in the actual network.

The primitive network for Fig. A 2.1 is shown in Fig. A 2.2.

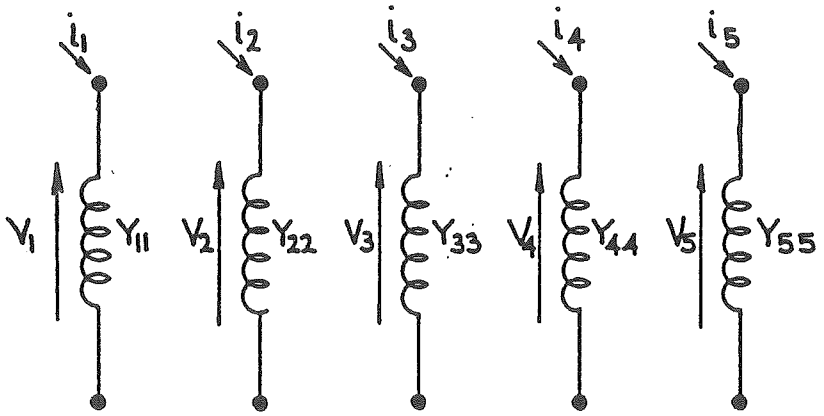

Fig. A2.2 Primitive or Unconnected Network

The primitive admittance matrix relationship is:

$$\begin{bmatrix} i_1 \\ i_2 \\ i_3 \\ i_4 \\ i_5 \end{bmatrix} = \begin{bmatrix} y_{11} & & & & \\ & y_{22} & & & \\ & & y_{33} & & \\ & & & y_{44} & \\ & & & & y_{55} \end{bmatrix} \begin{bmatrix} v_1 \\ v_2 \\ v_3 \\ v_4 \\ v_5 \end{bmatrix}$$

$$[Y_{PRIM}]$$

Off-diagonal terms are present when mutual couplings between branches are present.

(4) Form the connection matrix [C].

This relates the nodal voltages of the actual network to the nodal voltages of the primitive network. By inspection of Fig. A 2.1

$$v_1 = V_a - V_b$$

$$v_2 = V_b - V_c$$

$$v_3 = V_a$$

$$v_4 = V_b$$

$$v_5 = V_c$$

giving the matrix [C] as

$$\begin{bmatrix} v_1 \\ v_2 \\ v_3 \\ v_4 \\ v_5 \end{bmatrix} = \begin{bmatrix} 1 & -1 & \\ & 1 & -1 \\ 1 & & \\ & 1 & \\ & & 1 \end{bmatrix} \begin{bmatrix} V_a \\ V_b \\ V_c \end{bmatrix}$$

[C]

(5) The actual network admittance matrix which relates the nodal currents to the voltages by,

$$\begin{bmatrix} I_a \\ I_b \\ I_c \end{bmatrix} = \begin{bmatrix} \quad \\ [Y_{abc}] \\ \quad \end{bmatrix} \begin{bmatrix} V_a \\ V_b \\ V_c \end{bmatrix}$$

can now be derived from,

$$[Y_{abc}] = [C]^T [Y_{PRIM}] [C]$$
$$3\times3 \quad 3\times5 \quad 5\times5 \quad 5\times3$$

which is a straightforward matrix multiplication.

A 2.2 COMPOUND COILS

When analysing three phase networks, where the three nodes at a busbar are always associated together in their interconnections, it is convenient to use compound coils to graphically represent the network, and matrix quantities to represent the admittances of the network.

The compound coil is a mathematical tool which provides graphical representation of the use which can be made of matrix partitioning to simplify calculations.

Consider six mutually coupled single coils, the primitive network of which is illustrated below in Fig. A 2.3.

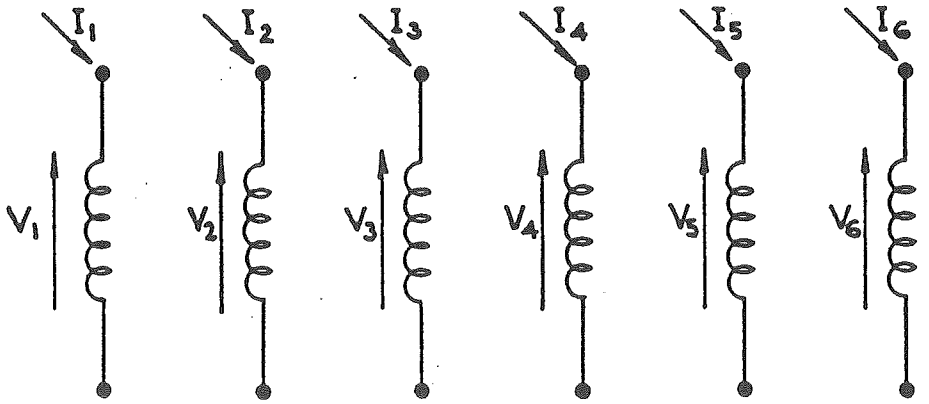

Fig. A2.3 Primitive Network of Six Coupled Coils

The primitive admittance matrix relates the nodal injected currents to the branch voltages as follows:

$$\begin{array}{|c|}\hline I_1 \\ \hline I_2 \\ \hline I_3 \\ \hline I_4 \\ \hline I_5 \\ \hline I_6 \\ \hline \end{array} = \begin{array}{|c|c|c|c|c|c|}\hline y_{11} & y_{12} & y_{13} & y_{14} & y_{15} & y_{16} \\ \hline y_{21} & y_{22} & y_{23} & y_{24} & y_{25} & y_{26} \\ \hline y_{31} & y_{32} & y_{33} & y_{34} & y_{35} & y_{36} \\ \hline y_{41} & y_{42} & y_{43} & y_{44} & y_{45} & y_{46} \\ \hline y_{51} & y_{52} & y_{53} & y_{54} & y_{55} & y_{56} \\ \hline y_{61} & y_{62} & y_{63} & y_{64} & y_{65} & y_{66} \\ \hline \end{array} \begin{array}{|c|}\hline V_1 \\ \hline V_2 \\ \hline V_3 \\ \hline V_4 \\ \hline V_5 \\ \hline V_6 \\ \hline \end{array} \qquad \text{(A 2.1)}$$

$6 \times 1 \qquad\qquad 6 \times 6 \qquad\qquad 6 \times 1$

Partitioning equation A 2.1 into 3 × 3 matrices and 3 × 1 vectors, the equation becomes,

$$\begin{array}{|c|}\hline [I_a] \\ \hline [I_b] \\ \hline \end{array} = \begin{array}{|c|c|}\hline [Y_{aa}] & [Y_{ab}] \\ \hline [Y_{ba}] & [Y_{bb}] \\ \hline \end{array} \begin{array}{|c|}\hline [V_a] \\ \hline [V_b] \\ \hline \end{array} \qquad \text{(A 2.2)}$$

where $[I_a] = [I_1\ I_2\ I_3]^T$, $[I_b] = [I_4\ I_5\ I_6]^T$ and

$$[y_{aa}] \begin{array}{|c|c|c|}\hline y_{11} & y_{12} & y_{13} \\ \hline y_{21} & y_{22} & y_{23} \\ \hline y_{31} & y_{32} & y_{33} \\ \hline \end{array} \qquad [y_{bb}] = \begin{array}{|c|c|c|}\hline y_{44} & y_{45} & y_{46} \\ \hline y_{54} & y_{55} & y_{56} \\ \hline y_{64} & y_{65} & y_{66} \\ \hline \end{array}$$

(A 2.3)

$$[y_{ab}] = \begin{array}{|c|c|c|}\hline y_{14} & y_{15} & y_{16} \\ \hline y_{24} & y_{25} & y_{26} \\ \hline y_{34} & y_{35} & y_{36} \\ \hline \end{array} \qquad [y_{ba}] = \begin{array}{|c|c|c|}\hline y_{41} & y_{51} & y_{61} \\ \hline y_{42} & y_{52} & y_{62} \\ \hline y_{43} & y_{53} & y_{63} \\ \hline \end{array}$$

Graphically we represent this partitioning as grouping the six coils into two compound coils (a) and (b), each composed of three individual coils. This is illustrated in Fig. A 2.4.

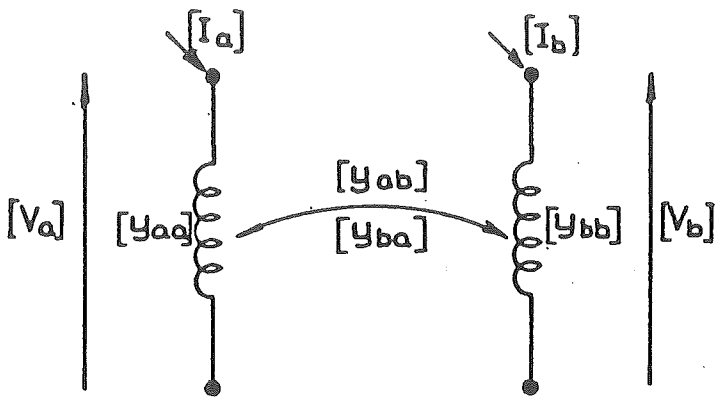

Fig. A2.4 Coupled Compound Coils

On examination of $[Y_{ab}]$ and $[Y_{ba}]$ it can be seen that,

$$[Y_{ba}] = [Y_{ab}]^T$$

if, and only if $Y_{ik} = Y_{ki}$ for i = 1 to 3 and k = 4 to 6. That is, if and only if the couplings between the two groups of coils are bilateral.

In this case equation A 2.2 may be written

$$\left[\begin{array}{c} [I_a] \\ \hline [I_b] \end{array}\right] = \left[\begin{array}{c|c} [Y_{aa}] & [Y_{ab}] \\ \hline [Y_{ab}^T] & [Y_{bb}] \end{array}\right] \left[\begin{array}{c} [V_a] \\ \hline [V_b] \end{array}\right] \qquad \text{(A 2.4)}$$

The primitive network for any number of compound coils is formed in exactly the same manner as for single coils, except that all quantities are matrices of the same order as the compound coils.

The actual admittance matrix of any network composed of the compound coils can be formed by the usual method of linear transformation; the elements of the connection matrix are now $n \times n$ identity matrices where n is the dimension of the compound coils.

If the connection matrix of any network can be partitioned into identity elements of equal dimensions greater than one, the use of compound coils is advantageous.

As an example, consider the network shown in Fig. A 2.5 - this represents a simple line section. The admittance matrix will be derived using single coils and compound coils to show the simple correspondence. The primitive networks and associated admittance matrices are drawn in Fig. A 2.6. The connection matrices are shown in Fig. A 2.7. The exact equivalence, with appropriate matrix partitioning, is clear.

The network admittance matrix is given by the linear transformation equation,

$$[Y_{NODE}] = [C]^T [Y_{PRIM}] [C]$$

This matrix multiplication can be executed using the full matrices or in partitioned form. The result in partitioned form is,

$$[Y_{NODE}] = \left[\begin{array}{c|c} [Y_A] + [Y_B] & -[Y_A] \\ \hline -[Y_A] & [Y_A] + [Y_C] \end{array}\right]$$

A 2.3 RULES FOR FORMING THE NETWORK ADMITTANCE MATRIX FOR SIMPLE NETWORKS

The method of linear transformation may be used to give the admittance matrix of any network. For the special case of networks where there is no mutual coupling between coils, simple rules may be

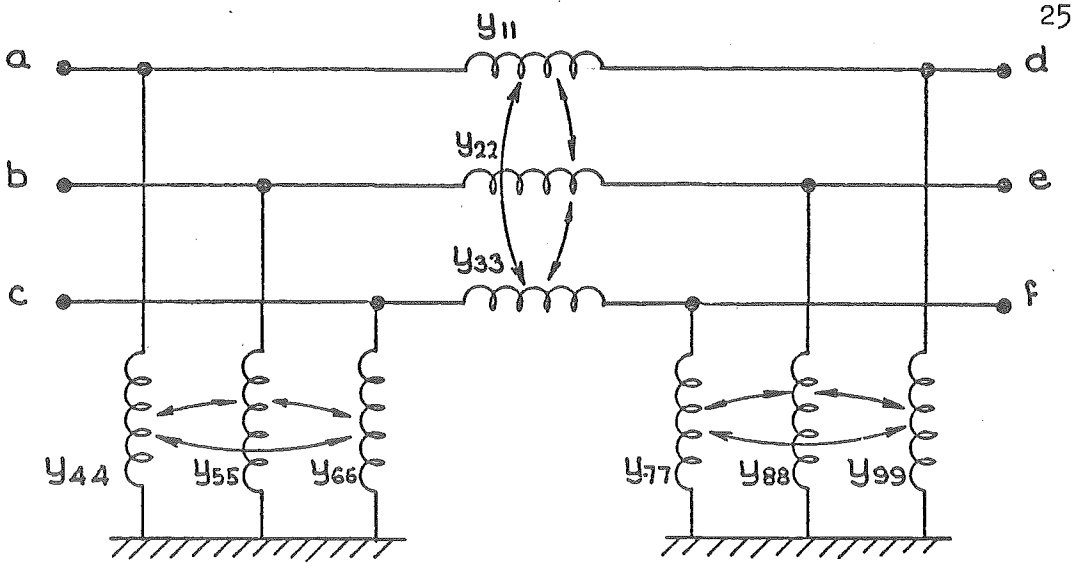

(i) SINGLE COIL.

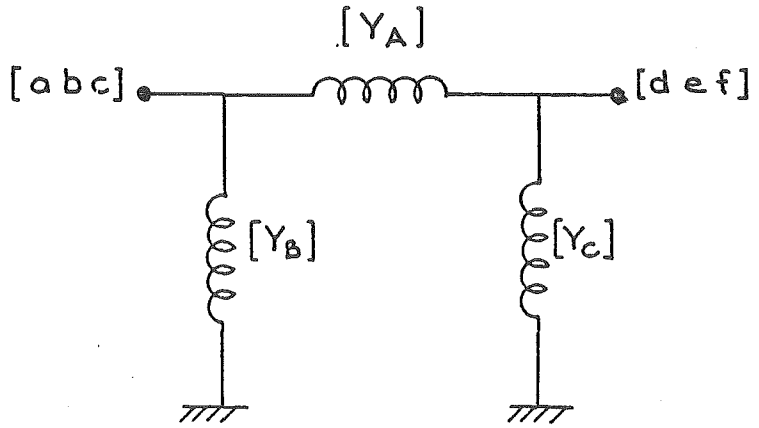

(ii) COMPOUND COILS

Fig. A2.5 Single and Compound Coil Network

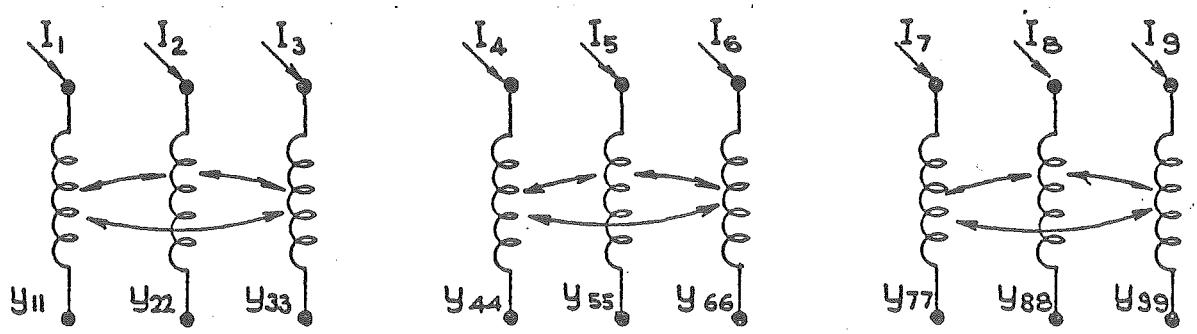

(i) PRIMITIVE NETWORK USING SINGLE COILS.

y_{11}	y_{12}	y_{13}						
y_{21}	y_{22}	y_{23}						
y_{31}	y_{32}	y_{33}						
			y_{44}	y_{45}	y_{46}			
			y_{54}	y_{55}	y_{56}			
			y_{64}	y_{65}	y_{66}			
						y_{77}	y_{78}	y_{79}
						y_{87}	y_{88}	y_{89}
						y_{97}	y_{98}	y_{99}

(ii) PRIMITIVE ADMITTANCE MATRIX.

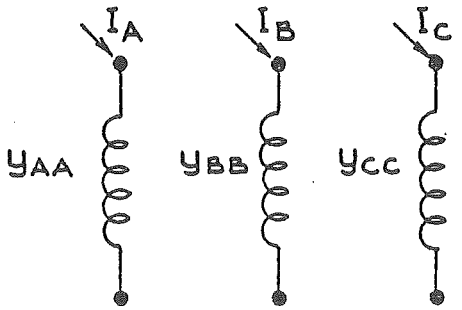

(iii) PRIMITIVE NETWORK USING COMPOUND COILS.

y_A		
	y_B	
		y_C

(iv) PRIMITIVE ADMITTANCE MATRIX.

Fig. A2.6 Single and Compound Coil Primitive Network

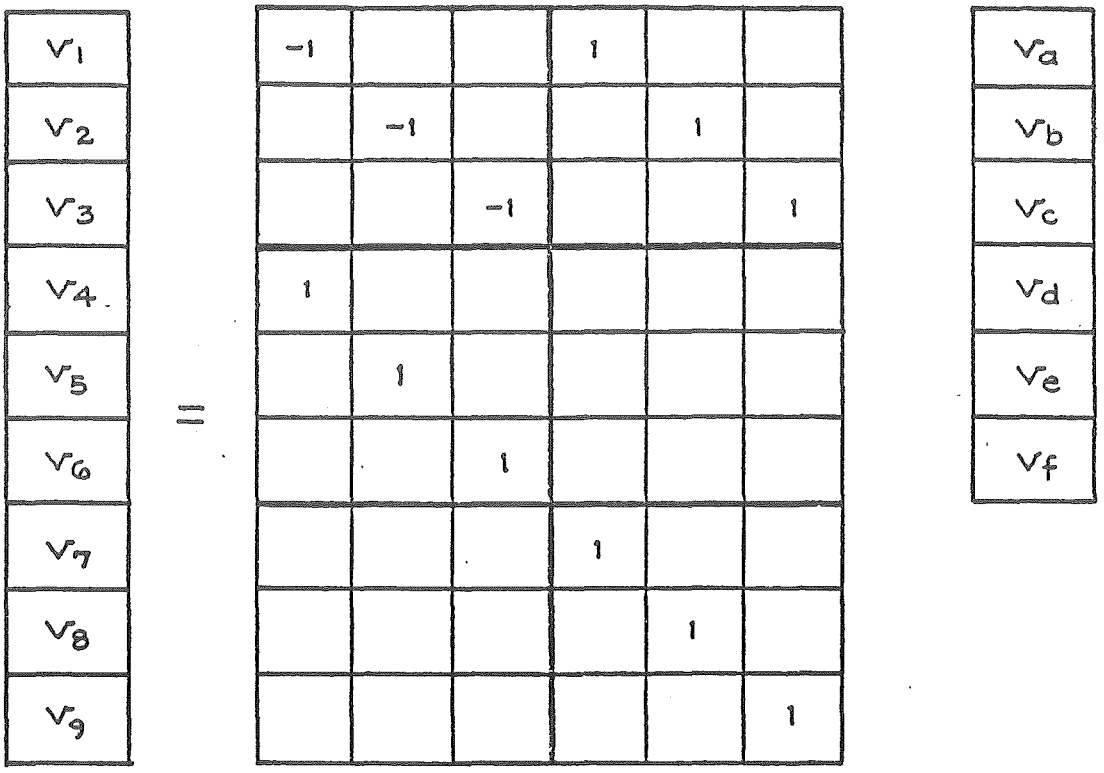

(i) SINGLE COIL NETWORK

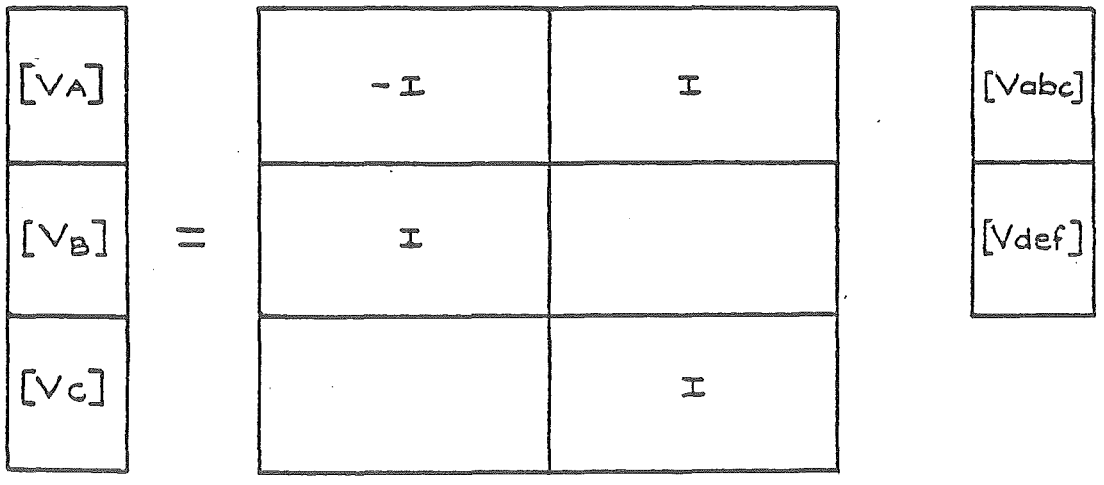

(ii) COMPOUND COIL NETWORK

Fig. A2.7 Single and Compound Connection Matrices

used to form the admittance matrix by inspection. These rules apply to compound networks with no mutual coupling between the compound coils.

These rules may be stated:[72]

(a) Any diagonal term is the sum of the individual branch admittances connected to the node corresponding to that term.

(b) Any off-diagonal term is the negated sum of the branch admittances which are connected between the two corresponding nodes.

APPENDIX 3

STAR-G/DELTA THREE PHASE TRANSFORMER MODEL

A 3.1 ADMITTANCE REPRESENTATION

Disregarding interphase mutual couplings the per unit primitive admittance matrix in terms of the transformer leakage admittance (y_{ti}) is:[9]

$$[Y_{prim}] = \begin{array}{|c|c|c|c|c|c|} \hline \frac{y_{t1}}{a_1^2} & & & \frac{-y_{t1}}{a_1} & & \\ \hline & \frac{y_{t2}}{a_2^2} & & & \frac{-y_{t2}}{a_2} & \\ \hline & & \frac{y_{t3}}{a_3^2} & & & \frac{-y_{t3}}{a_3} \\ \hline \frac{-y_{t1}}{a_1} & & & y_{t1} & & \\ \hline & \frac{-y_{t2}}{a_2} & & & y_{t2} & \\ \hline & & \frac{-y_{t3}}{a_3} & & & y_{t3} \\ \hline \end{array}$$

where a_1, a_2 and a_3 are the off-nominal taps on windings 1,2 and 3 respectively. In addition any windings connected in delta will, because of the per unit system, have an effective tap of $\sqrt{3}$

The nodal admittance matrix for the transformer windings is:

$$[Y_{node}] = [C]^T [Y_{prim}] [C]$$

where [C] is the connection (windings to nodes) matrix.

The connection matrix and connection diagram for a DY11 connection is illustrated in Fig. A 3.1.

The resulting $[Y_{node}]$ is,

$$[Y_{node}] = \begin{array}{|c|c|c|c|c|c|} \hline \frac{y_{t1}}{a_1^2} & & & \frac{-y_{t1}}{\sqrt{3}a_1} & \frac{y_{t1}}{\sqrt{3}a_1} & \\ \hline & \frac{y_{t2}}{a_2^2} & & & \frac{-y_{t2}}{\sqrt{3}a_2} & \frac{y_{t2}}{\sqrt{3}a_2} \\ \hline & & \frac{y_{t3}}{a_3^2} & \frac{y_{t3}}{\sqrt{3}a_3} & & \frac{-y_{t3}}{\sqrt{3}a_3} \\ \hline \frac{-y_{t1}}{\sqrt{3}a_1} & & \frac{y_{t3}}{\sqrt{3}a_3} & \frac{y_{t1}+y_{t3}}{3} & \frac{-y_{t1}}{3} & \frac{-y_{t3}}{3} \\ \hline \frac{y_{t1}}{\sqrt{3}a_1} & \frac{-y_{t2}}{\sqrt{3}a_2} & & \frac{-y_{t1}}{3} & \frac{y_{t2}+y_{t1}}{3} & \frac{-y_{t2}}{3} \\ \hline & \frac{y_{t2}}{\sqrt{3}a_2} & \frac{-y_{t3}}{\sqrt{3}a_3} & \frac{-y_{t3}}{3} & \frac{-y_{t2}}{3} & \frac{y_{t2}+y_{t3}}{3} \\ \hline \end{array}$$

Usually all three phase units are symmetrical i.e.,

$$y_{t1} = y_{t2} = y_{t3} = y_t$$

and

$$a_1 = a_2 = a_3 = a$$

A simple equivalent circuit is shown in Fig. A 3.2 for the symmetrical case with unity off-nominal taps.

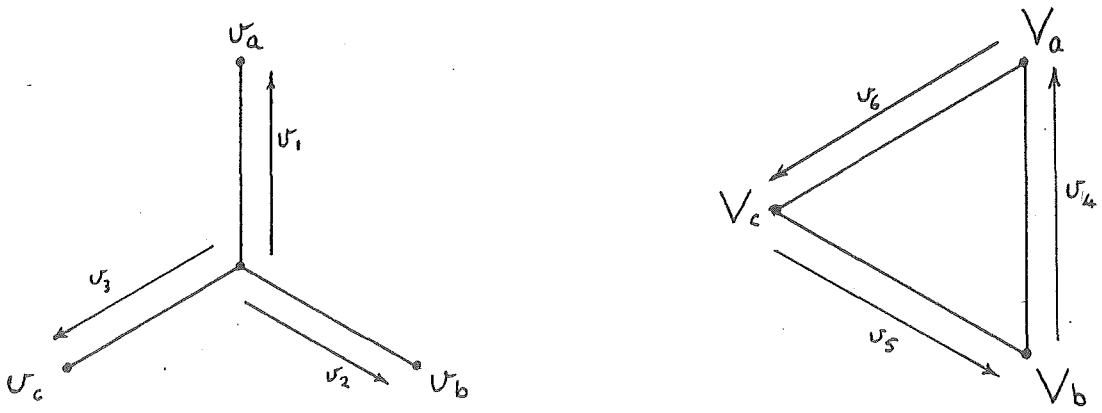

(i) Connection Diagram

υ_1	1					υ_a
υ_2		1				υ_b
υ_3			1			υ_c
υ_4				1	-1	V_a
υ_5					1	-1 V_b
υ_6				-1		1 V_c

(ii) Connection matrix

Fig. A3.1 Connection Matrix for Star-g/delta (DY11) Connection.

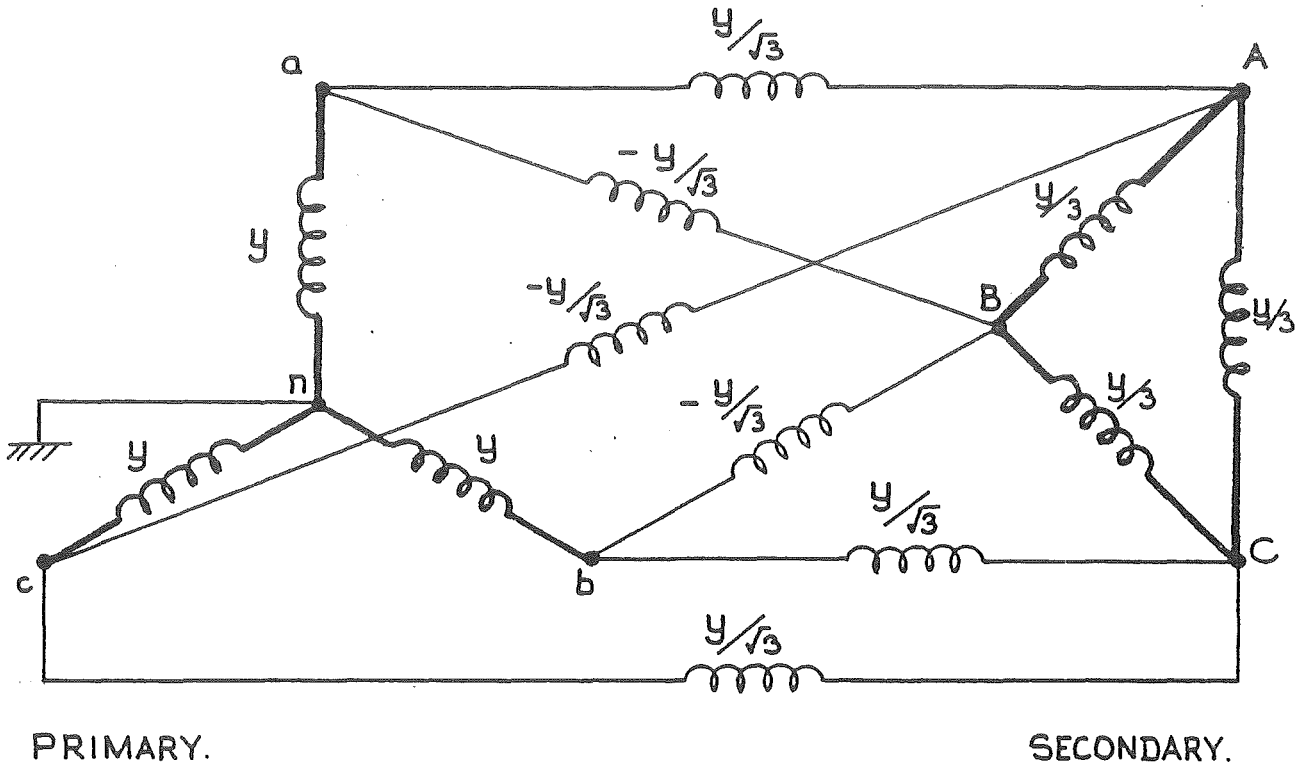

Fig. A3.2 Equivalent Circuit for Symmetrical Star-g/delta Transformer (unity tap ratio)

APPENDIX 4

SINGLE PHASE LOAD FLOW PROBLEM AND THE FAST DECOUPLED SOLUTION ALGORITHM

A 4.1 PROBLEM FORMULATION

The aim of the single phase load flow is to find the operating state of the balanced power system under the specified conditions of load, generation and system configuration.

The operating state is defined by,

$$[\bar{V}, \bar{\theta}]$$

where $\bar{V}_i$ is a vector of voltages at all system busbars i.e.

$i = 1,nb$

$\bar{\theta}_i$ is a vector of angles at all busbars (except one, which is assigned $\theta = 0$ and is taken as a reference) i.e. $i = 1,nb-1$.

It should be noted that $[\bar{V}, \bar{\theta}]$ is a minimum set of variables i.e. they are all independent variables.

To enable the use of a Newton-Raphson based technique it is necessary to formulate a set of $2nb-1$ independent algebraic equations in terms of the $2nb-1$ variables. These equations or constraints are derived from the specified operating conditions. Only a limited number of specified operating conditions apply to the balanced power system and it is customary to place the system busbars in categories as follows:

(i) Load Busbars. (P - Q)

The active and reactive power loading at the busbar is specified.

(ii) Generator Busbars (P - V)

The active power injection is known and the voltage is specified and controlled by the voltage regulator.

(iii) Slack Busbar

This is a special case of a generator busbar. As the total system losses are unknown it is impossible to specify the power injections at all busbars. One busbar, designated the slack busbar, must remain a source or sink of real power to enable an overall power balance to be maintained.

The following equations are derived from these specified conditions.

(i) $$V_i^{sp} - V_i = 0 \qquad \text{(A 4.1)}$$

for i = 1, ng i.e. at all generator busbars.

(ii) $$\Delta P_i(\bar{V}, \bar{\theta}) = P_i^{sp} - P_i(\bar{V}, \bar{\theta}) \qquad \text{(A 4.2)}$$

for i = 1, nb -1 i.e. at all busbars except the slack machine.

(iii) $$\Delta Q_i(\bar{V}, \bar{\theta}) = Q_i^{sp} - Q_i(\bar{V}, \bar{\theta}) \qquad \text{(A 4.3)}$$

for i = 1, nb - ng i.e. at all load busbars.

A total of 2nb - 1 equations have been formed. Clearly, equations A 4.1 are trivial and do not require solution and these equations and the corresponding voltage variables are removed from the problem formulation.

The problem may therefore be formulated as the solution of:

$$\begin{bmatrix} \Delta P(\bar{V}, \bar{\theta}) \\ \Delta Q(\bar{V}, \bar{\theta}) \end{bmatrix} = 0 \qquad \text{(A 4.4)}$$

for the unknown voltages and angles.

The power mismatches are written in terms of the problem variables and the system admittance matrix as follows,

$$P_i = R_e [V_i \cdot I_i^*] \qquad \text{(A 4.5)}$$

$$Q_i = I_m [V_i \cdot I_i^*] \qquad \text{(A 4.6)}$$

where

$$I_i = \sum_{k=1}^{n} Y_{ik} \cdot V_k \qquad \text{(A 4.7)}$$

and

$$Y_{ik} = G_{ik} + j B_{ik} \qquad \text{(A 4.8)}$$

The equations are:

$$\Delta P_i = P_i^{sp} - V_i \sum_{k=1}^{n} V_k [G_{ik} \cos \theta_{ik} + B_{ik} \sin \theta_{ik}] \qquad \text{(A 4.9)}$$

$$\Delta Q_i = Q_i^{sp} - V_i \sum_{k=1}^{n} V_k [G_{ik} \sin \theta_{ik} - B_{ik} \cos \theta_{ik}] \qquad \text{(A 4.10)}$$

A 4.2 NEWTON-RAPHSON ALGORITHM

The general Newton-Raphson method consists of successive solutions of,

$$\bar{F}(\bar{x}) = - [J][\Delta \bar{x}] \qquad \text{(A 4.11)}$$

where [J] is the jacobian matrix of first order partial derivatives. for the changes in variables $\Delta \bar{x}$. The variables $\bar{x}$ are then updated until the set of equations

$$\bar{F}[\bar{x}] = 0$$

can be considered solved.

Defining,

$$\bar{F} = \begin{bmatrix} \Delta \bar{P} \\ \Delta \bar{Q} \end{bmatrix} \quad \text{and} \quad \Delta \bar{x} = \begin{bmatrix} \Delta \bar{\theta} \\ \Delta \bar{V}/\bar{V} \end{bmatrix} \qquad \text{(A 4.12)}$$

The algorithm involves repeat solutions of,

$$\begin{bmatrix} \Delta \bar{P} \\ \Delta \bar{Q} \end{bmatrix} = \begin{bmatrix} H & N \\ J & L \end{bmatrix} \begin{bmatrix} \Delta \bar{\theta} \\ \Delta \bar{V}/\bar{V} \end{bmatrix} \qquad \text{(A 4.13)}$$

The Jacobian elements H, N, J and L are given by:

$$H_{ik} = \partial \Delta P_i / \theta_k \qquad N_{ik} = V_k [\partial \Delta P_i / \partial V_k]$$

$$J_{ik} = \partial \Delta Q_i / \partial \theta_i \qquad L_{ik} = V_k [\partial \Delta Q_i / \partial V_k]$$

The right hand side variable $[\Delta\bar{V}/\bar{V}]$ in equation (A 4.13) is usually taken as it is found to give better computational results than the use of $[\Delta\bar{V}]$ alone.

Equation (A 4.13) is solved for the changes in the variables $[\Delta\bar{V}/\bar{V}]$ and $[\Delta\bar{\theta}]$, the variables $[\bar{V}]$ and $[\bar{\theta}]$ are then updated, the mismatch functions $[\Delta\bar{P}]$ and $[\Delta\bar{Q}]$ re-evaluated and equation (A 4.13) solved again. This process is continued until $[\Delta\bar{P}]$ and $[\Delta\bar{Q}]$ are all small enough to be considered zero.

It should be noted that the Jacobians H, N, J and L must be re-evaluated at each solution of equation (A 4.13) as these are functions of $\bar{V}$ and $\bar{\theta}$ which are changing at each iteration.

A 4.3 DERIVATION OF THE SINGLE PHASE FAST DECOUPLED ALGORITHM

In decoupled load flow methods[30,34] the coupling matrices [N] and [J] are set to zero. This is the mathematical implementation of the following, well justified statements:

(a) A change $\Delta\bar{\theta}$ affects the real power flows with only a small change in the reactive power flow.

(b) A change $\bar{V}$ affects the reactive power flows with only a small change in the real power flows.

This yields the two decoupled equations:

$$[\Delta\bar{P}] = [H] \; [\Delta\bar{\theta}] \qquad \text{(A 4.14)}$$

$$[\Delta\bar{Q}] = [L] \; [\Delta\bar{V}/\bar{V}] \qquad \text{(A 4.15)}$$

The Jacobian matrices [H] and [L] are given by,

$$H_{km} = L_{km} = V_k V_m [G_{km} \sin \theta_{km} - B_{km} \cos \theta_{km}]$$

$$H_{kk} = - B_{kk} V_k^2 - Q_k$$

$$L_{kk} = - B_{kk} V_k^2 + Q_k$$

Stott[8] then makes the following assumptions:

(1) $\cos \theta_{km} = 1$

(2) $G_{km} \sin \theta_{km} << B_{km}$

(3) $Q_k << B_{kk} V_k^2$

These are almost always valid for the single phase representation of the balanced power system. Equations (A 4.14) and (A 4.15) may then be approximated to:

$$[\Delta \bar{P}] = [\bar{V}][B'][\bar{V}][\Delta \theta] \qquad \text{(A 4.16)}$$

$$[\Delta \bar{Q}] = [\bar{V}][B'']][\bar{V}][\Delta \bar{V}/\bar{V}] \qquad \text{(A 4.17)}$$

where at this stage [B'] and [B''] are simply the elements of the matrix [-B]. The use of equations (A 4.16) and (A 4.17) have been found to be only partially successful. Further modifications to the equations yield:

$$[\Delta \bar{P}/\bar{V}] = [B'][\Delta \bar{\theta}] \qquad \text{(A 4.18)}$$

$$[\Delta \bar{Q}/\bar{V}] = [B'']][\Delta \bar{V}] \qquad \text{(A 4.19)}$$

where the modifications may be listed:

(a) Omit from [B'] those elements that predominantly affect MVAr flows. This includes shunt ractances and in phase transformer taps.

(b) Omit from [B''] the angle shifting effects of phase shifters.

(c) Neglect series resistance in the calculation of the elements of [B']. This is of minor importance.

(d) Rearrange the equations (A 4.16) and (A 4.17) by taking the defining functions as $[\Delta\bar{P}/\bar{V}]$ and $[\Delta\bar{Q}/\bar{V}]$.

(e) Set the remaining right hand side $[\bar{V}]$ terms in (A 4.16) to one p.u., removing the affects of MVAr flows on the calculation of $\Delta\bar{\theta}$.

The equations (A 4.18) and (A 4.19) form the basis of the fast decoupled method. The constant approximated Jacobians [B'] and [B"] correspond to fixed approximated tangent slopes to the multidimensional surfaces formed by the right hand side defining functions.

Each iteration comprises one solution of (A 4.18) for $[\Delta\bar{\theta}]$, then updating $[\bar{\theta}]$, followed by one solution of (A 4.19) for $[\Delta\bar{V}]$, then updating $[\bar{V}]$. The iteration cycle, illustrated in Fig. A 4.1, is continued until both $[\Delta\bar{P}/\bar{V}]$ and $[\Delta\bar{Q}/\bar{V}]$ are small enough so that they can be considered as zero. This method has been found to be highly successful in solving many load flow problems, even those with convergence difficulties by other methods.

The main feature of the fast decoupled method, which makes it computationally superior to the full Newton-Raphson formulation, is the use of the constant Jacobians [B'] and [B"]. These need be inverted only once during the load flow, providing for fast repeat solutions of (A 4.18) and (A 4.19).

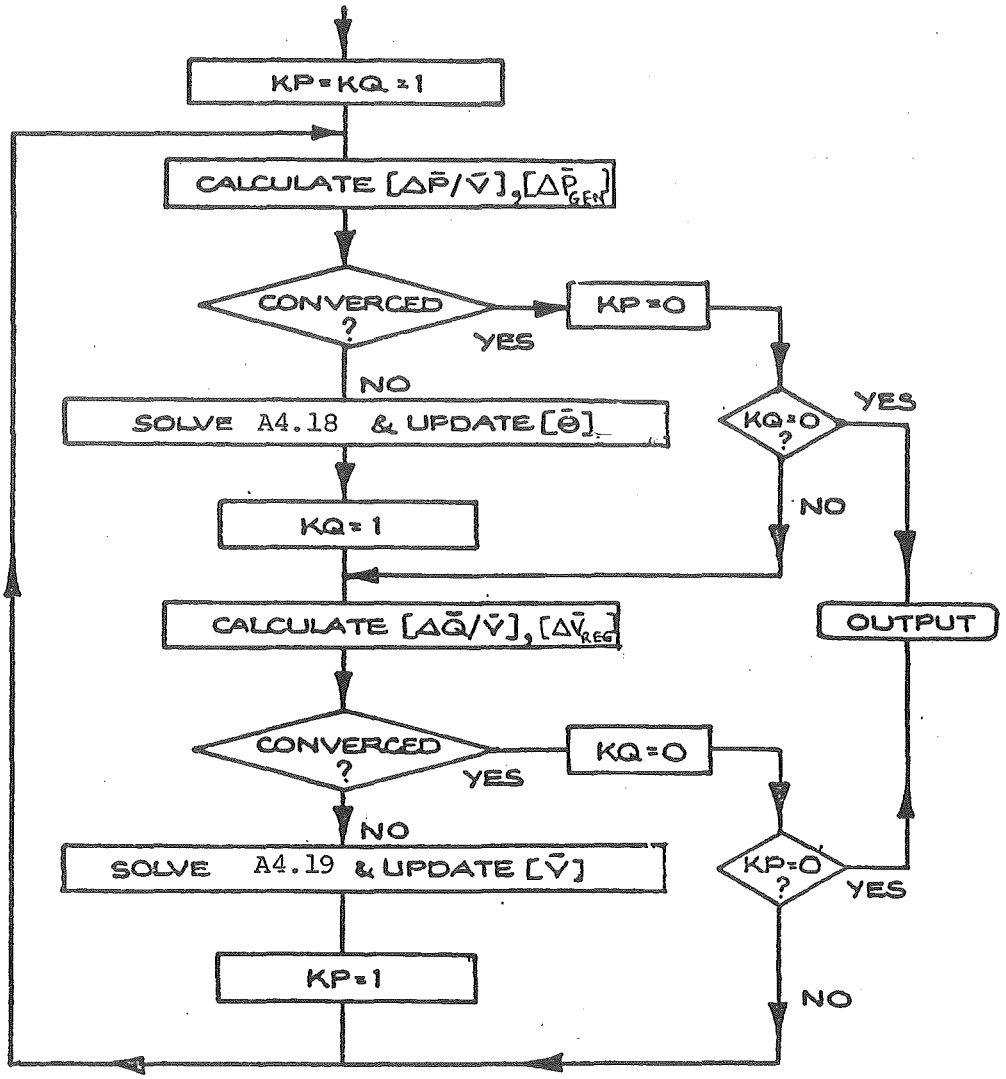

Fig. A4.1 Flow Chart of Single Phase Fast Decoupled Algorithm.

APPENDIX 5

Fast-decoupled three-phase load flow

Prof. J. Arrillaga, M.Sc. Tech., Ph.D., C.Eng., F.I.E.E., and B.J. Harker, M.E.

Indexing terms: *Load (electric), Modelling, Power-transmission lines, Reactive power, Transmission-network calculations*

Abstract

Using as a reference the single-phase fast-decoupled algorithm, this paper describes the modifications required to produce an efficient three-phase fast-decoupled load flow. The compound-coil concept is used in the representation of power-system components, and the effect of automatic voltage regulators is modelled as part of the reactive-power Jacobian-matrix equation. It is shown that the three-phase modified fast-decoupled load flow displays all the characteristics of the original single-phase version.

List of principal symbols

$[I]$ = vector of nodal injected currents
$[V]$ = vector of nodal voltages $[|V|e^{j\theta}]$
$[Z] = [R] + j[X]$ = matrix of impedances
$[Y] = [G] + j[B]$ = matrix of admittances
ΔP_i^p = real power mismatch at busbar i with phase p
ΔQ_i^p = reactive power mismatch at busbar i with phase p
$(P_i^p)^{SP}$ = specified real power at busbar i with phase p
$(Q_i^p)^{SP}$ = specified reactive power at busbar i with phase p
$|V|_i^p$ = voltage magnitude at busbar i with phase p
$\theta_{ik}^{pm} = \theta_i^p - \theta_k^m$ = angle between busbar i with phase p, and busbar k with phase m
G_{ik}^{pm} = value of matrix G relating busbar i with phase p, and busbar k with phase m
$|V|_{int.j}$ = voltage magnitude at the internal busbar of the jth generator
$\theta_{int.j}$ = voltage phase angle at the internal busbar of the jth generator
$P_{gen.j}^{SP}$ = specified total power output of jth generator
$V_{term.j}^{SP}$ = voltage regulator specification for the three terminal voltages for generator j
nb = number of system busbars, excluding generator internal busbars
n = total number of system busbars
ng = number of system generators

1 Introduction

Accurate models of power-system components using phase parameters are available in the literature.[1-3] Two recent publications[4,5] have integrated such models with a Newton-Raphson method for the solution of three-phase load flows. In balanced studies however the conventional Newton algorithm has been displaced by the computationally superior fast-decoupled method. Because computational requirements (time and storage) are more demanding with three-phase models, it would appear that the conventional Newton method should give way to the more powerful decoupled algorithms.

A preliminary investigation carried out to assess the applicability of the fast-decoupled algorithm to three-phase studies gave negative results. Owing to the greater degree of representation used in three-phase models (transformer connections, mutual inductances etc.), the simplifications made in the development of the single-phase fast-decoupled algorithm could not be justified for three-phase load flows, and convergence was poor.

A deeper investigation into decoupling techniques and three-phase power system components indicated that, with suitably modified simplifications, an efficient fast-decoupled three-phase load flow could be achieved with similar characteristics to the single-phase fast-decoupled method.

The development of such an algorithm is described in this paper, emphasis being placed on those features peculiar to the three-phase case.

2 Three-phase power-system modelling

The compound-coil concept provides the basis for a systematic modelling procedure. Linear transformations can be applied to compound coils by simply replacing the single quantities of ordinary networks with appropriate admittance matrices.[6]

Paper 8098 P, first received 17th May 1977 and in revised form 23rd January 1978

Prof. Arrillaga is with the Department of Electrical Engineering, University of Canterbury, Christchurch 1, New Zealand, and Mr. Harker is with the New Zealand Electricity Department, Christchurch 1, New Zealand

The network is first subdivided into subsystems (e.g. generators, transformers, transmission lines), with the restriction that there should not be mutual coupling between the branches of different subsystems. With this restriction the subsystem admittance matrices can be combined as follows:

(*a*) The self-admittance matrix of any busbar is the sum of all the individual self-admittance matrices at that busbar
(*b*) The mutual-admittance matrix between any two busbars is the sum of the individual mutual-admittance matrices from all subsystems containing those two busbars.

A transmission-line subsystem may itself need sectionalising to account for transpositions, changes of line parameters, series capacitors etc. In such cases, the parameters for each section are first found and then combined by matrix multiplication to obtain the overall subsystem parameters.

2.1 Transmission lines

For power frequency analysis, a three-phase transmission line can be modelled by three lumped π circuits, with mutual coupling between both the series and shunt branches of all three circuits. This is illustrated by the matrix equivalent of Fig. 1*a* and its compound coil equivalent of Fig. 1*b*.

The subsystem of Fig. 1*b* can be represented by matrix eqn. 1:

$$\begin{bmatrix} [I_i] \\ [I_k] \end{bmatrix} = \begin{bmatrix} [Z_{ik}]^{-1} + [Y_{ik}]/2 & -[Z_{ik}]^{-1} \\ -[Z_{ik}]^{-1} & [Z_{ik}]^{-1} + [Y_{ik}]/2 \end{bmatrix} \begin{bmatrix} [V_i] \\ [V_k] \end{bmatrix} \quad (1)$$

The effect of earth wires and the influence of ground currents is included in the self and mutual reactances of the phase conductors.[1,7] For a long line it may be necessary to consider the line as composed of two or three lumped π sections in series.

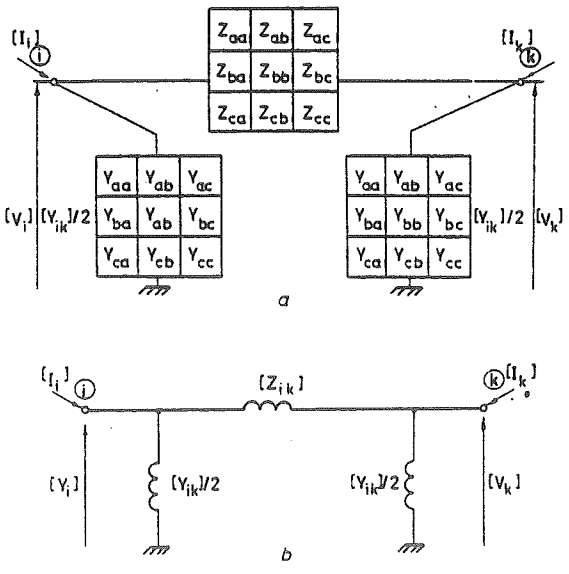

Fig. 1
Transmission-line model

a Matrix representation
b Equivalent circuit using three-phase compound coils

2.1.1 *Mutually-coupled three-phase lines*

It is common for up to four transmission lines to occupy the same right of way for a considerable length. Their electrostatic and electromagnetic coupling must then be considered.

Applying the method of linear transformation for compound coils, and assuming bilateral mutual couplings (i.e. $Y_{21} = Y_{12}^T$ etc.), we can write the following matrix equation for the case of two coupled lines, shown in Fig. 2:

$$\begin{array}{|c|}\hline I_A \\ \hline I_B \\ \hline I_C \\ \hline I_D \\ \hline \end{array} = \begin{array}{|c|c|c|c|}\hline Y_{11}+Y_{33} & Y_{12}+Y_{34} & -Y_{11} & -Y_{12} \\ \hline Y_{12}^T+Y_{34}^T & Y_{22}+Y_{44} & -Y_{12}^T & -Y_{22} \\ \hline -Y_{11} & -Y_{12} & Y_{11}+Y_{55} & Y_{12}+Y_{56} \\ \hline -Y_{12}^T & -Y_{22} & Y_{12}^T+Y_{56}^T & Y_{22}+Y_{66} \\ \hline \end{array} \begin{array}{|c|}\hline V_A \\ \hline V_B \\ \hline V_C \\ \hline V_D \\ \hline \end{array} \quad (2)$$

12 × 1 · 12 × 12 12 × 1

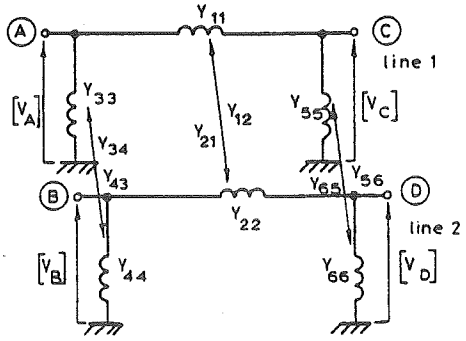

Fig. 2
Two coupled three-phase lines

By the combination of pairs of coupled 3 × 3 coils as a single 6 × 6 compound coil, the matrix equivalent of Fig. 3 results.

The corresponding matrix equation is as follows:

$$\begin{bmatrix} [I_A] \\ [I_B] \end{bmatrix} = \begin{array}{|c|c|}\hline [Z_S]^{-1}+[Y_{S1}] & -[Z_S]^{-1} \\ \hline -[Z_S]^{-1} & [Z_S]^{-1}+[Y_{S1}] \\ \hline \end{array} \cdot \begin{bmatrix} [V_A] \\ [V_B] \end{bmatrix} \quad (3)$$

Eqn. 3 now has the same form as eqn. 1, the series impedance $[Z_s]$ and shunt admittance $[Y_s]$ matrices being of orders 3 × 3, 6 × 6, 9 × 9, or 12 × 12 for cases of one, two, three or four coupled three-phase lines, respectively.

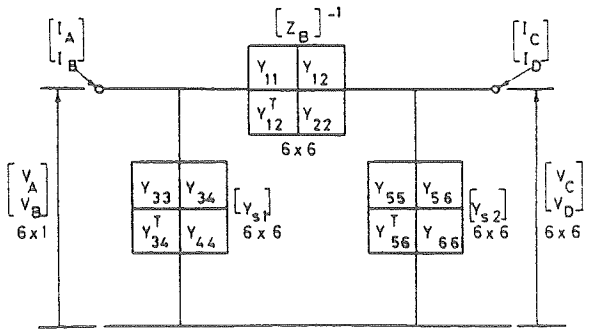

Fig. 3
6 × 6 matrix representation of Fig. 2

2.2 Synchronous machines

With reference to Fig. 4, the synchronous machine is represented by a compound coil $Y_{gen.}$, which interconnects an internal busbar of balanced three-phase voltages and a terminal busbar. The three terminal busbar voltages are used to control the balanced internal voltages according to some prespecified relationship.

The following matrix equation applies:

$$\begin{bmatrix} I_i \\ I_k \end{bmatrix} = \begin{array}{|c|c|}\hline [Y_{gen}] & -[Y_{gen}] \\ \hline -[Y_{gen}] & [Y_{gen}] \\ \hline \end{array} \begin{bmatrix} V_i \\ V_k \end{bmatrix} \quad (4)$$

where Y_{gen} is a 3 × 3 admittance matrix derived from the sequence component impedances of the machine.

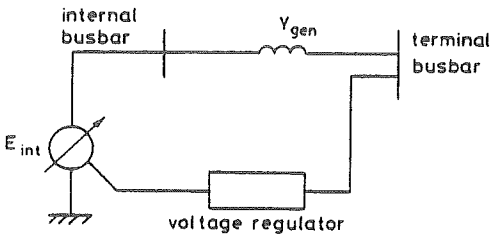

Fig. 4
Synchronous-generator model

2.3 Transformers

In general, any two-winding three-phase transformer can be represented using two coupled compound coils $[Y_{pp}]$, $[Y_{ss}]$, i.e.

$$\begin{bmatrix} i_p \\ i_s \end{bmatrix} = \begin{array}{|c|c|}\hline [Y_{pp}] & [Y_{ps}] \\ \hline [Y_{sp}] & [Y_{ss}] \\ \hline \end{array} \begin{bmatrix} V_p \\ V_s \end{bmatrix} \quad (5)$$

This procedure is carried out for the common connections in Reference 1, and it is shown that three basic types of submatrix result. For each type of transformer connection, Table 9 in Appendix 10.1 indicates the appropriate submatrix to be used in the corresponding position of the nodal admittance matrix of eqn. 5. The generality of the model can be increased by modifying these submatrices to include primary- and secondary-winding off nominal taps, which is achieved by

(*a*) dividing the primary self-admittance matrix by α^2
(*b*) dividing the secondary self-admittance matrix by β^2
(*c*) dividing the mutual admittance matrix by $\alpha\beta$.

where α and β are the primary and secondary tap ratios, respectively. In the p.u. system, a delta winding has an effective tap of $\sqrt{3}$.

3 Newton-Raphson solution

To find the state of the system (i.e. the voltage magnitudes and their phase-angle relationships) so that the specified conditions at the busbars are satisfied, a Newton-Raphson solution requires the following mismatch equations:

(i) For each of the three phases (p) at every load or generator terminal busbar (i),

$$\Delta P_i^p = (P_i^p)^{SP} - |V|_i^p \sum_{k=1}^{n} \sum_{m=1}^{3} |V|_K^m [G_{ik}^{pm} \cos\theta_{ik}^{pm} + B_{ik}^{pm} \sin\theta_{ik}^{pm}] \quad (6)$$

$$\Delta Q_i^p = (Q_i^p)^{SP} - |V|_i^p \sum_{k=1}^{n} \sum_{m=1}^{3} |V|_k^m [G_{ik}^{pm} \sin\theta_{ik}^{pm} - B_{ik}^{pm} \cos\theta_{ik}^{pm}] \quad (7)$$

(ii) For each internal busbar of each generator, where the nodal voltages are constrained to form a balanced three-phase set, only two equations are required for the unknown voltage ($|V|_{int.}$) and unknown angle ($\theta_{int.}$), i.e.

$$\Delta P_{gen.j} = P_{gen.j}^{SP} - \sum_{p=1}^{3} |V|_{int.j} \sum_{k=1}^{n} \sum_{m=1}^{3} |V|_k^m [G_{ik}^{pm} \cos\theta_{ik}^{pm} + B_{ik}^{pm} \sin\theta_{ik}^{pm}] \quad (8)$$

$$\Delta|V|_{reg.j} = |V|^{SP}_{term.j} - |V|_{term.j}(|V|^p_j) \quad (9)$$

where $|V|^p_j$ are the three terminal voltages at busbar j.

The simplest equation results when the voltage regulator monitors one phase ($|V|^A$) only, i.e.

$$\Delta|V|_{reg.j} = |V|^{SP}_{term.j} - |V|^A_j \quad (10)$$

These sets of nonlinear equations are expressed by the equation

$$\begin{bmatrix} \Delta P \\ \Delta P_{gen} \\ \Delta Q \\ \Delta|V|_{reg} \end{bmatrix} = \begin{bmatrix} [A] & [E] & [I] & [M] \\ [B] & [F] & [J] & [N] \\ [C] & [G] & [K] & [P] \\ [D] & [H] & [L] & [R] \end{bmatrix} \begin{bmatrix} \Delta\theta \\ \Delta\theta_{int} \\ \Delta|V|/|V| \\ \Delta|V|_{int} \ |V|_{int} \end{bmatrix} \quad (11)$$

The right-hand-side matrix is the usual Jacobian matrix of partial derivatives. Eqn. 11 is solved iteratively for the right-hand-side vector, the corresponding variables are updated, and the Jacobians are then re-evaluated. The procedure continues until the left-hand-side mismatches are within tolerance.

4 Decoupled algorithm

In decoupled solutions, the effects of $\Delta\theta$ on reactive-power flows and $\Delta|V|$ on real-power flows are ignored, i.e. we can simplify eqn. 11 by making

$$[I] = [M] = [J] = [N] = 0$$

and

$$[C] = [G] = 0$$

Moreover, it follows from eqn. 10 that

$$[D] = [H] = 0$$

Eqn. 11 can thus be written in decoupled form, i.e.

$$\begin{bmatrix} \Delta p^p_i \\ \Delta P_{gen\,j} \end{bmatrix} = \begin{bmatrix} [A] & [E] \\ [B] & [F] \end{bmatrix} \begin{bmatrix} \Delta\theta^p_i \\ \Delta\theta_{int\,j} \end{bmatrix} \quad (12)$$

for $i = 1, nb$ and $j = 1, ng - 1$ (excluding the slack generator)

$$\begin{bmatrix} \Delta Q^p_i \\ \Delta|V|_{reg\,j} \end{bmatrix} = \begin{bmatrix} [K] & [P] \\ [L] & [R] \end{bmatrix} \begin{bmatrix} \Delta|V|^p_i/|V|^p_i \\ \Delta|V|_{int\,j}/|V|_{int\,j} \end{bmatrix} \quad (13)$$

for $i = 1, nb$ and $j = 1, ng$ (including the slack generator).

The coefficients of the Jacobian submatrices for eqns. 12 and 13 are given in Appendix 10.2.

5 Three-phase fast-decoupled algorithm

The basis of a fast-decoupled algorithm is the use of constant Jacobian matrices. Approximations similar to those used in the single-phase-load-flow case are justifiable in eqns. 12 and 13 as follows:

(*a*) at all nodes

$$Q^m_k \ll B^{mm}_{kk}(|V|^m_k)^2$$

(*b*) between connected nodes of the same phase

$$\cos\theta^{mm}_{ik} \approx 1$$

and

$$G^{mm}_{ik}\sin\theta_{ik} \ll B^{mm}_{ik}$$

The three-phase Jacobian submatrices in eqns. 12 and 13 require a further approximation to remain constant, namely, ignoring the phase-angle unbalance

$$\theta^{pm}_{ik} = \pm 120^\circ \quad \text{for} \quad m \neq p$$

The above 'procedural' approximations, however, must not be confused with the 'actual' phase-angle differences or degrees of angle unbalance that the algorithm can handle.

Substituting these values into the Jacobian submatrices of Appendix 10.2 yields

$$\begin{bmatrix} \Delta P^p_i \\ \Delta P_{gen.j} \end{bmatrix} = \begin{bmatrix} [|V|^p_i M^{pm}_{ik}|V|^m_k] & \begin{bmatrix} \sum_{m=1}^{3} |V|^p_i M^{pm}_{il}|V|_{int.l} \end{bmatrix} \\ \begin{bmatrix} \sum_{p=1}^{3} |V|_{int.j} M^{pm}_{jk}|V|^m_k \end{bmatrix} & \begin{bmatrix} \sum_{m=1}^{3}\sum_{p=1}^{3} |V|_{int.j} M^{pm}_{jl}|V|_{int.l} \end{bmatrix} \end{bmatrix} \begin{bmatrix} \Delta\theta^p_k \\ \Delta\theta_{int.l} \end{bmatrix} \quad (14)$$

$$\begin{bmatrix} \Delta Q^p_i \\ \Delta|V|_{reg.j} \end{bmatrix} = \begin{bmatrix} [|V|^p_i M^{pm}_{ik}|V|^m_k] & \begin{bmatrix} \sum_{m=1}^{3} |V|^p_i M^{pm}_{il}|V|_{int.l} \end{bmatrix} \\ [L] & [O] \end{bmatrix} \begin{bmatrix} \Delta|V|^m_k/|V|^m_k \\ \Delta|V|_{int.l}/|V|_{int.l} \end{bmatrix} \quad (15)$$

where $M^{pm}_{ik} = G^{pm}_{ik}\sin\theta^{pm}_{ik} - B^{pm}_{ik}\cos\theta^{pm}_{ik}$

All terms in the matrix $[M]$ are constant, and their values are given by substitution of the following:

$$\theta^{mm}_{kk} = 0$$

$$\theta^{mm}_{ik} = 0$$

and

$$\theta^{pm}_{ik} = \pm 120^\circ \quad \text{for} \quad m \neq p$$

The matrix $[M]$ is the same as matrix $[B]$, except for the offdiagonal terms that connect nodes of different phases, which are modified by allowing for the $\pm 120^\circ$ angle, and adding the $G^{pm}_{ik}\sin\theta^{pm}_{ik}$ terms.

Eqns. 14 and 15 are then modified as follows:

(i) The left-hand-side defining functions are redefined as $[\Delta P^p_i/|V|^p_i]$, $[\Delta P_{gen.j}/|V|_{int.j}]$ and $[\Delta Q^p_i/|V|^p_i]$

(ii) In eqn. 14, the remaining right-hand-side $|V|$ terms are set to 1 p.u., removing the influence of reactive-power (MVAr) flows on the calculation of $\Delta\theta$ and $\Delta\theta_{int}$.

(iii) In eqn. 15, the remaining right-hand-side $|V|$ terms are cancelled with the corresponding ones at the right-hand-side vector.

This yields

$$\begin{bmatrix} [\Delta P^p_i/|V|^p_i] \\ [\Delta P_{gen\,j}/|V|_{int\,j}] \end{bmatrix} = \underbrace{\begin{bmatrix} M^{pm}_{ik} & \sum_{m=1}^{3} M^{pm}_{il} \\ \sum_{p=1}^{3} M^{pm}_{jk} & \sum_{p=1}^{3}\sum_{m=1}^{3} M^{pm}_{jl} \end{bmatrix}}_{[B']} \begin{bmatrix} \Delta\theta^p_k \\ \Delta\theta_{int\,l} \end{bmatrix} \quad (16)$$

$$\begin{bmatrix} \Delta Q^p_i/|V|^p_i \\ \Delta|V|_{reg\,j} \end{bmatrix} = \underbrace{\begin{bmatrix} M^{pm}_{ik} & \sum_{m=1}^{3} M^{pm}_{il} \\ [L''] & [O] \end{bmatrix}}_{[B'']} \begin{bmatrix} \Delta|V|^m_k \\ \Delta|V|_{int\,l} \end{bmatrix} \quad (17)$$

where $[B']$ and $[B'']$ are constant approximated Jacobian matrices.

5.1 Modification of constant Jacobian matrices

The decoupling process is completed by further modifying matrices $[B']$ and $[B'']$ as follows.

It is important that the constant Jacobian matrices represent a reliably approximate tangent slope to the corresponding surface, independent of the minor changes in shape that occur during the iterative process. For the surface defined by $[\Delta p/V]$, these changes in shape can be viewed as localised deformities of the surface. These deformities are most pronounced along the axis that corresponds to the busbars where shunt admittances are present. If the terms that reflect these localised deformities into the tangent hyperplane are ignored, a reliably approximate tangent slope is obtainable. This is effectively done in single-phase fast-decoupled load flows[8] by removing from $[B']$ the representation of the network elements that predominantly affect reactive-power (MVAr) flows.

In the modelling of some three-phase transformer connections (the most common example being the star-delta connection), large shunt admittances are effectively introduced into the system. This is illustrated for the case of a star-delta transformer in Fig. 5.

When the shunts are excluded from the $[B']$ matrix, convergence is inhibited. With the inclusion of these shunts, an excellent convergence is obtained, consistent with the usual single-phase load-flow characteristics.

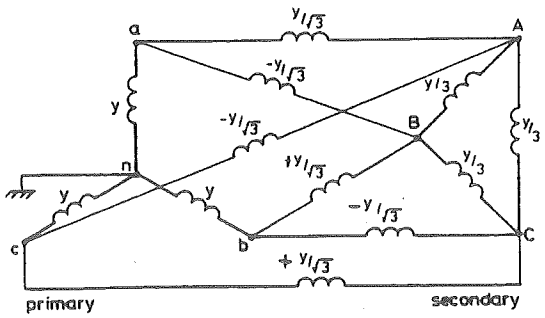

Fig. 5
Equivalent circuit for the star-delta transformer

The difference with respect to the normal system shunt elements is purely one of magnitude. The shunt admittances from the transformer model are extremely large (20 p.u. for a 5% leakage reactance transformer), and will therefore alter the entire shape of the multidimensional surface defined by $[\Delta P/V]$. These shunts must be included in $[B']$ if this is to be representative of the tangent hyperplane to the surface. All other shunts should be excluded from $[B']$ to avoid the localised-deformity problem discussed earlier.

This yields the following two three-phase fast-decoupled matrix equations:

$$\begin{bmatrix} \Delta P/|V| \\ \Delta P_{gen.}/|V|_{int.} \end{bmatrix} = \begin{bmatrix} B'_M \end{bmatrix} \begin{bmatrix} \Delta\theta \\ \Delta\theta_{int.} \end{bmatrix} \quad (18)$$

$$\begin{bmatrix} \Delta Q/|V| \\ \Delta|V|_{reg.} \end{bmatrix} = \begin{bmatrix} B''_M \end{bmatrix} \begin{bmatrix} \Delta|V| \\ \Delta|V|_{int.} \end{bmatrix} \quad (19)$$

The constant approximated Jacobians $[B'_M]$ and $[B''_M]$ correspond to fixed approximated tangent slopes to the multidimensional surfaces formed by the right-hand-side defining functions. Eqns. 18 and 19 are then solved successively, as in the single-phase fast-decoupled method, i.e. according to the flow diagram illustrated in Fig. 6.

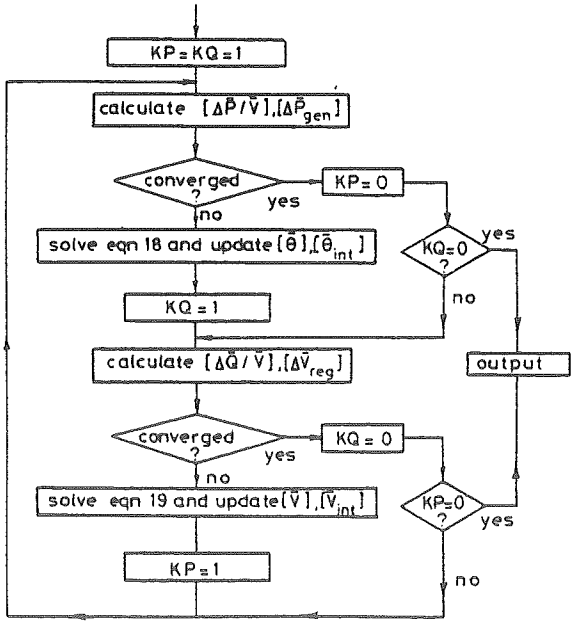

Fig. 6
Flow chart of basic iterative procedure

The solution of eqns. 18 and 19 is carried out using sparsity techniques and near-optimal ordering, as embodied in Zollenkopf's bifactorisation[9] technique.

In decoupled load flows, the multidimensional surface defined by $[\Delta P/V]$ is considered to be independent of the values of $[V]$. This is not strictly correct, and the changing $[V]$ values will alter the surface defined by $[\Delta P/V]$.

6 Test system

The developed algorithm has been applied to the power system shown in Fig. 7, which includes synchronous generators, a synchronous compensator, a section of four mutually-coupled three-phase lines, star-delta-connected transformers with earthed neutrals, and both primary and secondary taps.

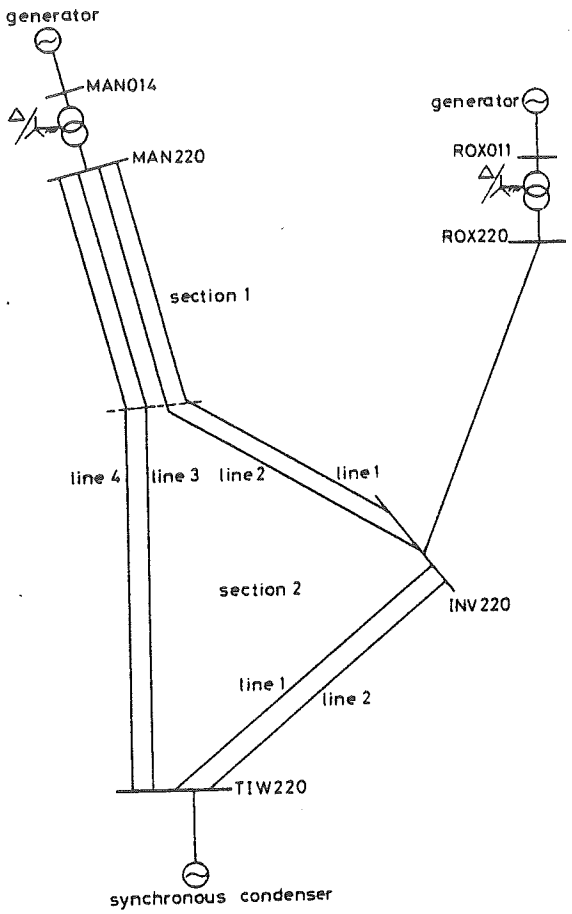

Fig. 7
Single-line diagram of the test system

Fig. 8 illustrates the system divided into eight natural sybsystems, each in terms of 3 × 3, 6 × 6, and 12 × 12 matrix blocks, representing the various elements and sections. The nodal admittance matrix is formed for each section, and these are then combined as discussed earlier.

The matrix blocks are formed from the input data illustrated in Tables 1–3. Because the input data for the coupled lines consist of various full matrices (up to and including two 12 × 12 matrices) representative data only are given in Table 3.

To investigate the convergence properties of the algorithm, the following studies were compared:

(*a*) Balanced operation of the balanced power system
 (i) with the generators effectively excluded by setting their sequence impedances to a low value (this is the three-phase equivalent of the usual single-phase load flow)
 (ii) with realistic generator modelling
(*b*) Unbalanced operation of the unbalanced power system (with busbar loading conditions as shown in Table 4)
 (i) generators effectively excluded
 (ii) realistic generator modelling
(*c*) As for case (*b*) (ii), except with the 30° phase shift due to the transformer connections ignored in the starting values

(*d*) For the unbalanced system under abnormal operating conditions
(i) large unbalanced real-power loading (as for case (*b*) (ii), except for INV220, which now has 300 MW in phase *A*)
(ii) large unbalanced reactive-power loading (as for case (*b*) (ii), except for INV220, which now has 500 MVAr reactive power in phase *A*)
(iii) large unbalanced real and reactive-power loading ((*d*) (i) and (*d*) (ii) loading conditions applied together).

6.1 Discussion of results

The number of iterations required for the maximum mismatches to be within the specified tolerance is shown in Table 5. These results and the authors' experience with other cases leads to the following conclusions as regards convergence properties of the developed algorithm:

(i) For a balanced system, convergence is similar to that of a single-phase load flow
(ii) The inclusion of generator plant and the modelling of the voltage regulator does not cause any significant deterioration in convergence
(iii) Starting values are not critical. Flat voltage and angle initial conditions are perfectly adequate
(iv) Convergence is achieved even in cases of extreme unbalance.

The resulting system voltages and angles for cases (*b*) (ii) and (*d*) (ii) are given in Tables 6 and 7, respectively, and the line power flows for case (*b*) (ii) in Table 8.

In addition to the significant unbalance, the following features are noticed in Tables 6–8:

(*a*) There is an approximate 30° phase shift due to the star-delta-connected transformers
(*b*) Balanced voltages occur at the generator internal busbars

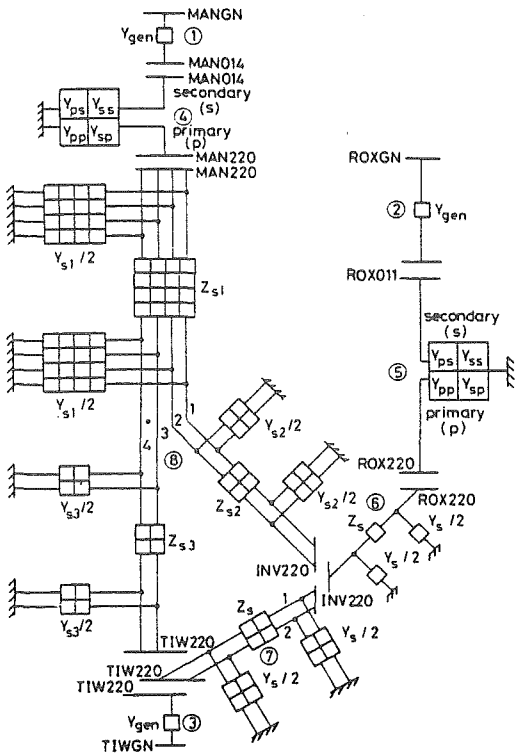

Fig. 8
Test system exploded into eight subsystems

Table 1
GENERATOR DATA

Generator	Sequence reactances			Power	Voltage
Name	X_0	X_1	X_2	P	V
MAN14	0·050	0·100	0·010	6·900	1·045
TIW220	0·050	0·100	0·010	0·000	1·020
ROX011	0·050	0·100	0·010	slack	1·050

Table 2
TRANSFORMER DATA

Busbar names	ROX220-ROX011	MAN220-MAN014
Connection	Star delta	Star delta
Leakage impedance	0·0060 + *j* 0·1164	0·0018 + *j* 0·0492
Primary tap (%)	0·022	0·025
Secondary tap (%)	0·732	0·732

Table 3
LINE DATA: INV220-TIW220 DOUBLE CIRCUIT $[Z_s]$ SERIES-IMPEDANCE MATRIX

	a	*b*	*c*	*a*	*b*	*c*
a	0·0069 + *j* 0·0440	0·0045 + *j* 0·0209	0·0043 + *j* 0·0219	0·0043 + *j* 0·0212	0·0045 + *j* 0·0185	0·0043 + *j* 0·0182
b	0·0045 + *j* 0·0209	0·0066 + *j* 0·0441	0·0044 + *j* 0·0207	0·0045 + *j* 0·0185	0·0046 + *j* 0·0182	0·0044 + *j* 0·0167
c	0·0043 + *j* 0·0219	0·0044 + *j* 0·0207	0·0065 + *j* 0·0442	0·0043 + *j* 0·0182	0·0044 + *j* 0·0167	0·0043 + *j* 0·0163
a	0·0043 + *j* 0·0212	0·0045 + *j* 0·0185	0·0043 + *j* 0·0182	0·0069 + *j* 0·0440	0·0045 + *j* 0·0209	0·0043 + *j* 0·0219
b	0·0045 + *j* 0·0185	0·0046 + *j* 0·0182	0·0044 + *j* 0·0167	0·0045 + *j* 0·0209	0·0066 + *j* 0·0441	0·0044 + *j* 0·0207
c	0·0043 + *j* 0·0182	0·0044 + *j* 0·0167	0·0043 + *j* 0·0163	0·0043 + *j* 0·0219	0·0044 + *j* 0·0207	0·0065 + *j* 0·0442

$[Y_s]$ shunt-admittance matrix

	a	*b*	*c*	*a*	*b*	*c*
a	*j* 0·0152	−*j* 0·0021	−*j* 0·0024	−*j* 0·0020	−*j* 0·0009	−*j* 0·0005
b	−*j* 0·0021	*j* 0·0142	−*j* 0·0022	−*j* 0·0009	−*j* 0·0011	−*j* 0·0004
c	−*j* 0·0024	−*j* 0·0022	*j* 0·0147	−*j* 0·0008	−*j* 0·0004	−*j* 0·0001
a	−*j* 0·0020	−*j* 0·0008	−*j* 0·0008	*j* 0·0152	−*j* 0·0021	−*j* 0·0024
b	−*j* 0·0009	−*j* 0·0011	−*j* 0·0004	−*j* 0·0021	*j* 0·0142	−*j* 0·0022
c	−*j* 0·0005	−*j* 0·0004	−*j* 0·0001	−*j* 0·0024	−*j* 0·0022	*j* 0·0147

Table 4
BUSBAR LOADING DATA

Bus name	Phase *A*		Phase *B*		Phase *C*	
	P	*Q*	*P*	*Q*	*P*	*Q*
INV220	50·000	15·000	45·000	14·000	48·300	16·600
MAN014	0·000	0·000	0·000	0·000	0·000	0·000
MAN220	0·000	0·000	0·000	0·000	0·000	0·000
ROX011	0·000	0·000	0·000	0·000	0·000	0·000
ROX220	48·000	20·000	47·000	12·000	51·300	28·300
TIW220	150·000	80·000	157·000	78·000	173·000	72·000
MAN.GN	0·000	0·000	0·000	0·000	0·000	0·000
TIW.GN	0·000	0·000	0·000	0·000	0·000	0·000
ROX.GN	0·000	0·000	0·000	0·000	0·000	0·000

Table 5
NUMBER OF ITERATIONS TO CONVERGENCE

Case study	Maximum initial mismatch*	Convergence tolerance*					
		0·1		0·01		0·001	
		θ	$\|V\|$	θ	$\|V\|$	θ	$\|V\|$
a (i)	2·45	2	1	3	2	5	3
a (ii)	2·45	2	1	4	3	6	4
b (i)	2·51	2	1	4	4	7	7
b (ii)	2·51	2	1	4	4	7	7
c	10·34	4	3	6	5	9	7
d (i)	2·88	4	4	7	7	11	10
d (ii)	3·14	6	6	9	9	12	12
d (iii)	3·14	6	6	10	10	13	12

*Tolerances and mismatches are in p.u. on a 100 MVA base

Table 6
SYSTEM VOLTAGES (V) AND ANGLES (DEGREES) FOR CASE *b* (ii)

Busbar name	Phase *A*		Phase *B*		Phase *C*		Generation	
	Voltage	Angle	Voltage	Angle	Voltage	Angle	MW	MVAr
INV220	1·021	29·447	1·022	−90·520	1·026	149·152	0·000	0·000
MAN014	1·045	11·235	1·046	−108·873	1·044	131·112	0·000	0·000
MAN220	1·059	35·399	1·053	−85·244	1·042	155·267	0·000	0·000
ROX011	1·050	−1·573	1·051	−121·550	1·051	118·412	0·000	0·000
ROX220	1·038	26·646	1·048	−93·247	1·035	146·354	0·000	0·000
TIW220	1·020	29·164	1·018	−90·908	1·023	148·845	0·000	0·000
MAN GN	1·111	22·584	1·111	−97·416	1·111	142·584	690·000	288·124
TIW GN	1·056	29·033	1·056	−90·967	1·056	149·033	0·000	114·641
ROX GN	1·078	0·000	1·078	−120·000	1·078	120·000	93·065	89·246

Table 7
SYSTEM VOLTAGES (V) AND ANGLES (DEGREES) FOR CASE *d* (ii)

Busbar name	Phase *A*		Phase *B*		Phase *C*		Generation	
	Voltage	Angle	Voltage	Angle	Voltage	Angle	MW	MVAr
INV220	0·884	28·782	1·162	−97·506	1·190	152·450	0·000	0·000
TIW220	1·020	27·345	1·137	−94·500	1·142	149·480	0·000	0·000
ROX220	1·013	25·944	1·084	−94·405	1·070	146·723	0·000	0·000
ROX011	1·050	−1·849	1·050	−121·739	1·052	118·190	0·000	0·000
MAN220	1·057	33·828	1·104	−87·051	1·095	153·583	0·000	0·000
MAN014	1·045	9·280	1·047	−110·561	1·049	129·263	0·000	0·000
MAN GN	1·049	21·416	1·049	−98·584	1·049	141·416	690·000	80·021
TIW GN	1·382	27·448	1·382	−92·552	1·382	147·448	0·000	1174·450
ROX GN	1·065	0·000	1·065	−120·000	1·065	120·000	105·447	48·534

Table 8
LINE POWER FLOWS FOR CASE (*b*) (ii)

Sending-end busbar name	Receiving-end busbar name	Sending end		Receiving end	
		MW	MVAr	MW	MVAr
MAN014	MAN GN	−215·188	−47·660	214·317	94·689
		−236·239	−32·027	239·036	83·135
		−238.^{577}	−57·358	236·651	110·300
TIW220	TIW GN	1·022	−48·856	−0·943	50·603
		13·968	−39·879	−14·459	41·417
		−14·990	−21·861	15·402	22·622
ROX011	ROX GN	−31·477	−32·397	31·380	34·123
		−27·102	−26·447	27·056	27·870
		−34·486	−25·625	34·629	27·253
MAN220	INV220	61·717	−0·449	−59·959	−3·060
		63·923	8·780	−63·029	−12·525
		55·884	9·433	−55·938	−12·890
MAN220	INV220	60·104	3·148	−58·834	−6·633
		60·697	8·862	−59·913	−12·893
		55·386	8·308	−55·251	−11·644
MAN220	TIW220	50·372	4·489	−50·036	−10·361
		45·195	8·696	−44·865	−15·661
		45·799	−2·050	−44·387	−4·002
MAN220	TIW220	50·280	1·766	−49·601	−7·803
		71·153	−10·392	−68·015	5·177
		66·716	21·838	−67·520	−25·218
INV220	TIW220	25·741	4·940	−25·740	−6·486
		29·094	12·418	−29·016	−13·818
		22·994	8·775	−23·049	−10·464
INV220	TIW220	25·755	4·932	−25·727	−6·494
		29·094	12·418	−29·016	−13·818
		23·008	8·782	−23·035	−10·456
INV220	ROX220	17·294	−15·180	−17·761	7·742
		19·699	−13·417	−18·814	8·668
		16·931	−9·624	−16·981	2·118
MAN220	MAN014	−222·495	−8·953	215·204	47·661
		−240·999	−15·945	236·242	32·027
		−223·842	−37·530	238·620	57·358
ROX220	ROX011	−30·247	−27·743	31·473	32·397
		−28·193	−20·668	27·099	26·447
		−34·329	−30·418	34·487	25·625

Total generation	783·0651 MW	492·0122 MVAr
Total load	769·6000 MW	335·9000 MVAr
System losses	13·3693 MW	156·1128 MVAr
Mismatch	0·0959 MW	−0·0006 MVAr

(c) Balanced angles occur at the generator internal busbars
(d) There is an apparent gain in active power flow in any one phase. This power flows through the mutual-coupling terms between phases. The overall active power shows a net loss as expected for a realistic system
(e) For the synchronous compensator the individual phases may carry real power; although the total three-phase power always sums to zero.

7 Conclusions

The high efficiency of fast-decoupled algorithms over the conventional Newton-Raphson (roughly six fast-decoupled iterations are equivalent to one full Newton-Raphson iteration) method has been extended in this paper to the solution of three-phase load flows. Such extension is not straightforward, and various modifications to the basic algorithm have been developed to cope with mutual effects between phases and between parallel transmission lines. Also, the presence of large shunt admittances in some transformer equivalent circuits have been found to influence convergence, and need to be included in the active power-mismatch Jacobian matrix. Sparsity techniques and near-optimal ordering have been used to provide fast-repeat solutions. The algorithm provides fast and reliable convergence even with extreme conditions of steady-state unbalance.

8 Acknowledgments

The authors are grateful to P.W. Blakeley, General Manager of the New Zealand Electricity Department and to the Computer Centre of the University of Canterbury for their help.

9 References

1 CHEN, M.S., and DILLON, W.E.: 'Power system modelling', *Proc. IEEE*, 62, 1974, pp. 901–915
2 LAUGHTON, M.A.: 'Analysis of unbalanced polyphase networks by the method of phase co-ordinates – Part 1. System representation in the phase frame of reference', *Proc. IEE*, 1968, 115, (8), pp. 1163–1172
3 BRAMELLER, A., and PANDEY, R.S.: 'General fault analysis using phase frame of reference', *ibid.* 121, (5), 1974, pp. 366–368
4 WASLEY, R.G., and SLASH, M.A., 'Newton-Raphson algorithm for 3-phase load flow', *ibid.* 121, (7), 1974, pp. 630–638
5 BIRT, K.A., GRAFFY, J.J., McDonald, J.D., and El-Abiad, A.H.: 'Three-phase load flow program', *IEEE Trans.*, PAS-95, 1976, pp. 59–65
6 KRON, G.: Tensor analysis of networks (MacDonald, London, republished 1965)
7 CLARKE, E.: 'Circuit analysis of a.c. power systems – Vol. 1' (Wiley, 1943)
8 STOTT, B., and Alsac, D.: 'Fast decoupled load flow', *IEEE Trans.* PAS-93, 1974, pp. 859–867
9 ZOLLENKOPF, K.: 'Bi-factorisation – Basic computational algorithm and programming techniques'. Conference on large sets of sparse linear equations, Oxford, 1970, pp. 75–96

10 Appendix

10.1 Submatrices for different transformer connections

Table 9

BASIC SUBMATRICES USED IN NODE-ADMITTANCE FORMULATION OF COMMON THREE-PHASE TRANSFORMER CONNECTIONS

Transformer connection		Self admittance		Mutual admittance
Bus P	Bus S	Y_{pp}	Y_{ss}	Y_{PS}, Y_{SP}^T
Wye – G	Wye – G	Y_{I}	Y_{I}	$-Y_{\mathrm{I}}$
Wye – G	Wye	$Y_{\mathrm{II}}/3$	$Y_{\mathrm{II}}/3$	$-Y_{\mathrm{II}}/3$
Wye – G	Delta	Y_{I}	Y_{Π}	$+Y_{\mathrm{III}}$
Wye	Wye	$Y_{\mathrm{II}}/3$	$Y_{\mathrm{II}}/3$	$-Y_{\mathrm{II}}/3$
Wye	Wye	$Y_{\mathrm{II}}/3$	Y_{Π}	Y_{III}
Delta	Delta	Y_{Π}	Y_{Π}	$-Y_{\Pi}$

The characteristic submatrices used in forming the transformer admittance matrices are as follows:

$$Y_{\mathrm{I}} = \begin{bmatrix} Y_t & & \\ & Y_t & \\ & & Y_t \end{bmatrix}$$

$$Y_{\mathrm{II}} = \begin{bmatrix} 2Y_t & -Y_t & -Y_t \\ -Y_t & 2Y_t & -Y_t \\ -Y_t & -Y_t & 2Y_t \end{bmatrix}$$

$$Y_{\mathrm{III}} = \begin{bmatrix} -Y_t & Y_t & \\ & -Y_t & Y_t \\ Y_t & & -Y_t \end{bmatrix}$$

10.2 Jacobian submatrices

Coefficients of matrix eqn. 12 are as follows:

(i) $[A_{ik}^{pm}] = [\partial \Delta P_i^p / \partial \theta_k^m]$

where

$$A_{ik}^{pm} = |V|_i^p |V|_k^m [G_{ik}^{pm} \sin \theta_{ik}^{pm} - B_{ik}^{pm} \cos \theta_{ik}^{pm}]$$

except

$$A_{kk}^{mm} = -B_{kk}^{mm} |V|_k^{m^2} - Q_k^m$$

(ii) $[B_{jk}^m] = [\partial \Delta P_{GEN.j} / \partial \theta_k^m]$

$$= \sum_{p=1}^{3} |V|_{int.j} |V|_k^m [G_{jk}^{pm} \sin \theta_{jk}^{pm} - B_{jk}^{pm} \cos \theta_{jk}^{pm}]$$

(iii) $[E_{il}^p] = [\partial \Delta P_i^p / \partial \theta_{int.l}]$

$$= \sum_{m=1}^{3} |V|_{int.l} |V|_i^p [G_{il}^{pm} \sin \theta_{il}^{pm} - B_{il}^{pm} \cos \theta_{il}^{pm}]$$

(iv) $[F_{jl}] = [\partial \Delta P_{gen.j} / \partial \theta_{int.l}]$

where $[F_{jl}] = 0$ for $j \neq l$ because the jth generator has no connection with the lth generator internal busbar

and

$$[F_{il}] = \sum_{m=1}^{3} -B_{il}^{mm} |V|_i^{m^2} - Q_i^m + \sum_{\substack{m=1 \\ m \neq p}}^{3} \sum_{p=1}^{3} |V|_{int.l} |V|_{int.l} [G_{il}^{pm} \sin \theta_{il}^{pm} - B_{il}^{pm} \cos \theta_{il}^{pm}]$$

Coefficients of matrix 13 are as follows

(i) $[K_{ik}^{pm}] = |V|_k^m [\partial \Delta Q_i^p / \partial |V|_k^m]$

where

$$K_{ik}^{pm} = |V|_k^m |V|_i^p [G_{ik}^{pm} \sin \theta_{ik}^{pm} - B_{ik}^{pm} \cos \theta_{ik}^{pm}]$$

except

$$K_{kk}^{mm} \equiv -B_{kk}^{mm} |V|_k^{m^2} + Q_k^m$$

(ii) $[L_{jk}^m] = |V|_k^m [\partial \Delta_{reg.j} / \partial |V|_k^m]$

where $L_{jk}^1 = -|V|_k^1$ where k is the terminal busbar of the jth generator and $L_{jk}^m = 0$ otherwise

(iii) $[P_{il}^p] = |V|_{int.l} [\partial \Delta Q_i^p / |V|_{int.l}]$

$$= |V|_{int.l} \sum_{m=1}^{3} |V|_i^p [G_{il}^{pm} \sin \theta_{il}^{pm} - B_{il}^{pm} \cos \theta_{il}^{pm}]$$

(iv) $[R_{jl}] = 0$ for all j, l

APPENDIX 6

3-phase a.c./d.c. load flow

B.J. Harker, B.E., M.E., and Prof. J. Arrillaga, M.Sc.Tech., Ph.D., C.Eng., F.I.E.E.

Indexing terms: D.C. power transmission, Load flow, Power convertors

Abstract

A phase-co-ordinate model of h.v. d.c. transmission systems suitable for integration into 3-phase load-flow analysis is developed in the paper. The model is sufficiently general to allow representation of alternative control strategies, such as the predictive and symmetrical firing control. The integration of the model into the load-flow analysis is described with particular reference to the 3-phase fast-decoupled algorithm. The results indicate the flexibility and powerful convergence of the proposed algorithm.

1 Introduction

The subject of a.c./d.c. load flow has been given some consideration in recent years but only under perfectly symmetrical operating conditions.[1] When the a.c. system is not balanced the interaction between convertor and a.c.-supply waveforms can only be assessed with a 3-phase load-flow model integrating the a.c. and d.c. equations.

Phase-angle control with minimum angles of delay (rectifier) or advance (inverter) in the steady-state condition constituted the basis of early h.v.d.c. control schemes. An alternative control, based on equidistant firings on the steady state, is generally accepted to provide more stable operation in the presence of weak a.c. systems and particularly during disturbances.[2]

Under normal steady-state and perfectly balanced generating conditions there is no difference between these two basic control strategies. However, their effect on the a.c. system and d.c. voltage and current waveshapes during normal, but not balanced, operation is quite different.

A 3-phase convertor model is described in this paper with flexibility to represent alternative control strategies and d.c. configurations. Although the model can be used with any type of 3-phase load flow, the paper describes a very efficient integration with the recently developed 3-phase fast decoupled algorithm.[3]

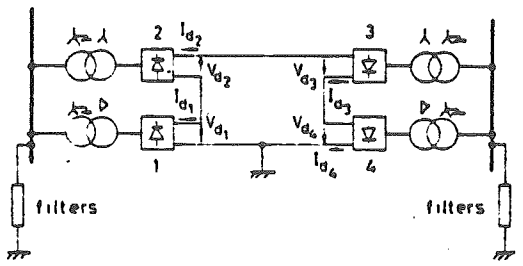

Fig. 1
Basic h.v. d.c. interconnection

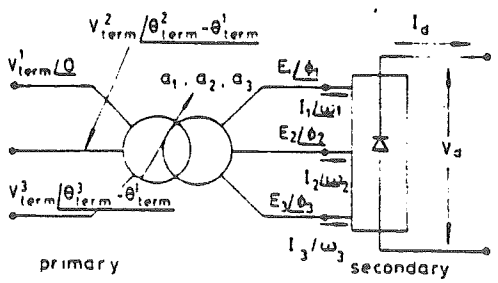

Fig. 2
Basic convertor unit

2 D.C. system modelling

The basic h.v. d.c. interconnection shown in Fig. 1 is used as a reference in the development of the model. The extension to other configurations is clarified throughout the development. All convertor units, whether rectifying or inverting, are represented by the same model (Fig. 2), and their equations are of the same form.

Paper 8420 P, received 25th June 1979

Mr. Harker is with New Zealand Electricity, Christchurch 1, New Zealand, and Prof. Arrillaga is with the Department of Electrical Engineering, University of Canterbury, Christchurch 1, New Zealand

Under unbalanced conditions the convertor transformer modifies the source voltages applied to the convertor and also affects the phase distribution of current and power. In addition, the a.c. system operation may be influenced (e.g. by a zero-sequence current flow to a star-g/delta transformer) by the transformer connection. Each bridge in Fig. 1 will thus operate with a different degree of unbalance, owing to the influence of the convertor transformer connections, and must be modelled independently.

A mathematical model of the d.c. system, suitable for inclusion into the load-flow analysis, consists of a set of independent equations $\bar{R}$ which completely define the operating state of the system in terms of the convertor variables $\bar{x}$ and the 3-phase a.c. voltages V^i_{term} and θ^i_{term} at the terminal busbars, i.e.

$$R(V^i_{term}, \theta^i_{term}, \bar{x})_k = 0 \qquad (1)$$

for $k = 1$ (number of convertors) and $i = 1, 3$ for the three phases at the terminal busbar.

2.1 Derivation of equations

To simplify the selection of variables and the formulation of eqn. 1 the following conditions are assumed:

(*a*) sinusoidal voltage supply on the system side of the convertor transformer
(*b*) perfectly smooth direct current
(*c*) rectangular approximation for the phase currents
(*d*) the supply to the convertor auxiliaries and control units is not affected by the degree of unbalance.

Regarding assumptions (*a*) and (*b*), previous work[7, 8, 9] has demonstrated the appearance of second-harmonic ripple on the d.c. side and nonzero-sequence triplen-harmonic currents on the a.c. side of static convertors under unbalanced a.c. system conditions. However, the harmonic levels produced are only significant in extreme cases of unbalance, e.g. during unbalanced short-circuit conditions.

The limit of voltage harmonic distortion permitted under steady-state operating conditions is normally below 1% for each individual harmonic at transmission-voltage levels, and, whenever such limits are surpassed, steps are taken to reduce them (e.g. the addition of a third-harmonic filter to the cross-channel link).

Although an exact solution would require accurate assessment of the harmonic content and harmonic penetration, there is no need for such detailed studies in power-flow analysis. (Further justification is given in Section 6.)

Approximation (*c*) is commonly accepted in load-flow studies[1] for the purpose of calculating the magnitude of the fundamental current. (The error involved under normal operating conditions with overlap angles below 30° is under 1%.) It must be clarified, however, that such approximation does not imply neglect of the effect of commutation reactance in the calculation of power factor, d.c. voltage levels etc. where the errors would be more pronounced.

Based on the above approximations the voltage and current waveforms illustrated in Fig. 3 apply. The convertor operating state can then be formulated in terms of the following 26 variables ($\bar{x}$) defined with reference to Fig. 2 and Fig. 3:

E_i/ϕ_i = fundamental-frequency voltages at the secondary side of the transformer
I_i/ω_i = fundamental-frequency line currents at the transformer secondary
a_i = off-nominal tap ratios on the primary side
U_{ij}/C_i = phase-phase source voltages for the convertor referred to the transformer secondary. C_i are therefore the zero crossings for the timing of firing pulses
α_i = firing-delay angle measured from the respective zero crossing

V_d = total average d.c. voltage from complete bridge
I_d = average d.c. current

where $i = 1, 2, 3$ for the three phases involved.

In the 3-phase a.c. load flow all angles are referred to the slack generator's internal busbar. The angle reference for the convertor variables is arbitrary. Similarly, for the single-phase a.c./d.c. load flow,[1] by using one of the convertor angles (e.g. θ^1_{term} in Fig. 2) as a reference, the mathematical coupling between the equations describing the a.c. system and those describing the convertor is weakened. This has a favourable effect on the rate of convergence, especially when a sequential solution technique is used.

Based on the p.u. system described in Appendix 10.1 a set of 26 independent equations is derived in the following subsections.

The complete set of equations is illustrated in Appendix 10.2.

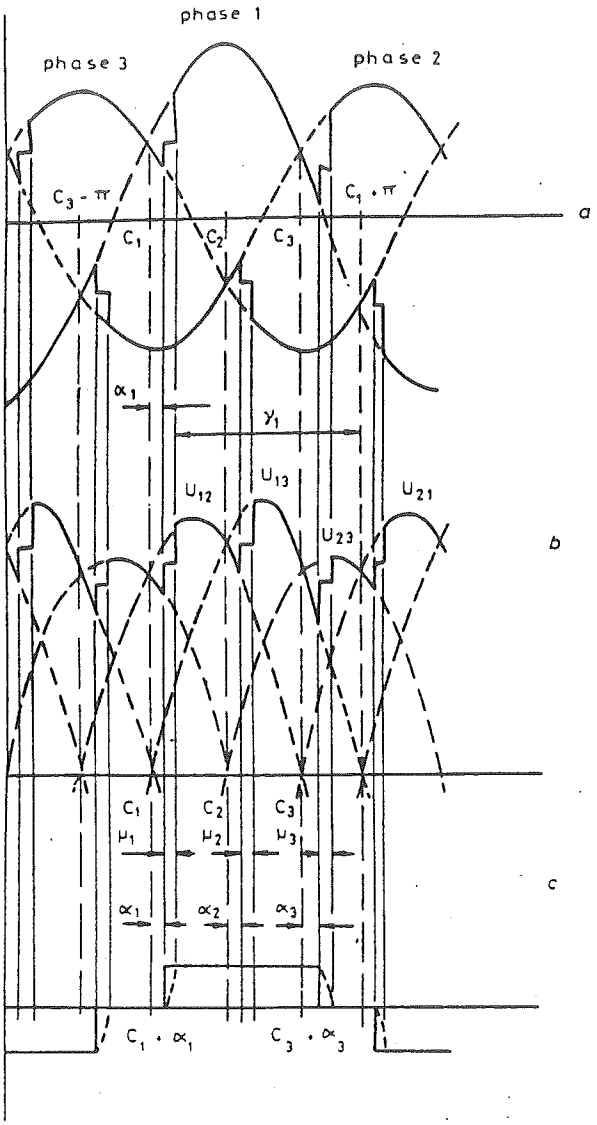

Fig. 3
Voltage and current waveforms

a Phase voltages
b Direct voltages
c Assumed current in phase 1 (actual waveform indicated in dotted line)

2.1.1 Current relationships

Relationships are derived for the fundamental-frequency real and imaginary current flows across the convertor transformer.

Off-nominal taps (a_1 a_2 a_3) are modelled on the system (primary) side of the transformer and for generality are assumed to be independently controllable.

The 3-phase convertor transformer is represented by its nodal admittance model, i.e.

$$Y_{node} = \begin{array}{|c|c|}\hline Y_{pp} & Y_{ps} \\ \hline Y_{sp} & Y_{ss} \\ \hline \end{array}$$

where p indicates the primary side and s the secondary side of the transformer.

The 3 × 3 submatrices (Y_{pp} etc.) for the various transformer connections, including modelling of the independent-phase taps, may be derived using Kron's connection-matrix technique as explained in Reference 6.

In terms of these submatrices, and on the assumption of a lossless transformer (i.e. $Y_{pp} = jb_{pp}$ etc.), the currents at the convertor-side busbar are expressed as follows:

$$I_i e^{j\omega_i} = -\sum_{k=1}^{3} \{jb^{ik}_{ss} E_k e^{j\phi k} + jb^{ik}_{sp} V^k_{term} \exp [j(\theta^k_{term} - \theta^1_{term})]\}$$

On subtracting θ^1_{term} in the above equation, the terminal busbar angles are related to the convertor angle reference. On separating this equation into real and imaginary components, the following six equations result:

$$I_i \cos \omega_i = \sum_{k=1}^{3} \{b^{ik}_{ss} E_k \sin \phi_k + b^{ik}_{sp} V^k_{term} \sin (\theta^k_{term} - \theta^1_{term})\} \quad (2)$$

$$I_i \sin \omega_i = \sum_{k=1}^{3} \{-b^{ik}_{ss} E_k \cos \phi_k - b^{ik}_{sp} V^k_{term} \cos (\theta^k_{term} - \theta^1_{term})\} \quad (3)$$

Three approximate relationships are derived[4] for the fundamental r.m.s. components of the line-current waveforms as shown in Fig. 3, i.e.

$$I_i = \frac{4I_d}{\sqrt{2}} \sin (T_i/2) \quad (4)$$

where T_i is the assumed conduction period of phase i.

2.1.2 Secondary-voltage reference

The voltage reference for the a.c. system is earth. In d.c. transmission the actual earth is placed on one of the convertors' d.c. terminal, and this point is used as a reference to define the d.c.-transmission voltages and the insulation levels of the convertor-transformers' secondary windings.

However, for the load-flow analysis, arbitrary references can be used for each convertor unit to simplify the mathematical model. The actual voltages to earth, if required, can then be obtained from knowledge of the particular configuration and earthing arrangements.

The transformer nodal admittance matrix of Section 2.1.1 relates the injected currents to the nodal voltages, where the nodal voltages are normally referenced to earth. In the case of the convertor-transformer secondary an arbitrary reference can be explicitly included. Using the zero-sequence secondary voltage as a reference yields the following equations:

$$\sum_{k=1}^{3} E_i \cos \phi_i = 0 \quad (5)$$

$$\sum_{i=1}^{3} E_i \sin \phi_i = 0 \quad (6)$$

2.1.3 Power relationship

The following expression is derived by equating the sum of the 3-phase a.c. powers to the total d.c. power:

$$\sum_{i=1}^{3} E_i I_i \cos (\phi_i - \omega_i) - V_d I_d = 0 \quad (7)$$

2.1.4 Convertor source voltages

The phase-phase source voltages referred to the transformer secondary are found by a consideration of the transformer connection and off-nominal turns ratio. For example, consider the star-star transformer of Fig. 4:

$$U_{13} \angle C_1 = \frac{1}{a_1} V^1_{term} \angle 0 - \frac{1}{a_3} V^3_{term} \angle (\theta^3_{term} - \theta^1_{term}) \quad (8)$$

$$U_{23} \angle C_2 = \frac{1}{a_2} V^2_{term} \angle (\theta^2_{term} - \theta^1_{term}) - \frac{1}{a_3} V^3_{term} \angle (\theta^3_{term} - \theta^1_{term}) \quad (9)$$

$$U_{21}\angle C_3 = \frac{1}{a_2} V^2_{term}\angle\theta^2_{term} - \theta^1_{term} - \frac{1}{a_1} V^1_{term}\angle 0 \quad (10)$$

Taking real and imaginary parts yields a further six equations.

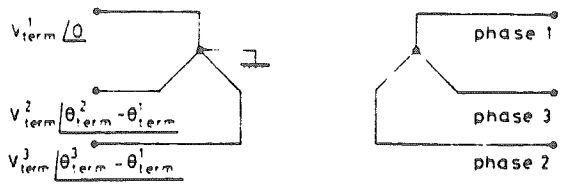

Fig. 4
Star-star transformer connection

2.1.5 Direct voltage

The direct voltage is found by integration of the waveforms in Fig. 3*b* and may be written in the form

$$\frac{V_d\pi}{\sqrt{2}} = U_{21}[\cos(C_1 + \alpha_1 - C_3 + \pi) - \cos(C_2 + \alpha_2 - C_3 + \pi)] + U_{13}[\cos(C_2 + \alpha_2 - C_1) - \cos(C_3 + \alpha_3 - C_1)] + U_{23}[\cos(C_3 + \alpha_3 - C_2) - \cos(C_1 + \alpha_1 + \pi - C_2)] - I_d(XC_1 + XC_2 + XC_3) \quad (11)$$

where XC_i is the commutation reactance for phase i.

2.1.6 D.C. interconnection

An equation is derived for each convertor from the d.c. system topology relating the d.c. voltages and currents. In general this equation is of the form

$$f(V_d, I_d) = 0 \quad (12)$$

For example, the system shown in Fig. 1 provides the following four equations:

$$\begin{aligned} Vd_1 + Vd_2 + Vd_3 + Vd_4 - Id_1Rd &= 0 \\ Id_1 - Id_2 &= 0 \\ Id_1 - Id_3 &= 0 \\ Id_1 - Id_4 &= 0 \end{aligned}$$

where clearly some redundancy results. This is the cost of complete generality in the d.c. interconnection.

2.1.7 Incorporation of control strategies

A further six equations are derived from the specific operating conditions. Any function of the 26 variables is a valid (mathematically) control equation so long as the equation is independent of all the others. In practice there are restrictions limiting the number of alternatives. Some control specifications refer to the characteristics of power transmission (e.g. constant power or constant current); others introduce constraints such as minimum delay or extinction angles.

As the consideration of the alternative firing controls is of particular interest their implementation is now discussed. Symmetrical firing is considered as being applied individually for each 6-pulse bridge, although, if required, the equations may be written to consider the firing controller operating on an integral 12-pulse bridge. For the 6-pulse unit the interval between firing pulses is specified as 60°. This provides two equations. The third equation results from the specification of minimum firing-angle control, i.e.

$$\alpha_i - \alpha_{min} = 0$$

where phase i is selected during the solution procedure such that the other two phases will have, in the unbalanced case, firing angles greater than α_{min}. With conventional phase-angle control the firing angle on each phase is specified as being equal to α_{min}, i.e.

$$\begin{aligned} \alpha_1 - \alpha_{min} &= 0 \\ \alpha_2 - \alpha_{min} &= 0 \\ \alpha_3 - \alpha_{min} &= 0 \end{aligned}$$

The remaining three control equations are derived from the operating conditions. Usually, the off-nominal taps are specified as being equal, i.e.

$$\begin{aligned} a_1 - a_2 &= 0 \\ a_2 - a_3 &= 0 \end{aligned}$$

The final equation will normally relate to the constant current or constant power controller, e.g.

$$I_d - I_d^{sp} = 0$$

or

$$V_d I_d - p_d^{sp} = 0$$

The above examples illustrate the ease with which the various control specifications are incorporated.

2.1.8 Invertor operation with minimum extinction angle

As the firing-delay angle α is used as a variable, the restriction on the extinction advance angle γ requires the implicit calculation of the commutation angle for each phase.

Taking the specification for γ as defined in Fig. 3, the following equation is used:

$$\cos\gamma_1^{sp} + \cos\alpha_1 - I_d\frac{(XC_1 + XC_3)}{\sqrt{2}U_{13}} = 0 \quad (13)$$

Similar equations apply to the other two phases with cyclic change of suffixes.

3 3-phase a.c./d.c. algorithm

Single and 3-phase load-flow formulations are basically the same. In the 3-phase case, however, the system-admittance matrix includes the effect of each separate phase as well as the interphase mutual couplings in generators, transformers and transmission systems. Moreover, the load active P and reactive Q powers are specified separately for each phase.

Generators require special consideration in 3-phase load flows. Their model includes

(*a*) a balanced set of internal voltages acting behind their synchronous-impedance matrix; i.e. an additional internal busbar is introduced for each generator

(*b*) the voltage-regulator action, which in general is specified as a function of the three terminal voltages, i.e. $f(V^1, V^2, V^3)$

(*c*) the total real-power generation, which is specified at all generating busbars except the slack busbar.

The following variables are required to define the operating state of the 3-phase system:

(i) the slack-generator internal-busbar-voltage magnitude $(V_{gen})_{SL}$

(ii) the internal-busbar-voltage magnitudes $(V_{gen})_j$ and angles $(\theta_{gen})_j$ at all other generators, i.e. for $j = 1, ng-1$ where ng is the number of generators.

(iii) the three voltage magnitudes (V_i^p) and angles (θ_i^p) at every generator terminal busbar and every load busbar, i.e. for $p = 1, 3$ for the three phases and $i = 1, nb$ where nb is the actual number of busbars.

To solve for the above variables, a total of $[2(ng-1) + 1 + 6nb]$ mismatch equations can be written from the specified conditions; these are

(*a*) at the generators' internal busbars (except the slack generator),

$$(\Delta P_{gen})_j = (P_{gen})_j^{sp} - (P_{gen})_j \quad (14)$$

$$(\Delta V_{reg})_j = f(V_j^1, V_j^2, V_j^3) = 0 \quad (15)$$

for $j = 1, ng-1$

(*b*) at the slack-generator internal busbar,

$$(\Delta V_{reg})_{SL} = f(V_{SL}^1, V_{SL}^2, V_{SL}^3) = 0 \quad (16)$$

(*c*) at every generator terminal busbar and every load busbar,

$$\Delta P_i^p = (P_i^p)^{sp} - (P_i^p)^{ac} = 0 \quad (17)$$

$$\Delta Q_i^p = (Q_i^p)^{sp} - (Q_i^p)^{ac} = 0 \quad (18)$$

for $p = 1, 3$ and $i = 1, nb$.

Eqns. 14 to 18 are written in terms of the unknown variables (normally V and θ). They may be solved by the direct Newton-

Raphson algorithm[5] or, more effectively, by a 3-phase fast-decoupled Newton-Raphson algorithm.[3] Using the latter technique, eqns. 14 to 18 can be decoupled in two groups and solved sequentially as follows:

$$\begin{bmatrix} \Delta P_i^P/|V_i^P| \\ (\Delta P_{gen})_j/|(V_{gen})_j| \end{bmatrix} = [B'] \begin{bmatrix} \Delta\theta_i^P \\ \Delta(\theta_{gen})_j \end{bmatrix} \tag{19}$$

$$\begin{bmatrix} \Delta Q_i^P/|V_i^P| \\ \Delta(V_{reg})_j \\ \Delta(V_{reg})_{SL} \end{bmatrix} = [B''] \begin{bmatrix} \Delta|V_i^P| \\ \Delta(V_{gen})_j \\ \Delta(V_{gen})_{SL} \end{bmatrix} \tag{20}$$

where B' and B'' are the Jacobian matrices approximated to constants.

The presence of the d.c. link is manifested in two ways:

(i) addition of 26 variables and the corresponding mismatch equations for each convertor, i.e. eqn. 1

(ii) modification of the constraint eqns. 17 and 18 at the convertor-terminal busbar as follows:

$$\Delta P_i^P = (P_i^P)^{sp} - (P_i^P)_{ac} - (P_i^P)_{dc} = 0 \tag{21}$$

$$\Delta Q_i^P = (Q_i^P)^{sp} - (Q_i^P)_{ac} - (Q_i^P)_{dc} = 0 \tag{22}$$

where $(Q_i^P)_{dc}$ and $(P_i^P)_{dc}$ are functions of the a.c.-terminal conditions and of the convertor variables.

Extensive load-flow studies have shown that in all cases where reasonable starting values are available a sequential integration of the d.c. equations into the load-flow algorithm led to convergence, the complexity of other approaches not being justified.

With the sequential approach the d.c.-convertor power demands in eqns. 21 and 22 are considered as constant loads, and eqns. 19 and 20 are used without modification for the a.c. solution.

For the solution of the link eqn. 1 the terminal voltages V_{term}^i and θ_{term}^i are considered constant, and the standard Newton-Raphson technique is applied; i.e. the equation

$$[R] = [J][\Delta x] \tag{23}$$

is used to iteratively solve eqn. 1.

The three sets of equations (i.e. eqns. 19, 20 and 23) are solved according to the iteration sequence illustrated in Fig. 5. This sequence acknowledges the fact that the convertor operation is strongly related to the magnitude of the terminal voltages and more weakly dependent on their phase angles. Therefore the convertor solution follows the update of the a.c.-terminal voltages. Also, to avoid compatibility problems between a.c. and d.c. tolerances, the convertor equations are continued to be solved until both sets of a.c. mismatches have converged. Final convergence, when a d.c. convertor is present, is always obtained via path C in the flow chart; paths A and B are possible only in the absence of d.c. convertors.

During the iterative procedure the unspecified convertor variables may go outside prespecified limits. In these cases the offending variable can be set to its limiting value and an appropriate control variable freed. In addition, once convergence is achieved, it may be necessary to set the transformer taps to the nearest discrete step and reconverge to obtain a practical operating condition. The reconvergence will, in general, be very fast.

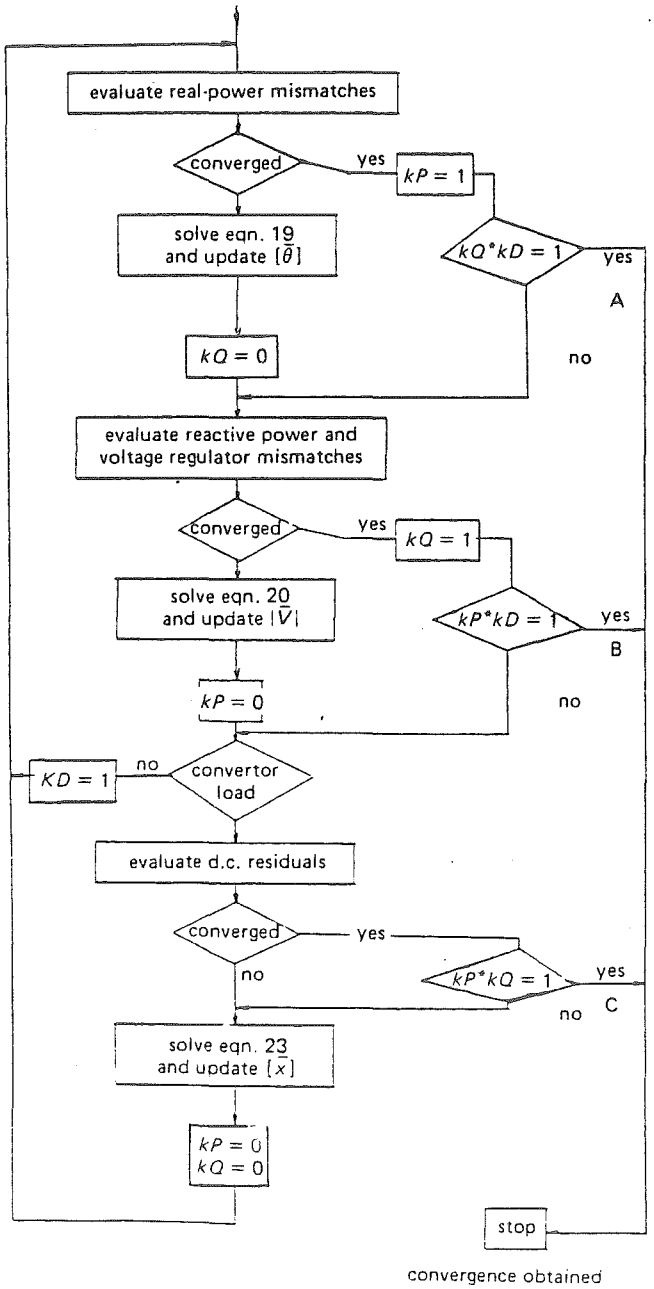

Fig. 5
Flow chart of iterative procedure

4 Programming aspects

Eqns. 19 and 20 are solved using sparsity techniques and near-optimal ordering. The solution of eqn. 23 is carried out using a modified Gaussian-elimination routine. The equations for each convertor are separate except for those relating to the d.c. interconnection.

This feature may be utilised, by appropriate ordering of variables, to yield a block sparsity structure for the d.c. Jacobian. On placing the direct-voltage variable last for each block of convertor equations and on placing all the direct-current variables after all convertor blocks, the d.c. Jacobian will have a structure as illustrated in Fig.6.

On using row pivoting only during the solution procedure, the block sparsity of Fig. 6 is preserved. Each block containing nonzero elements is stored in full, but only nonzero elements are processed.

This routine requires less storage than a normal sparsity programme for nonsymmetrical matrices and the solution efficiency is improved.

5 Test system and results

The test system, Fig. 7, consists of two a.c. subsystems interconnected by an h.v. d.c. link. The 20-busbar system is a representation of the 220 kV a.c. network in the South Island of New Zealand. It includes mutually coupled parallel lines, synchronous generators and condensers, star-star and star-delta connected transformers and has a total generation in excess of 2000 MW. The d.c.-link parameters are those of the Cook Strait link between the two islands.

At the other end of the link a fictitious 5-busbar system represents 800 MW of remote hydrogeneration feeding balanced loads at busbars 1 and 2 and connected to the convertor terminal by long untransposed high-voltage lines.

The small system is used to test the algorithm and to enable detailed discussion of results. The New Zealand d.c. link should have considerable influence, as the link power rating (600 MW) is comparable to the total capacity of the small system.

Table 1
CONTROL SPECIFICATIONS AND CONVERGENCE RESULTS

Case	Case description and rectifier specifications	Number of iterations to convergence (0·1 MW/MVAr)	
		20-busbar system	5-busbar system
(*a*)	Convertor modelled by equivalent balanced loads*	8	6
(*b*) (i)	phase-angle control: $\alpha_1 = \alpha_2 = \alpha_3 = \alpha_{min}, a_1 = a_2 = a_3, P_{dc} = P_d^{sp}$	8	7
(ii)	symmetrical firing; $\alpha_i = \alpha_{min}$ " "	8	7
(iii)	as for case (*b*)(i): with large unbalanced load at busbar 03	8	7
(iv)	as for case (*b*)(ii): with large unbalanced load at busbar 03	8	7
(v)	symmetrical firing; $\alpha_1 = \alpha_{min}, a_1 = -10°7, a_2 = 0, a_3 = +10°7$	8	7

*Loading for case *a* derived from results for case *b* (i)

Table 1 illustrates specifications and convergence results for a few selected cases. In all cases the following specifications apply at the receiving end:

(i) symmetrical firing control with reference phase on minimum-exinction angle
(ii) off-nominal taps equal in the three phases
(iii) d.c. voltage specified

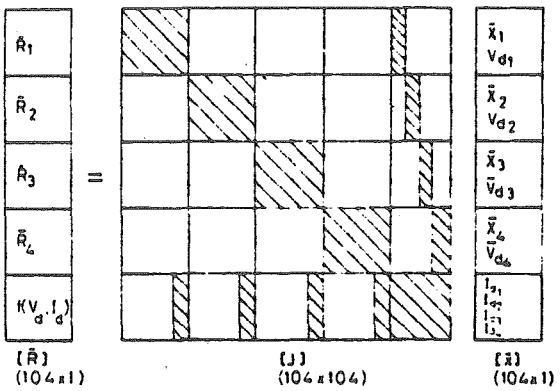

Fig. 6
Jacobian structure for a 4-convertor d.c. system (nonzero elements indicated)

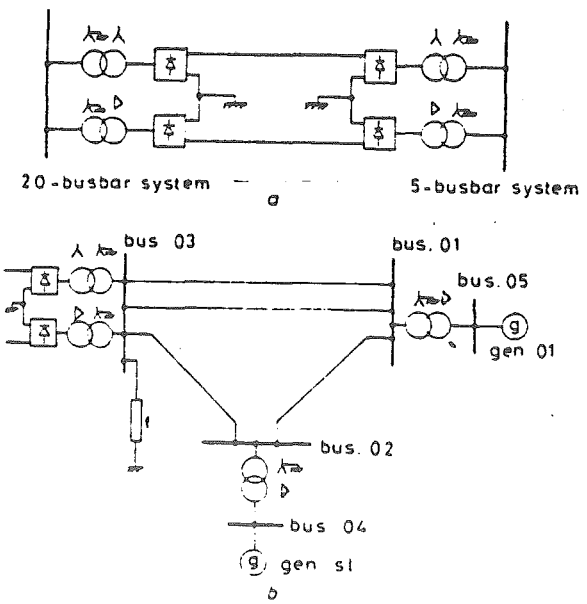

Fig. 7
Test system

a H.V. d.c. interconnection
b 5-busbar a.c. system

The case descriptions are summarised below:

(*a*) equivalent balanced loading with the convertors modelled by specified real and reactive powers at the terminal busbars
(*b*) accurate convertor representation:

(i) phase-angle control with all taps constrained to be equal and the total real power specified
(ii) as for case (i) but with symmetrical-firing control
(iii) as for case (i) but with unbalanced loading at busbar 3
(iv) as for case (iii) but with symmetrical firing
(v) all taps independently controlled on each phase, with symmetrical firing.

Only cases (i) and (ii) are representative of practical load-flow operating conditions. Cases (iii) and (iv) have been included to illustrate the capability of the algorithm to handle extreme levels of load unbalance (although it is realised that the approximations of Section 2.1 will lead to larger errors under such conditions). Finally, case (v) has been added to show the flexibity of the model regarding control specifications. The operating states of each convertor at the rectifier end are given in Table 2. The results have not been adjusted to the nearest discrete tap ratio to facilitate their interpretation.

To provide some understanding of the influence of the convertor-transformer connection on the unbalance, the zero-sequence components of voltage and current are indicated for case *b*(i) in Fig. 8.

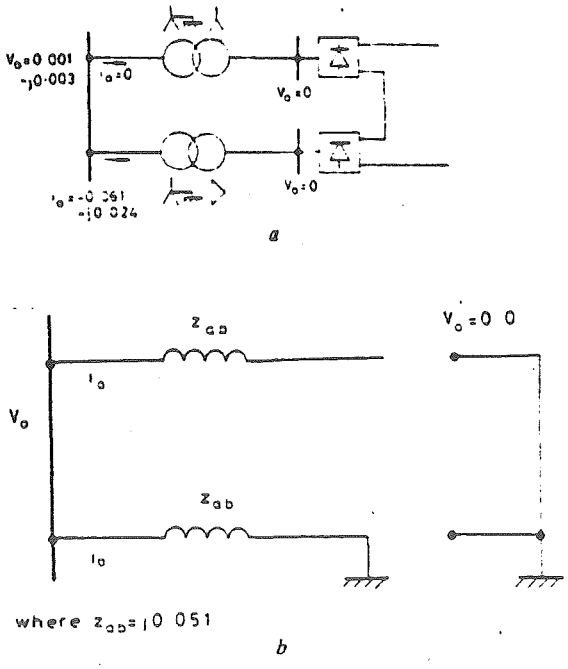

Fig. 8
Zero-sequence behaviour of convertor transformers (corresponding to test example (b)(i))

a Zero-sequence voltages and currents
b Equivalent zero-sequence network
Transformer-secondary-zero sequence reference is provided by eqns. 5 and 6

OPERATING STATES AT THE RECTIFIER END

Case	Phase	Convertor 1 (star-star) firing angle α_i, deg	tap ratio a_i, %	commutation angle μ_i, deg	terminal powers real P_i, MW	terminal powers reactive Q_i, MVAr	d.c. conditions voltage V_{d1}, kV	d.c. conditions current I_{d1}, kA	Convertor 2 (star-g/delta) firing angles α_i, deg	tap ratio a_i, %	commutation angle μ_i, deg	terminal power real P_i, MW	terminal power reactive Q_i, MVAr	d.c. conditions voltage V_{d2}, kV	d.c. conditions current I_{d2}, kA
b (i)	1	7·00	5·5	29·79	98·1	48·1	292·8	1·0246	7·00	5·5	29·80	97·3	49·2	292·8	1·0246
	2	7·00	5·5	29·32	101·7	50·8	–	–	7·00	15·5	29·60	102·6	53·2		
	3	7·00	5·5	29·61	100·3	48·3	–	–	7·00	5·5	29·32	100·14	44·7	–	
b (ii)	1	7·00	5·3	29·78	98·6	49·0	292·8	1·0246	8·03	5·2	28·97	96·4	50·0	292·8	1·0246
	2	7·20	5·3	29·14	100·9	51·3	–	–	7·00	5·2	29·57	102·7	52·9	–	
	3	8·43	5·3	28·50	100·6	47·8	–	–	8·55	5·2	28·08	100·87	45·66	–	
b (iii)	1	7·00	4·8	29·17	95·6	39·5	292·8	1·0246	7·00	4·3	30·63	67·9	13·0	292·8	1·0246
	2	7·00	4·8	29·16	101·9	50·5	–	–	7·00	4·3	28·92	95·5	89·4	–	
	3	7·00	4·8	30·43	102·44	57·2	–	–	7·00	4·3	28·90	136·6	53·7	–	
b (iv)	1	7·00	3·9	29·03	97·6	39·1	292·8	1·0246	7·00	3·0	30·48	70·9	17·9	292·8	1·0246
	2	11·64	3·9	25·63	101·8	54·7	–	–	14·95	3·0	23·25	90·1	94·1	–	–
	3	9·37	3·9	28·56	100·6	57·7	–	–	13·41	3·0	24·25	138·9	52·2	–	–
b (v)	1	11·00	−10·0	24·32	104·6	49·4	314·1	0·9483	8·08	−10·0	25·42	88·9	65·3	314·7	0·9483
	2	7·00	0·0	27·76	101·1	45·4	–	–	8·38	0·0	27·30	122·6	49·9	–	
	3	7·55	10.0	26·08	92·1	44·03	–	–	7·00	10·0	26·96	86·9	24·2	–	

6 Discussion

With reference to Table 1, the following general features of the algorithm can be identified:

(*a*) The number of iterations to convergence is not significantly increased by the presence of the d.c. convertors.
(*b*) Convergence is not dependent on the specific control specifications applied to each convertor.
(*c*) The algorithm exhibits good reliability even under conditions of extreme steady-state unbalance.

In comparison with single-phase a.c./d.c. load flows[1] the somewhat slower convergence of the 3-phase fast-decoupled load flow leads to a greater degree of reliability for the 3-phase a.c./d.c. algorithm.

The results, shown in Table 2, clearly demonstrate the need for accurate 3-phase modelling of the convertor plant. Differences of up to 20% are noticed in the reactive powers of the three phases of case *b*(i). The use of balanced *P*, *Q*-power injections at the convertor busbars is therefore unacceptable, even for small degrees of unbalance.

On the other hand, the errors owing to approximations made in the analytical model (Section 2.1) are comparatively small. For voltage distortion, for instance, the addition of 1% third-harmonic voltage results in about one-degree firing error in the worst possible case (i.e. when the third-harmonic voltages are in antiphase at the fundamental-voltage zero crossing) and the corresponding maximum changes in fundamental power components are of the order of 1%.

The use of symmetrical firing control results in higher reactive-power consumption by the convertors, and, to maintain the levels of direct voltage and power, increases in transformer-tap boost are required.

The computed results also indicate that, in general, the convertors have a balancing effect on the system voltage profile.

It can be seen from Fig. 8 that under unbalanced conditions a zero-sequence voltage may appear at system busbars. As the convertor has no zero-sequence path, zero-sequence current will only flow when the convertor transformer provides a path, as in the case of the star-g/delta transformer. Accurate convertor-transformer models must therefore be included in the convertor modelling.

7 Conclusions

A model of the steady-state behaviour of unbalanced h.v. d.c. transmission systems under normal operating conditions has been developed. Its sequential integration with a 3-phase fast-decoupled a.c. load-flow solution has been successfully implemented without impairing the efficiency and convergence of the original fast-decoupled algorithm.

The results indicate that a realistic assessment of the phase voltages and line-power flows, in the presence of voltage unbalance, requires a detailed 3-phase representation of the convertor and convertor transformer. Reactive-power differences of the order of 20% can occur as a result of normal transmission-system unbalance, i.e. under perfectly-balanced generating and loading conditions.

The maximum prescribed levels of voltage harmonic distortion have negligible effect for the purpose of power-flow studies. It must be made clear, however, that waveform distortion cannot be ignored in the calculation of current harmonic content to be used in harmonic-penetration studies, and further work is required in this area.

8 Acknowledgments

The authors are grateful to P.W. Blakely, General Manager of New Zealand Electricity, and the Computer Centre at the University of Canterbury for their help.

9 References

1 ARRILLAGA, J., and BODGER, P.: 'Integration of h.v. d.c. links with fast-decoupled load-flow solution', *Proc. IEE.*, 1977, 124, (5), pp. 463–468
2 AINSWORTH, J.D.: 'Harmonic instability between controlled static convertors and a.c. networks', *ibid.*, 1967, 114, (7), pp. 949–957
3 ARRILLAGA, J., and HARKER, B.J.: 'Fast decoupled three-phase load flow', *ibid.*, 1978, 125, (8), pp. 734–740
4 ARRILLAGA, J., and EFTHYMIADIS, A.E.: 'Simulation of convertor performance under unbalanced conditions', *ibid.*, 1968, 115, (12), pp.1809–1818
5 WASLEY, R.G., and SHLASH, M.A.: 'Newton-Raphson algorithm for 3-phase load flow', *ibid.*, 1974, 121, (7), pp. 630–638
6 CHEN, M.S., and DILLON, W.E., 'Power system modelling', *Proc. IEEE*, 1974, 62, pp. 901–915
7 GIESNER, D.B., and ARRILLAGA, J.: 'Behaviour of h.v. d.c. links under unbalanced-a.c.-fault conditions', *Proc. IEE.*, 1972, 119, (2), pp. 209–215
8 PHADKE, A.G., and HARLOW, J.H.: 'Generation of abnormal harmonics in high-voltage a.c.-d.c. power systems', *IEEE Trans.*, 1968, PAS-87, pp. 873–882
9 REEVE, J., and KRISHNAYYA, P.C.S.: Unusual current harmonics arising from high-voltage d.c. transmission, *ibid.*, 1968, PAS-87, pp. 883–893

10 Appendixes

10.1 Per-unit system

Computational simplicity is achieved by using common power and voltage bases on both sides of the convertor. The 3-phase a.c.-system base values are as follows:

MVA_{base} = base power per phase

V_{base} = phase: neutral voltage base

With common power and voltage bases the current base on the a.c. and d.c. sides are also equal, and therefore no constants appear in the equations owing to the p.u. system.

10.2 Convertor equations

The 26 equations ($\bar{R}$) which define the operation of each convertor are as follows:

$$R(1) = \sum_{i=1}^{3} E_i \cos \phi_i = 0$$

$$R(2) = \sum_{i=1}^{3} E_i \sin \phi_i = 0$$

$$R(3) = \sum_{i=1}^{3} E_i I_i \cos (\phi_i - \omega_i) - V_d I_d$$

$$R(4) = I_1 - \frac{4}{\pi\sqrt{2}} \frac{I_d}{} \sin (T_1/2)$$

$$R(5) = I_2 - \frac{4}{\pi}\frac{I_d}{\sqrt{2}} \sin(T_2/2)$$

$$R(6) = I_3 - \frac{4}{\pi}\frac{I_d}{\sqrt{2}} \sin(T_3/2)$$

$$R(7) = I_1 \cos\omega_1 - \sum_{k=1}^{3} [b_{ss}^{1k} E_k \sin\phi_k + b_{sp}^{1k} V_{term}^k \sin(\theta_{term}^k - \theta_{term}^1)]$$

$$R(8) = I_2 \cos\omega_2 - \sum_{k=1}^{3} [b_{ss}^{2k} E_k \sin\phi_k + b_{sp}^{2k} V_{term}^k \sin(\theta_{term}^k - \theta_{term}^1)]$$

$$R(9) = I_3 \cos\omega_3 - \sum_{k=1}^{3} [b_{ss}^{3k} E_k \sin\phi_k + b_{sp}^{3k} V_{term}^k \sin(\theta_{term}^k - \theta_{term}^1)]$$

$$R(10) = I_1 \sin\omega_1 + \sum_{k=1}^{3} [b_{ss}^{1k} E_k \cos\phi_k + b_{sp}^{1k} V_{term}^k \cos(\theta_{term}^k - \theta_{term}^1)]$$

$$R(11) = I_2 \sin\omega_2 + \sum_{k=1}^{3} [b_{ss}^{2k} E_k \cos\phi_k + b_{sp}^{2k} V_{term}^k \cos(\theta_{term}^k - \theta_{term}^1)]$$

$$R(12) = I_3 \sin\omega_3 + \sum_{k=1}^{3} [b_{ss}^{3k} E_k \cos\phi_k + b_{sp}^{3k} V_{term}^k \cos(\theta_{term}^k - \theta_{term}^1)]$$

$R(13)$
$\vdots$ depend on transformer connection
$R(18)$

$R(19)$
$\vdots$ depend on control specifications
$R(24)$

$$R(25) = V_d\pi - \sqrt{2}U_{21}[\cos(C_1 + \alpha_1 - C_3 + \pi) - \cos(C_2 + \alpha_2 - C_3 + \pi)] - \sqrt{2}U_{13}[\cos(C_2 + \alpha_2 - C_1) - \cos(C_3 + \alpha_3 - C_1)] - \sqrt{2}U_{23}[\cos(C_3 + \alpha_3 - C_2) - \cos(C_1 + \alpha_1 + -C_2)] + I_d(XC_1 + XC_2 + XC_3)$$

$R(26) = f(V_{dl}, I_{dl})$ from d.c.-system topology

APPENDIX 7

EFFECT OF HARMONIC VOLTAGES ON FUNDAMENTAL FREQUENCY OPERATION OF D.C. CONVERTORS

The three phase model of the d.c. convertor, as formulated in chapter 6, assumes perfectly sinusoidal voltages at the convertor terminal busbar. Without this assumption the steady state load flow formulation would be extremely complex due to the difficulty of calculating the harmonic voltages to any accuracy.

Harmonic voltages and currents present in the a.c. system cause many well documented[43] undesirable effects. Power authorities therefore specify maximum permissible values for these quantities. It is reasonable to restrict accuracy requirements to those systems which fall within these limits.

The presence of harmonic voltages at the convertor terminal busbar will alter the fundamental frequency power flows primarily because the actual zero crossings of the phase to phase voltages will be shifted from those calculated from the fundamentals alone. Other secondary effects will also be present but these may be ignored as the allowable harmonic voltages are small.

The term 'error' refers to the difference between the actual quantity in question and that calculated when the harmonics are ignored i.e. from the fundamentals alone as in the load flow equations of chapter 6.

A 7.1 HARMONIC VOLTAGE LIMITS

Recommended limits for harmonic voltages in the United Kingdom are given[74] below:

Supply Voltage	Odd Harmonic %	Even Harmonic %
415 V	4	2
33 kv	2	1
110/132 kv	1	0.5

The Total Harmonic Distortion (THD) is also limited to 1.5% for 110/132 kv where,

$$THD = \sqrt{\sum_{n=2}^{\infty} V_n^2}$$

In addition limits are placed on the harmonic current magnitude but these are not relevant to the present discussion.

A 7.2 ASSESSMENT OF POSSIBLE ERRORS

A 7.2.1 Shift in Zero Crossing of Phase-Phase Voltages

There is considerable difficulty in assigning a realistic worst case for the investigation of the influence of harmonic voltages. The following considerations apply:

- Under balanced conditions the characteristic harmonic orders do not influence the intervals between firing pulses i.e. all firings are shifted by equal amounts. Therefore these voltages will have very little effect on the magnitude of the fundamental currents.
- Harmonic limits are usually applied at the point of common coupling to the supply network which may or may not be the convertor terminal busbar as assumed by the load flow.
- The majority of the allowed triplen harmonics will consist of the usual zero sequence components and these have no influence on the position of phase to phase crossings.

The order of the non-zero sequence triplen harmonics, which may be considered to cause the most significant shifts, is not important as, under balanced conditions with the subsequent crossings 120 degrees apart, a small magnitude of any lower order triplen harmonic will result in comparable shifts for all three phases.

As a consequence of these features it is considered reasonable to investigate the worst case effect of 2% of non-triplen third harmonic voltage.

The worst case for a shift in any zero crossing is for all harmonics to add to the fundamental voltage on one phase and to subtract from the other phase at the position of actual zero crossing. This situation is illustrated in Fig. A 7.1 where a phasor diagram for non zero sequence third harmonic is shown.

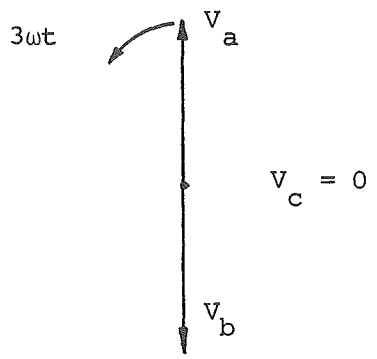

Fig. A7.1 Phasor Diagram of Third Harmonic Voltages

With consequent zero crossings 60^{o} apart i.e. one half rotation of the third harmonic phasors, then one subsequent shift will be approximately half the initial worst case, and the third shift will be equal to the worst case initial shift except in the opposite direction.

For 2% non zero sequence third harmonic the worst case shift is approximately one degree.

The order of magnitude of the resultant errors can be assessed on the basis of nominally balanced operation and by interpreting shifts in zero crossings as firing angle errors determined in accordance with the firing controller in operation.

For a convertor operating with fixed tap ratios and specified d.c. current, any firing angle errors are reflected into the convertor operation through errors in the calculated d.c. voltage and in the calculated magnitudes for the fundamental component of the phase current waveforms. Both errors occur to some extent with both firing controllers.

A 7.2.2 Errors in Calculated Phase Current Magnitudes

Appreciable errors occur with the case of phase angle control; errors with symmetrical firing are limited to the effects of commutation angle unbalance.

The effect of a 2 degree modulation has been investigated on the basis of the current waveform of a convertor with commutation angle of ten degrees and balanced voltages. Ignoring the shifts in commutation angle which will occur with an alteration of firing angle the effect of alteration in the period of conduction has been investigated using a Fourier Transform algorithm. The results are shown in Table A 7.1. In addition to the fundamental the percentages of the harmonics are also given. Note that no even harmonics are present as the waveform was assumed to be symmetrical.

It is important to note that the percentage errors presented in the Table are the maximum that can occur; in all practical cases there will be an alteration in the commutation angle which will

inhibit the change in the waveform. This effect will be most noticeable at small firing angles as can be seen in the results of chapter 8. In general therefore the harmonic changes will be less than those indicated in the Table.

The change in fundamental is not, therefore, expected to exceed 1% of the value calculated by the load flow.

Table A 7.1

Harmonic content of current waveform with period between valve firings of T and commutation angle of 10 degrees.

Order	Period T		
	120^{o}	121^{o}	122^{o}
0	-	-	-
1	100.00	100.50	100.99
3	0.01	0.95	1.92
5	17.85	17.3	16.89
7	11.32	11.64	12.04
9	0.01	0.68	1.35
11	4.88	4.57	4.25
13	3.09	3.26	3.41
15	0.01	0.29	0.56
17	1.05	0.94	0.82
19	0.75	0.81	0.85

A 7.2.3 Error in Calculated Average D.C. Voltage

The largest error occurs with symmetrical firing where any shift in the firing angle of the reference phase is reflected as a shift on all phases. The error depends upon the nominal firing angle. An example of possible errors is shown in Table A 7.2.

Table A 7.2

Percentage Errors in Calculated D.C. Voltage

Nominal Firing Angle	Error due to shift in Zero Crossing		
α	1^o	2^o	3^o
10^o	0.3	0.7	1
20	0.6	1.3	2
40	1.1	2.3	3.5
70	1.6	3.3	5.0

- % of V_{do}

The errors are small at small firing angles but may become significant at large firing angles.

A 7.3 CONCLUSION

The errors discussed in the previous sections may cause an alteration in the operating state of the convertor and lead to errors in the calculated values of real and reactive power flows for each phase.

The errors are minimal at small control angles which are usually applicable in load flow investigations. In addition, the nature of the harmonic voltages which will exist in any practical situation are unlikely to satisfy worst case conditions and any errors are not considered significant in the context of load flow investigations.

The modulation in the valve conduction periods which may occur are, however, significant if harmonic frequency current generation is being considered.

APPENDIX 8

IMPROVEMENT IN APPROXIMATIONS FOR PHASE CURRENT MAGNITUDES

The approximations for the fundamental magnitude of the phase currents may be improved in accuracy by adding an additional iterative loop to the load flow solution. After the load flow has converged to a moderate tolerance (e.g. five times the final tolerance) a Fourier Transform may be performed for the fundamental magnitudes. This may be performed by the Fast Fourier Transform algorithm as described in chapter 8. The correction factor (0.995 in equation 6.25) is then recalculated separately for each phase.

Convergence may then proceed to the final tolerance.

The phase currents may be calculated to any accuracy desired by repeated application of this procedure.

With one correction as discussed above the fundamental magnitudes have been within 0.2% for all examples considered. Only a marginal increase in the number of iterations is usually incurred by the introduction of this discontinuity.